Part B

Extended Abstracts of

Poster presentations

The order is in topical blocks as in the programme (pages *x-xvii*)
and within them numbered consecutively (nn = 01, ..., max):

Pnn	for	Precipitation Processes
Cnn	for	Climate Aspects
Bnn	for	Boundary Layer Processes
Dnn	for	Dynamical Aspects
Snn	for	Snow Pack

Observations of convection initiation and development from the Doppler on Wheels radars and comparison with high resolution WRF simulations

Lindsay J. Bennett[1], Alan M. Blyth[1,2], Tammy M. Weckwerth[3]

[1] School of Earth and Environment, University of Leeds, Leeds, UK
[2] National Centre for Atmospheric Science, UK
[3] Earth Observing Laboratory, National Center for Atmospheric Research, Boulder, Colorado, USA
E-mail: *l.j.bennett@leeds.ac.uk*

Abstract: Observations and model simulations are presented of convection initiation on IOP15a, 12 August 2007.

***K*eywords:** *convection initiation, mobile radar, WRF*

1 INTRODUCTION

Two mobile X-band Doppler on Wheels (DOW) radars were operated during the Convective and Orographically-Induced Precipitation Study (COPS). Their objectives were to (1) provide high resolution wind fields in regions not covered by the operational radar network, (2) observe areas of convergence and determine their role in the initiation of convection, and (3) observe the evolution of convective cells and the influence of the terrain on their propagation.

Observations from the DOWs during IOP15a, 12 August 2007 are presented and compared with simulations using the Weather and Research Forecasting (WRF) model. Early results show that the model simulations of the timing and location of precipitation compare well with the observations and suggest that the clouds formed as a result of converging upslope flows.

2 DATA

The location of the DOW radars are shown in Fig. 1 along with the COPS supersites, the POLDIRAD radar and the main river valleys. DOW2 was located at Hohbuhn in the Rhine Valley, whilst DOW3 was located at Schopfloch on the eastern side of the Black Forest.

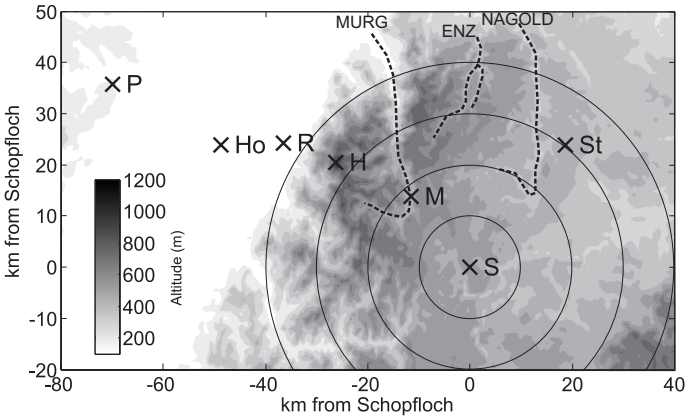

Figure 1: Map showing Black Forest topography (grey scale contours), major river valleys (black dashed lines) and site locations (crosses): Poldirad (P), Hohbuhn (Ho), Schopfloch (S), Achern (R), Hornisgrinde (H), Murg (M) and Stuttgart (St).

The Advanced Research WRF (ARW) model Version 3.0 was used to simulate this case study. The model was run with an outer domain and two higher resolution nests. The horizontal resolution of the domains were 6.3, 2.1 and 0.7 km respectively. The inner domain was centred over the COPS region. The model was run with 121 vertical levels, initialised at 0000 UTC and run for 18 hours, and the outer domain was driven by either 1°GFS or 0.25° ECMWF analyses, updated every 6 hours.

3 EARLY RESULTS

Sequences of PPI scans from DOW3 showed that small convective cells began to develop between 10 and 30 km north of the radar from approximately 1000 UTC. Larger cells developed from about 1130 UTC and examples of

these are shown in Figs. 2a and b. Satellite images reveal that shallow convective clouds were widely distributed across the northern Black Forest, but the locations of the first echoes observed by DOW3 (Fig. 2c) indicates that precipitating clouds only occurred on the eastward facing slope, between the Murg and Nagold valleys.

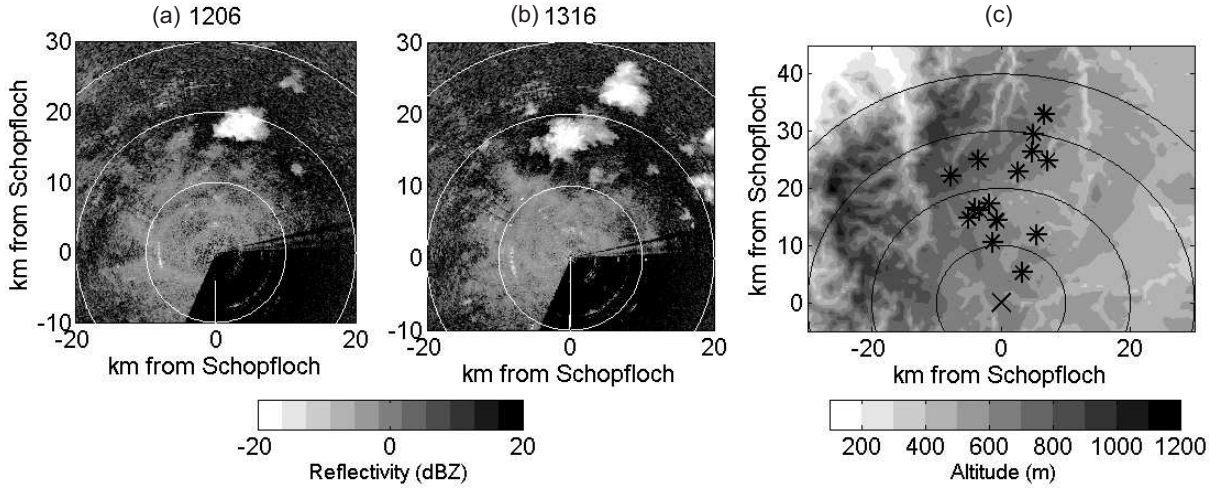

Figure 2: Examples of convective cells observed by DOW3 at (a) 1206 and (b) 1226 UTC. The location of the first precipitation echoes of all significant cells is shown in (c).

Figure 3 shows examples of simulated 10 m horizontal wind vectors overlaid on orography. At 0700 UTC down-valley and down-slope winds are occurring. The wind direction is southerly along the Murg and Nagold valleys and south-westerly along the Enz and down the eastward facing slope. By 0900 UTC, the wind direction has shifted 180 degrees to a northerly flow along the centre of the valleys and to an upslope north-easterly or north-westerly along the valley sides. These flows lead to areas of convergence that results in the development of clouds by 1000 UTC. Clouds develop widely across the northern Black Forest but those that precipitate are confined to the eastern slope (not shown).

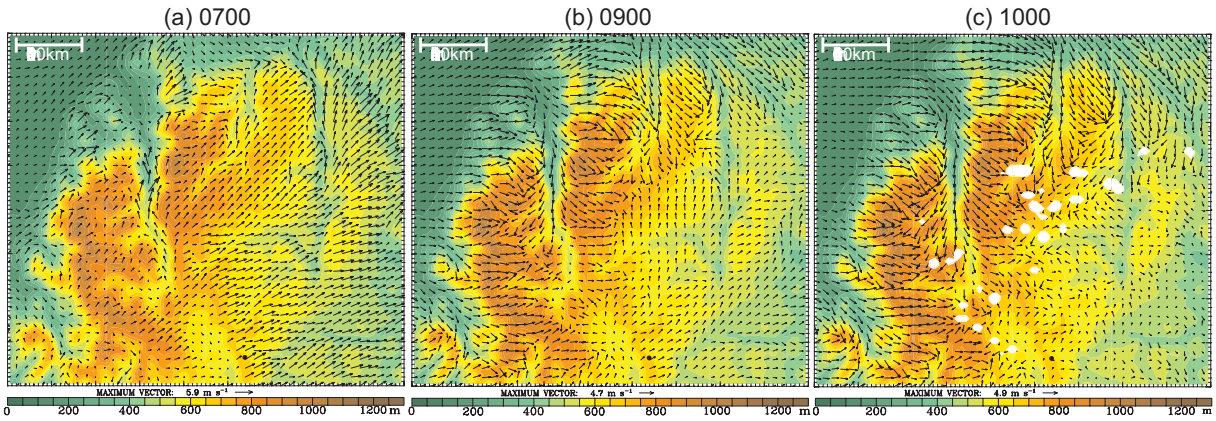

Figure 3: Output from model runs initialised with GFS analyses. A subsection of the inner domain is shown at (a) 0700, (b) 0900 and (c) 1000 UTC. The contours show orography and the vectors are the 10 m horizontal wind. The black dot marks the location of DOW3.

4 FUTURE WORK

Investigations are under way into the processes creating the convergence zones on the eastern slope. In particular, the influence of topographic shading and differential heating will be evaluated. Comparisons will also be made between the DOW observations on several other days and WRF runs to examine the ideas found in this study that the convergence lines produced by the valley flows are responsible for the initiation of precipitating convection.

CHARACTERIZATION OF THE CONVECTIVE ACTIVITY IN THE EASTERN IBERIAN RANGE, SPAIN

Samuel Buisán [1], Francisco Espejo [1], Gerardo Sanz[1]
Francisco Cortés[2], Cristina Lafragüeta[2]

[1] State Meteorology Agency (AEMET), Aragón Regional Office, Zaragoza, Spain
E-mail: *sbuisan@inm.es*
[2] SODEMASA – Environmental Department, Aragón Regional Government, Spain

Abstract: Mediterranean climates are characterized by dry summers. However, this work presents a region which, despite its being close to the Mediterranean Sea, shows a different precipitation pattern that presents a maximum between May and September. This is mainly due to the high convective activity developed in this area. The main contributing factors are the geographical situation, favourable to the appropriate synoptic weather conditions, the elevated altitude, and the convergence of two different air masses, the first one characterized by a continental dry and hot air from the central plateau of the Iberian Peninsula and the second one by cool and humid air from the sea. All these factors lead to the remarkably high number of violent storms reported.

Keywords: *Altitude, Mediterranean Sea, severe weather, mountainous area, Iberian Range*

1 INTRODUCTION

The Eastern Iberian Range, shown in Figure 1, is located in the Northeast of Spain roughly aligned in a NW-SE direction along some 400 Km. Our area of interest lies on its easternmost part, the closest one to the Mediterranean Sea, covering a surface of around 7000 km^2 in the Spanish province of Teruel, in the region of Aragón. It is a plateau-like morphology with a mean elevation of around 1500 m, reaching 2020 m at the Javalambre peak. The distance to the Mediterranean Sea is on average 50 km along its eastern side.

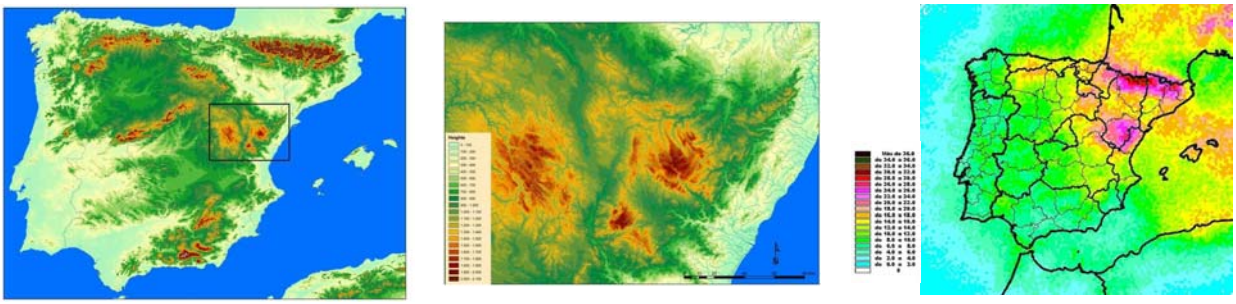

Figure 1. A and B) Eastern Iberian Range, characterized by its elevation and closeness to the Mediterranean Sea. C) Average thunderstorm days per year (2000 – 2007 period), from [1].

2 DESCRIPTION OF CONVECTIVE ACTIVITY

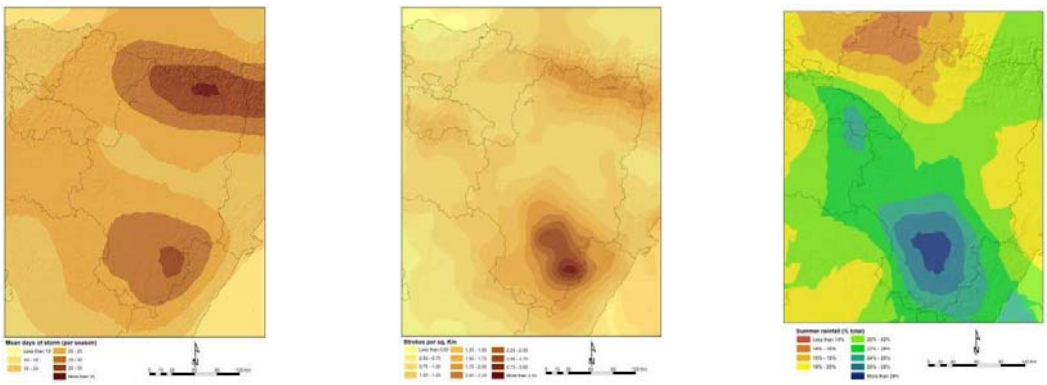

Figure 2. A) Average thunderstorm days during warm season (Apr.-Sep./2002-08) B) Flash rate density per square kilometre during the warm season (Apr.-Sep./2002-08) C) Percentage of summer rainfall from the annual mean.

This area is characterized by a significant high number of storms as shown on Figure 1C) with around 30 thunderstorm days per year, these figures are only exceeded on the Pyrenees. Most of these days are concentrated in the spring and summer months with an average of 5 thunderstorm days per month, Figure 2A). The study area is the first one in flash rate density in Spain recording an average of more than 3 cloud-to-ground flashes per km2, Figure 2B), during the warm season (Apr.-Sep.). Taking into account the number of strokes per flash, the real number of strokes could well double these figures. Comparing Figure 2A) and Figure 2B) it is clear how, in spite of the lower number of thunderstorm days on the Eastern Iberian Range, their severity is higher, fact that is also confirmed by forecasting experience. The focus of convective activity is found in the Sierra del Rayo (Lightning's Sierra), a great example of accuracy in traditional toponymy.
Finally, Figure 2C) shows how the precipitation during the summer months (JJA) accounts for around 30 percent of the annual precipitation.

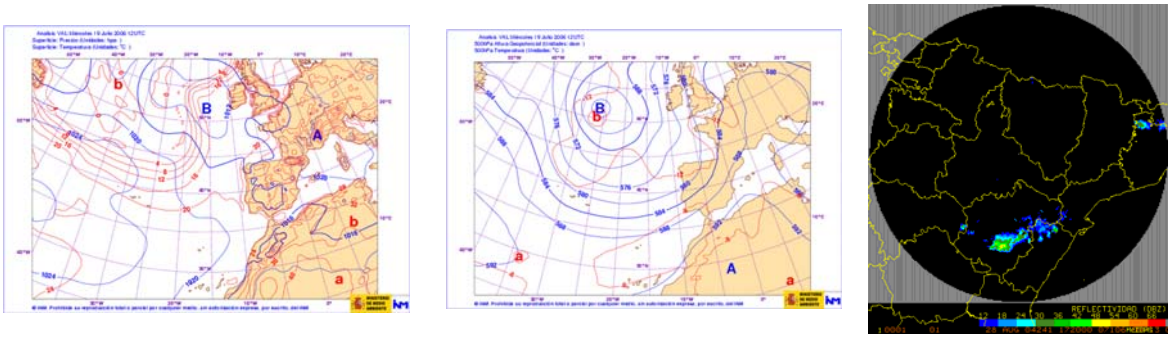

Figure 3. Typical synoptic conditions associated with severe weather. A) Surface pressure and temperature at 12 UTC (19.07.06) B) 500-hPa geopotential height and temperature at 12 UTC (19.07.06) C) Radar observed supercell (28.08.04)

Intensive heating during the warm season produces a thermal low, Figure 3A), in the centre of the Iberian Peninsula, which together with the high altitude of the region facilitates the convection. This relative low pressure enhances the ascending southeast humid low level flow from the sea providing moisture and wind shear. When midlevel instabilities and/or dynamical forcing are present, Figure 3B), all the ingredients are then favourable for severe weather to develop.

Numerous episodes of severe weather including severe thunderstorms, supercells, Figure 3C), and mesoscale convective systems, occur each season. Severe hail has been frequently observed during these episodes. Moderate and significant tornadoes have been reported, including some severe F3 tornadoes such as those of the Sierra del Rayo in 1999, near the town of Alcañiz in 2003, and Corbalán in 2004.

Flash floods are also frequent especially during cut-off low conditions over the Mediterranean Sea, particularly at the end of summer and the beginning of autumn.

3 CONCLUSIONS

This part of Spain is sparsely populated and for this reason numerous episodes of severe weather have not been reported. The expansion of human activities due to the opening of new motorways and tourism makes this area a new focus of interest, apart from the mere fact that this is probably one of the regions of Europe more prone to severe weather events. The weather forecast office of the Spanish State Meteorology Agency (AEMET) in Aragón must provide timely and accurate forecasts and must watch for severe weather giving the appropriate warnings, including fire alerts, which are issued to local emergency management and public safety officials. A deeper study of these phenomena is currently carried out in order to better understand these processes.

Acknowledgements:
Evelio Álvarez, Francisco Pérez Puebla, César Zancajo, Ramón Vazquez and Margarita Palmer (AEMET).
All the current and former staff at the weather forecast office of the Spanish State Meteorology Agency (AEMET) in Aragón.

REFERENCES

[1] Francisco Pérez Puebla y César Zancajo Rodríguez: El carácter tormentoso del año 2008 en España, 6º Simposium do APMG, Lisboa - Portugal

THE IMPACT OF CONVERGENCE ZONES ON THE INITIATION OF DEEP CONVECTION: A CASE STUDY FROM COPS

B. Adler[1], N. Kalthoff[1], Ch. Barthlott[1], U. Corsmeier[1], S. Mobbs[2], S. Crewell[3], K. Träumner[1], Ch. Kottmeier[1], A. Wieser[1], V. Smith[4]

[1] Institute for Meteorology and Climate Research, Karlsruhe Institute of Technology (KIT), Karlsruhe, Germany
E-mail: *bianca.adler@imk.fzk.de*
[2] National Centre for Atmospheric Science, Leeds, United Kingdom
[3] Institute for Geophysics and Meteorology, University of Cologne, Cologne, Germany
[4] Institute for Climate and Atmospheric Science, University of Leeds, Leeds, United Kingdom

Abstract: During the 'Convective and Orographically-induced Precipitation Study' (COPS) performed in summer 2007, deep convection developed on July 15, although convective available potential energy was only moderate and convective inhibition was high. Data analysis revealed that the convection was triggered by the optimal superposition of a mesoscale and an upslope-wind induced convergence zone.

Keywords: *boundary layer, slope winds, convection indices, convective inhibition, updraught*

1 INTRODUCTION

Development of moist convection requires some kind of instability and a trigger mechanism like i.e. mid- and upper-tropospheric lifting or forcing by planetary boundary-layer (PBL) processes. Convergence zones of different origin are important PBL phenomena which initiate deep convection (Wilson et al., 1992).

The "Convective and Orographically-induced Precipitation Study" (COPS) was performed in summer 2007 in south-western Germany (Black Forest) and eastern France (Vosges). The case study reported here deals with the interaction of different low-level convergence zones and their impact on the initiation of deep convection on July 15, 2007. To investigate the different mechanisms which were responsible for triggering convection data analysis based on radiosondes, standard meteorological instruments, aircraft measurements, and remote sensing systems was carried out.

2 SYNOPTIC CONDITIONS AND DEEP CONVECTION ON JULY 15, 2007

The COPS area was located in the transition zone between an eastern European ridge stretching from the Mediterranean Sea to Poland and a high-amplitude eastern Atlantic trough. The large-scale forcing resulted in weak lifting concentrating on the western part of the domain. Near the surface, the investigation area was in the transition zone between a surface low in the west and a surface high in the east accompanied by convergence in between. Consequently, low-level SE wind dominated in the COPS domain in the morning (Fig. 1 left). While the surface low was approaching, the area with convergence moved towards the east, such that SW wind prevailed in the PBL of the whole COPS area in the afternoon (Fig. 1 right).

The atmosphere was characterised by warm, but dry air masses which did not favour atmospheric instability. A PBL-capping inversion, a weak inversion at about 2200 m asl, and some minor mid-tropospheric inversions existed. In the Rhine valley, CAPE was small and CIN rather high. East of the Black Forest crest at Heselbach, CAPE and CIN reached moderate values. LFC was higher than 3200 m asl at all sites.

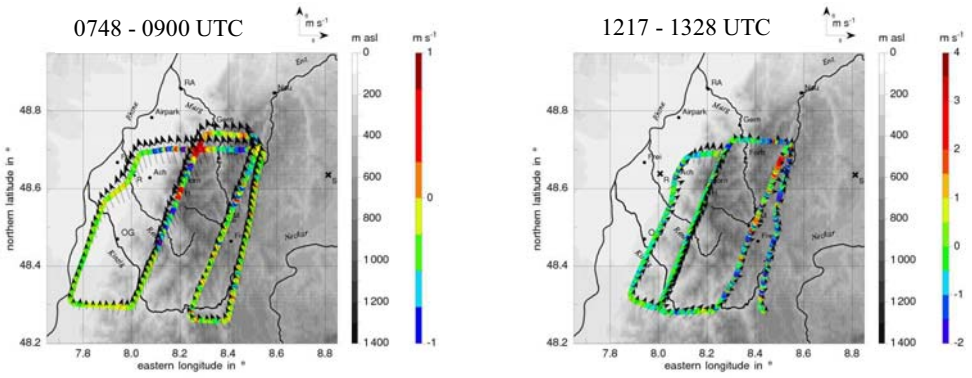

Figure 1. Horizontal wind vectors and vertical wind (colour code) as measured by the Dornier 128 aircraft on July 15.

First cumulus clouds formed over the Black Forest at about 1115 UTC. At about 1230 UTC shallow clouds were detected by satellite over the Vosges. Until 1400 UTC two cloud bands had developed over the Black Forest. During the next hour three isolated deep convective cells developed from the cloud bands. The cell southeast of Freudenstadt even developed into a mature cumulonimbus. At 1730 UTC all clouds in the COPS area had disappeared.

3 INITIATION OF CONVECTION BY BOUNDARY LAYER PROCESSES

Thermally induced wind systems developed over the Vosges and Black Forest. The resulting vertical wind of the two upslope wind systems at the western and eastern slope of the Black Forest crest, based on the continuity equation, was about 0.1 m s^{-1} at the top of the convergence zone above the Black Forest crest between 0830 and 1130 UTC. Thermally induced upvalley winds developed within the valleys of the northern Black Forest. Based on the wind profile in the Kinzig valley a rough estimate of the mean vertical wind at the top of the valley wind layer at the valley head was performed. Maximum values of about 0.5 m s^{-1} were reached between 1100 and 1300 UTC. Thus, slope and valley winds were too weak to overcome the CIN and trigger convection on this day.

To elaborate the characteristics of the mesoscale flow structure the local change of the horizontal wind was analysed: At Meistratzheim (V) and Achern (R) change of the low-level wind from SE to SW was completed at 1000 UTC and at 1030 UTC, respectively, which indicated the end of the passage of the convergence zone (Fig. 2 left). At Oberkirch (OBE) and the Hornisgrinde (H) the convergence zone had passed at 1100 UTC (Fig. 2). During its passage over the mountain crest, it optimally superimposed on the convergence zone generated by the stationary slope winds. Consequently, strong upward motion occurred which penetrated the capping inversion at 2100 m asl (Fig. 2 right) and roughly reached the LFC. The strong updraughts were accompanied by a change in the wind direction from SE to W and an increase in humidity. At Barongartenhütte (BAR), the convergence zone had passed at 1330 UTC and at Igelsberg (IGE) and Heselbach (M) at about 1400 UTC, respectively (Fig. 2 left). The humidity and temperature profiler at Heselbach showed that during the passage of the convergence zone an increase in humidity occurred up to about 4.5 km asl. Applying the continuity equation to the Heselbach wind profiler data, a mean vertical wind speed at the top of the convergence zone of 1.2 m s^{-1} resulted. The Dornier 128 aircraft measurements between 1317 and 1328 UTC revealed updraughts of about 3.5 m s^{-1} below individual convective cells within the convergence zone (Fig. 1 right).

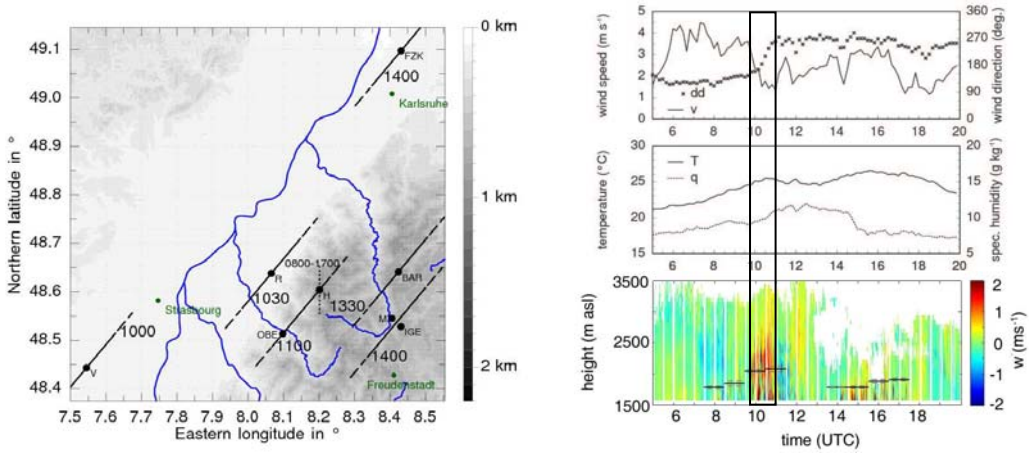

Figure 2. Left: Position and end of passage time of the mesoscale convergence zone (solid dashed lines) and duration and position of the upslope wind-induced convergence zone (dotted line). Right: Surface measurements and vertical wind speed profile measured by the wind lidar at Hornisgrinde.

4 SUMMARY

Deep convection developed on July 15, 2007 over the Black Forest. The analysis showed that an optimal superposition of an eastward moving mesoscale and a stationary upslope wind-induced convergence zone over the mountain crest initiated the convection (Kalthoff et al., 2009).

REFERENCES

Kalthoff, N., B. Adler, C. Barthlott, U. Corsmeier, S. Mobbs, S. Crewell, K. Träumner, C. Kottmeier, A. Wieser, V. Smith, P. Di Girolamo, 2009: The impact of convergence zones on the initiation of deep convection: A case study from COPS. Atmos. Res. doi: 10.1016/j.atmosres.2009.02.010.

Wilson, J.W., G.B. Foote, N.A. Crook, J.C. Fankhauser, C.G. Wade, J.D. Tuttle, C. Mueller, 1992: The role of boundary-layer convergence zones and horizontal rolls in the initiation of thunderstorms: a case study. Mon. Wea. Rev. **120**, 1785 – 1815.

INFLUENCE OF LOCAL OROGRAPHY ON FORECAST OF PRECIPITATION IN CASE OF FLASH FLOODS IN SLOVENIA ON SEPTEMBER 18, 2007

Vanja Kovač[1], Jure Cedilnik[1], Nedjeljka Žagar[2], Mark Žagar[2]

[1]Environmental Agency of the Republic of Slovenia, Ljubljana, Slovenia
[2]University of Ljubljana, Faculty of Mathematics and Physics, Chair of Meteorology, Ljubljana, Slovenia
E-mail: vanja.kovac@gmail.com

Abstract: The influence of the Slovenian orography on the ALADIN model forecasts is studied in flash flood case which occurred on September 18, 2007. Various modifications of model orography were tested, resulting in amplitude of the differences in the 24-hour accumulated rainfall around ±30 % of the precipitation amounts in the reference experiment over the same area.

Keywords: *numerical weather prediction, ALADIN model, orography modelling, extreme precipitation*

1 INTRODUCTION

On September 18, 2007 heavy precipitation occurred across the northwestern Slovenia causing severe flash floods with a death toll of 6 and the damage about 250 million Euros. Extreme precipitation was measured at many stations across the country and 24-hour cumulative amounts locally exceeded 400 mm. Precipitation occurred ahead of the cold front related to the intense low-level moisture advection from the southwest and a relatively strong vertical wind shear over the Slovenian region. The operational forecasts, while able to predict heavy rains sufficiently well so that the weather service issued the flash flood warnings, systematically underestimated the amounts of precipitation and failed to provide details of the spatial distribution.

The purpose of this study is to estimate the influence of the local orography on the operational forecasts of the mesoscale model ALADIN-SI. The emphasis is on the intensity and spatial distribution of the simulated precipitation. In order to gain a quantitative estimate of the orography impact, several sensitivity studies with altered orography are carried out and preliminary results are presented. Since the ALADIN applications used operationally in neighbouring countries had a few differences compared to the operational ALADIN-SI at the time of the flash flood event, they can be studied as a limited area ensemble; we show some results of the comparison of several ensemble members.

2 COMPARISON OF OPERATIONAL ALADIN RESULTS

We choose to present the precipitation forecast from simulations which mimic the operational ALADIN applications in Slovenia (ALADIN-SI), Croatia (ALADIN-HR) and Slovakia (ALADIN-SK). Their only difference is the horizontal resolution and the domain size. In each case the model orography was prepared using the variational approach of Bouteloup (1995). Resulting topographic features of Slovenia had somewhat different shape and height of orographic peaks. The cumulative precipitation distributions showed to be strongly correlated with the underlying orography. In each case the distribution of 30-hour cumulative precipitation resembles the models' orography (not shown). Precipitation maxima differ significantly: from 90 mm in ALADIN-SI to 107 mm in ALADIN-HR and 165 mm in ALADIN-SK (Fig. 1). Forthcoming work aims at studying in more detail methods for preparing the mesoscale model orography.

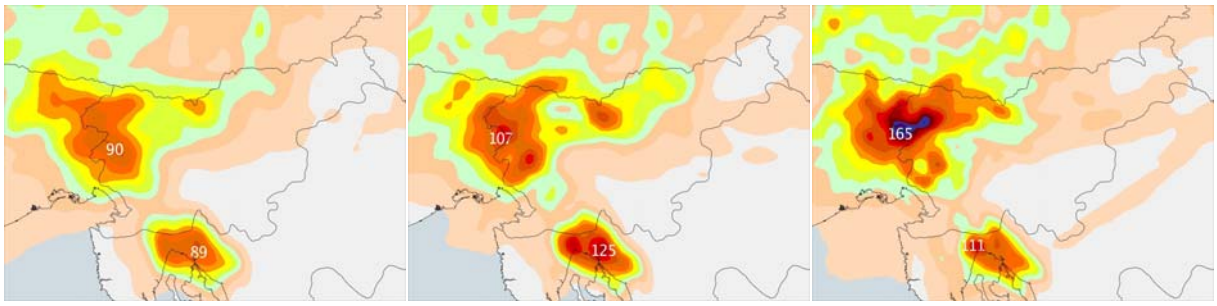

Figure 1. 30-hour accumulated precipitation at 18 UTC September 18, 2007 (contour intervals 10 mm). Left: ALADIN-SI, middle: ALADIN-HR and right: ALADIN-SK.

3 SENSITIVITY STUDIES ON THE IMPACT OF SLOVENIAN OROGRAPHY

Sensitivity studied performed 30-hour simulations starting on September 17, 2007, 12 UTC. Various experiments tested the impact of different mountains across the northwestern Slovenia. For these experiments, we

applied a more recent, ALARO version of ALADIN model, which includes a set of new physical parametrizations. Sensitivity experiments varied from removing or lowering down selected mountains to removing the whole mountain system such as the Kamnik Alps. The reference orography and two examples of the orography used in sensitivity simulations, denoted NO_JKA and NO_KA, are presented in Fig. 2.

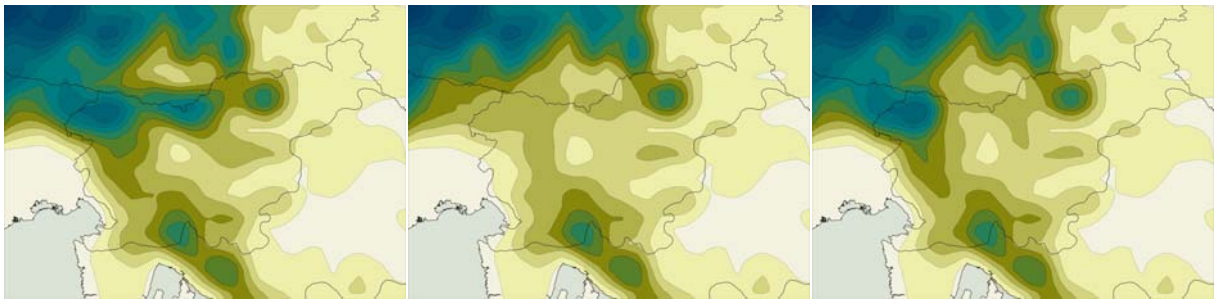

Figure 2. Examples of the orography used in sensitivity experiments (contour intervals 200 m). Left: reference orography (REFR), middle: experiment in which the Julian and the Kamnik Alps were removed (NO_JKA), right: experiment without the Kamnik Alps (NO_KA).

As expected, results show that the orography considerably impacts the moist and potentially unstable flow in the lower troposphere and so the location and amounts of precipitation. The position and strength of the low-level convergence zone ahead of the front are defined by the orography. The spatial distribution of the differences between the reference and sensitivity experiments agrees well with the changes in the terrain (Fig. 3 versus Fig. 2). When the terrain is raised the airflow slows down, and in the opposite case, when new gaps open the airflow accelerates. In the former case the precipitation increases on the windward side while in the latter case more moisture reaches areas behind the original terrain. Compared with the REFR experiment which produced up to 135 mm of rain within 24 hours, the precipitation in the NO_KA experiment changed between -40 mm to +22 mm. In the NO_JKA experiment the change with respect to REFR varied between -33 mm and +43 mm. The orography impact on the precipitation distribution is limited to the surroundings of the modified terrain (Fig. 3).

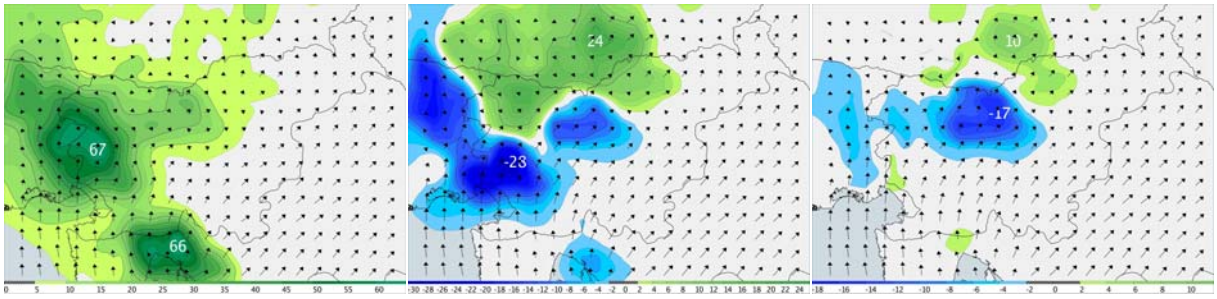

Figure 3. 10 m wind field and 18-hour accumulated precipitation at 12 UTC September 18 for three experiments: REFR (left), NO_JKA (middle) and NO_KA (right). For experiments NO_JKA and NO_KA the precipitation difference with respect to reference (REFR) is shown. The largest arrows represent wind speed of 12 m/s.

4 OUTLOOK

We are working on additional experiments at higher resolution to perform more in-depth study of the model sensitivity to the details of the terrain representation.

REFERENCES:

Bouteloup, Y., 1995: Improvement of the spectral representation of the earth topography with a variational method. Mon. Wea. Rev. **123,** 1560–1574.

Kovač, V., 2008: The influence of local orography on the precipitation forecast with ALADIN for 18 September 2007. Bsc Thesis, University of Ljubljana (In Slovenian), 58 pp.

Piriou, J.-M., Redelsperger, J.-L., Geleyn, J.-F., Lafore, J.-P. and Guichard, F., 2007: An Approach for Convective Parameterization with Memory: Separating Microphysics and Transport in Grid-Scale Equations. J. Atmos. Sci. **64**, 4127-4139.

Žagar, M., 2008: Analysis of causes and numerrical modelling of heavy precipitation on 18 September 2007. Ujma **22**, 101-104.

THE OROGRAPHIC IMPACT ON PATTERNS OF EMBEDDED CONVECTION DURING THE AUGUST 2005 ALPINE FLOOD

Wolfgang Langhans[1], Alexander Gohm[2], Günther Zängl[3]

[1] Institute for Atmospheric and Climate Science, ETH Zurich, Switzerland
[2] Institute of Meteorology and Geophysics, University of Innsbruck, Austria
[3] DWD, Offenbach, Germany
E-mail: *wolfgang.langhans@env.ethz.ch*

Abstract: Convective precipitation structures during a heavy Alpine precipitation event in August 2005 are investigated utilizing a mesoscale non-hydrostatic numerical model and observational data. The focus is on the mechanism of convective initiation during the very beginning of the event, when organized cellular updrafts enhanced the precipitation. A set of sensitivity experiments with systematically modified topography is conducted in order to investigate the role of single topographic obstacles in initiating and arranging convection.
***K*eywords:** *banded convection, August 2005 Alpine flood, orographic precipitation*

1 INTRODUCTION

The August 2005 heavy precipitation event has been selected for investigations, as it features a period of intense embedded convective precipitation, which resulted in locally intensified rainfall. The convective cells are embedded in the northeasterly low-level jet and cause heavy precipitation over the low-mountain terrain in southern Germany and northern Alpine slopes during an early stage of the event. Furthermore, observations and simulations suggest that these downstream propagating convective cells become aligned in a banded manner (Langhans, 2008). Previous studies highlighted the potential of convective bands to enhance precipitation in mountainous regions (e.g., Cosma et al., 2002; Fuhrer and Schär, 2007; Kirshbaum et al., 2007). In this study the mechanisms of convective initiation during the period of interest are determined, whereby special attention is also given to the influence of topographic obstacles. Therefore, numerical experiments with partly removed or flatened orography and others with additional idealized orographic obstacles are performed.

2 EXPERIMENTAL SETUP

The Weather Research and Forecasting modeling system (WRF) is used for numerical simulations. Three two-way nested model domains are used with a horizontal mesh size of 30 km, 10 km, and 2 km, respectively. The innermost domain encloses the Alpine area, i.e., Switzerland, Austria, and the German Alpine foreland. Convective clouds are treated explicitly within this model domain. The initial and boundary conditions are obtained from the European Centre for Medium Range Weather Forecasts (ECMWF) operational analysis. Several sensitivity simulations are conducted using modified topography. The reference run (REF) uses a 30" orography in the innermost domain. The influence of individual mountain ridges is explored by the experiments NOBF and NOSA, in which the Bavarian Forest and the Swabian Alb, respectively, are removed. Within the NOALPS run the terrain elevation in the innermost Alpine domain is limited to 500 m, which completely removes the Alpine arc. Idealized ridges are added to the flatened NOSA topography in two experiments: with respect to the Swabian Alb, in the ADDRIDGE1 run the ridge is located slightly further north, whereas in the ADDRIDGE2 simulation the ridge is right at its original location. The simulated precipitation fields are validated against a dense network of daily rain gauge measurements and the CERAD (Central European Weather Radar Network) radar composite.

3 RESULTS

Two precipitation bands are observed by the CERAD radar measurements (not shown) over the northern Alpine foreland. Also rain gauge records indicate these banded regions of relatively high daily accumulated precipitation (see Fig. 1a). The REF run reproduces these patterns over southwestern Germany very well (see Fig. 1b). Compared to the radar product the REF simulation shows a qualitatively similar development of precipitation structures. Convective cells become aligned and form two flow-parallel bands during the afternoon of 21 August. The REF simulation reveals the presence of two low-level convergence lines, which are the driving mechanism for initiating the cells in this banded manner. The northern band is located over the Swabian Alb, while the southern band seems to trail downstream of the Bavarian Forest. However, removing specific mountain ranges (NOBF, NOSA) results in small modifications of the spatial distribution and intensity of daily accumulated precipitation and the

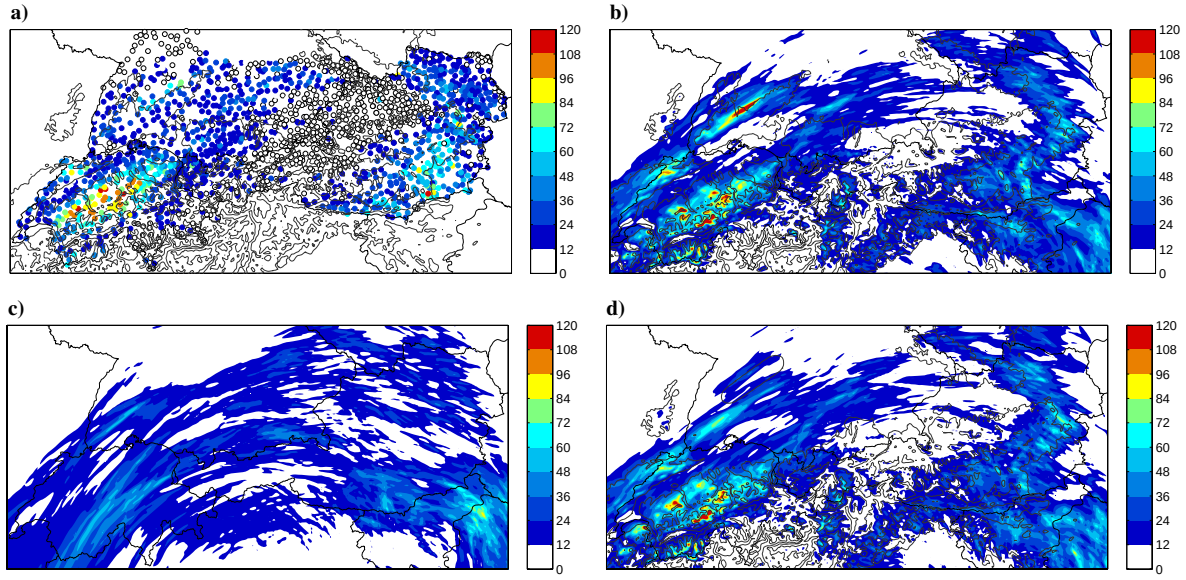

Figure 1: Daily accumulated precipitation (mm) over the northern Alps between 0600 UTC 21 August and 0600 UTC 22 August 2005 from (a) rain gauge measurements, (b) REF, (c) NOALPS, and (d) ADDRIDGE1. Orography is indicated every 1000 m.

arrangement of the cells appears even more banded. Only the NOALPS simulation (see Fig. 1c) shifts the position of both convergence lines, thereby modifying the regions of convective updrafts.

Further knowledge about the impact of the Swabian Alb on the convective initiation in the northern convergence line is gained from ADDRIDGE1 and ADDRIDGE2. The former, in which the convergence line is positioned slightly to the south of the ridge, produces much higher convective inhibition, that results in less continuous triggering in the convergence zone, scattering and weakening of convective updrafts (see Fig. 1d). ADDRIDGE2, in which the position of the ridge is in phase with the position of the convergence line, retains the banded shape and intensity of convection.

4 CONCLUSIONS

A primary mechanism for both the initiating and aligning of convective cells over the northern Alpine foreland during the afternoon of 21 August 2005 is given by the presence of two synoptically forced low-level convergence lines. A sensitivity study reveals no significant influence of mountains, as the primary mechanism consistently triggers moist convection at the same locations. However, the experiments show that the orography (e.g., Swabian Alb) constitutes a secondary mechanism for triggering convection. Enhancement (weakening) of the alignment of convective cells is achieved, when the convergence line is located above (next to) a ridge.

Acknowledgements: *Rain gauge data was provided by the national weather services ZAMG, DWD, MeteoSwiss, and by the Austrian hydrological service HZB. Thanks to all weather services contributing to the CERAD product, especially to Kurt Zimmermann (ZAMG). The Central IT Services (ZID) as well as the High-Performance-Computing (HPC) Consortium of the University of Innsbruck are acknowledged for access to their Linux Compute Clusters.*

REFERENCES

Cosma, S., E. Richard, and F. Miniscloux, 2002: The role of small-scale orographic features in the spatial distribution of precipitation. *Quart. J. Roy. Meteor. Soc.*, **128**, 75–92.

Fuhrer, O., and C. Schär, 2007: Dynamics of orographically triggered banded convection in sheared moist orographic flows. *J. Atmos. Sci.*, **64**, 3542–3561.

Kirshbaum, D.J., G. Bryan, and R. Rotunno, 2007: The triggering of orographic rainbands by small-scale topography. *J. Atmos. Sci.*, **64**, 1530–1549.

Langhans, W., 2008: Cloud-resolving simulations of the August 2005 Alpine flood: the sensitivity to microphysics parameterizations. Master's thesis, University of Innsbruck, 114 pp.

ANALYSIS OF DIFFERENT ALADIN FORECAST RUNS FOR THE FLASH FLOOD CASE IN SLOVENIA, 18 SEPTEMBER 2007

Jože Rakovec[1], Rahela Žabkar[1] and Mark Žagar[1,2]

[1]University of Ljubljana, Faculty of Mathematics and Physics, Chair of Meteorology, Ljubljana, Slovenia
E-mail: *joze.rakovec@fmf.uni-lj*
[2]Vestas Wind Systems A/S, Randers, Denmark; and part time with UL FMF

Abstract: The strong precipitation case of September 18th, 2007 in Slovenia is analyzed as regards the different forecast lead times. Relevat characteristics for strong precipitation are studied along the trajectories leading to the location of the event.

Keywords: *precipitation, convection, orographic enhancement, flash flood*

On the 18 September 2007 extreme prefrontal precipitation in Julian Alps, extending also to Kamnik Alps, caused severe floods in Slovenia. Heaviest rainfall occurred ahead of the cold front passing Slovenia in the evening of that day. The 24-hours precipitation accumulation, measured with rain gauges exceeded 300 mm (Figure 1). Radar measurements offered information that strong prefrontal convection was repeatedly forming at the upslope side of the orographic obstacles in the impinging SW flow (Figure 2): the main reasons for strong precipitation were constant inflow of moist and conditionally unstable air from southeast, wind shear in higher atmospheric layers, and the terrain complexity.

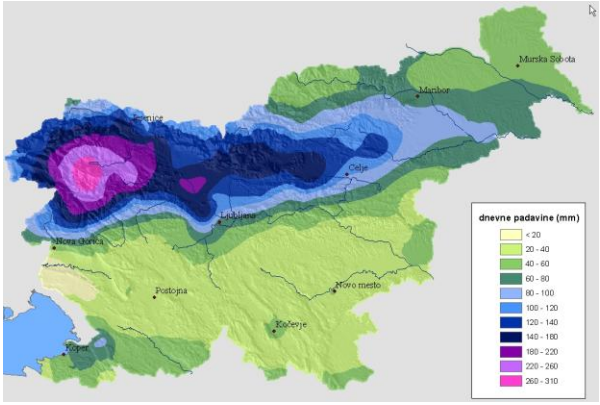

Figure 1 The 24-hour precipitation accumulation measured with rain gauges.

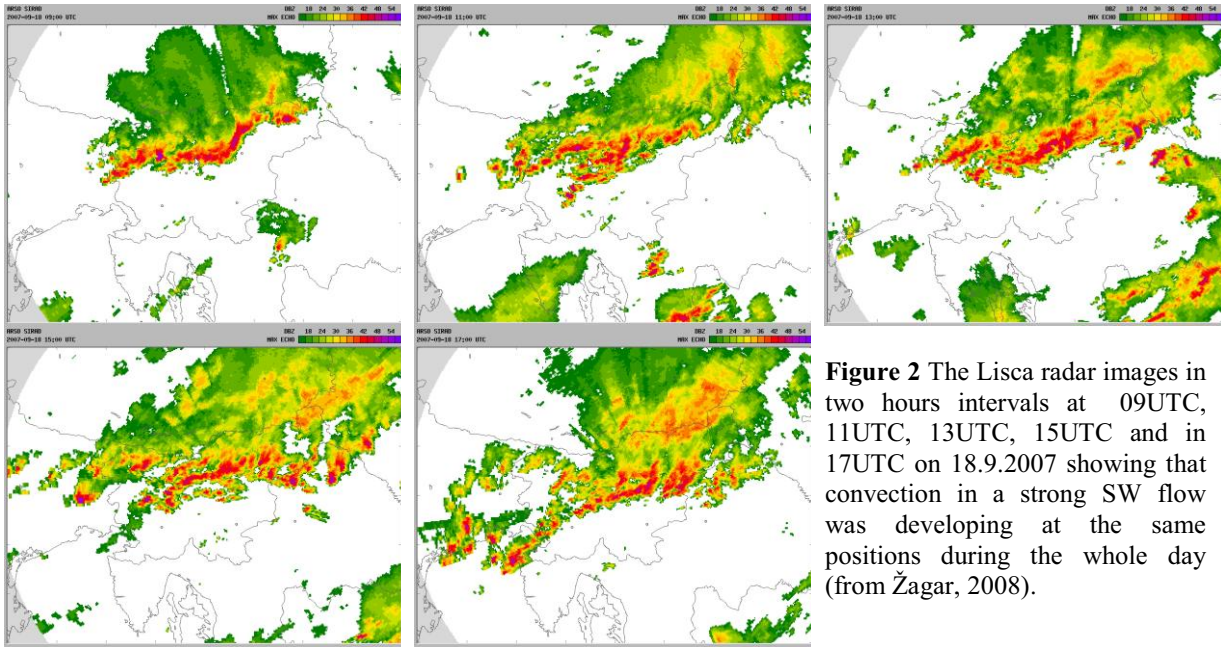

Figure 2 The Lisca radar images in two hours intervals at 09UTC, 11UTC, 13UTC, 15UTC and in 17UTC on 18.9.2007 showing that convection in a strong SW flow was developing at the same positions during the whole day (from Žagar, 2008).

The operational limited area hydrostatic model ALADIN at Environmental Agency of Republic of Slovenia with 9 km resolution forecasted the precipitation occurrence for September 18 well, but not its quantity and the intensity. The rate of precipitation underestimation varied from one model's run to another, reaching 200 mm for the 24 hours precipitation accumulation.

In the present study we evaluate and compare forecasts with different lead-time (+72, +60, …, +12 hours ahead) of operational ALADIN model for the September 18 (Figure 3). With comparison of 3D trajectories calculated for different forecast runs we focus on relation between the accuracy of precipitation forecast and representation of moist air advection in numerical prediction (Figure 3).

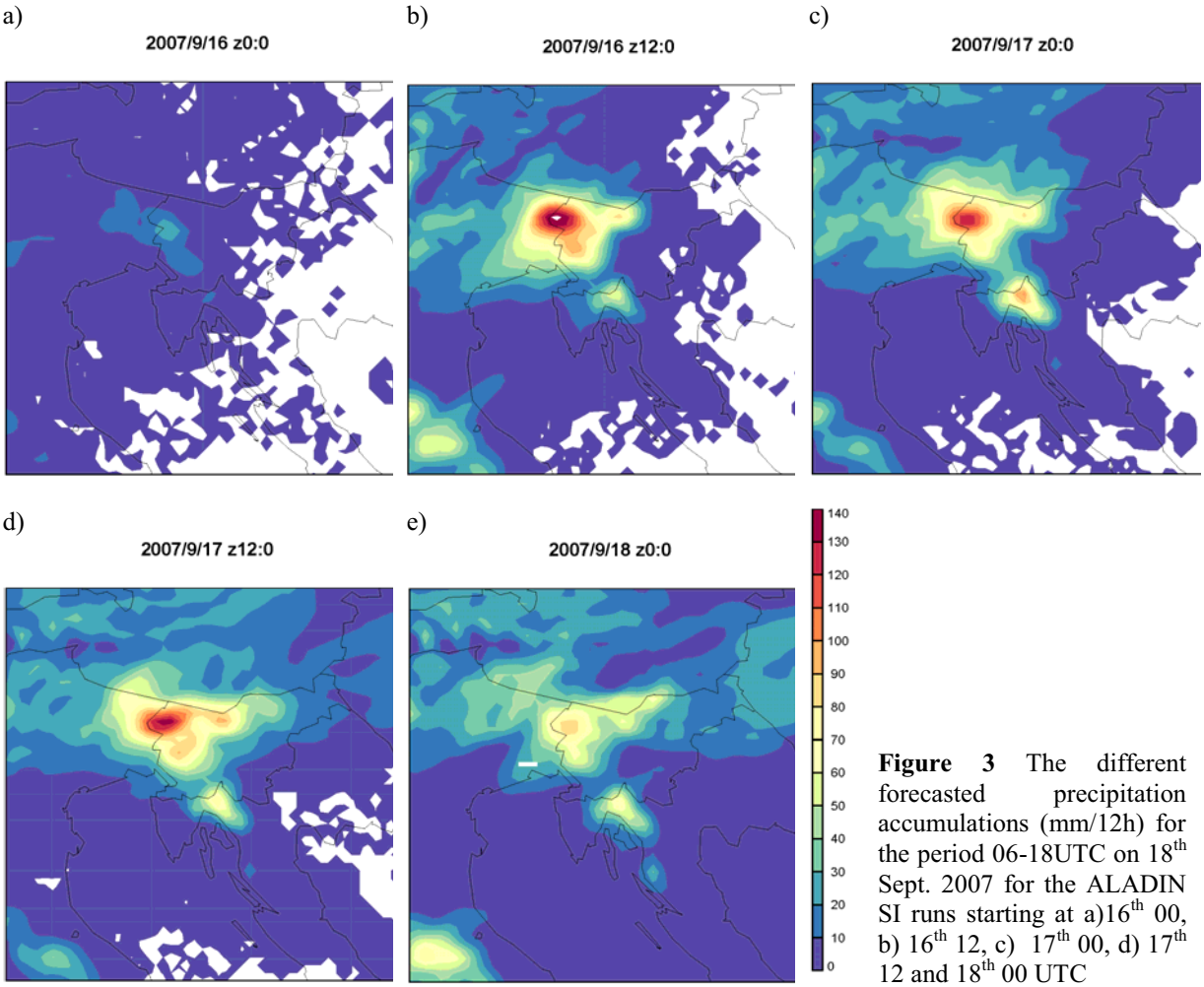

Figure 3 The different forecasted precipitation accumulations (mm/12h) for the period 06-18UTC on 18th Sept. 2007 for the ALADIN SI runs starting at a)16th 00, b) 16th 12, c) 17th 00, d) 17th 12 and 18th 00 UTC

The moisture divergence, equivalent potential temperature, CAPE etc. at different levels along these trajectories reveal the main differences between the forecasts, and so contribute to the explanation of different forecasts of precipitation amount by different forecast runs. These results (more details in poster) we evaluate in the light of the other possible sources of different lead-time forecast error and compare them with some other sources of uncertainties, e.g. representation of orography in the model (Kovač, 2008).

REFERENCES

M. Žagar, 2008: Analiza vzrokov in numerično modeliranje močnih padavin 18. septembra 2007 = Analysis of causes and numerical modelling of heavy precipitation on 18 September 2007. *Ujma (Ljublj.)*, **22**, 101-104.

V. Kovač: The influence of local orography on the precipitation forecast with ALADIN for 18. Sept. 2007, (Diploma work at UL FMF, supervisor: N. Žagar, in Slovenian), 58 pp.

THE IMPACT OF MULTI-SCALE SYSTEMS ON FREEZING RAIN AND SNOW STORMS OVER SOUTHERN CHINA

Jianhua SUN and Sixiong ZHAO
Institute of Atmospheric Physics, Chinese Academy of Sciences, Beijing，China
Email: sjh@mail.iap.ac.cn

Abstract: Synoptic weather patterns, quasi-stationary fronts, surface conditions, and stratification associated with severe freezing precipitation and snow storms during January-February 2008 are diagnosed in this paper. The impact of multi-scale systems on freezing rain and snow storms over southern China are obtained.

Keywords- *quasi-stationary front, freezing rain, stratification*

1 INTRODUCTION

Freezing precipitation, including freezing drizzle (FZDZ), freezing rain (FZRA), and ice pellets (IPE) (Carrière et al., 2000; Bernstein, 2000), is a major hazard that impacts many economic and social activities. During 11 January – 2 February 2008, record damage (since 1950) from snow and freezing precipitation occurred over southern China. Four periods of heavy snowfall and freezing precipitation occurred continuously over southern China: 0000 UTC 11 – 0000 UTC 17 January, 0000 UTC 18- 0000 UTC 22 January, 0000 UTC 25 – 0000 UTC 30 January and 0000 UTC 31 January – 0000 UTC 02 February. The persistent of snowfall and freezing precipitation affected transportation, electric power, communication, agriculture, and forestry seriously. In paper, we will try to get some answer for following questions. What kind of large-scale circulation is responsible for sustaining freezing precipitation? What are the impacts of the quasi-stationary front on the formation of freezing precipitation and the snow storm? What is favorable surface and stratification for the formation of freezing precipitation in southern China.

2 RESULTS

2.1 The synoptic weather pattern for the four periods

The long period anomaly of the atmospheric circulation is one of the important reasons for the freezing precipitation and snow storms. For example, the blocking high pressure (BHP) in the middle latitudes was located near west Siberia for more than 20 days, and also the west Pacific Subtropical High (WPSH) was to the north and west of its normal position. There was a transverse trough between the BHP and WPSH, which is very favorable to the southward invasion of cold air from North China. The BHP and trough in middle latitudes existed from the lower to upper troposphere, and could be found clearly even at 200hPa. The trough (disturbance) in the south branch (TSB) of the westerlies stayed for a long period and was very active. The southwest current ahead the TSB can transport very rich moisture to the Chinese continent. Cold/dry air from the north and warm/moist air from the south converged toward each other, and then the favored environment for snowfall and freezing rain could appear in different areas at different stages.

2.2 The quasi-stationary front

The east-west oriented quasi-stationary front (or shear line) located in southern China was the most important system producing freezing rain and the snow storms. This kind of quasi-stationary front has hardly been observed before during wintertime. The position of the stationary front is, to some extent, similar to that of the Meiyu front in summer. The denser isolines of pseudo-equivalent potential temperature and higher temperature of inversion were in the west part of front, thus, of the conditions of west front was more favorable for the formation of freezing precipitation. The strongest moisture convergence occurred ahead of the front at low levels and then climbed slantwise along the front to the middle troposphere.

2.3 The surface conditions and the stratification associated with freezing precipitation

The formation of freezing rain was very sensitive to some key influencing factors. The preferred ground surface temperature for freezing rain was from - 1 to - 3℃. The warm layer and inversion existed while freezing rain occurred, and at the same time, the formation of freezing rain was sensitive to both the thickness of the warm layer and the near surface frozen layer. The incomplete melting of snowflakes in the warm layer may be the mechanism of ice pellet formation. In addition, the warm rain and melting processes could be the mechanisms of freezing rain formation.

Finally, one kind of the conceptual model for multi-scale systems that sustain freezing precipitation has been proposed (Fig.1), including the synoptic conditions, details of the quasi-stationary front, and the sounding profiles associated with freezing rain and ice pellets.

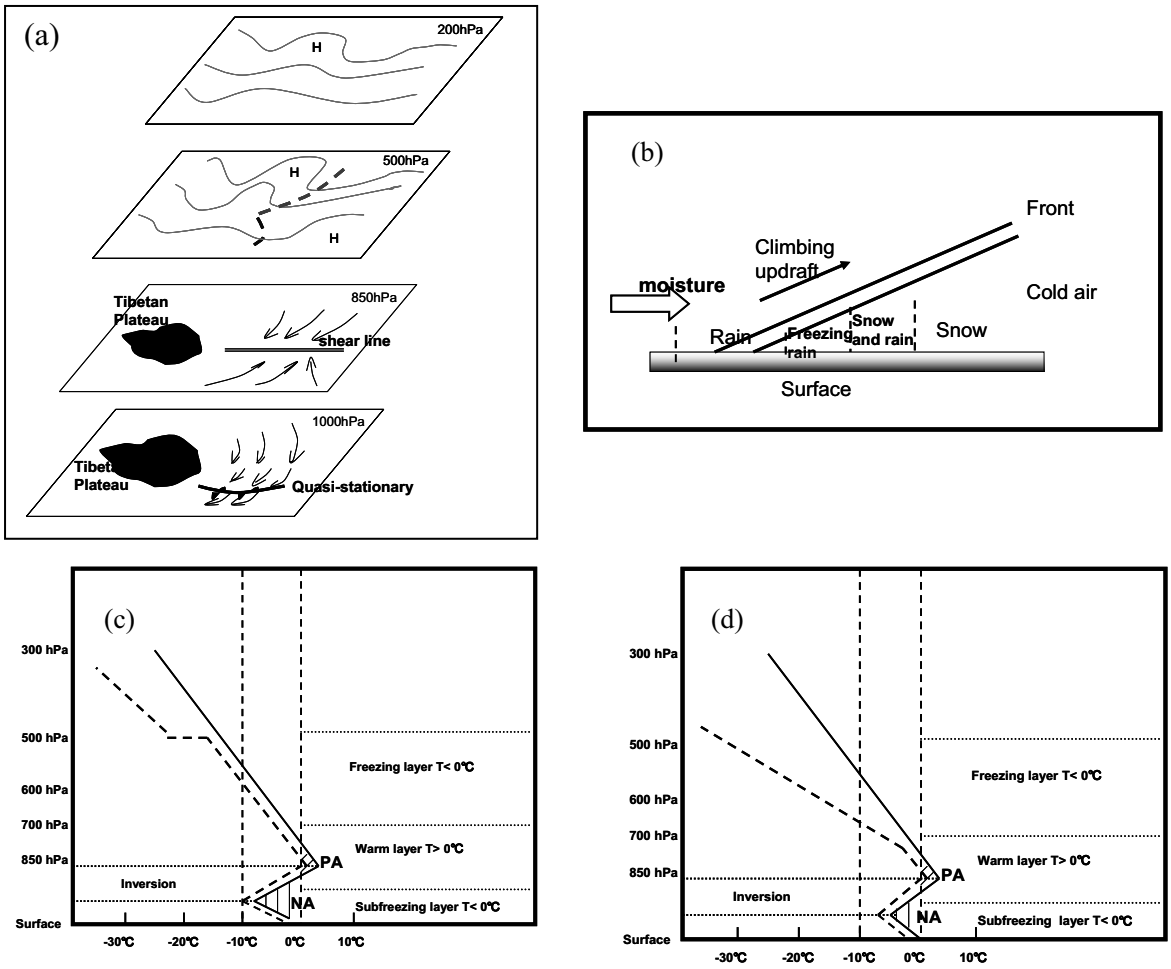

Fig.1 The multi-scale conceptual model for sustaining freezing precipitation in southern China: (a) The synoptic weather pattern, (b) the structure of quasi-stationary front, (c) the stratification condition for ice pellet and for (d) freezing rain

3 CONCLUSION

A long duration of freezing precipitation was caused by stationary and anomalous synoptic weather patterns, such as a blocking high pressure system and the trough in the south branch of westerlies, which induced the meeting of cold air from the north and warm, wet air from the south in southern China.The conditions of west part of front were very favorable for the formation of freezing precipitation. The moisture convergence occurred ahead of the front at low levels and then lifted slantwise along the front up to the middle levels. Favorable conditions at the ground surface for freezing precipitation occurred with temperature at about - 1 ~ - 3℃ and weak wind. The warm layer and inversion layer existed while freezing rain occurred.

Acknowledgements: *This research was supported by the National Natural Science Foundation of China under Grant No. 40875021 and 40605016, and foundation of Institute of Heavy Rain, China Meteorological Administration, Wuhan*.

REFERENCES

Bernstein, B. C., 2000: Regional and local Influences on freezing drizzle, freezing rain, and ice pellet events. *Wea. Forecasting*, **15,** 485–508.

Carrière, J. M., C. Lainard, C. Le Bot, and F. Robart, 2000: A climatological study of surface freezing precipitation in Europe. *Meteorol. Appl.*, **7,** 229–238.

MISREPRESENTATION OF THE SEEDER-FEEDER MECHANISM BY KESSLER-TYPE AUTOCONVERSION SCHEMES

Günther Zängl, Axel Seifert

Deutscher Wetterdienst, Offenbach, Germany
E-mail: *Guenther.Zaengl@dwd.de*

Abstract: Idealized simulations of moist flow over narrow isolated mountains have been conducted to investigate the ability of various autoconversion schemes to adequately represent the seeder-feeder effect, which in particular requires that no significant amounts of rainfall are generated in the absence of seeding. From the considered schemes, the Kessler scheme is found to have the largest deficits in this respect.

***K*eywords:** *Orographic precipitation, seeder-feeder mechanism, cloud microphysics*

1 INTRODUCTION

The seeder-feeder mechanism, i.e. local intensification of larger-scale (frontal) precipitation within orographic clouds, is known to be one of the most important mechanisms of orographic precipitation. The relevance of the ambient precipitation lies in the different microphysical time scales for autoconversion and accretion. Autoconversion, i.e. initiation of rain due to the coalescence/collision of cloud drops, has a typical time scale of 15–30 min depending on the cloud water density and the number concentration of cloud droplets. In comparison, precipitation growth due to accretion of cloud water by rain or frozen precipitation particles is a much faster process. This implies that for given ambient conditions, narrow mountain ridges may not receive significant precipitation amounts in the absence of ambient precipitation, but experience a marked local rainfall intensification when seeding is present. To obtain realistic simulated precipitation amounts at very high resolution ($\Delta x \lesssim 1$ km), it is thus important to reasonably discriminate between the microphysical timescales of autoconversion and accretion. Here, we focus on idealized simulations of moist flow over isolated mountains, investigating the precipitation amounts occurring in the absence of seeding. Ideally, these should exhibit a marked dependence on the mountain width, getting very small when the advective timescale for the flow over the mountain is smaller than the microphysical conversion time.

2 MODEL SETUP

The simulations presented here have been conducted with the Penn State/NCAR mesoscale model MM5, using (depending on the mountain width) three or four interactively nested model domains with a finest horizontal mesh size of 2250 m and 750 m, respectively. The model topography consists of four isolated mountains with a height of 400 m, 800 m, 1200 m and 1600 m, respectively, and a base-to-base width of about 36 km (12 km) in the wide-mountain (narrow-mountain) case. The atmospheric conditions assumed in the simulations involve a weakly moist stable ridge-normal flow with positive shear from 12.5 m s^{-1} at sea level to 25 m s^{-1} at tropopause level, and constant wind speed higher above, and a nearly saturated moisture field up to a pressure of 400 hPa. Two weakly moist stable temperature profiles are considered with freezing levels at 2300 m (denoted as T1) and 1500 m (T2), respectively. Thus, the ice phase does not play a significant role in precipitation initiation. Taking into account some upstream deceleration, the time required for the flow to cross the windward slope of the mountain is about 30 min (10 min) in the wide-mountain (narrow-mountain) case, so that only small amounts of precipitation should be generated in the latter one. The simulations use a PBL parameterization to account for surface friction and a mixed-phase microphysics scheme including graupel (Thompson et al., 2004). By default, this scheme uses the Berry and Reinhardt (1974) parameterization for autoconversion, which is based on the stochastic collection equation. Sensitivity tests consider the simple Kessler-type parameterization implemented in older versions of this scheme and the more recent Seifert and Beheng (2001) parameterization, in which both autoconversion and accretion are derived from the stochastic collection equation. In the simulation acronyms used in the following, we will use BR, KES and SB to refer to these parameterizations.

3 RESULTS

The results of our simulations are presented in Fig. 1. Apart from a general precipitation increase with mountain height, all cases considered here exhibit higher precipitation maxima for the wide mountains than for the narrow mountains. The latter is opposite to the respective dependence of the condensation rate, which is proportional to the slope (and thus inversely proportional to the mountain width) at least at low levels where gravity-wave

effects are weak. This implies that for all microphysical schemes considered here, the dependence of the simulated precipitation amounts on the mountain width has the expected sign.

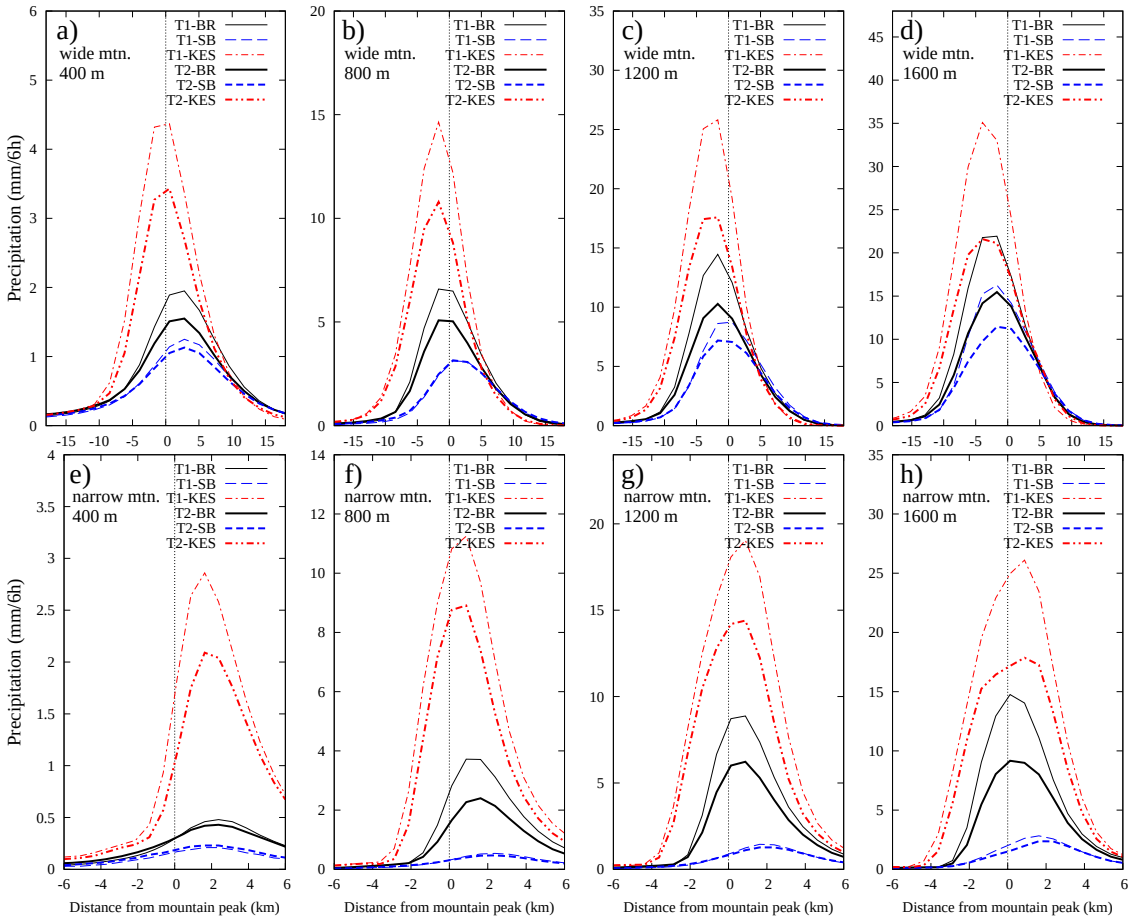

Figure 1: 6h-accumulated precipitation for wide (top) and narrow (bottom) mountains with a height of (a,e) 400 m, (b,f) 800 m, (c,g) 1200 m and (d,h) 1600 m. See text for explanation of simulation acronyms.

Nevertheless, there are tremendous differences between the autoconversion schemes, which in turn depend on the mountain width and height. While the KES scheme always produces the highest rainfall amounts, the more physically based BR and SB schemes are reasonably close together for the wide mountains. In that case, the relative difference between the two latter schemes does not show a clear dependence on mountain height. However, the additional precipitation produced by the KES scheme is, in relative amounts, largest for the lowest mountain (Fig. 1a). For the narrow mountains, the discrepancies between the autoconversion schemes become even more pronounced. The rainfall amounts obtained with the KES scheme now exceed those produced by the SB scheme by roughly one order of magnitude. The differences between BR and SB are now also much larger than for the wide mountains, with a clear tendency to increase with increasing mountain height.

4 CONCLUSIONS

As a conclusion, we note that the KES scheme does not appear to be suitable for simulating the seeder-feeder effect, because it still produces unrealistically large amounts of rain in the absence of seeding and thus does not allow for a proper discrimination between the seeding and no-seeding regimes.

REFERENCES

Berry, E. X., and R. L. Reinhardt, 1974: An analysis of cloud drop growth by collection: Part IV. A new parameterization. *J. Atmos. Sci*, **31,** 2127–2135.

Thompson, G., R. M. Rasmussen, and K. Manning, 2004: Explicit forecasts of winter precipitation using an improved bulk microphysics scheme. Part I: Description and sensitivity analysis. *Mon. Wea. Rev.*, **132,** 519–542.

Seifert, A., and K. D. Beheng, 2001: A double-moment parameterization for simulating autoconversion, accretion and selfcollection. *Atmos. Res*, **59-60**, 265–281.

WATER VAPOR FIELDS RETRIEVE WITH TOMOGRAPHY SOFTWARE

Mathieu Reverdy[1], J. Van Baelen[1], A. Walpersdorf[2], G. Dick[3], M. Hagen[4], E. Richard[5]

[1] Laboratoire de Météorologie Physique, Aubière, France
E-mail: *m.reverdy@opgc.univ-bpclermont.fr*
[2] Laboratoire de Géophysique Interne et Tectonophysique, Grenoble, France
[3] GeoForschungsZentrum-GFZ, Potsdam, Germany
[4] DLR Oberpfaffenhofen, Wessling, Germany
[5] Laboratoire d'Aérologie, Toulouse, France

Abstract**:** As part of the COPS campaign, a GPS project as collected data during the summer period of 2007 to study water vapor in Rhine valley. An initial GPS network has been deployed with 50 GPS stations (including a dense area of 16 GPS stations) to study water vapor density through a GPS tomography software. In addition, rain data were provided by two different radar.

Keywords: *ICAM, Water vapor, tomography, GPS, inverse problem*

1 INTRODUCTION

Water vapor is a very important parameter in atmospheric sciences. However, due to the spatial and temporal variability of water vapor, it is a parameter which is difficult to estimate with classical methods. Since few decades, this quantity can be estimated using remote sensing technologies as for example radio sounding, spectrometers, lidars, radiometers, and so on. Since the early 90's, researchers have focused on the study of the water vapor using the Global Positioning System. Indeed, the GPS offers an autonomous, all-weather and continuous system for the restitution of the water vapor. With such a technology we can retrieve the IWV (Integrated Water Vapor) over an area. This quantity has been validated by means of comparisons with other measurements and is now tested for assimilation in numerical weather prediction models. In addition, when a dense network of GPS stations exists, we can use the GPS to perform tomography in order to retrieve the 3 dimensional distribution of water vapor density. Tomography is a powerful mathematical tool of inversion which is used to retrieve information based on distant data.

As part of the COPS (Convective and Orographically-induced Precipitation Study), a project dedicated to the study of precipitation occurrences and the formation of convective systems in Rhine valley, a GPS project as collected data during the summer period of 2007. An initial GPS network has been deployed with 50 GPS stations (including a dense area of 16 GPS stations) to study water vapor.

To do so, collected GPS data has been used in tomography software to retrieve the 3 dimensional repartition of the density of water vapor over the studied area. Tomography allow us to study water vapor with very good precision (order of g/m^3) regarding to spatial and temporal variability of water vapor.

In addition, rain data were provided by two different radar. Poldirad radar working in C band and a X-band radar. The resulting data display the rain reflectivity over the same area that a part of the GPS network for comparison and further correlation.

2 SOFTWARE METHOD

The tomography algorithm is based on SIWV inputs: the IWV along the receiver to satellite baselines. The principle of the tomography is as follow: the volume above the GPS network is divided into voxels. The height of the voxels is function of the altitude in order to provide a better resolution in the low layers of the atmosphere where the water vapor is concentrated. Then, an algorithm looks at the repartition of each SIWV through the voxels. Using this repartition, *a priori* solution as initialization and weighted matrix, the mathematical inversion is done to retrieve the 3 dimensional distribution of water vapour as shown in equation 1.

$$m = m_0 + W_m^{-1} \times G^t \times \left(G \times W_m^{-1} \times G^t + \alpha^2 \times W_e^{-1}\right)^{-1} \times \left(d - G \times m_0\right) \quad (1)$$

Where m are the density of water vapor in g/m^3; m_0 are the *a priori* solution, G is the matrix of the SIWV repartition, d are our data (in our case the SIWV) and W_x and *alpha* are the weighted matrix. Another method based on direct STD (Slant Total Delay) as been tested on COPS campaign.

3 RESULTS

Among all the GPS and radar data, we will focus on an event which took place in August the 12th and 13th. A convective system passed over the GPS network (Figure 1 left), allowing us to study the role of the water vapor in the formation and maintain of convective cells (Figure 1 right).

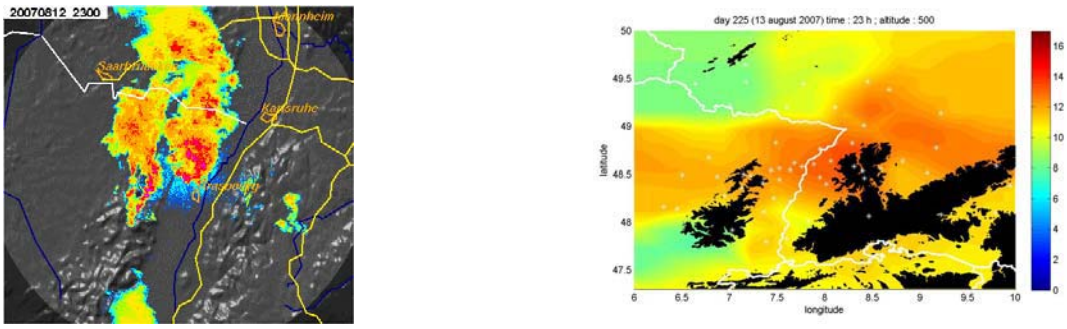

Figure 1. Left: radar precipitation from POLDIRAD during COPS-2007; right: tomography result of the water vapour density (g/.m^3). Horizontal cut at 500m.

This case is of great interest since the area is part of the Vosges and black-forest region allowing us to study water vapor structures with strong orographic effects through vertical cut (Figure 2).

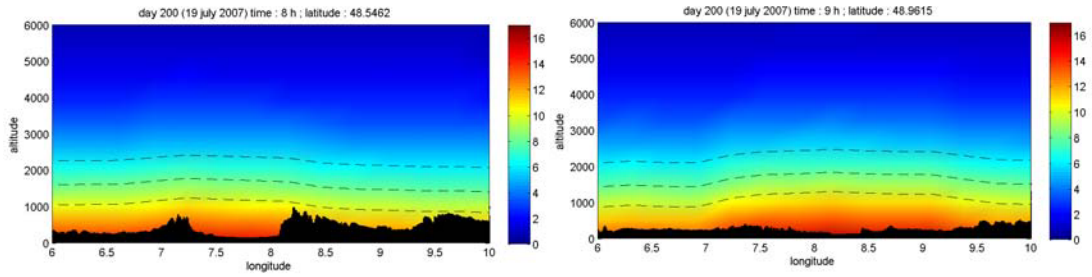

Figure 2. Water vapour density in g/m^3. East-West and North-South over the GPS network. Dashed lines correspond to isolines 10, 8 and 6 g/m^3.

In addition, we will also present preliminary results for some different cases which took place in June and July 2007. Those periods are really different from the first one regarding to the reflectivity map and the water vapor distribution.

4 CONCLUSIONS AND OUTLOOKS

The next step of this work will be to do inter-comparison with GFZ-Potsdam tomography results using different inversion methods. Likewise, comparison with model outputs as well as lidar measurements, balloon sounding, etc, will also be done to study the accuracy of the GPS tomography. In addition, water vapor density retrieval will be performed over a smaller area where the dense GPS network is available. The algorithm will use SIWV passing entirely through the voxel as well as the SIWV coming from GPS stations outside the voxels area.

REFERENCES

Flores A., Ruffini G., Rius A., (2000), 4D tropospheric tomography using GPS slant wet delays, *Annales Geophysicae, 18,* 223–234.

Reverdy M., Van Baelen J., (2007), Estimation des paramètres atmosphériques à partir des signaux GPS, CNES contract n°04/CNES/1928-5.

Van Baelen, J., J-P Aubagnac, A. Dabas (2005), Comparison of near real-time estimates of integrated water vapor derived with GPS, radiosondes, and microwave radiometer, *J. of Atmosph. Ocean Techn., 22*, 201-210.

Walpersdorf A., Bock O., Doerflinger E., Masson F., Van Baelen J., Somieski A., Bürki B., (2004), Data analysis of a dense GPS network operated during the ESCOMPTE campaign: first result, *Physics and Chemistry of the Earth, 29, 201-211.*

SIMULTANEOUS X-BAND AND K-BAND STUDY OF PRECIPITATION TO DERIVE SPECIFIC Z-R RELATIONSHIPS

F. Tridon, J. Van Baelen, Y. Pointin

Laboratoire de Météorologie Physique, UMR CNRS/UBP 6016,
24, avenue des Landais, 63177 Aubière cedex, France
E-mail: *F.Tridon@opgc.univ-bpclermont.fr*

Abstract : Using a simple scanning X-band radar and a vertically looking K-band radar, we show the need in using several specific Z-R relationships to improve the rain estimates by taking into account the high variability of rain regimes within the precipitations systems. To determine these specific Z-R relationships, we propose some simple classification schemes based on the trend of the reflectivity intensity.

***K*eywords :** *ICAM, radar, Z-R relationship, drop size distribution, precipitation estimation*

1 INTRODUCTION

During more than 50 years of development, ground-based weather radar became a tool fitted to quantitative rainfall measurements. The major source of errors lie in the conversion of the radar reflectivity factor Z ($mm^6\ m^{-3}$) to rain rate R ($mm\ h^{-1}$). These two parameters are related to each other via the raindrop size distribution (DSD) which cannot be inferred by conventional weather radar measurements. Hence, it has been common practice to take a simple power law relationship between Z and R, like the well known Marshall-Palmer relationship. DSD is extremely variable in time and space even within a single precipitating event. Thus, many of these relationships have been proposed, nevertheless, in most of the cases, a unique relationship is used for one precipitating event.

The aim of this work is to categorize the different rain regimes that might occur even within individual precipitation cells to derive the corresponding specific relationships. Then we will confront the rain estimates with these specific relationships to the classical approach using one single relationship in order to investigate their potential for improve rain estimation. To do so, we analyse the simultaneous measurements of a scanning X-band radar and a vertically pointing K-band radar in their common volume.

In section 2, we will describe the radars and data. In section 3, we will present the methods and their performances. Finally, we will outline some conclusions and perspective for future developments.

2 EXPERIMENTAL SET-UP

During the summer of 2007, for the international COPS (Convective and Orographically induced Precipitations Study)(Wulfmeyer et al., 2008) campaign, the X-band radar was installed on a small hill at the foot of the Vosges mountains in order to overlook a largely instrumented site where we had installed the K-band radar.

The K-band (24.15 GHz) radar is a Micro Rain Radar (MRR) : it is a FMCW system which provides Doppler spectra with 64 lines over a range of 0.8–12.2 m/s in 30 range gates of 100 m with a typical time resolution of 10 s. Under the assumption of zero vertical wind, profiles of DSD are derived using the relation between the drop diameter and the terminal fall velocity. These profiles of DSD allow to correct for the rain attenuation, and to derive reflectivity factor and rainrate. Further details are described in Peters et al. (2005).

The X-band (9.41 GHz) radar is scanning at a fixed elevation of 5° with a time resolution of 30 s, a range resolution of 60 m up to a maximum range of 20 km, and an azimuth resolution of 2° with a beam width of 2.4°. Furthermore, attenuation correction was also taken into account by applying the classical Hitschfeld and Bordan (1954) method to the X-band radar reflectivity measurements. Finally, we performed a statistical cross calibration between the X-band and MRR reflectivity wich allow a relative comparison of rain rate between the two systems.

An example of the resulting reflectivity measured by the two systems during the night of August 07 2007, is presented in figure 1 (right). The reflectivities correspond very well and show very similar features. However, one can notice slight differences which could be attributed to the differences between the sampling strategies and the two volumes sounded by the radars. Indeed, the geometrical dimensions of the radar beams are noticeably different with a volume ratio close to 100 (see figure 1 (left)). Thus, the X-band radar volume can include parts of the precipitating system not seen by the MRR.

3 RAIN REGIMES CLASSIFICATION AND PRECIPITATION ESTIMATION

The figure 1 (right) gives us confidence in using observations from common volume in order to investigate the Z-R relationships to be applied to the X-band reflectivity field. In a first step, we will focus on this common

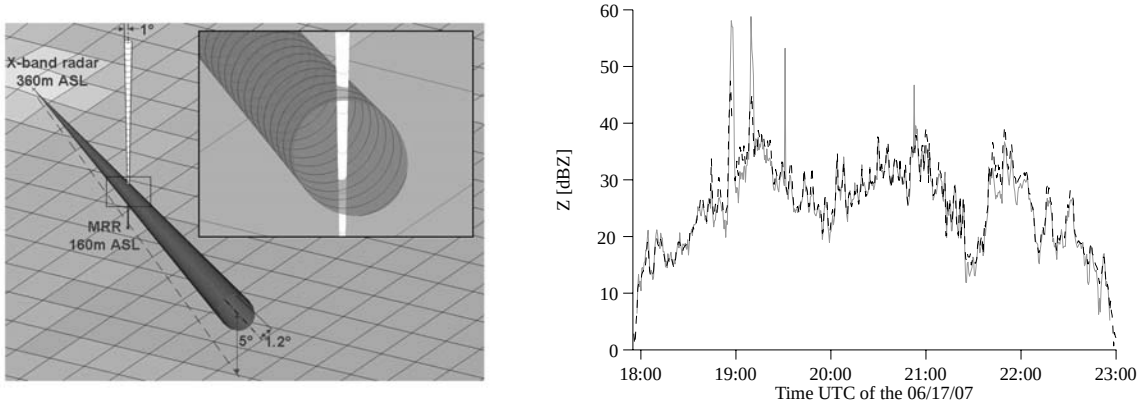

FIG. 1: Left : Representation of the X-band radar and MRR common volume. Right : Time series of the reflectivities of the MRR (dash line) and the X-band radar (solid line) for the precipitating event of June 17, 2007.

volume only. Our objective is to find simple techniques to categorize rain regimes from the X-band reflectivity. We propose different schemes based on the trend of this reflectivity intensity (increasing, decreasing, stagnating) or on its intensity itself. The MRR measured reflectivity and estimated rain-rate are used to derive the corresponding Z-R relationship which is then applied to the X-band radar reflectivity measurements in order to calculate a corresponding rain-rate which, in turn, is compared to the MRR derived value. This procedure is biased towards the MRR estimation which we will use as a reference, but the goal at this point of the project is to evaluate candidate rain regime selection scheme to later improve rainfall estimates.

The table 1 presents the results of the two methods in terms of total accumulated rainfall for the entire COPS campaign data set. It shows that the classification based on intensity degrades precipitation estimation whereas the increasing-stagnating-decreasing classification slightly improves it. Thus, this results give us confidence in using this last method in order to determine the specific Z-R relationships.

MRR	single Z-R relationship	Increasing, stagnating and decreasing intensity classification	Rain intensity classification
73.51	68.23 (-7.18%)	68.67 (-6.58%)	65.04 (-11.52%)

TAB. 1: Total rainfall (in mm) estimated by the different methods, and difference (%) from the MRR reference.

4 CONCLUSIONS AND PERSPECTIVES

We have shown the need in using specific Z-R relationships to account for the high variability of rain regimes within the precipitations systems. To determine these specific Z-R relationships, the classification scheme based on the trend of the reflectivity intensity (increasing, stagnating, decreasing) shows great promises for improvement of the rain estimation.

We are still working on the improvement of this classification scheme in order to extend and validate this study by rainfall comparisons with a network of raingages over the domain covered by the X-band radar.

Acknowledgements:
Participation to the COPS campaign was made possible with the support of the French ANR research grant BLAN06-3_136575 and INSU LEFE funding.

REFERENCES

Hitschfeld W. and J. Bordan, 1954: Errors inherent in the radar measurement of rainfall at attenuating wavelengths. *J. of the Atmos. Sci.*, **11**, 58–67.

Peters, G., B. Fischer, H. Münster, M. Clemens, A. Wagner, 2005: Profiles of Raindrop Size Distributions as Retrieved by Micro Rain Radars. *J. Appl. Meteorol.*, **44**, 1930-1949.

Wulfmeyer, V. and co-Authors, 2008: The Convective and Orographically-induced Precipitation Study: A Research and Development Project of the World Weather Research Program for improving quantitative precipitation forecasting in low-mountain regions. *Bull. Amer. Meteor. Soc.* **89**(10), 1477–1486, DOI:10.1175/2008BAMS2367.1.

Environmental conditions and radar observations of organized thunderstorms

Helge Tuschy[1, 2, 3], Martin Hagen[1], Georg J. Mayr[2]

[1] Deutsches Zentrum für Luft-und Raumfahrt (DLR) Oberpfaffenhofen, Germany
[2] University of Innsbruck, Innsbruck, Austria
[3] European Severe Storms Laboratory, ESSL
E-mail: *Helge.Tuschy@dlr.de*

Abstract: Different cases of organized thunderstorms are reviewed: a bow echo, a mesoscale convective system, a supercell and a hailstorm. The high resolution COnsortium for Small-Scale MOdelling (COSMO) model of the German weather service (DWD) is utilized to calculate the parameters for severe weather. In addition, the polarization diversity doppler weather radar (POLDIRAD) at DLR, Oberpfaffenhofen is used to detect the storms and to gain more detailed information about their structure. Finally several significant severe weather outbreaks in central Europe are included into this study (03 August 2008 eastern France, 25 June 2008 Czech Republic and 15 August 2008 southwest Poland).

***K*eywords:** *deep moist convection, wind shear, tornado, radar, COSMO*

1 INTRODUCTION

Despite the rapid enhancement of models' resolution and the increase in the calculating capacity, forecasting the initiation or the future tracks of thunderstorms remains difficult. Several organized thunderstorms, like bow echoes, mesoscale convective systems, supercells and hail storms are studied and the efficiency of the model is assessed by means of the calculation of forecasting parameters for severe thunderstorms (e.g. convective available potential energy (CAPE), directional and speed shear, convective inhibition (CIN) ...). Additionally, parameters like the significant tornado parameter (STP), the energy helicity index, or the SWEAT index are calculated to compare those results with studies from Switzerland (e.g. Huntrieser,1996 or Houze Jr.,1993) and North America (e.g.Craven,2002, Edwards et al.(2000, 2004)). To get a better insight in the structure of thunderstorms, the POLDIRAD was used, where not only rotation but also precipitation distribution and different type of precipitation can be analyzed.

2 SETUP

POLDIRAD operates at C-band (5.5027 GHz, 5.45cm). Research measurements are performed either in operational mode (radar range:120km) or in surveillance mode (radar range:300km). A subjective study of special features like hail spikes or hook echoes is carried out for the extensive archive of the POLDIRAD. 9 cases were selected for the final study, six occurred over southern Germany and 3 of them over NE-France, the Czech Republic and SW-Poland, respectively.
Data assimilations from the high resolution model of the national German weather service (DWD), the COSMO-DE, are used for those case studies. It is a high resolution version of the non-hydrostatic weather forecasting model of the COSMO community. The model domain contains 421x461 grid points, spaced 2.8km apart with 50 vertical levels. Severe thunderstorm forecast parameters are computed from model level data to achieve a better vertical resolution. The intent is to describe the imminent environment where thunderstorms evolve with the most effective/latest weather model and to see how the model assimilation performs different situations. There is also the chance to get a unique insight into those thunderstorms, which moved nearby the polarimetric radar station where hail cores or concentrated swaths of damaging wind became visible. The parameters are compared with studies of North America or Switzerland.

3 FIRST RESULTS

On the 15 August 2008, COSMO-DE performed well in highlighting the area of interest over southwest Poland (Fig.1, 2), where a regional tornado outbreak occured. In comparison to GFS (calculated at the European Storm Forecast Experiment (ESTOFEX, http://www.estofex.org/), COSMO-DE had strong hints in the parameter fields (e.g. the significant tornado parameter was above 3 just around the region, where tornadoes evolved).
The investigation of the radar already procured numerous interesting features like intense hail spikes, persistent bounded weak echo regions or hook echoes. The evolution of long lived outflow boundaries can be examined, which are a focus for thunderstorm initiation later-on and serve as an area, where wind shear increases significantly and hence enhances the potential for severe thunderstorm events.

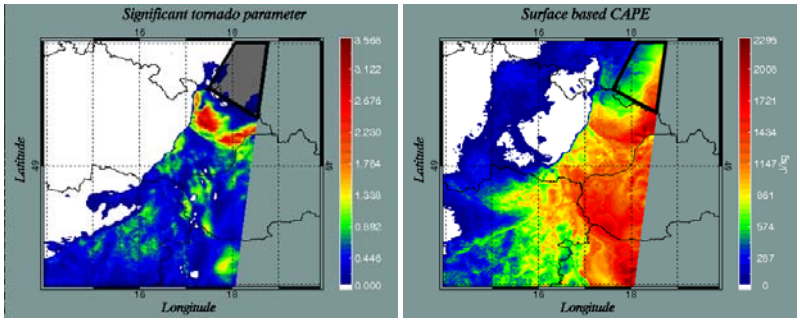

Figure 1: 15 August 2008, both at 15UTC: The significant tornado parameter (Edwards et al.2004) (left) and surface based convective available potential energy (J/kg) (right). Tornadoes evolved in the highlighted area between 15Z-19UTC. (coloured: http://www.pa.op.dlr.de/icam2009/extabs/)

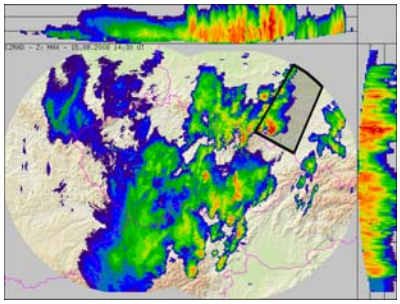

Figure 2: 15 August 2008, at 14.30UTC: The maximum radar reflectivity composed from radars Brdy and Skalky (source: CHMI). Tornadoes evolved in the highlighted area between 15Z-19UTC. (coloured: http://www.pa.op.dlr.de/icam2009/extabs/)

4 FUTURE WORK

The remaining cases are investigated in more detail and the parameters are compared to results from studies in Switzerland and North America in order to find out similarities or geographical differences. Of special interest are the F4 tornado at Hautmont in northeast France on 3 August 2008 and the significant derecho over the Czech Republic on 23 June 2008.

Acknowledgements:
The authors want to thank Meteo France, the Institut Royal Météorologique (KMI), the Institute of Meteorology and Water Management (IMGW), the Czech Hydrometeorological Institute (the Radar Department and the Satellite Department, CHMI), the European Organisation for the Exploitation of Meteorological Satellites (EUMETSAT) and the German weather service (DWD) for the provision of data.

REFERENCES

Craven, J.P. et al., (2002): *Baseline climatology of sounding derived parameters associated with deep, moist convection. Preprints, 21st Conf. Severe Local Storms, San Antonio*

Edwards, R. et al., (2000): *RUC-2 Supercell proximity soundings, Part II: An independent assessment of supercell forecast parameters. Preprints, 20th Conf. Severe Local Storms, Orlando FL*

Edwards, R. et al., (2004): An update to the supercell composite and significant tornado parameters. Preprints, 22nd Conf. Severe Local Storms, Hyannis MA

Huntrieser, H. et al., (1996): *Comparison of traditional and newly developed thunderstorm indices for Switzerland. Weather and forecasting, volume **12**, 108–125*

Houze, R.A. et al., (1993): Hailstorms in Switzerland: Left movers, right movers and false hooks. Monthly weather review, volume **121**, 3345–3370

MODIFICATION OF ATMOSPHERIC PARAMETERS BY DEEP CONVECTION OVER COMPLEX TERRAIN DURING COPS

Holger Mahlke, Ulrich Corsmeier, Christoph Kottmeier

Institut für Meteorologie und Klimaforschung (IMK), Karlsruhe Institute of Technology (KIT), Germany
E-mail: *holger.mahlke@imk.fzk.de*

Abstract: The goal of the study is to investigate the interactions between deep convection events over complex terrain (e.g. cumulonimbus development) and their atmospheric environment based on observational data obtained during the COPS field campaign in summer 2007.

Keywords: *ICAM, COPS, deep convection, low mountain area*

1 INTRODUCTION

Not all aspects of how deep convection interacts with its atmospheric environment are understood in detail, especially over complex terrain. Deep convection is a complex four dimensional process, governed by scale dependent interactions of numerous factors such as the vertical distribution of the meteorological parameters, the cold outflow causing gust fronts, the shading by the storm's anvil cloud, and the cooling of evaporating hydrometeors. Another important factor is the orographic structure of the underlying terrain, since often secondary flows develop over mountainous regions during the day which can trigger deep convection (Barthlott et al., 2005). These processes need to be understood in detail for improved forecasts of convective events that can strongly affect societal living (risk of wind storms, flash flood events, hail damages etc). A suitable way is to perform case studies based on measurements and simulations.

2 DATA AND METHOD

The Convective and Orographically Induced Precipitation Study (COPS) field campaign (Wulfmeyer et al., 2008) in summer 2007 in the Black Forest, the Rhine valley, and the Vosges mountains, provided the opportunity to investigate the above interactions due to temporally and spatially dense data obtained from various measurement platforms (remote sensing systems, ground stations, radiosondes, research aircraft etc.) and by performing of numerical simulations. Multiple data sets were obtained of days with deep convection present.

One of the measurement systems used was a mobile radiosonde system developed at IMK (Kottmeier et al., 2001). During COPS, 78 of these balloon-borne sondes were launched simultaneously by up to 4 mobile teams that were sent to different sites in the northern Black Forest, where convection was expected. The aim was to get "snapshots" of the convective development by measuring prior to, during and after convective cells passed the aerological stations.

Based on data derived from these soundings and measurements made by other instruments case studies are composed on COPS days where deep convection occurred and interacts with its environment. The results are compared to respective numerical simulations using the COSMO-DE model (resolution: 2.8 km).

3 EXAMPLE

On 20 July 2007, some thunderstorms and showers developed around noon across the northern Black Forest in front of a shortwave trough which triggered a mesoscale convective system (MCS) over eastern France (Fig. 1). The showers were mainly a result of the gust front of the MCS. The model forecast by COSMO-DE did not capture the development adequately, since no precipitation was simulated before 16:30 UTC.

Comparisons between the model output and radiosonde profiles from Hornisgrinde Mountain, close to where the initiation of a first convective cell took place, showed that: 1. The passage of the gust front was correctly forecast by the model, but the model was prior to the passage of the front and even more after the passage distinctly too warm (~10 K, Fig. 2). 2. A significant increase in specific humidity (~3 g kg^{-1} at 8 UTC) in the boundary layer a few hours before the initiation of convection was underestimated by the model (Fig. 3). Probably this was the reason why the model did not simulate the initiation of deep convection.

High values of boundary layer humidity were also observed at the mobile radiosonde site Dornstetten (Fig. 4) about 15 minutes before two convective cells passed the site. Thirty minutes later, during the second cell's passage, another radiosonde showed within the convective cell and in its vicinity lower values of temperature below 2 km, higher air temperature in the upper two thirds of the troposphere, and an increase of humidity in heights above the boundary layer depth. The boundary layer cooling was also observed in profiles from radiosondes released some time after a cell passage. Afterwards there was only little further convective activity

in the northern Black Forest until the evening due to the reduced amount of convective available potential energy (CAPE; e.g. 17 J kg^{-1} at Hornisgrinde Mountain at 14:05 UTC, ~0 J kg^{-1} in Dornstetten 16:14 UTC).

4 CONCLUSIONS AND OUTLOOK

A measurement strategy using mobile radiosondes teams proved to be a good approach to investigate deep convection processes if they are embedded in the framework measurements of a field campaign. Subject of future work will also be to analyse whether the temporal and spatial variability of the parameters going along with the convective development is well represented in the COSMO-DE model.

REFERENCES

Barthlott, Ch., U. Corsmeier, C. Meißner, F. Braun and Ch. Kottmeier, 2005: The influence of mesoscale circulation systems on triggering convective cells over complex terrain, *Atmos. Res.* **81**, 150-175.

Kottmeier, C., Reetz, T., Ruppert, P., and N. Kalthoff, 2001: A New Aerological Sonde for Dense Meteorological Soundings, *J. Atmos. Oceanic Technol.*, **18**, 1495-1502.

Wulfmeyer, V., A. Behrendt, and H.-S. Bauer, Ch. Kottmeier, U. Corsmeier, A. Blyth, G. Craig, U. Schumann, M. Hagen, S. Crewell, P. Di Girolamo, C. Flamant, M. Miller, A. Montani, S. Mobbs, E. Richard, M.W. Rotach, M. Arpagaus, H. Russchenberg, P. Schlüssel, M. König,, V. Gärtner, R. Steinacker, M. Dorninger, D.D. Turner, T. Weckwerth, A. Hense, and C. Simmer, 2008: The Convective and Orographically-induced Precipitation Study: A Research and Development Project of the World Weather Research Program for improving quantitative precipitation forecasting in low-mountain regions. *Bull. Amer. Meteor. Soc.* **89**, 1477-1486.

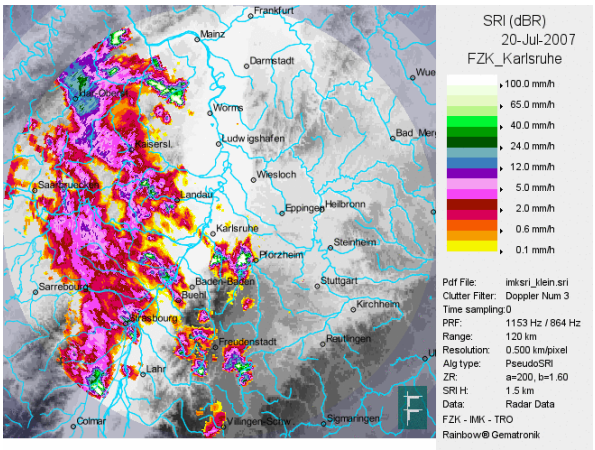

Figure 1. Convective precipitation rate derived from IMK-C-band rain radar on 20 July 2007, 10:30 UTC. Courtesy of Jan Handwerker.

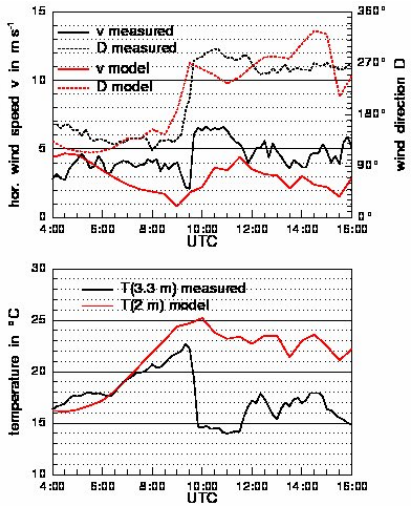

Figure 2. Wind speed (D) and direction (v, above) and temperature (below) measured by ground station at Hornisgrinde and forecast by COSMO-DE model, on 20 July 2007. Courtesy of Christian Barthlott and Norbert Kalthoff.

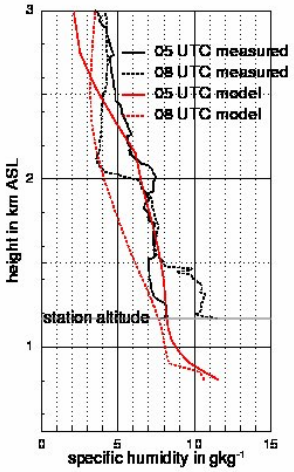

Figure 3. Comparison of specific humidity measured by radiosondes at Hornisgrinde Mountain and forecast by COSMO-DE model, on 20 July 2007.

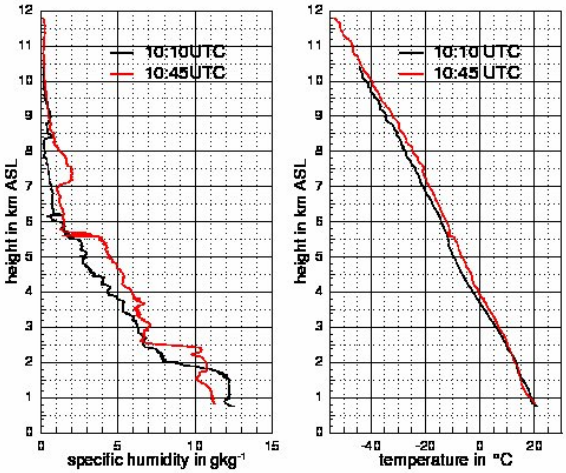

Figure 4. Specific humidity (left) and temperature (right) above height of two radiosondes at Dornstetten on 20 July 2007, 10:10 UTC (black) and 10:45 UTC (red).

CONVERGENCE INDEX: A NEW PERFORMANCE MEASURE FOR THE JUMPINESS OF OPERATIONAL RAINFALL FORECASTS

Uwe Ehret[1]

[1] TU München, Department for Hydrology, München, Germany
E-mail: *u.ehret@bv.tum.de*

Abstract: The degree of jumpiness of a sequence of rainfall forecasts strongly influences the end-users perception of its reliability. To objectively evaluate forecast convergence, a new performance measure termed 'convergence index' is proposed. It is applied on areal-averaged rainfall observations and forecasts of several numerical weather models in the mesoscale alpine catchment of the river Iller/Germany. It is shown that in combination with the root mean square forecast error, the convergence index allows useful evaluation of forecast quality: From the models used (Median of Cosmo-Leps, GME, Cosmo-EU, Persistence), the Median forecast scored highest.

Keywords: *rainfall forecast, convergence index, jumpiness, Cosmo-Leps*

1 INTRODUCTION

Rainfall forecasts serve as important prerequisite for many aspects of disaster management. In flood management for example, this ranges from the pre-flood drawdown of reservoir water levels to the preparation of protective measures such as the publication of warnings or timely evacuation.

In this context, the inevitable jumpiness of deterministic rainfall forecasts, which is partly even a positive sign of a models flexibility and ability to capture the full spectrum of atmospheric states, is distracting as firstly, many decisions in flood management are threshold-dependent and require forecasts consistently above (or below) the threshold and secondly, repeated switches from warning to all-clear erodes credibility in the eyes of non-expert users and the public. Consequently, for flood managers, evaluation of a rainfall forecasts jumpiness is useful. However, to date objective evaluation criteria are rare.

In this work, a new method termed 'convergence index' to evaluate a forecasts convergence is proposed. The work is structured in three parts: The first (Data & Methods) introduces the convergence index and the test data set used. The second (Results) displays results of its application on the test data set. In the third part (Conclusions), conclusions are drawn and the usefulness of the new performance measure is critically evaluated.

2 DATA & METHODS

2.1 Rainfall observations

Hourly rainfall observations from 26 raingauges were used to calculate mean areal rainfall (linear interpolation) in the alpine catchment of the river Iller/Germany up to Kempten (area: 954 km^2). The timeseries extends from 01.08.2005 to 30.04.2008, excluding the snow-influenced winter months November through March. The timeseries includes a 300-year flood event in August 2005.

2.2 Rainfall forecasts

The following rainfall forecasts were used (abbreviations in brackets): GME (GME), Cosmo-EU (LME), Cosmo-Leps Median (CLM), and, as reference, a simple persistence forecast (PER).

The forecasts were disaggregated to 1-hour sums (necessary for Cosmo-Leps and GME) and areal-averaged in the same manner as the rainfall observations. From all forecasts, only the 00:00 and 12:00 runs, cut to a maximum forecast depth of 48 hours were used to assure comparability. Accordingly, persistence forecasts were also generated only for the same initial times and forecast depths.

2.3 Convergence index

Based on a set of forecasts for a given observation, ordered by decreasing lead time, the convergence index (KONV) sums up the instances where the values, from on forecast to the next, do not approach the observed value (divergence) and the instances where forecasts switch from over- to undershooting (oscillation). The sums are divided by the maximum of possible occurrences and thus normalized to [0,1], where 0 means perfect convergence without oscillation.

To suppress the influence of small changes, a tolerance range, expressed in percent of the actual rainfall observation value, is applied. Times where forecast fluctuations are within the tolerance range are not

considered. Also, divergence and oscillation occurrences are inversely weighted by the forecast lead time to reduce the influence of poor (and less relevant) forecasts with long lead time.

However, KONV only expresses how good a series of forecasts approaches the observation in relative terms and even a series which is far off in absolute values may attain high scores. Therefore, KONV should be evaluated in combination with a measure that expresses forecast quality in absolute terms. Here, the root mean square error (RMSE) of the forecast series for each observation, also inversely weighted by lead time, was calculated.

2.4 Test setup

KONV and RMSE were calculated for each areal rainfall observation in the timeseries exceeding a threshold of 2.4 mm/h, which delineates the upper 5% of rainfall observations above a detection limit of 0.1 mm/h. Thus, only strong, flood-relevant rainfall events were considered. The tolerance range of KONV (as explained in 2.3) was set to 5%. From all values of KONV and RMSE, the mean was calculated (shown in Figure 1).

3 RESULTS

The main results (as shown in Figure 1) are: i) The persistence forecast exhibits the highest RMSE and ii) the lowest KONV, which indicates that it shows poor absolute values but good convergence. While the first result is in accordance with intuition, the latter is not. Further, iii) the Cosmo-Leps Median forecast shows the best overall performance (indicated by the smallest distance from the graphs point of origin), followed by GME and Cosmo-EU. The latter three iv) differ mainly with respect to KONV, not to RMSE.

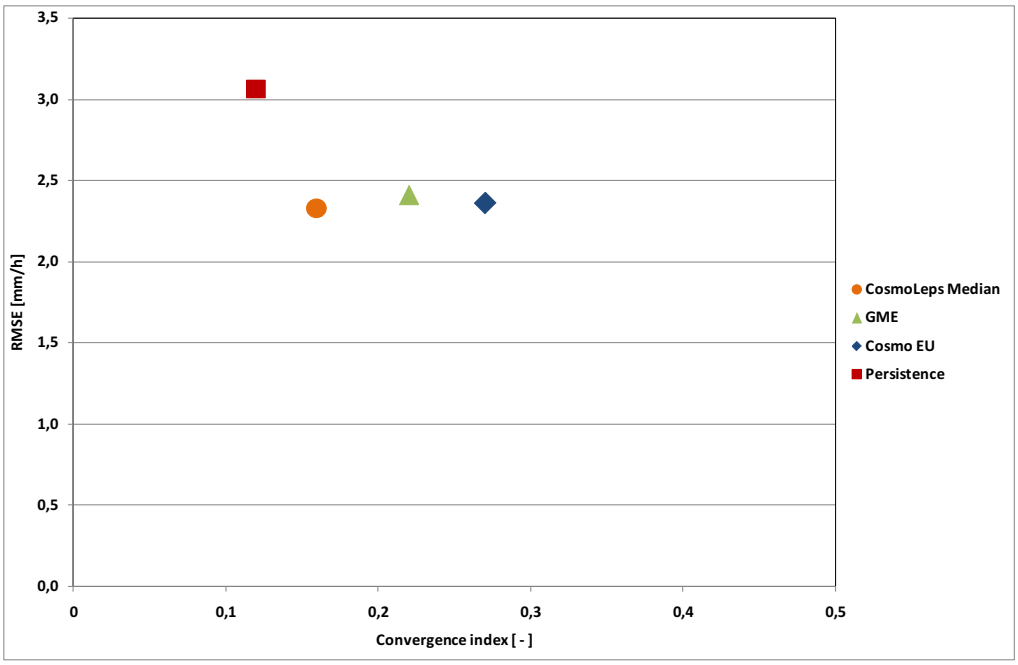

Figure 1. Performance of different forecasts with respect to Convergence index (0=optimal) and RMSE (0=optimal). Shown are mean values of the time series 01.08.2005-30.04.2008.

4 CONCLUSIONS

A new method to quantify the jumpiness of forecasts was proposed and applied on a series of areal rainfall observations and forecasts in a mesoscale alpine catchment. From the forecasts investigated, the Cosmo-Leps Median performed best. These findings are in accordance with other investigations by the author (not shown here), assessing rainfall forecast quality in alpine regions, where the Cosmo-Leps Median forecast often outperformed deterministic forecasts.

In combination with a measure that expresses forecast quality in absolute terms (here: RMSE), the convergence index may be useful for flood managers to find the most reliable rainfall forecast.

Acknowledgements:
The author expresses his gratitude to the Bavarian Agency for the Environment (LfU) for supplying the data for this work.

HYMEX, AN EXPERIMENTAL PROGRAM DEDICATED TO THE HYDROLOGICAL CYCLE IN THE MEDITERRANEAN

Véronique Ducrocq[1], Philippe Drobinski[2], Piero Lionello[3] and the HyMeX ISSC

[1] GAME-CNRM, Météo-France & CNRS, Toulouse, France
E-mail: veronique.ducrocq@meteo.fr
[2] IPSL-LMD, CNRS, Palaiseau, France
[3] Department of Science of Materials, University of Lecce, Italy

Keywords: *Mediterranean, water cycle, high-impact events, coupled processes*

1 INTRODUCTION

The Mediterranean basin has quite a unique character that results both from physiographic conditions and historical and societal developments. The region features a nearly enclosed sea surrounded by very urbanized littorals and mountains from which numerous rivers originate (Fig. 1). This results in a lot of interactions and feedbacks between ocean-atmosphere-land processes that play a predominant role on climate and on high-impact weather. The Mediterranean area concentrates indeed the major natural risks related to water cycle, which include heavy precipitation and flash-flooding during the fall season, severe cyclogenesis associated with strong winds and large sea waves during winter, and heat waves and droughts accompanied by forest fires during summer. The capability to predict such high-impact events remains weak because of the contribution of very fine-scale processes and their non-linear interactions with the larger scale processes.

Water resource is a critical issue for a large part of the Mediterranean basin. Freshwater is rare and unevenly distributed in time and space with few short duration heavy precipitation and long drought periods. Moreover, this happens in a situation of increasing water demands and climate change. The Mediterranean region has been indeed identified as one of the two main "hot-spots" of climate change, which means that its climate is especially responsive to global change. Large decrease in mean precipitation and increase in precipitation variability during dry (warm) season are expected as well as large increase in temperature. There are still, however, large uncertainties on the future evolution of the climate in the Mediterranean. Progress has to be made in the monitoring and modelling of the Mediterranean coupled climate system (atmosphere-land-ocean) in order to quantify the on-going changes and to better predict their future evolution in order to provide guidelines for development of adaptation measures.

These societal and science issues motivate the HyMeX (HYdrological cycle in the Mediterranean Experiment, http://www.hymex.org/) program, which is an experimental program aiming at a better quantification and understanding of the water cycle in Mediterranean - with emphases on intense events.

2 HYMEX SCIENCE OBJECTIVES

HyMeX proposes to monitor and modelling the Mediterranean coupled system (atmosphere-land-ocean), its variability (from the event scale, to the seasonal and interannual scales) and characteristics over one decade in the context of global change (2010-2020). In particular, HyMeX aims at addressing key issues related to (1) the water budget of the Mediterranean basin, (2) the continental hydrological cycle and related water resources, (3) heavy precipitation and flash-flooding and (4) intense air-sea exchanges produced by severe regional winds and cyclogenesis. HyMeX aims also at monitoring vulnerability factors and adaptation strategies developed by different Mediterranean societies to accommodate the impacts of climate change and intense events. The reader is referred to the HyMeX White book (Beranger et al, 2008) for a comprehensive description of the science issues addressed in HyMeX.

Figure 1 illustrates one of the coupled phenomena addressed in HyMeX. The Mediterranean Sea is characterized by several key-spots of intense air-sea exchanges associated with very strong winds, which are caused by the orographic response to the large scale forcing (e.g. Mistral, Bora, Sirocco, Tramontana, etc), deep cyclogenesis (e.g. Genoa cyclogenesis, etc) and high/low pressure patterns. These successive intense air-sea exchange events and the associated sea surface cooling affect considerably the heat and water budget of the Mediterranean Sea with formation of dense water and deep ocean convection during winter and early spring. Modifications of the ocean mixed layer in their turn influence the atmospheric boundary layer.

3 HYMEX OBSERVATION STRATEGY

A three-level nested observation strategy is proposed:

• *A long-term observation period* (LOP) lasting about 10 years to gather and provide additional observations of the whole coupled system in order to analyze the seasonal-to-interannual variability of the water cycle and to estimate the water budget. It is proposed that the LOP consists in enhancing the current operational observing systems and existing long-term observatories in hydrology, oceanography and meteorology, not excluding the setup of new networks. There is a general agreement that the LOP will have to cover the whole Mediterranean basin, developing and maintaining the acquisition of the long-term time series required to study its seasonal and interannual variability.

• *An enhanced observation period* (EOP) for both budget and process studies. The Enhanced Observation Period is envisaged lasting for at least 4 years, embracing the SOP periods. However, EOP may cover only part of the year, i.e. activities may be restricted for some aspects to specific periods (e.g. autumns for heavy precipitation, extending to winter for severe cyclogenesis and strong winds).

• *Special observation periods* (SOP) lasting several months, which will aim at providing detailed and specific observations to study key processes of the water cycle in specific Mediterranean regions. A first series of SOPs will take place in Northwestern Mediterranean in order to document heavy precipitation systems during fall and intense air-sea fluxes and dense water formation at the end of winter. The first HyMeX SOP over Nortwestern Mediterranean is now foreseen for September-October 2012.

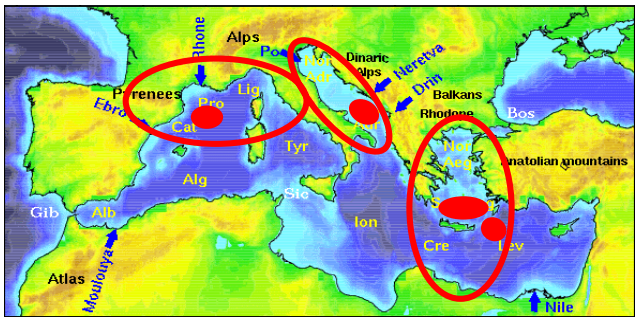

Figure 1. The four major sites of dense water formation (red line) and of deep ocean convection (red spots) over the Mediterranean basin.

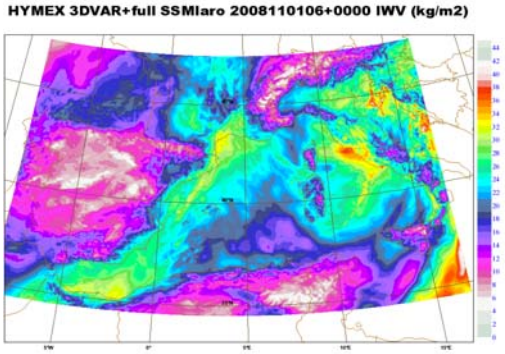

Figure 2. Integrated Water Vapour (mm) simulated by the 2.5-km AROME –WMED model (Courtesy: G. Jaubert).

4 HYMEX MODELING STRATEGY

The modelling strategy associated with the observation strategy includes :

- The development of regional coupled systems (ocean-atmosphere, atmosphere-land, ocean-land-atmosphere) to reduce uncertainties of the future regional projections. Validation of these systems includes measuring their skill in accurately simulating the Mediterranean water budget by using the HyMeX multidisciplinary databases.
- The development and improvement of high-resolution deterministic or ensemble modelling systems to improve the prediction capabilities of extreme events. Some of these systems will run in real-time during the SOPs to serve as guide for the deployment of dedicated instrumentation. Figure 2 illustrates one of this system currently developed for real-time application during the HyMeX SOPs. The AROME-WMED model is a version of the AROME NWP system running its own 3-hourly rapid update assimilation cycle at 2.5 km over the western Mediterranean. Such high-resolution large domain allows to include the major mountain ranges of the western Mediterranean region (Atlas, Pyrenees, Alps, Massif Central, etc) and to describe their influence on the atmospheric circulation .
- The development of new process modelling, parameterization development, novel data assimilation systems for the different Earth compartments. For example, improvement of air-sea flux parameterizations or development of data assimilation in cloud and precipitation systems are major objectives of HyMeX and part of the observation strategy is designed to serve these objectives.

REFERENCES

Béranger K., Braud I., Carlotti F., Chanzy A., Claud C., Delrieu G., Doerenbecher A., Despiau S., Drobinski P., Ducrocq V., Dulac F., Durrieu de Madron X., Elbaz-Poulichet F., Escadafal R., Estournel C., Giordani H., Guieu C., Guiot J., Hallegate S., Kageyama M., Jacob F., Lachassagne P., Lang M., Li L., Martin E., Médail F., Noilhan J., Moussa R., Perrin J.L., Plu M., Prieur L., Ricard D., Rinaudo J.C., Radakovitch O., Roux F., Lutoff C., Somot S., Taupier-Letage I., 2008: HyMeX (Hydrological cycle in the Mediterranean Experiment): Towards a major field experiment in 2010-2020. Eds. P. Drobinski, V. Ducrocq, available at http://www.cnrm.meteo.fr/hymex/, version 1.3.2, February 2008, 124 pp.

OPERATIONAL PERFORMANCE OF DISCHARGE PREDICTION IN ALPINE REGIONS

Frédéric Jordan[1], Javier Garcia Hernandez[2], Alexandre Gal[3]

[1] e-dric.ch, Le Grand-Chemin 73, CH-1066 Epalinges, Switzerland
E-mail: *fred.jordan@e-dric.ch*
[2] Ecole Polytechnique Fédérale Lausanne, Dept. of Civil Engineering, Station 18, CH-1015 Lausanne, Switzerland
[3] Groupe E, Route de l'Abbaye, CH-1025 Posieux, Switzerland

Abstract: The Groupe-e is an electricity provider, operating 6 dams with large reservoirs located in the Saane river basin in Switzerland. The 1800 km^2 Saane river basin is an alpine catchment area, with elevations from 450 m a.s.l. (Laupen) to 3200 m a.s.l. (Wildhorn). Due to its specific electricity market, the Groupe e company is able to self-produce only a moderate part of its electricity sales, the remaining part has to be bought on the spot electricity market. For this reason, it is of highest importance to predict the future inflows in the reservoirs in order to adjust the hydroelectricity production and the electricity trades on the spot market.

During 2007 and 2008, a hydrological prediction model was developed, including the functioning of the 6 existing hydropower schemes. In this semi-distributed conceptual model, the Saane river basin is decomposed into 43 sub-basins. Each one is cut into 300m elevation bands in order to take into account the temperature-driven processes (snow melt, glacier melt, rainfall-snow separation, PET).

Different deterministic numerical weather prediction models are used in the system, such as ECMWF, COSMO-7 and COSMO-2 models. The system was able to provide relevant information during 2008, such as high flows and small floods due to snow melt and summer storms. The 2008 operational performance of the whole system is presented below, comparing the different predicted inflow models. The results are compared with persistence, continuous simulation based on observations and updated continuous simulation.

Keywords: *Hydrology, Discharge prediction, Flood*

1 INTRODUCTION

Discharge prediction is a powerful tool for hydroelectricity production. However, the uncertainty associated to the inflow forecasts is important, depending on particular meteorological situations. For this reason, ensemble discharge forecasts are now used by researchers in order to quantify the related uncertainty. For daily use of inflow forecasts, the ensemble forecasts are of complicated use and do not suit yet for operational systems. The aim of this contribution is to present the operational performance of the RS3.0 system (Garcia et al., 2007), a discharge prediction system after its first year of operational use.

2 MODEL DESCRIPTION

The Saane river is located in the North side of the Alps in Switzerland (Fig. 1, left). Its 1800 km^2 catchment area is mountainous with snow covered areas during 4 months per year including a small glacier. The basin has elevations from 450 to 3200 m a.s.l. The Groupe-e company is owner of 6 hydropower schemes with 2 large reservoirs located in this catchment area. In the simulation model (Fig. 1, right), the catchment area is divided into 43 sub-basins with 40 km^2 of average area. Each sub-basin is divided into 300 m elevation bands to take into account the temperature effects. The computed hydrological processes are separation between solid and liquid precipitation, snow melt, glacier melt, real evapo-transpiration, soil infiltration, surface runoff and river routing. The model computes hydraulic schemes as well (Jordan, 2007).

3 SIMULATION

The performance analysis compares continuous simulation results, filtered simulation results and forecast results. The simulation results (continuous and filtered) are obtained with observed meteorological input data, while forecast results are obtained with predicted meteorological input data from the COSMO-7 model of Meteoswiss. The performance is evaluated with the Nash indicator computed on a whole year simulation period. The continuous simulation is obtained by a direct hydrological simulation during the period. The filtered simulation is obtained by updating the initial conditions of the model every 12 hours. The updating procedure allows comparing simulated and observed discharges at every discharge measuring gauge. Finally, the forecasts

are computed by using 2 numerical weather forecasts per day during the same year period. Different lead times are analyzed, from 0-12 h to 60-72 h ahead.

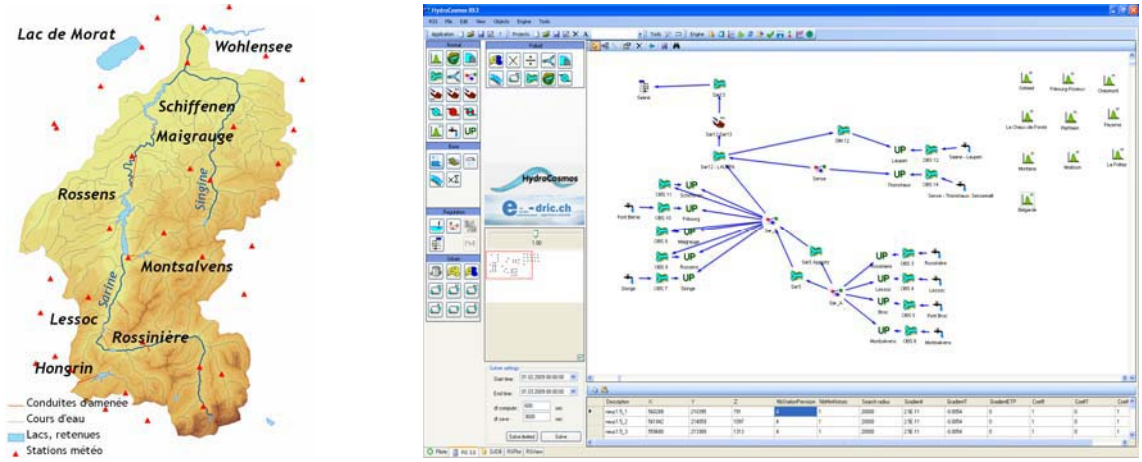

Figure 1. Map of the Saane river basin (left) with the sub-catchments, rivers, reservoirs and meteorological measuring stations. Corresponding RS3.0 model (right) with the main user interface.

4 PERFORMANCE OF THE MODEL

Fig. 2 presents the whole year forecasts at Rossinière dam for 24h lead time (left). The good correlation between observed and predicted discharge is due to good quality 24h meteorological forecasts and a relatively long 12 h response time of the basin. Systematic simulation and forecasts results show 3 different elements (Fig. 2, right). First, the filtered simulation provides a much better performance that the continuous simulation, which is expected. For this reason, the filtered simulation provides the operational initial conditions of the hydrological forecast. Second, the average forecast performance is lower than the one of the filtered simulation. Nevertheless, it can be better than the continuous simulation one, at least for lead times lower than 48 hours. Finally, the forecast performance (COSMO7) strongly decreases for lead times higher than 36 hours, and the persistence theoretical model (PERS) provides in average better Nash values.

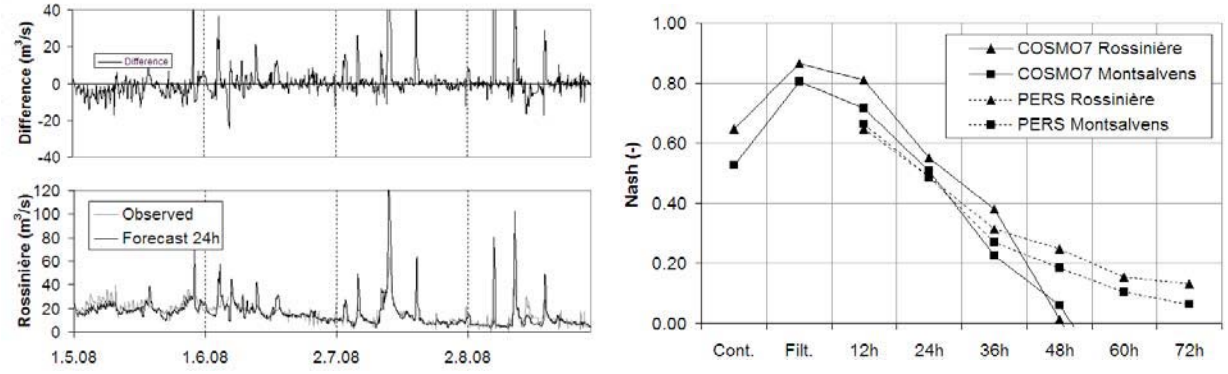

Figure 2. Comparison between observed and predicted inflows 24h ahead at the Rossinière dam (left). Differences (prediction minus observation) are also presented. Synthetic analysis of Nash coefficients computed during the year 2008 (right). Cont. = continuous simulation ; Filt. = filtered ; 12h – 72h = lead times.

A detailed analysis will provide useful information in order to assess the part of the uncertainty due to the hydrological model and the part due to the meteorological forecast. These results illustrate the difficulties to predict discharges more than 48h ahead with the COSMO7 deterministic model.

REFERENCES

García Hernández, J., Jordan, F., Dubois, J., Boillat, J.-L. & Schleiss, A. (2007). Routing System II: Flow modelling in hydraulic systems, Communication du Laboratoire de Constructions Hydrauliques N°32, ed. A. Schleiss, EPFL, Lausanne.

Jordan, F. (2007). Modèle de prévision et de gestion des crues - optimisation des opérations des aménagements hydroélectriques à accumulation pour la réduction des débits de crue. PhD Thesis N°3711, Ecole Polytechnique Fédérale de Lausanne.

ANALYSIS OF PRECIPITATION PATTERNS ON MOUNT BALDO (ITALY)

Giacomo Poletti[1], Massimiliano de Franceschi[1,2], Alberto Bellin[1], Dino Zardi[1]

[1] Dipartimento di Ingegneria Civile e Ambientale, Univesità di Trento, Trento, Italy
E-mail: *Dino.Zardi@ing.unitn.it*
[2] Seminario Maggiore, Diocesi di Bolzano-Bressanone, Bressanone, Italy

Abstract: Preliminary results are shown from a research work aiming at retrieving and organising in a dataset precipitation data from 16 stations disseminated on Mount Baldo, in order to produce a climatological analysis of precipitation in the area. The final dataset covers an overall 90 year span (1919-2008), although the various stations have been operated very discontinuously in it. The analysis of the 11 most representative time series provides an overview of typical annual and seasonal mean values along with their trends. Correlation analysis between total monthly precipitation data shows that stations located on the same side of the mountain are better correlated with respect to other lying closer, but on the opposite side. Suitable mapping through Kriging techniques allows to infer the spatial distribution of precipitation under various seasonal and typical weather patterns. 100 precipitation events have been classified into 7 typical meteorological scenarios, identified on the basis of patterns from ECMWF reanalysis. Specific features of each scenario are evaluated and discussed.

Keywords: *orographic lifting, precipitation, mountain, rain gauge, Kriging.*

1 INTRODUCTION

The mountain chain of Mount Baldo, in the southern Prealps, lies between the Lake Garda and the Lagarina Valley (Figure 1). Ranging from 65 m a.m.s.l. of the mountain feet at the shore of Lake Garda up to about 2200 m a.m.s.l. of its main crests, Mount Baldo displays a remarkable variety of local microclimates, geographical characters and ecosystems, in particular flora (since it received the name of *Hortus Europae*, i.e. Europe's Garden). Precipitation over Mount Baldo originates both from evaporation and up-slope advection of water vapour, especially from the side of Lake Garda, and from the lifting of moist airflows, especially from south. These effects may variously occur and interact under different meteorological scenarios.

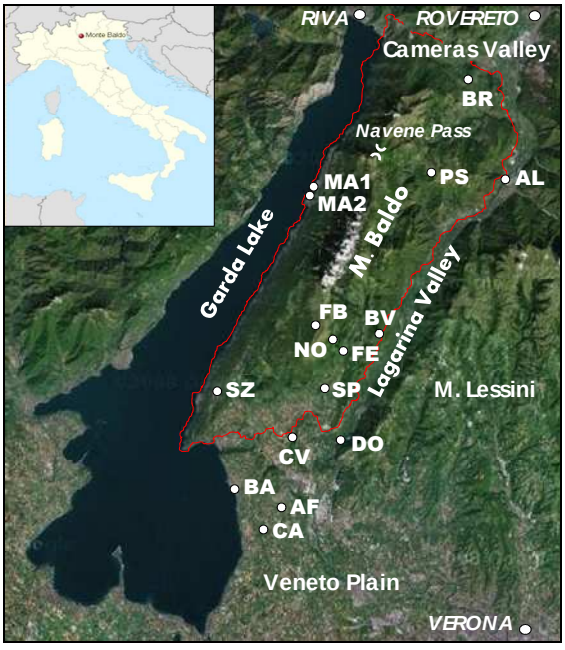

Figure 1. Map of Mount Baldo with the precipitation measuring stations: Affi (AF), Ala (AL), Bardolino (BA), Brentonico (BR), Belluno Veronese (BV), Calmasino (CA), Caprino Veronese (CV), Dolcè (DO), Ferrara di Monte Baldo (FE), Rifugio Fiori del Baldo (FB), Malcesine (MA1, MA2), Prà da Stua (PS), Spiazzi di Monte Baldo (SP), San Zeno di Montagna (SZ).

2 DATASET

The dataset collected for the present analysis includes data from 16 weather stations disseminated on the mountain (Figure 1) and covers an overall period of 90 years (1919-2008). Since the various stations have been operated very discontinuously, the analysis focused on the 11 most representative time series and provides an

overview of typical annual and seasonal mean values along with their trends. Correlation coefficients between total monthly precipitation data (Table 1) show that stations located on the same side of the mountain are better correlated with respect to other lying closer, but on the opposite side.

	AL	BV	BR	CA	CV	DO	FE	MA	PS	SZ	SP
AF	0.805	0.783	0.744	0.947	0.897	0.784	0.790	0.713	0.797	0.770	0.787
	AL	0.854	0.860	0.818	0.854	0.738	0.847	0.876	0.893	0.783	0.813
		BV	0.795	-	0.853	0.712	0.889	0.824	0.855	0,762	0.794
			BR	0.795	0.805	0.731	0.792	0.794	0.901	0.728	0.774
				CA	-	0.870	-	-	-	-	-
					CV	0.840	0.848	-	-	0.746	0.826
						DO	0.750	0.624	0.745	0.637	0.753
							FE	-	-	0.690	0.797
								MA	0.856	0.736	0.774
									PS	0.823	0.776
										SZ	0.759

Table 1. Correlation coefficients *r* between monthly total precipitation (orange: $r > 0.85$, yellow: $0.75 < r < 0.85$, white $r < 0.75$). Dashes denote 11 couples displaying no overlapping periods so that correlation coefficient could not be evaluated.

3 PRECIPITATION MAPPING AND ANALYSIS

Suitable mapping through Kriging techniques allowed to infer the spatial distribution of precipitation under various seasonal and typical weather patterns. In an area characterized by various weather conditions, 100 precipitation events were classified into 7 typical meteorological scenarios, identified on the basis of patterns from ECMWF reanalysis. Specific features of each event are evaluated and discussed (an example in Figure 2).

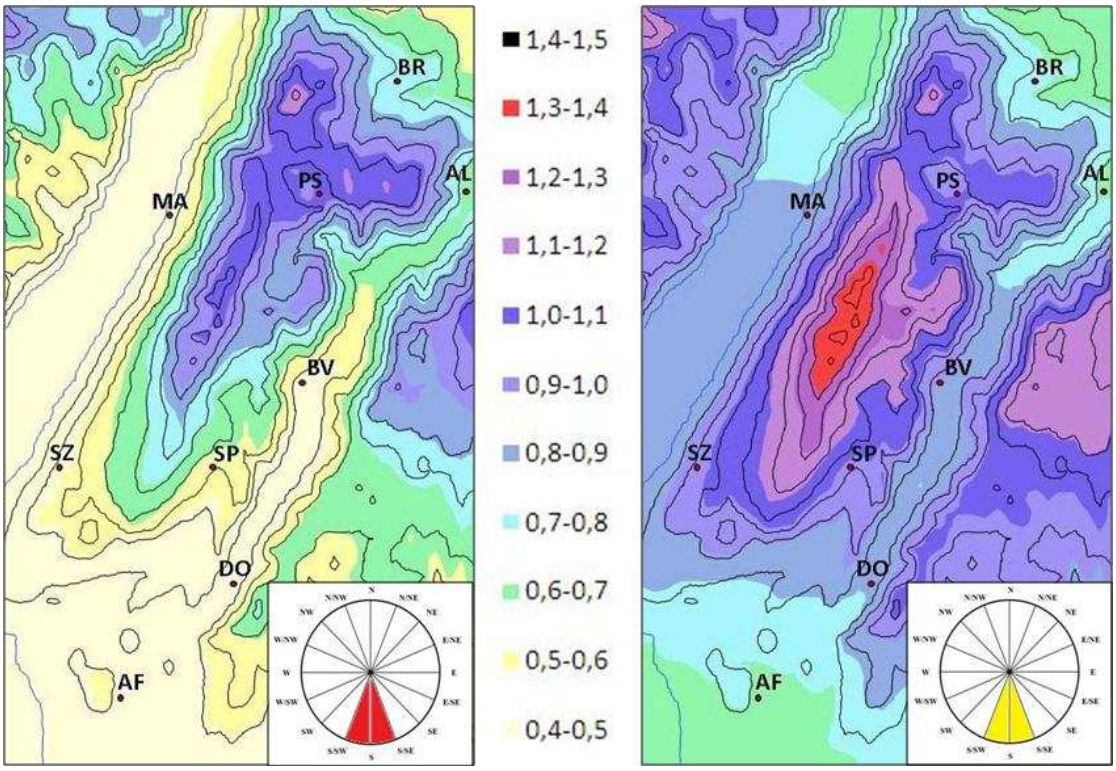

Figure 2. Average distribution of precipitation for two events with strong (left) and moderate (right) southerly flows. Scale is normalised to the maximum measured total precipitation value. Height contours every 250 m.

ASSIMILATION OF LEANDRE2 WATER VAPOR OBSERVATIONS WITH THE AROME 3D-VAR CYCLE FOR COPS

Matthias Grzeschik[1], Genevieve Jaubert[2], Cyrille Flamant[3], Evelyne Richard[1]

[1] Laboratoire d'Aérologie, CNRS and University of Toulouse, Toulouse, France
[2] Centre National de Recherches Météorologiques, Météo-France, Toulouse, France
[3] Service d'Aéronomie, CNRS and University Pierre et Marie Curie, Paris, France
E-mail: *Matthias.Grzeschik@aero.obs-mip.fr*

Abstract: This study is investigating the sensitivity of forecast quality on initial conditions with respect to the water vapor field and the possible contribution of high resolution lidar measurements to an improvement of precipitation forecast. The airborne Leandre2 Differential Absorption Lidar (DIAL) system was measuring water vapor profiles during the Convective and Orographically-induced Precipitation Study (COPS) in mattress patterns to observe the 3D distribution of water vapor. This quasi volume information of the water vapor field promises a positive impact on the quality of the modeled humidity field and also improvements of the precipitation forecast can be expected. The observations was assimilated with the AROME 3D-Var cycle and the impact was studied by comparing short range forecasts from analysis with and without additional water vapor information.

***K*eywords:** *ICAM, data assimilation, water vapor, airborne, lidar, DIAL*

1 INTRODUCTION

Leandre2 measures water vapor profiles with a high spatial and temporal density. The data collected during the COPS IOPs of July 2007 represent a total of 22 hours. The outstanding property of these data is the high resolution of $20\,\mathrm{m}$ vertically and $5\,\mathrm{sec}$ in time. Since the water vapor was observed along the aircraft track, while it was flying mattress patterns, the measurements give good information about the spatial distribution of water vapor in the boundary layer. These data set is to be used to investigate the role of the distribution of water vapor on the initialization of convection by forcing the model towards the observed humidity field.

2 DATA PROCESSING

The Leandre2 data were provided as water vapor mixing ratios together with estimated observation error in netCDF format. These data were prepared to be used with the AROME 3D-Var system.

For the assimilation, it had to be assured, that no bad data are used. Therefore, the dataset was first cleaned by removing data with an absolute error larger than $1.5\,\mathrm{g/kg}$, a relative error larger than $50\,\%$, and a relative error smaller than $2\,\%$. Further data were removed after inspecting the data by human eye.

The water vapor profiles were averaged in horizontal to profiles with a minimum distance of $20\,\mathrm{km}$ and with a temporal interval not larger than two minutes. In vertical, the profiles were roughly averaged to the AROME model levels. The resulting super observations, see figure 1, were furthermore used for the screening.

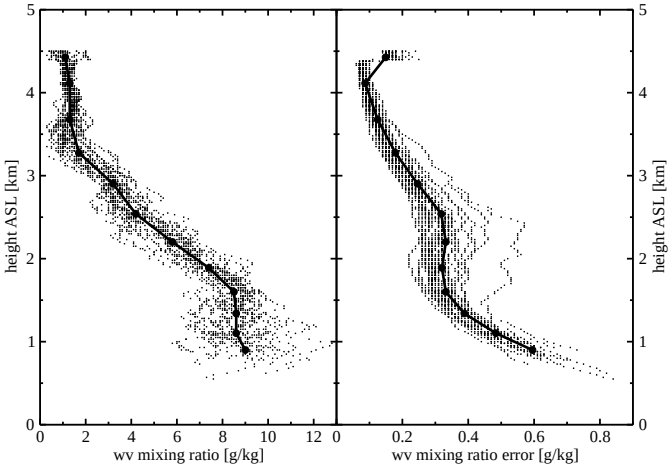

Figure 1: Result of thinning for an example of one super observation profile. The left panel shows the water vapor mixing ratio observation and the right panel shows the corresponding measurement error. The raw observation are represented as small dots, while the super observation are marked as larger dots, connected by lines.

During the screening, all available super observations were compared with AROME $3\,\mathrm{h}$ forecasts of the corresponding observation time. The resulting statistics of Leandre2 observations for July 2007 are shown in figure 2. This comparison yielded to a dry bias at the bottom of the profiles of about $0.5\,\mathrm{g/kg}$ and a RMS of about $1.5\,\mathrm{g/kg}$. The distribution of deviations can be roughly assumed to be gaussian after removing the bias of panel one of figure 2.

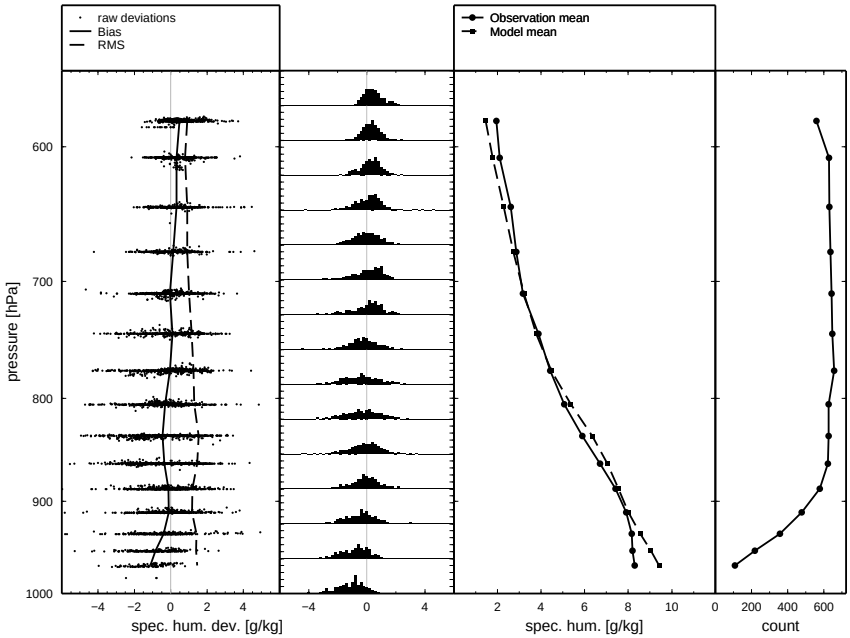

Figure 2: Statistics of all Leandre2 observations against AROME forecasts. The first panel shows the deviation Leandre2 - AROME of specific humidity for each super observation as dots. The solid line is the mean of the deviation and represents the bias, while the dashed line is the RMS. The second panel shows the histogram of the deviations for each level, while the third panel shows the mean of the absolute specific humidity for the observation and AROME. At last, the fourth panel shows the number of observations for each level over the whole period.

3 ASSIMILATION

In a next step the super observations were introduced in the AROME assimilation cycle every three hours, with the 3D-Var technique in a resolution of 2.5 km. Figure 3 shows the difference of water vapor in 2 km height for the analysis at 12 UTC, while additional observations were already assimilated at 9 and 12 UTC. A clear impact of the order of 3 g/kg is visible in the cops region.

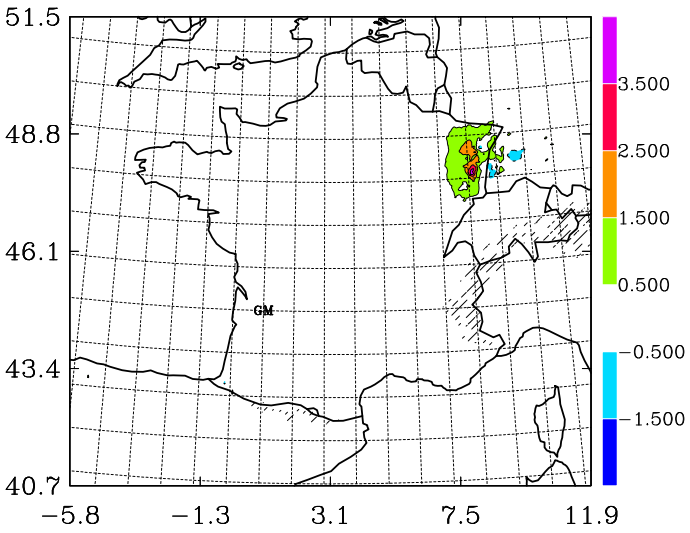

Figure 3: Water vapor differences (with Leandre2 minus the control experiment) at 2 km height for 14 of July, 12 UTC after assimilating Leandre2 observations at 9 UTC and at 12 UTC.

4 OUTLOOK

The impact of these data should be further investigated. How does it evolve in the further assimilation cycle? Is the influence of Leandre2 on the forecast positive, compared with other observations as TEMP, AMDAR, and so on? Does the modification of the water vapor field yield to an improved forecast in terms of convection and precipitation and the reasons for this change in the water vapor field.

Additionally is currently in development the assimilation of DIAL data from the DLR Falcon system, which provided similar data during COPS.

Acknowledgements:
Christoph Kiemle, DLR, Institut für Physik der Atmosphäre for providing DLR Falcon DIAL data.

PROPOSAL OF A NEW METHOD TO SELECT THE REFERENCES SERIES: FIRST RESULTS

Fiorella Acquaotta[1], Simona Fratianni[1]

[1] Department of Earth Science University of Turin, Turin, Italy
E-mail: *fiorella.acquaotta@unito.it*

Abstract: Most techniques used to adjust daily climatological time series for reconstruction the missing values and for inhomogeneities require a reference series obtained from neighbouring stations. In many cases, the selection of reference series is obtained using only statistical methods and neglecting the climatological peculiarities of the meteorological station.
In this study we have tried to estimate the importance of climatological features compared with the statistical methods. We have studied the maximum and minimum daily temperatures series of the Piedmont (NW Italy). We have selected the candidate series (to reconstruct or to homogenize) and the neighbouring series. For each selected station we have carried out a climate analysis and we have applied the statistical tests in the period 1998-99. The methods have allowed to assess which reference series "better represent" the candidate series.

Keywords: *References series, maximum and minimum temperatures, statistical tests, climate indexes.*

1 INTRODUCTION

The techniques for the reconstruction of the missing values or to create homogeneous reference series are becoming more important in the international field (Della Marta et al. 2006) in order to estimate the real climate changes of a region. However, in many cases, the reference series selection is obtained using only statistical methods and neglecting the climatological peculiarities of the meteorological stations (Peterson et al. 1994, Eischeid et al. 1995).

In this paper we have tried to use both methods, statistic and climate, so to consider all the factors that cause the state of a meteorological variable.

2 DATA AND METHODS

We have used an objective method to select, from a set of neighbouring stations, the reference series more suitable to reconstruct the missing values or to homogenise a candidate series.

We have chosen as candidate series the minimum (Tn) and maximum (Tx) daily temperatures of Turin, for the period 1998-1999. Then we have been selected the neighbouring series (Tab. 1) that were operating continuously in the considered period.

For each station we have carried out a climate analysis using climate indexes. For the minimum daily temperature we have used the frost day (Tn<0°C), day with Tn>10°C and tropical nights (Tn>20°C), while for the maximum daily temperatures the summer day (Tx>25°C), day with Tx>10°C and ice day (Tx<0°C). To quantify the "climate differences", for each climate index, we have calculated the difference in day between the values obtained from the candidate series and the neighbouring series for each month.

Subsequently, for each month, we have made a statistical analysis. We have identified and excluded the outliers (between 2nd and 98th quantiles), and evaluated the maximum, the minimum, the median, the average and the standard deviation. On each set of values we have applied the Shapiro-Wilk test to assess whether the data assume a normal distribution and, thank to results of this test, we have applied the Student test, parametric test, or the Wilcoxon signed-rank test, nonparametric test, to evaluate if the two series, candidate and neighbouring, have the same average. The Kolmogorov-Smirnov test, nonparametric test, has been applied in order to estimate if the two series have the same distribution and then the correlation coefficient has been calculated.

The results obtained from climate indices and statistical tests have been classified by appropriate conversion tables that allow us to highlight the best results (Tab. 2). The values obtained by the division into classes of the comparison methods have been added to detect, for each month, the four best neighbouring series suitable to interpolate the candidate series.

3 RESULTS

The analysis on the minimum daily temperatures series has revealed the low possibility to use the daily values of neighbouring series to reconstruct or to homogenise the series of Turin. In fact, in many months, we have not identified the reference series because the sum of the results had low scores (Tab. 3). It was possible to identify only an exception, in October, for the meteorological station of Luserna S. Giovanni.

Good results were obtained from the maximum daily temperatures series (Tab. 3). In each month, except August, we have found at least one reference station. In the months of February and May most of neighbouring stations are suitable to interpolate the daily values of the candidate station.

Stations	E [m]	Latitude	Longitude
Torino	240	45°04'49"	7°40'25"
Varallo	470	45°49'14	8°16'30"
Lucerna	475	44°48'50"	7°14'32"
Asti	117	44°53'09"	8°12'48"
Vercelli	135	45°19'32"	8°23'26"
Cumiana	327	44°57'53"	7°23'31"
Pino T.se	608	45°02'32"	7°45'58"
Lanzo	580	45°17'23"	7°29'38"
Piverone	230	45°25'53"	8°02'04"
Verolengo	163	45°11'10"	8°00'43"

Table 1. Geographical localization of the meteorological stations analyzed, E = elevation.

Climate indexes		Statistical tests	
Difference (days)	**Score**	**Results**	**Score**
0	6	1	6
±1	5	0.96-0.99	5
±2	4	0.92-0.95	4
±3	3	0.88-0.91	3
±4	2	0.84-0.87	2
±5	1	0.80-0.83	1
≥±6	0	<0.80	0

Table 2. Classification of the results obtained from climate indices and from statistical tests. We have assigned a score equal to 6 for the best result climbing up to 0 for the worst results.

M	Jan	Feb	Mar	Apr	May	Jun	Jul	Ago	Sep	Oct	Nov	Dec
1	5/0.55	8/0.87	8/0.89	7/0.80	6/0.72	10/0.68	5/0.58	2/0.76	3/0.84	6/0.85	2/0.85	4/0.61
2	8/0.68	7/0.82	3/0.79	0/0.53	1/0.83	0/0.70	0/0.40	0/0.75	0/0.79	4/0.62	4/0.81	6/0.71
3	5/0.73	14/0.90	7/0.93	2/0.86	13/0.86	2/0.85	5/0.70	2/0.81	6/0.86	7/0.85	5/0.86	7/0.81
4	5/0.72	15/0.92	15/0.94	11/0.86	10/0.88	2/0.84	4/0.75	3/0.90	5/0.87	8/0.92	7/0.87	3/0.62
5	10/0.91	10/0.94	8/0.95	12/0.93	10/0.93	3/0.90	3/0.84	3/0.91	7/0.94	8/0.94	4/0.92	8/0.87
6	8/0.81	10/0.94	6/0.95	8/0.92	11/0.96	5/0.90	3/0.85	4/0.93	8/0.96	8/0.94	8/0.91	11/0.63
7	6/0.80	10/0.93	6/0.95	9/0.93	4/0.95	3/0.89	1/0.82	3/0.91	9/0.92	8/0.91	10/0.90	5/0.76
8	10/0.88	19/0.94	10/0.95	3/0.90	18/0.91	5/0.88	12/0.84	7/0.92	12/0.94	9/0.96	4/0.93	9/0.89
9	8/0.85	21/0.92	17/0.95	8/0.88	13/0.93	3/0.88	5/0.85	3/0.91	7/0.95	8/0.95	19/0.94	8/0.88
m	**Jan**	**Feb**	**Mar**	**Apr**	**May**	**Jun**	**Jul**	**Ago**	**Sep**	**Oct**	**Nov**	**Dec**
1	1/0.50	3/0.88	6/0.71	0/0.76	0/0.58	0/0.73	0/0.32	0/0.71	1/0.80	0/0.79	5/0.91	0/0.78
2	0/0.54	5/0.91	5/0.77	0/0.62	6/0.56	3/0.84	0/0.52	0/0.69	0/0.67	16/0.84	9/0.89	0/0.76
3	0/0.29	2/0.84	6/0.55	0/0.56	0/0.34	1/0.51	0/0.42	0/0.62	0/0.70	3/0.82	6/0.83	0/0.71
4	0/0.22	1/0.83	6/0.50	4/0.56	0/0.59	6/0.76	2/0.41	0/0.56	0/0.60	4/0.71	5/0.77	5/0.71
5	0/0.74	4/0.94	9/0.89	3/0.89	4/0.68	3/0.84	0/0.39	0/0.75	0/0.78	2/0.84	8/0.88	2/0.87
6	4/0.39	6/0.79	4/0.74	3/0.86	5/0.66	4/0.91	0/0.56	0/0.79	3/0.75	2/0.70	5/0.79	0/0.48
7	0/0.49	3/0.88	9/0.88	3/0.90	0/0.67	2/0.84	0/0.43	0/0.74	1/0.80	2/0.85	6/0.91	0/0.70
8	0/0.51	3/0.88	6/0.79	1/0.75	6/0.64	6/0.85	0/0.68	1/0.80	3/0.73	4/0.84	8/0.87	1/0.83
9	0/0.21	3/0.90	6/0.55	0/0.55	0/0.35	0/0.73	0/0.27	0/0.50	0/0.66	0/0.72	5/0.77	0/0.71

Table 3. Results obtained by comparison of the maximum (M) and minimum (m) temperatures series and corresponding correlation coefficient; Stations: 1= Varallo, 2= Luserna S. Giovanni, 3= Asti, 4= Vercelli, 5= Cumiana, 6= Pino T.se, 7= Lanzo, 8= Piverone and 9= Verolengo.

4 CONCLUSIONS

The results obtained by this first pilot methodology on the minimum and maximum daily temperatures series have allowed to highlight that, in many cases, the simple presence of neighbouring stations with a good correlation coefficient is not enough to affirm that the series are "similar". The climate peculiarities play a key role in the climate determination because their features can create important effects on the trends of the meteorological variables, even for some periods of the year.

REFERENCES

Della Marta P., H. Wanner, 2006: A method of homogenizing the extremes and mean of daily temperature measurements, Journal of Climate, Volume **19**, 4179-4197.

Eischeid, J., C. Baker, T. Karl and H. Diaz, 1995: The quality control of long-term climatological data using objective data analysis, Journal of Applied Meteorology, Volume **34**, 2787-2795.

Peterson T., D. Easterling, 1994: Creation of homogeneous composite climatological reference series, International Journal of Climatology, Volume **14**, 671-679.

A quality control and bias correction method developed for irregularly spaced time-series of observational pressure- and temperature-data

Stefan Sperka[1], Dieter Mayer[1], Reinhold Steinacker[1]

[1] Department of Meteorology und Geophysics, University of Vienna, Vienna, Austria
E-mail: *stefan.sperka@univie.ac.at*

Abstract: Within the creation of the MESOCLIM-dataset (3 hourly MSLP, potential- and equivalent potential temperature VERA-analyses for a 3000 times 3000 km_2 area centered over the Alps from 1971-2005) a method to detect and correct occurring biases in the observational raw data had to be developed. The method is based on an automated variational algorithm that minimizes second spatial derivates in meteorological fields.

***K*eywords:** *MESOCLIM, Bias correction, MSLP-analyses*

1 INTRODUCTION

There are many reasons for a change of a measurement site's performance, for example a change in the instrumentation, a slight modification of the location or a different way of data processing (pressure reduction). For the creation of a 3 hourly MSLP, potential- and equivalent potential temperature VERA-analyses-dataset, a method to estimate these artificial influences was developed, using an automated variational algorithm that minimizes second spatial derivates in meteorological fields and calculates deviations for each observation (Steinacker (2000)). These deviations were calculated for each station at each time, using a piecewise functional fitting approach that considers the stations primary and secondary neighbours. The resulting timeseries of deviations were then used to estimate a bias correction for each meteorological parameter at each measurement site. Additionally, the data was checked for gross errors by comparing it to ERA-40 gridded data.

2 Bias Correction: Theory

The output of the automated quality control algorithm was checked for inhomogeneities, that could be caused by artificial shifts in the stations records, with a Standard Normal Homogeneity Test (SNHT). The variant of the SNHT used here was developed by Haimberger (2007) for testing analysis feedback data of radiosonde temperatures and is defined as:

$$T_k = (\frac{N}{2}(\mu_{1k} - \mu)^2 + \frac{N}{2}(\mu_{2k} - \mu)^2)/\sigma_k \quad (1)$$

$\frac{N}{2}$ denotes the sample length, μ_{1k}, μ_{2k} and μ the mean deviations in interval one, two and over both of them and σ_k is the standard deviation. Synthetic timeseries were generated to test the tests capability to detect inhomogeneities of different sizes, and to determine the significant threshold level for the SNHT values. The results suggest that it is possible to detect breaks $\geq 2\sigma$, while smaller breaks can be lost in the noise. Once the assumed artificial breaks are determined, the median of the deviations between breaks is used as bias correction estimate.

3 Results

In the top panel of figure 1 the deviation timeseries of station 11022 (Retz, Austria) is shown in black and the red vertical lines indicate detected breaks. To correct these inhomogeneities the median of the deviations between two breakpoints was used as correction estimate. The middle and bottom panels of figure 1 show the uncorrected and corrected MSLP timeseries of the same station and their trends. Considering that the long term trend of MSLP should be rather close to zero, the correction seems to have a good effect on the timeseries.

4 Conclusions

In general the bias correction reduces the standard deviation of the stations trends and helps to produce smoother fields. Most MSLP-trends of stations with long records, that were differing from zero, could be reduced by the bias estimates. For potential and equivalent potential temperature the standard deviation of trends from stations with records longer than 20 years could be reduced by 10 percent.

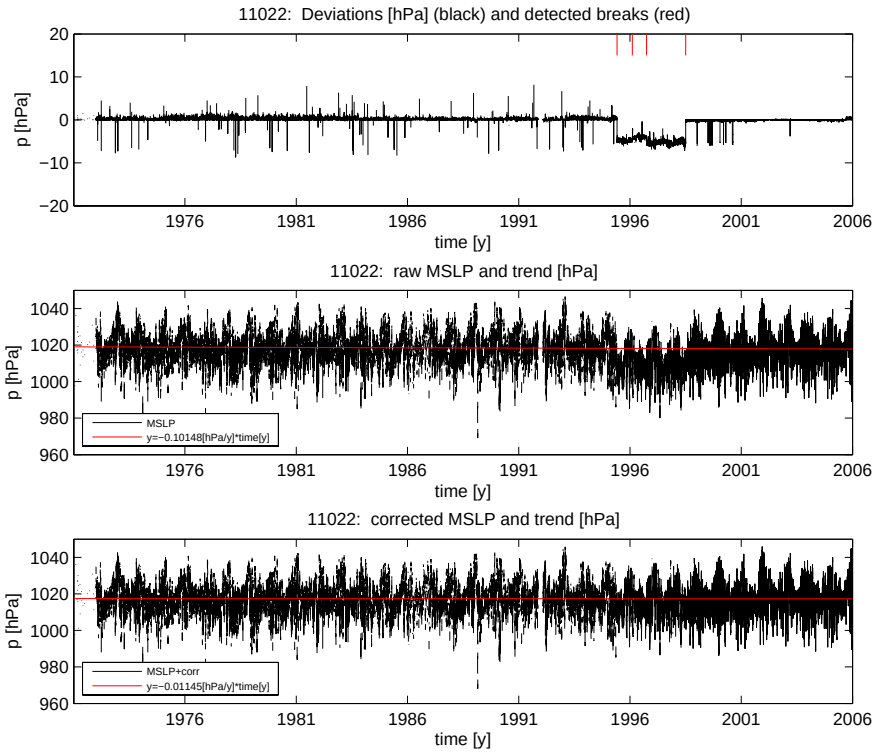

Figure 1: Deviations, uncorrected and corrected MSLP

REFERENCES

Haimberger, L. 2007. Homogenization of radiosonde temperature timeseries using innovation statistics. *Journal of Climate*, **20**(7), 1377–1403.

Steinacker, et al. 2000. A Transparent Method for the Analysis and Quality Evaluation of Irregularly Distributed and Noisy Observational Data. *Monthly Weather Review*, **128**(7), 2303–2316.

RADAR-BASED HAIL CLIMATOLOGY OF EASTERN SLOVENIA

Mark Žagar[1,2] and Benedikt Strajnar [2]

[1] University in Ljubljana, Faculty for mathematics and physics
[2] Environmental Agency of the Republic of Slovenia, Ljubljana, Slovenia
E-mail: *Benedikt.strajnar@rzs-hm.si*

Abstract: Several hail diagnostic and detection methods were applied on the three-dimensional radar reflectivity data. Nominal resolution of the data was 1km in the horizontal as well as in the vertical direction. Most methods use a certain value of the reflectivity as a threshold and combine the information of the temperature profile of the atmosphere to assess the depth of the column with freezing temperatures, an important parameter in the detection algorithms. The temperature profile was taken from the radiosonde data. We have produced a map, showing the 5 year average number of events with probable hail fall over each of 1 km squares covering the NE Slovenia. When sufficiently long data series is used to prepare the climatology it can also be used to provide the probability of hailstorm events in the future. The hail probability estimate based on this study should be used with caution, but can nevertheless present valuable additional information to ease decision making in case of crop and vines insurance and physical protection with nets.

Keywords: *ICAM, radar hail detection, hail climatology*

1 INTRODUCTION

Agriculture largely depends on meteorological and climatic conditions. Extreme weather phenomena comprise spring and summer thunderstorms with hail, which is one of the most limiting factors in agriculture in eastern and north-eastern parts of Slovenia. Lack of sufficiently dense traditional (surface) hail observational network calls for alternative approaches for creation of spatially complete hail climatology. The weather radar is an obvious choice, even though the presence of complex terrain with hills up to 1500 m high does present a certain difficulty for the region of eastern Slovenia due to occultation.

2 DATA AND METHODS

Data used were the 3-dimensional radar reflectivity maps from Slovenian C-band single-polarization weather radar, located at Mt Lisca. In our case only 5 seasons (May-August, 2002 - 2006) were used, primarily due to suboptimal quality of the radar system at Mt. Lisca prior to year 2002. Three methods were designed and applied, mainly following the hail detection algorithms used at other national weather services (e.g. Holleman, I., 2001) and in literature. The method based on the data from Grossversuch hail suppression experiment (Waldvogel et al., 1979; Federer, B., 1986) calculates the probability of hail p using polynomial expression

$$p = -1.20231 + 1.00184 \cdot \Delta h_0 - 0.17018 \cdot \Delta h_0^2 + 0.01086 \cdot \Delta h_0^3 \qquad (1)$$

where Δh_0 is the difference between 45 dBZ echo-top and freezing level height in km. Modified version requires continuous reflectivity exceeding threshold. Another methodology, used at Austrian meteorological service (Gmoser H. et al., 2006), examine columns of 5 km depth with sufficiently high radar reflectivity.

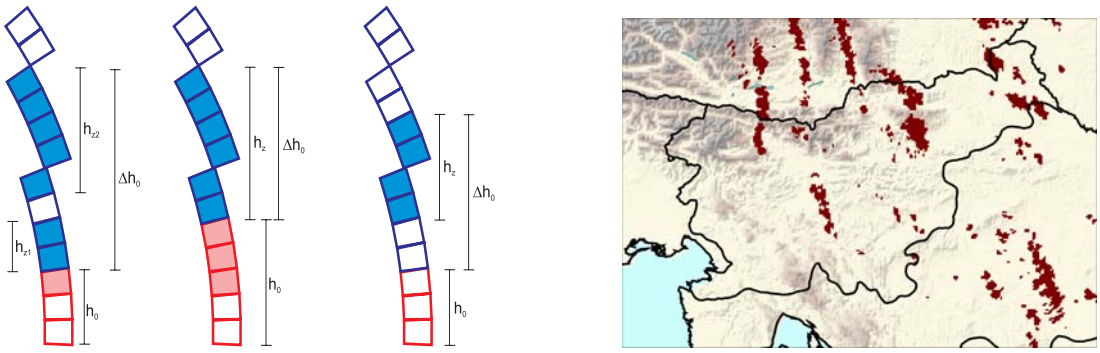

Figure 1. Left: illustration of hail detection. Depending on the method, actual height and extent of high reflectivity columns (solid rectangles) in cold parts of the cloud (blue colours) are parameters which determine hail probability; right: hail occurrence in the stormy day (August 9th, 2004). Daily contributions are summed up to give the climatology maps.

To estimate the freezing level height, Ljubljana radiosoundings (or, if missing, Zagreb or Udine) were used. Verification was performed subjectively from case to case, hail detection products was compared to some available ground measurements and damage reports from newspapers, civil protection etc.

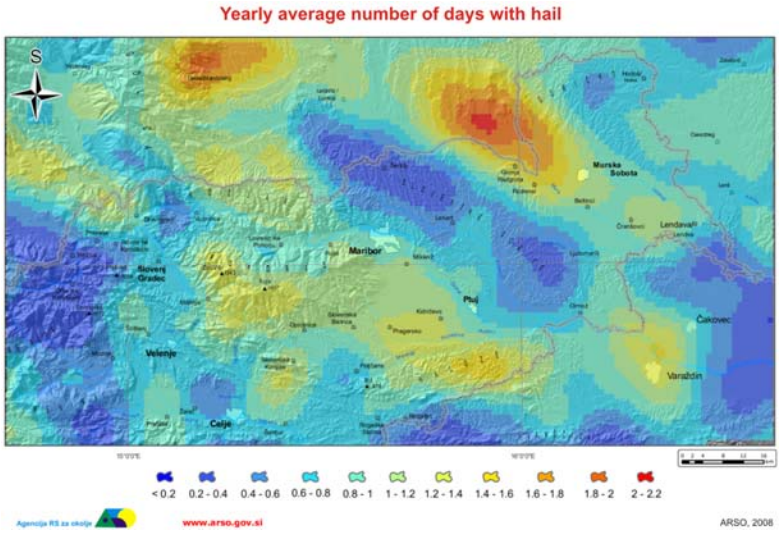

Figure 2. A map of spring and summer hail fall frequency for the period of 2002-2006. The raw map is smoothed by a spatial filter.

3 RESULTS

The results of the radar data analysis are spatial maps of yearly days with occurrence of hailstorms. An example of the product (average over both) is shown in Fig. 2, representing the average number of days in a year a hailstorm occurs over a geographic location of SE Slovenia. In this figure, the results are smoothed by a 5 km filter for reducing noise, i.e. preventing the end users from assuming that the spatial resolution of the product of 1 km is anywhere relevant.
Results show significant spatial distribution of detected hailstorm frequency. While the average is about 1 per year per square kilometer, we also observe values from 0.2 to around 2. These values agree quite well with climatological frequencies in the vegetation period on some Slovenian climatological stations (Dolinar, 2005). Maximums are located over the Drava and Mura river basins and lowlands and regions close to the line connecting them (e.g. Pohorje mountain range). This can be explained by more moisture available for convection. Minimums occur over the hilly regions in between.

4 CONCLUSIONS

The remote sensing derived climatology of hail has many potential sources of error, especially those originating from radar technology, and because it is indirect. But it can help us understand the spatial distribution of hail events. Because of large data set, we decided to focus only on the time period of most frequent hail. There are for sure some missed hail events, especially in September and rarely in other months of the year.
The hail frequency maps are typically meant to enter further algorithms, such as various decision trees in order to obtain a scientifically based estimation of potential economical impact of hail to unprotected crops. Successively, cost of protecting crops (e.g. hail nets or insurance) can be compared to potential damage.
Using also the newest data, this product could for sure be significantly improved in the future.

Acknowledgements
The authors would like to thank Anton Zgonc from Environmental agency of Slovenia for help in preparing radar dataset. This study was supported by Slovenian research agency project no. CRP V4-0359.

REFERENCES

Dolinar M., 2005: Prostorska in časovna analyze neviht in toče v vegetacijskem obdobju (1961-2004). Environmental agency of the Republic of Slovenia, Ljubljana.

Federer, B., A. Waldvogel, W. Schmid, H. Schiesser, F. Hampel, M. Schweingruber, W.Stahel, J. Bader, J. Mezeix, N. Doras, G. D'Aubigny, G. DerMegreditchian, and D.Vento, 1986: Main Results of Grossversuch IV. *J.Appl.Meteor.*, **25**, 917–957.

Gmoser H., Zwatz-Meise V., 2006: Warning System of ZAMG for Austria - Concept and Applications. Subgroup on Regional Aspects of Public Weather Services, Bucurest, 4. – 7. December 2006.

Holleman, I., 2001: Hail Detection using Single-Polarization Radar, KNMI Scientific Report, WR-2001-01.

Strajnar B. and Žagar M., 2007: A radar-based hailstorm climatology for Slovenia. 4th European Conference on Severe Storms, Trieste, 10-14 September 2007.

Waldvogel, A., B. Federer, and P. Grimm, 1979: Criteria for the Detection of Hail Cells. *J. Appl. Meteor.*, **18**, 1521–1525.

An Enhanced Hail Detection Algorithm for the WSR-88D. *Wea. Forecasting*, **13**, 286–303.

SPATIAL VARIABILITY AND TRENDS OF HAILSTORM FREQUENCY AND THE RELATION TO ATMOSPHERIC CHARACTERISTICS IN SOUTHWEST GERMANY

Michael Kunz, Marc Puskeiler

Institute for Meteorology and Climate research (IMK), Universität (TH) / Forschungszentrum Karlsruhe, Germany
E-mail: *kunz@kit.edu*

Abstract: By combining radar reflectivity data with loss data from a building insurance company, hail streaks between 1997 and 2007 are determined for a region that covers most parts of Baden-Württemberg (southwest Germany). In the mean, the hail patterns exhibit a high spatial variability that can be attributed to triggering or amplification mechanisms for convection by orographic features. In the last three decades, hail days and total hail damage have increased significantly due to changes in static stability. Several convective indices that depend upon surface temperature and moisture reveal a positive trend regarding both the annual extreme values and the number of days above/below specific thresholds.

***K*eywords:** *hail, hail damage, climate change, convective indices, low mountain ranges*

1 INTRODUCTION

Severe thunderstorms and associated extreme events, like heavy rainfall, gusts, or hail, pose a significant threat to modern societies and their assets. In the federal state of Baden-Württemberg (southwest Germany), almost a quarter of the total damage on residential buildings is related to large hail, yielding a mean annual loss of around 26.9 Mio €. In the past, single severe hailstorms caused up to 100 Mio € damage to buildings in this region. Loss prevention and risk management purposes require information about the local probability of occurrence of severe hail storms as well as identification of possible trends related to climate change.

2 DATA AND METHODS

Due to their small horizontal extent, convection-related phenomena like hail are usually not captured accurately by one single conventional observation system (Houze, 1993). Therefore, data sets from different observation systems are used to supplement this study: data from a building insurance company (Sparkassenversicherung) to determine hail days and affected regions, radar data to identify hail streaks and to estimate the intensity, and convective indices derived from radiosonde observations (Stuttgart) at 12:00 UTC to assess long-term changes of the convective potential of the atmosphere.

By applying the cell tracking algorithm TRACE3D (Handwerker, 2002) on 3D radar reflectivity data between 1997 and 2007, individual storm tracks are identified for a region that covers most parts of Baden-Württemberg. From this sample, damage-related hail streaks are separated using the insurance loss data that are available for five-digit postal code zones. These streaks are projected on a 10×10 km^2 grid in order to quantify hail track density. By statistical modelling of extremes, a cumulative distribution function (generalized Pareto distribution) is estimated, which relates radar reflectivity and probability of occurrence.

From the Stuttgart soundings between 1974 and 2003, various convective indices are derived that allow to quantify the thunderstorm potential of the atmosphere. In order to estimate long-term changes, different percentiles of the annual frequency distribution (90th, 95th, and 99th percentiles) as well as the number of days per year above/below appropriate thresholds of the indices according to the study of Kunz (2007) are calculated.

3 RESULTS

The identified hail streaks show a significant spatial variability in the occurrence probability that is supposed to be due to orographic influences (Fig. 1, left). Lowest probabilities are found over the rolling terrain in the north as well as over the elevated terrain of Black Forest and Swabian Jura. Between the two mountain ridges, the probability of hail streaks to occur is highest. One may assume that air masses that partly goes around the mountains in cases of southwesterly flow directions favour the development of convergence zones downstream of Black Forest. Also a flow deviation at the upstream border of the Swabian Jura, indicated by a sharp gradient of the hail streaks, may facilitate the formation of convergence zones in this area. Note that the high number of storm tracks behind the northern Black Forest mountains in radial direction to the radar location is an indication that beam shielding at the mountains does not substantially modify the results.

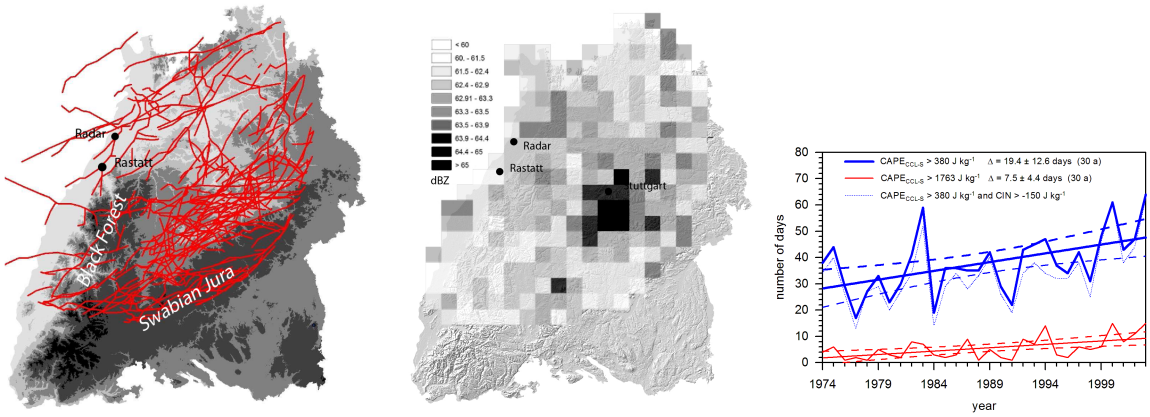

Figure 1: Damage-related hail tracks according to IMK-radar data for a radar reflectivity of $\geq$ 55 dBZ (left) and radar reflectivity for a return period of 1 year (middle), both between 1997 and 2007. Number of days per year with a CAPE above two specific thresholds (solid lines) and for a combination of CAPE and convective inhibition (CIN; thin dotted line) (right).

Considering not only the number but also the intensity of severe thunderstorms in terms of radar reflectivity for specific return periods, does not substantially change the spatial distribution of the hail patterns (Fig. 1, middle). The highest intensities are well correlated with the highest track densities. Again, the lowest values occur over the mountains of Black Forest and Swabian Jura.

By examining atmospheric stability in a 30-year perspective, it is found that most of the commonly used convective indices that depend upon near-surface temperature and moisture reveal a positive trend regarding both the annual extreme values and the number of days above/below specific thresholds. An example is shown in Fig. 1 (right) for the convective available potential energy (CAPE) as integrated from the convective condensation level (CCL) to the equilibrium level (EL) and assuming a surface-based parcel (S) that was lifted. A relationship can be established between the indices and the annual number of hail damage days, yielding correlation coefficients between 0.65 and 0.80 (Kunz et al., 2009). In contrast to this, indices derived from temperature and moisture at higher levels exhibit either a negative or no significant trend. The trend directions of the indices can be attributed to different temperature and moisture stratification in the various atmospheric layers. The significant positive trends of both surface temperature and water vapour can be concisely expressed by an increase in wet-bulb potential temperature. This indicates the presence of warmer parcels throughout the whole troposphere during convection.

4 CONCLUSIONS

Although it is impossible to deduce a direct relationship between orography and hail frequency, local effects like flow channelling or orographically induced wind systems are certainly decisive for the spatial variability of hail streaks. In particular for hot spots as identified in this study, it is very important to know whether severe thunderstorms will further increase in intensity and/or probability in the light of global warming. Even if our analysis provides an indication for an increase of severe thunderstorms in the past decades due to an decrease of static stability, these trends cannot be projected into the future. Hence, the next steps are to apply the methods to reanalysis data and to regional climate simulations to quantify possible changes of the hailstorm potential in the next decades. Both data sets are available at IMK at the very high resolution of approx. 7 km.

Acknowledgements: *We thank the Sparkassenversicherung (SV) for the provision of detailed loss data, Jan Handwerker for providing the radar data and the tracking algorithm TRACE3D, and the German weather service for the provision of the radiosonde data.*

REFERENCES

Handwerker, J., 2007: Cell tracking with TRACE3D, a new algorithm. *Atmos. Res.*, **61**, 15–34.

Houze, R. A., Jr. 1993: *Cloud dynamics, International Geophysics series*, volume **53**. Academic Press. 573 pp.

Kunz, M., J. Sander and Ch. Kottmeier, 2009: Recent trends of thunderstorm and hailstorm frequency and their relation to atmospheric characteristics in southwest Germany. *Int. J. Climatol.*, DOI: 10.1002/joc.1865.

Kunz, M., 2007: The skill of convective parameters and indices to predict isolated and severe thunderstorms. *Nat. Hazards Earth Syst. Sci.*, **7**, 327–342.

ANALYSIS OF SNOW COVER CHARACTERISTICS CHANGE IN SLOVAKIA

Pavol Faško[1], Milan Lapin[2], Jozef Pecho[1] and Katarína Mikulová[1]

[1]Slovak Hydrometeorological Institute, Bratislava, Slovakia, e-mail: pavol.fasko@shmu.sk
[2]Faculty of Math, Phys. and Informat., Comenius Univ., Bratislava, Slovakia, e-mail: lapin@fmph.uniba.sk

Abstract: Snow cover information is very frequently used. For many people it is in the centre of interest during all winter season. On the other hand snow cover is one of the mostly impacted due to ongoing climate change. Recently some increase in winter precipitation has been registered, mainly in the northern Slovakia. This resulted in significant increase of new snow in the high mountain localities at some extreme events (above 1300 m a.s.l.). Such examples are well known not only in Slovakia, but also at many sites in the Alps (the newest events occurred in the 2008/2009 winter). On the other side significant decrease of snow cover days was observed in the lowlands.

There are about 700 precipitation gauges in Slovakia every year since 1951 and some lower number since 1921. In 1980 the Slovak Hydrometeorological Institute decided to create precipitation database, including all snow data (climatologic database is ready for 1961-2008). Altogether 600 station data are complete in 1981-2008. In spite of shorter 30-year period, it is considered long enough to identify principal changes in snow cover during current climate change. This snow cover series is very valuable also for future analysis in some years or decades. In the paper the new and the total sow cover data observed once a day are analyzed. The elaboration brought plenty of characteristics, never issued in Slovakia up to present. Because of existence of limited snow characteristics for the period 1921-2000, some comparisons are included as well. Limited area in the paper enables to present selected information only.

The analysis presented here is focused mainly on the changes in annual regime and territorial distribution of snow cover due to warming of climate and change in precipitation. Very important is the dividing line between the influence of rising temperature and increasing winter precipitation. It is considered that currently it lies about 900 m a.s.l. and it tends slowly to increase. Below this boundary decrease of snow is observed and above it some increase. Finally some extreme events with high new and total snow cover depth are listed. Snow cover analysis is highly important also in prevention of dangerous avalanche events occurring in Slovakia every year.

Keywords: *snow cover regime changes in Slovakia, statistical analysis of snow cover characteristics, long-term changes of liquid, solid and mixed precipitation rate, fresh snow cover depth chages and extremes*

1 INTRODUCION

Analysis of snow cover regime changes within the territory of Slovakia represents the essential goal of this contribution. Snow cover characteristics, such as snow cover depth as well as snow water equivalent, play an important role in different climatological and hydrological analyses and they are widely used in operative meteorological service, particularly during the winter season.

Liquid, solid and mixed precipitation proportion of total precipitation value is considered to be relevant characteristic indicating sufficiently noticeable the long-term changes of temperature as well as precipitation conditions. More precisely the change of regime of particular precipitation state (liquid, solid and mixed) could be used as significant indicator of climate change evidence in specified region. Recently the snow cover extreme events, particularly calamitous flurries of fresh snow are occurring more frequent and theirs impact on society activities are becoming more obvious and serious in Slovakia. Regarding this fact we have decided to prepare a statistical analysis of selected characteristics of snow cover emphasizing the fresh snow cover extremes at particular meteorological stations in Slovakia within the 1951-2009 period.

2 RESULTS AND CONCLUSIONS

The analysis of long-term series of precipitation state ratio (liquid, solid and mixed) at selected meteorological stations has confirmed the existence of positive trend in the case of annual liquid and mixed precipitation rate and on the contrary the negative trend of annual solid precipitation rate in the south as well as north part of Slovakia, including mountain regions (e.g. the High Tatras; Figure 2). Analogous or even more expressive trends of proportion of particular precipitation state have been revealed for individual months as well as for period when solid and mixed precipitation predominate (in the cold half-year). Similarly the results of fresh snow cover depth analysis have shown an expected increase at considered meteorological stations in Slovakia in the winter (e.g. Oravská Lesná, Figure 1). The fresh snow cover depth maxima raking and its temporal occurrence support an exceptional status of the values recorded in the last decade of the 20th century and in the first decade of the 21st century, as well. In the case of n-days sum maxima (particularly 3-, 4- and 5-days sum) of fresh snow cover depth as well as the number of days with higher values of fresh snow cover depth the statistical analysis have preliminarily detected a significant positive trend for the most of territory of Slovakia in the winter (Figure 1).

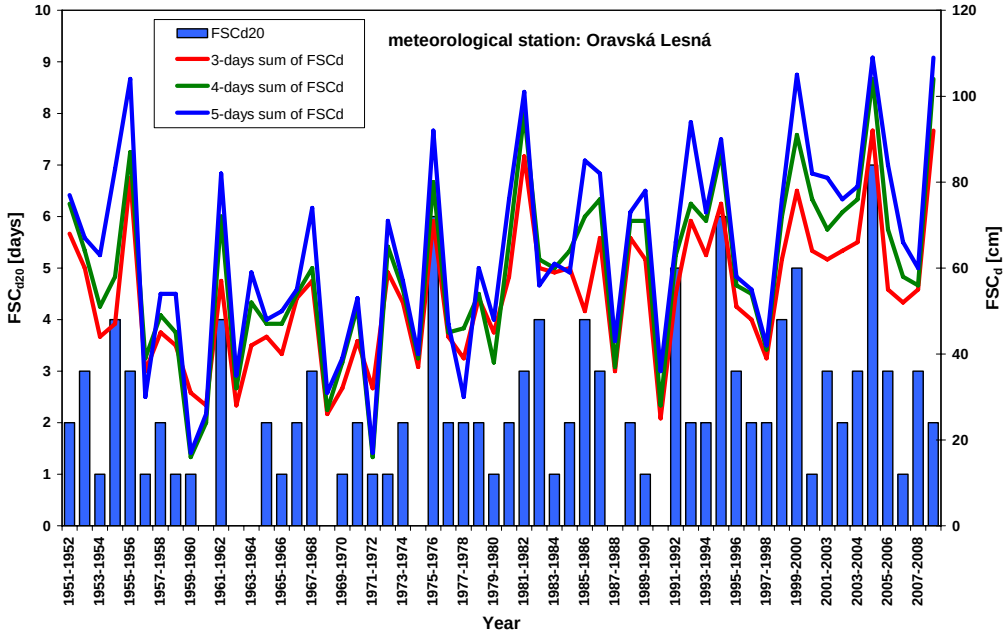

Figure 1. Number of days with fresh snow cover depth ≥ 20 cm (FSC_{d20}) and n-days sum of fresh snow cover depth (FSC_d) at mateorological station Oravská Lesná (780 m a.s.l.) in the 1951/1952-2008/2009 winter.

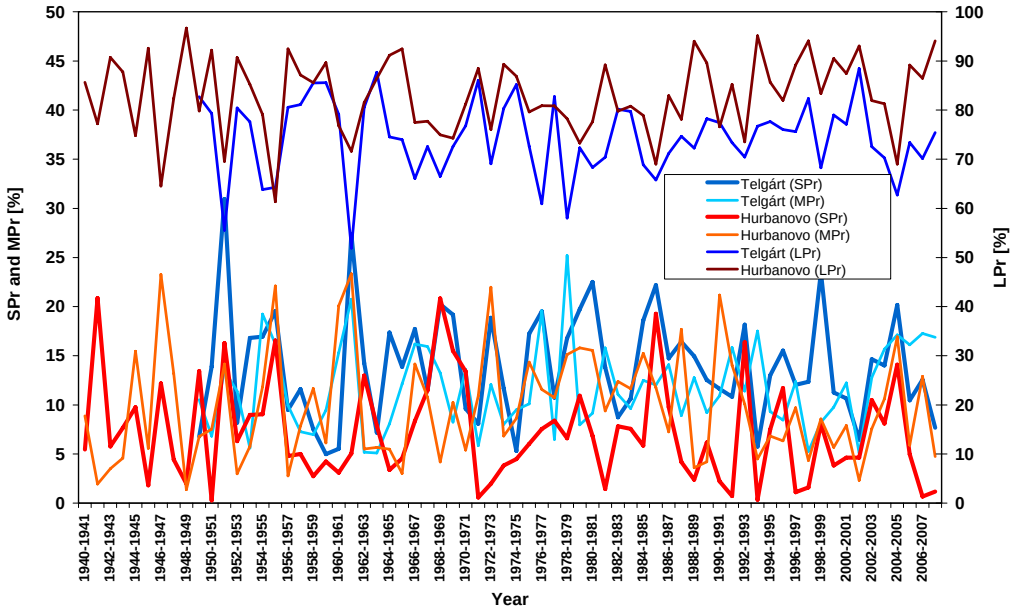

Figure 2. Liquid (LPr), solid (SPr) and mixed (MPr) precipitation rate at meteorological stations Hurbanovo (115 m a.s.l.) and Telgárt (901 m a.s.l.) in the 1941/1942-2008/2009 winter.

Acknowledgements: *We thank all contributors for their cooperation on the paper.*

REFERENCES

Faško, P., Handžák, Š., Lapin, M., 1997. Selected snow cover characteristics change in the Low Tatras region (Slovakia) in 1921-1995. In: National Climate Programme of the Slovak republic. Vol. 7, Slovak Ministry of the Environment and Slovak Hydrometeorological Institute, Bratislava 1997, p. 47-67.

Lapin, M., Faško, P., Pecho, J., 2007. Snow Cover Variability and Trends in the Tatra Mountains in 1921-2006. In: Proceedings of the 29th International Conference on Alpine Meteorology, Chambéry, France, 4.-8.6.2007.

Lapin, M., Melo, M., Faško, P., Pecho, J. (2007): Snow Cover Changes Scenarios for the Tatra Mountains in Slovakia. In: Proceedings of the 29th International Conference on Alpine Meteorology, Chambéry, France, 4.-8.6.2007.

Vojtek, M, Faško, P., Šťastný, P., 2003. Some selected snow climate trends in Slovakia with respect to altitude. In: Acta Meteorologica Universitatis Comenianae 32; p. 17-27.

15 YEARS OF SPECTRAL UV-MEASUREMENTS AT SONNBLICK OBSERVATORY: INVESTIGATION OF SHORT- AND LONG-TERM CHANGES AT AN ALPINE HIGH ALTITUDE STATION

Michael Fitzka, Stana Simic, Philipp Weihs, Helga Kromp-Kolb

Institute for Meteorology, University of Natural Resources and Applied Life Sciences, Vienna, Austria
E-mail: *michael.fitzka@boku.ac.at*

Abstract: Monitoring of spectral UV radiation and total ozone at Sonnblick observatory (3,106 m a.s.l.) is performed since 1994, representing the longest available time series of spectral UV in Austria. A current goal is to quantitatively understand the influence of clouds, ozone and surface albedo on spectral UV. Continuous measurements are examined alongside model calculations (SDISORT). The increases in surface UV during the last decades are calling for more detailed investigations. Long-term trends in UV irradiance are investigated based on clear sky measurements using trend tests. Results from Simic et al. (2008) show significant downward trends for several combinations of solar zenith angle and wavelength, which are apparently caused by an increase in sunshine duration during periods of high values of total ozone. Due to large variations and the serious dependence on various atmospheric parameters, detection of significant trends is notably hampered.

Keywords: *ICAM, UV radiation, ozone, albedo, short-term changes, trend detection, radiation transfer model*

1 INTRODUCTION

Surface UV levels are influenced by the concentration of total ozone and by clouds, surface albedo and aerosols. Knowledge of spectral UV radiation and its dependence on these parameters, which may change in the course of a changing climate, are prerequisites to quantitatively understand and estimate future UV radiation.

Increase of UV radiation during the last decades is reported where a decrease of stratospheric ozone has been observed (Bartlett and Web 2000). The magnitude of this change and their causes are, however, uncertain, calling for more detailed investigations of the influence of clouds, albedo, and other atmospheric parameters (Bais and Lubin et al. 2007). Monitoring of spectral UV exists since the beginning of the 1990ies. Thus, studies on long-term changes are hampered by the limited lengths of available data series (Glandorf et al. 2005).

The present study aims at estimating the impact of changing cloud cover, total ozone and surface albedo on spectral UV irradiance at Sonnblick observatory, using continuous measurements of spectral UV and radiation transfer model calculations. Additionally it is attempted to analyze the measurements of spectral UV irradiance for potentially underlying trends over the measurement period (Simic et al. 2008).

2 DATA & METHOD

Spectral UV irradiance and total ozone are being measured with a Brewer spectrophotometer at Sonnblick observatory since 1993 and an additional Bentham DM150 spectroradiometer since 1997. Brewer data were used for both short- and long-term investigations. Data from the Bentham spectroradiometer were employed in ancillary analysis (e.g. influence of changing snow-line). Cloud observations are regularly performed by the Austrian Weather Service, providing the input data for estimating cloud effects. A semi-empirical algorithm for the reconstruction of albedo based on snow observations was developed and deployed (Simic 2006).

The analysis of short-term changes in surface UV levels is based on a combination of measurements and model calculations (Arola et al. 2003). First off, actual measurements were reconstructed using the radiation transfer model SDISORT. A second data-set was created using a combination of daily climatological means of the model input data along with actually measured data. The variation of UV irradiance due to a specific parameter X (e.g. ozone, albedo, clouds) was then estimated as the ratio of modeled UV using the actual value of parameter X and climatological data of the *remaining* variables to modeled UV using climatological data of *all* variables, including parameter X. The amplitude was calculated as the spread of ratios divided by the mean ratio on a daily and on a monthly basis. The amplitude can then be regarded as the maximum variability due the specific parameter during a day respectively a month.

Long-term changes in surface UV levels were investigated for several combinations of wavelength and solar zenith angle in the time series of monthly deviations from the 13-year climatological mean values of UV irradiance under clear-sky conditions. Trends were identified through the use of regression models (R^2, Theil-Sen estimate) and tested for significance through various trend tests.

3 RESULTS

Throughout the year, ozone is the dominating parameter influencing surface UV levels. On a daily basis, ozone can cause variability of more than 200%, the highest values are found during late winter and spring, the period of the strongest interannual variation in stratospheric ozone. Enhanced cumulus convection surpasses the effect of ozone during summer, daily variability of more than 150% can be reached. Cloud influence is notably reduced during the rest of the year. Additionally, due to the station's high altitude, cloud-layer thickness is smaller, reducing the influence of clouds compared to lower altitude stations (Arola et al. 2003). Albedo has its greatest influence in April. This is the period of snow-melt, causing the snow-line height and therefore albedo to change rapidly. Variability due to albedo can reach a maximum of 32% on a daily basis. On a monthly time-scale, despite being significantly reduced in magnitude, variations show the same behavior throughout the year.

Due to the relatively short time-series and the strong variations therein, only few trends could be reliably identified. Most of the significant changes were found at a solar zenith angle of 55°, representing the data selection criteria yielding the greatest number of available measurements. Trends were only found at wavelengths of 305 nm and higher, as variations are distinctly increasing with decreasing wavelength. Unexpectedly, the significant trends display decreases, rather than increases. This would suggest an increase in stratospheric ozone, but no significant changes were found in the time series starting in 1994.

The decreases my therefore be explained by increasing sunshine duration during spring and summer over the period of investigation: At a solar zenith angle of 55°, an increase of almost 19% per decade is present in the number of available clear-sky spectra over the whole period. At the same time, the increase during January to June is almost 45%/dec. This may explain the observed highly significant downward trends, since more measurements of UV irradiance during higher total ozone concentrations were included in the latter parts of the investigation period. The same behavior is found at different zenith angles, although less pronounced and significant. Tab. 1 summarizes the calculated trends.

SZA	305 nm	310 nm	315 nm	324 nm
45°	-9.5 $^{+}$	-11.1 $^{+}$	-10.5 $^{+}$	-9.8 $^{+}$
55°	-23.9 *	-19.9 *	-15.6 *	-14.4 *
65°	-3.8 $^{-}$	-5.7 $^{+}$	-4.6 $^{+}$	-6.0 $^{+}$

Table 1. Linear trends in relative departures of UV radiance from climatological monthly mean values, trends given in percent per decade, symbols to the right indicate trend significance (-: insignificant, +: significant, *: highly significant).

4 CONCLUSION

Surface UV levels show strong dependencies from the influencing factors ozone, clouds and albedo on different time scales. Seasonal variations in the influencing factors also lead to distinctly varying seasonal impacts on surface UV levels. The knowledge of the factors' contributions to UV variability is a prerequisite for the estimation of surface UV levels and the assessment of UV induced risks for human health, as well as the estimation of future UV levels in the course of a changing climate.

Investigations focusing on long-term changes in spectral UV radiation are still notably hampered by the high variations in the relatively short time-series. Despite being based on one of the longer time-series available today, only precautious statements regarding actual trends in surface UV levels can be given at a decent level of resilience. Longer time-series are a crucial basis for further assessments.

Acknowledgements:
This work has been funded by the Austrian Ministry of Agriculture, Forestry, Environment and Water Management and by the Commission of the European Communities, project "Stratosphere-Climate Links with Emphasis on the UTLS, Scout-03".

REFERENCES

Arola, A., Lakkala, K., Bais, A., Kaurola, J., Meleti, C., and Taalas, P.: Factors affecting short- and long-term changes of spectral UV irradiance at two European stations, J. Geophys. Res., 108(17), 9, 1–11, 2003.

Bais, A., Lubin, D., Arola, A., Bernhard, G., Blumthaler, M., Chubarova, N., Erlick, C., Gies, H., Krotkov, N., Lamtz, K., Mayer, B., McKenzie, R., Piacentini, R., Seckmeyer, G., Slusser, J., Zerefos, C., Feister, U., Fioletov, V., Gröbner, J., Kyrö, E., and Slaper, H.: Surface ultraviolet radiation: past, present and future, Scientific assessment of ozone depletion: 2006, 7(21), 1 – 54, 2007.

Bartlett, L. M. and Webb, A. R.: Changes in ultraviolet radiation in the 1990s: Spectral measurements from Reading, England, J. Geophys. Res.-Atmos., 105(D4), 4889–4893, 2000.

Glandorf, M., Arola, A., Bais, A., and Seckmeyer, G.: Possibilities to detect trends in spectral UV irradiance, Theor. Appl. Climatol., 81, 33–44, 2005.

Simic, S.: Investigations on the transfer of ultraviolet radiation on the Hoher Sonnblick, doctoral thesis, BOKU Vienna, 2006

Simic, S., Weihs, P., Vacek, A., Kromp-Kolb, H., and Fitzka, M.: Spectral UV measurements in Austria from 1994 to 2006: investigations of short- and long-term changes. Atmos. Chem. Phys., 8, 7033-7043; ISSN 1680-7324, 2008.

SATELLITE REMOTE SENSING ASSESSMENT OF CLIMATE RISKS AND IMPACTS ON ROMANIAN MOUNTAIN FORESTS

Maria Zoran

National Institute of R&D for Optoelectronics
Bucharest Magurele, 409 Atomistilor Street, MG 5, 077125 Romania
E-mail: *maria@dnt.ro*

Abstract: During last years, due to anthropogenic and climatic stressors, most Carpathian Mountain forests in Romania had experienced environmental degradation. As in mountain areas, climate changes rapidly with height over relatively short horizontal distances, mountain forests represent unique areas for the detection of climatic change and the assessment of climate-related impacts. Mountain forest landscape pattern and the biogeophysical variables controlling observed patterns can be addressed through time series remote sensing satellite imagery, which provide useful information on spatial variations in physiological characteristics, productivity, successional patterns, forest structure and decline. Multispectral, multiresolution and multitemporal satellite imagery is used to classify and map various forest and/or land-use types. The specific aims of this paper are to: 1) quantify the changes and rates of change between 1990 and 2008 in vegetative composition across a forest landscape in Romanian Carpathians on Prahova Valley using Landsat TM and ETM, MODIS data; 2) examine the changes in landscape structure in relation with climatic changes and extreme events; 3) assess the climate risks and their potential impact on Romanian mountain forests; 4) investigate and discuss the spatio-temporal changes observed in the landscape composition, pattern and structure o in the context of forest management activities and other disturbances. The preservation and enhancement of mountain forest vegetation cover in natural, semi-natural forestry ecosystems is an essential factor in sustaining environmental health and averting natural hazards. In order to decrease the risk for socio-economic impacts, long-term adaptive strategies in modern silviculture seem necessary.

Keywords: *Satellite remote sensing, climate change,. extreme events, Carpathian Mountain forests, Romania*

1 INTRODUCTION

The continuing and accelerating rate of global climate change and its potentially severe impacts on nature and mountain forest ecosystems addresses scientific and policy responses for possible help adaptation to the partly inevitable consequences. Monitoring the vegetation dynamics of the Carpathian Mountains forests in Romania is important for understanding the consequences of climate-driven changes in these areas. The transitional height regions of the mountain forests is expected to be sensitive to even small changes in environmental variables and thus it can offer early insight into potential changes in forest vegetation driven by climate and anthropogenic changes. Climate change is likely to change existing forest systems, as changes in phenology, length of growing season and northwards shift of forest species can be related to climate change (Olesen et al., 2007;IPCC, 2007). The anticipated increase in both climate variability and extreme events may influence forest health and biomass production (Leckebusch et al., 2007). In spite of the potential of adaptive capacity of forest systems to adjust to climate change (Schar, et al., 2004), an increase in the number of hot days, changes to potential evapotranspiration and more frequent occurrence of drought periods will have a direct impact on mountain forest condition. Climate impacts are of increasing concern to societies, particularly in regions with high climatic variability in context of local, regional and global climatic changes.

2 SATELLITE REMOTE SENSING IN FOREST RESEARCH

Satellite remote sensing, based on building spectral databases, global large datasets, refining validation, calibration procedures in multi-source, multi-temporal environment is an important investigation tool of land vegetation and forest cover monitoring at regional, national, and global scales. In order to estimate climate and anthropogenic impacts on forest vegetation, during the last years, satellite imagery has been used for the analysis of bio-geophysical parameters of forest ecosystems as well as for assessment of the soil moisture content, CO_2 (carbon dioxide), O_3 (ozone) and NO (nitrogen oxide) concentrations in forest ecosystems.
As forests act as sinks for carbon dioxide, these play a fundamental role in mitigating climate change, being very vulnerable to changes in meteorological variables as temperature, precipitation and extreme weather events, which can have destructive impacts and reduce the carbon sequestration potential of the forest. On the other hand, forest fires events have an even more negative effect since destroying the forest increases the amount of carbon dioxide in the atmosphere.

3. RESULTS

To evaluate the climate risk and impacts of the management practice on biophysical properties of the mountain forest system, a set of biophysical variables have been estimated from time series Landsat TM ,

ETM+ and MODIS data over 1990 - 2008 period. The data included vegetation indices, surface broadband albedos. To study climatic and anthropogenic impacts , have been done several classifications of forest vegetation (evergreen, mixed , decidous) over tested area- Prahova Valley, located in Southern Carpathian Mountains (Figure 1). Image pairs of the same vegetation index, for subsequent years, were subtracted producing continuous maps indicating areas of change. Statistical analysis was carried out to see if there is a correlation between the two sets of output. The analysis of different classifications over selected test area have shown mountain forest changes due to high levels of atmospheric pollution mainly close of main road traffic air masses dynamics at regional level as well as due to deforestation for land-use conversion.and disease epidemics.

The relationship between phenological development of mountain forests and climate variability is a critical element in understanding current and future impacts of global climate change. Based on Normalized Difference Vegetation Indices (NDVI) derived from satellite data , phenological changes observed in Crapathian temperate forest are strongly related to global climate change. Figure 2 represents NDVI map from MODIS TERRA 16/08/2007 image for Prahova Valley, Carpathian mountain forest test area.Some conclusions have been obtained : average satellite phenology is scalable from fine (IKONOS) to coarse (Landsat) satellite sensors scales, but important fine-grain distinctions (such as microclimates) are lost at coarser scales; interannual phenological variability recorded from MODIS satellites data has a great potential to be used in spectral/climatic models in synergy with in-situ monitoring data of biogeophysical parameters. Based on time series satellite data, continued analyses of interannual phenology will be an effective tool for monitoring mountain forest responses to global-scale climate variability as well as for assessment of climate risks and its impact on mountain environment. Forest cover has also a great impact on local mountain climate.

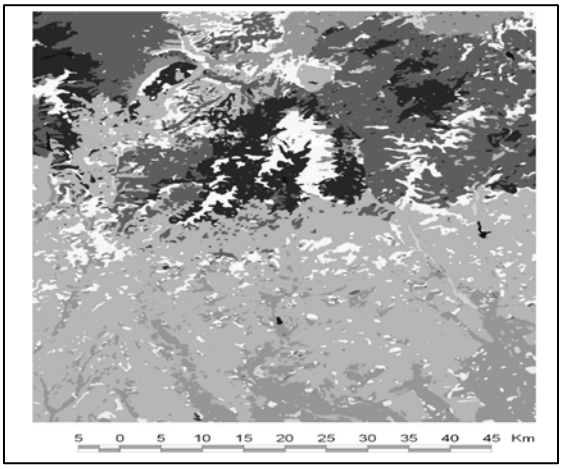

Figure 1. Forest vegetation classification on Landsat ETM+ 16/08/2007 for test area.

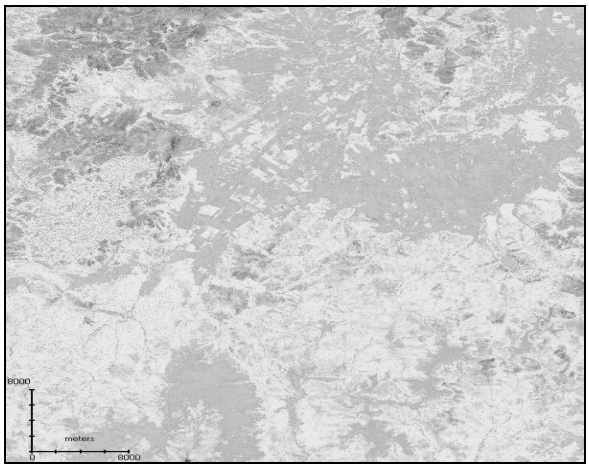

Figure 2. NDVI map from MODIS TERRA 16/08/2007 for Prahova Valley, Carpathian mountain forest test area

4 CONCLUSIONS

As a result of global climate change, there is a growing evidence that some of the most severe weather events could become more frequent in Romania over the next 50 to 100 years. In the case of Carpathian mountain forests, winter storms and heat waves are considered key climate risks, particularly in prealpine and alpine areas. Effects of climate extremes on forests can have both short-term and long-term implications for standing biomass, tree health and species composition. The preservation and enhancement of mountain forest vegetation cover in natural, semi-natural forestry ecosystems is an essential factor in sustaining environmental health and averting natural hazards. Romanian mountain forest system is under continuous influence of characteristic meteorological-climatic fluctuations of continental climate. For a better management and decision making is important to be performed medium and long term changes forecasting.

REFERENCES

Olesen, J., Fronzek, S., Heidmann, T., et al., 2007: Uncertainties in projected impacts of climate change on European agriculture and ecosystems based on scenarios from regional climate models. Climate Change **81**, 123–143.

IPCC (2007): Intergovernmental Panel on Climate Change Working Group II. Climate Change 2007: Impact, Adaptation and Vulnerability. IPC Working Group II [http://www.ipcc.ch].

Leckebusch, C.G., Ulbrich, U., Fro¨ hlich, L., Pinto, J.G., 2007: Property loss potentials for European midlatitude storm in a changing climate. Geophysical Research Letters 34, 05703.

Schar, C., Vidale, P.L., Lu¨ thi, D., Frei, C., Ha¨ berli, C., Liniger, M., Appenzeller, C., 2004: The role of increasing temperature variability in European summer heat waves.Nature 427, 332–336.

EEA Report No 4/2008, Impacts of Europe's changing climate - 2008 indicator-based assessment.

TRENDS IN HEAVY PRECIPITATION IN MOUNTAINOUS AND LOWLAND AREAS IN CENTRAL EUROPE: ARE THE DIFFERENCES RELATED TO CHANGES IN CIRCULATION?

Jan Kysely[1]

[1] Institute of Atmospheric Physics AS CR, Prague, Czech Republic
E-mail: *kysely@ufa.cas.cz*

Abstract: Trends in winter-time indices of heavy precipitation are evaluated at rain-gauge stations covering the Czech Republic over 1961-2005. The study focuses on differences between mountainous and lowland areas and other regional patterns. For all characteristics of heavy precipitation, spatially coherent increasing trends are identified; they are more pronounced in the western than eastern part of the country, with relative magnitudes mostly between +20 and +30% over the 45 years. The increases in heavy precipitation are generally stronger at sites in higher-elevated and mountainous regions that are windward in prevailing southwestern to northwestern flows, which points to the fact that changes in the frequency and intensity of zonal circulation play important roles in governing changes in precipitation extremes. The analysis partly supports an emerging global picture of prevailing positive trends in precipitation extremes over the mid-latitudinal land areas of the Northern Hemisphere in winter. However, the differences between mountainous and lowland regions and the cut-off between the western and eastern parts of the Czech Republic indicate that (i) the observed trends are to a large extent driven by changes in zonal circulation, and (ii) the pattern of changes becomes more complex and less coherent in regions where the changes in zonal circulation play less important role.

Keywords: *heavy precipitation, trend analysis, atmospheric circulation, central Europe*

1 INTRODUCTION

Trends towards higher frequency and intensity of winter-time precipitation extremes have been found in many extratropical regions of the world, including western and central Europe (e.g. Moberg and Jones 2005; Hundecha and Bardossy 2005; Schmidli and Frei 2005). The present study evaluates regional patterns of trends in various indices of heavy precipitation, and differences between mountainous and lowland areas, using high-quality dataset from rain-gauge stations covering the Czech Republic. For details concerning quality of the data, methodology used, results for other seasons and their interpretation refer to paper in *International Journal of Climatology* (Kyselý 2009).

2 DATA AND METHODS

Daily precipitation totals measured over 1961-2005 at 175 stations are used as an input dataset. The altitudes of stations range from 150 to 1322 m a.s.l. There were no significant station displacements during 1961-2005, and the daily series of precipitation records are uninterrupted.

Common indices are selected to characterize various aspects of the intensity of heavy precipitation events in winter (DJF); they include maximum seasonal *k*-day precipitation amounts, 'rain intensity index' (RII), defined as the mean precipitation amount per wet day, and percentage of total precipitation falling on days above long-term seasonal 90th and 95th percentiles of daily amounts (%P90, %P95).

Non-parametric Kendall's tau is used to estimate linear trends; statistical significance of the trends is evaluated by the Mann-Kendall test.

3 RESULTS

Increasing trends dominate over the western part of the Czech Republic in all indices of heavy precipitation in winter (Fig. 1). The trends are positive at about 90% of stations, and approximately one third of them are significant at p=0.10. For rain intensity index (RII), the positive significant trends appear at 50%/36% of sites if evaluated at p=0.10/0.05. Relative magnitudes of the trends are usually between 3 and 10% per 10 years, but they exceed 10% per 10 years at about one tenth of sites for the *k*-day winter maxima, and at one fifth (two fifths) of sites for the percentage of precipitation occurring on days above the long-term seasonal 90th (95th) percentiles (%P90, %P95). In most characteristics, the positive trends are more pronounced and spatially more uniform in the south (the Vltava river basin) than the north areas (the Elbe river basin) of the western region. For some of the indices (e.g. R5, %P90), relatively large areas appear in the southwest where all (or nearly all) locations posses increasing trends that are significant at p=0.10.

Over the eastern part of the Czech Republic, increasing trends are more frequent than decreasing ones for most indices of heavy precipitation (except for RII), but they are insignificant and spatially incoherent. The fraction of positive trends significant at p=0.10/0.05 does not exceed 12%/9% in any characteristics of extremes.

Increases prevail in the mountainous and highland areas while decreases or trends close to zero in the lowland regions, mainly in the eastern part of the country. This appears to be related to the enhanced influence of windward slopes under

more frequent and intense zonal circulation in winter (cf. Jacobeit et al. 2001). The spatial pattern of trends in heavy precipitation in winter is also linked to trends in mean precipitation which are increasing in the western part of the country while there is no clear trend (with decreases being more frequent) in the eastern region (Kyselý 2009).

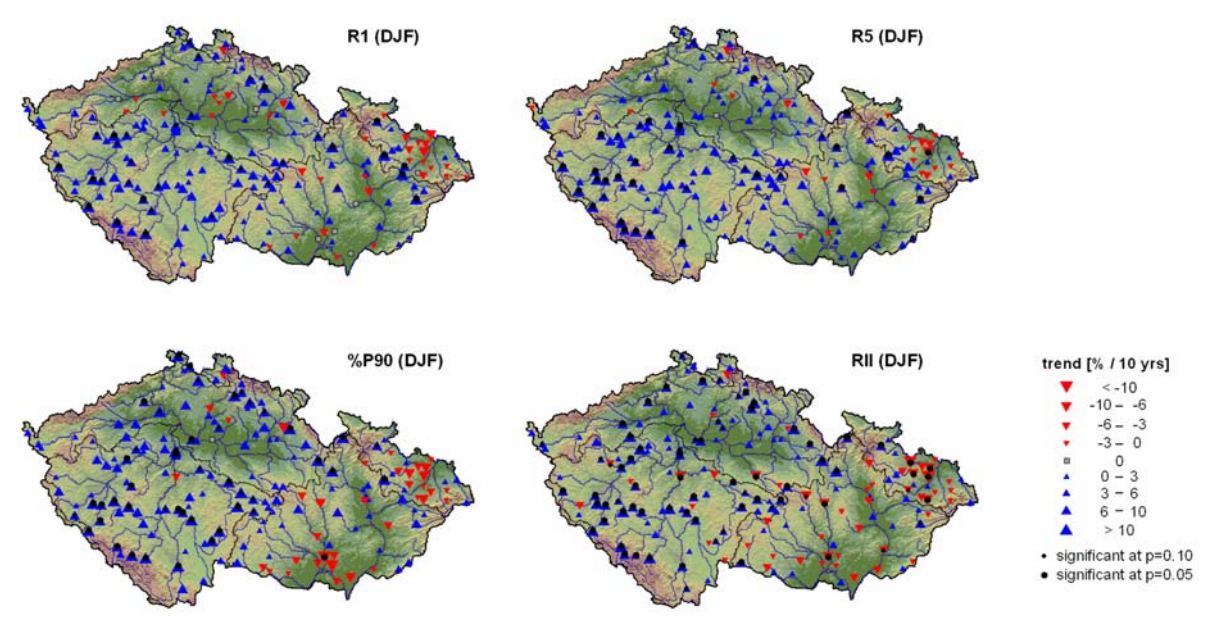

Figure 1. Trends in characteristics of heavy precipitation in winter. Increasing (decreasing) trends are marked by ▲(▼).

4 CONCLUSIONS

Spatially coherent and statistically significant increasing trends have been identified for all indices of winter-time heavy precipitation in the western part of the Czech Republic. This finding is in accord with results for relatively nearby regions in Germany (Hundecha and Bardossy 2005), Switzerland (Schmidli and Frei 2005) and northern Italy (Brunetti et al. 2001). The mean rise of 21-26% over the 45 years for 1-day to 20-day winter maxima (averaged over the stations), and 30-35% for the fraction of precipitation falling on days exceeding the long-term 90th and 95th percentiles is relatively large compared e.g. with the centennial increases in high quantiles and the seasonal 1- to 10-day extremes in Switzerland, which were between 10 and 30% in winter (Schmidli and Frei 2005). However, this change is the only widespread and spatially uniform trend in heavy precipitation over all seasons, and it is not clearly observed in the eastern part of the Czech Republic where Mediterranean influences play more important roles in producing heavy precipitation events. The trends are generally more pronounced in the western than eastern parts of the country and in mountainous than lowland sites, which suggests that the increases are linked to the modes of the North Atlantic climate variability (e.g. the North Atlantic Oscillation) and changes in the intensity of the zonal circulation.

Acknowledgements: *The study was supported under project B300420801 of the Grant Agency of AS CR. Thanks are due to O.Halásová, Czech Hydrometeorological Institute, Hradec Králové, for drawing the maps, and P.Štěpánek, Czech Hydrometeorological Institute, Brno, for providing the daily precipitation dataset and performing quality checks.*

REFERENCES

Brunetti M, Maugeri M, Nanni T. 2001. Changes in total precipitation, rainy days and extreme events in northeastern Italy. *International Journal of Climatology* **21**: 861-871

Hundecha Y, Bardossy A. 2005. Trends in daily precipitation and temperature extremes across western Germany in the second half of the 20th century. *International Journal of Climatology* **25**: 1189-1202

Jacobeit J, Jönsson P, Bärring L, Beck C, Ekström M. 2001. Zonal indices for Europe 1780-1995 and running correlations with temperature. *Climatic Change* **48**: 219-241

Kyselý J. 2009. Trends in heavy precipitation in the Czech Republic over 1961-2005. *International Journal of Climatology*, doi: 10.1002/joc.1784.

Moberg A, Jones PD. 2005. Trends in indices for extremes in daily temperature and precipitation in central and western Europe, 1901-99. *International Journal of Climatology* **25**: 1149-1171

Schmidli J, Frei C. 2005. Trends of heavy precipitation and wet and dry spells in Switzerland during the 20th century. *International Journal of Climatology* **25**: 753-771

SCENARIOS OF AIR HUMIDITY AND SATURATION DEFICIT CHANGE FOR SLOVAKIA

Milan Lapin and Martin Kremler

Faculty of Mathematics, Physics and Informatics, Comenius Univ. in Bratislava, Slovakia
E-mail: lapin@fmph.uniba.sk, kremler@fmph.uniba.sk, Web: www.dmc.fmph.uniba.sk

Abstract: About 30 meteorological stations in Slovakia have complete and good quality observations since 1951 (1961). Most of them well represent important sub-regions, like the Danubian lowland and area round the Tatra mountain. The paper presents detail daily air humidity and daily saturation deficit analysis from 6 stations in 1961-2008, including some information on air temperature and humidity (5 of those stations lie in the Tatra mountains, Hurbanovo in the lowland). In 2007 the newest Canadian CGCM3.1 model with daily data outputs have been analyzed (IPCC emission scenarios SRES-A2 and B1 applied). Based on the CGCM3.1 outputs the scenarios of daily data in 1961-2100 are presented for selected stations.

Keywords: *measured air humidity, Canadian GCM3.1 outputs, modeled humidity data, modeled evapotranspiration.*

1 INTRODUCTION

Temperature increase by 1.6°C and precipitation decrease by 25 mm (3.1%) was registered in Slovakia in the 1881-2008 period. On the other hand annual relative air humidity means decreased in the lowlands by 5% since 1901. This decrease was less significant in the mountains. Water vapor pressure had insignificant trend in 1901-2008 in all year round with some lower values in 1976-1993. Significant increase in air temperature and changes in precipitation occurred in Slovakia predominantly after 1985. These changes influenced regime of air humidity, potential (E_o) and actual (E) evapotranspiration, soil moisture and runoff mainly in southern Slovakia. For example, E_o increased at Hurbanovo (lowland, 115 m a.s.l.) by 17.5% in 1951-2008.

2 METHOD AND RESULTS

Saturation deficit (d) enables to calculate monthly E_o sums by several methods (Lapin et al. 2008). A common formula can be expressed as $E_o = k.d$, where k is a coefficient different for any month and any region. The CGCM3.1 based scenarios of E_o were are calculated using simple Zubenok formula and saturation deficit (d – difference between saturated and actual water vapor pressure). Selected data and humidity scenarios from the CGCM3.1 outputs downscaling for Slovakia are in Tables 1 and 2.

Modeled d means will increase up to 2100, both at A2 and B1 scenarios. More intense increase is modeled for A2 scenario (Table 2), in the April to September season (Growing season – GS) 2071-2100 up to 20% compared to period 2001-2030 (up to 40% trend in 1961-2100), and only by 8% at the B1 scenario (up to 17% trend in 1961-2100). If the A2 scenario will fulfill, the increase in E_o can reach even 25-30% in the GS compared to 1951-1980 averages. The d and E_o increase will be less significant in the mountains (Table 2 and Figure 1).

Because of insignificant change in precipitation totals is supposed (some small decrease is more probable in the lowlands), it is expected a decrease in soil moisture up to 25% and runoff decrease up to 25% in Slovakia. The presented method of water balance related variables calculation can be applied also for other Slovak localities with sufficiently reliable data on air humidity and temperature.

Acknowledgement:
Some parts of this paper are based on the results of project VEGA No. 1/4033/07 and the observed SHMI data.

Table 1. Deviations of Growing Season (GS = April to September) mean values in selected periods between SRES A2 and SRES B1 scenarios and between SRES A2 scenario and measured averages in 1961-1990 (T – air temperature, e – water vapor pressure, U – relative humidity, Hurbanovo, 115 m a.s.l., Strbske Pleso, 1360 m a.s.l.).

Station	Element		1961-1990	1991-2020	2021-2050	2051-2080	2071-2100	1996-2025	2016-2045	2061-2090
Hurbanovo	T (A2-B1)	[°C]	0.0	0.2	0.0	1.1	1.7	0.2	0.2	1.0
Hurbanovo	T (A2-M)	[°C]	0.0	0.7	1.8	2.8	3.9	1.0	1.7	3.2
Hurbanovo	e (A2-B1)	[hPa]	0.0	0.0	0.1	0.8	1.5	0.0	0.0	1.0
Hurbanovo	e (A2-M)	[hPa]	0.1	0.6	1.5	2.5	3.5	0.7	1.3	2.9
Strbske Pleso	U (A2-B1)	[%]	0.0	-0.9	0.0	-0.9	-1.0	-0.6	-0.9	0.0
Strbske Pleso	U (A2-M)	[%]	0.6	0.4	-0.2	0.5	-0.2	0.0	-0.5	0.7
Hurbanovo	U (A2-B1)	[%]	0.0	-1.1	0.2	-0.6	-0.7	-1.2	-0.8	0.2
Hurbanovo	U (A2-M)	[%]	-1.0	-1.8	-1.5	-1.4	-1.6	-2.1	-1.9	-0.9

Table 2. Mean values of Growing Season (GS) saturation deficit *d* [hPa] in selected periods (Mean – average of daily $d = e^* - e$; MeMax – average of GS maxima in daily *d*; e^*, *e* – saturated and actual atmospheric water vapor pressure 2 m above ground; M1961-1990 – based on measurements, other columns – modified CGCM1.3 SRES A2 model values, A2-B1 – difference of *d* between Mean SRES A2 and Mean SRES B1, selected periods represent the scenarios frames used in Slovakia).

Station Altitude	*d* [hPa]	M1961-1990	1961-1990	1991-2020	2021-2050	2051-2080	2071-2100	1996-2025	2016-2045	2061-2090
Poprad	Mean	**4.0**	**4.1**	**4.4**	**4.8**	**4.9**	**5.3**	**4.5**	**4.9**	**5.0**
695 m	MeMax	11.3	11.2	12.4	13.9	14.2	14.4	13.0	14.0	14.4
	A2-B1		0.0	0.2	0.1	0.5	0.6	0.1	0.2	0.4
Telgart	Mean	**3.0**	**3.2**	**3.4**	**3.8**	**3.9**	**4.2**	**3.5**	**3.8**	**3.9**
901 m	MeMax	9.2	9.7	10.6	12.4	12.4	12.5	11.3	12.3	12.5
	A2-B1		0.0	0.2	0.1	0.5	0.5	0.1	0.2	0.3
Lipt. Hradok	Mean	**4.3**	**4.5**	**4.7**	**5.2**	**5.3**	**5.7**	**4.9**	**5.2**	**5.4**
640 m	MeMax	12.9	12.4	13.4	15.2	15.1	15.5	14.2	15.2	15.2
	A2-B1		0.0	0.2	0.1	0.5	0.7	0.2	0.2	0.4
Strbske Pleso	Mean	**3.1**	**3.2**	**3.4**	**3.8**	**3.9**	**4.2**	**3.5**	**3.8**	**3.9**
1360 m	MeMax	11.1	11.3	12.4	14.0	14.7	14.5	13.0	14.1	14.8
	A2-B1		0.0	0.2	0.0	0.4	0.6	0.1	0.2	0.3
Sliac	Mean	**5.0**	**5.2**	**5.5**	**6.0**	**6.2**	**6.6**	**5.7**	**6.0**	**6.3**
313 m	MeMax	13.2	13.2	14.3	15.7	16.1	16.4	14.9	15.8	16.0
	A2-B1		0.0	0.2	0.1	0.6	0.8	0.2	0.3	0.5
Hurbanovo	Mean	**6.5**	**6.6**	**7.1**	**7.6**	**8.0**	**8.7**	**7.3**	**7.7**	**8.2**
115 m	MeMax	17.6	17.1	18.1	19.8	21.8	22.0	18.9	19.9	21.8
	A2-B1		0.0	0.4	0.0	0.7	1.1	0.3	0.2	0.7

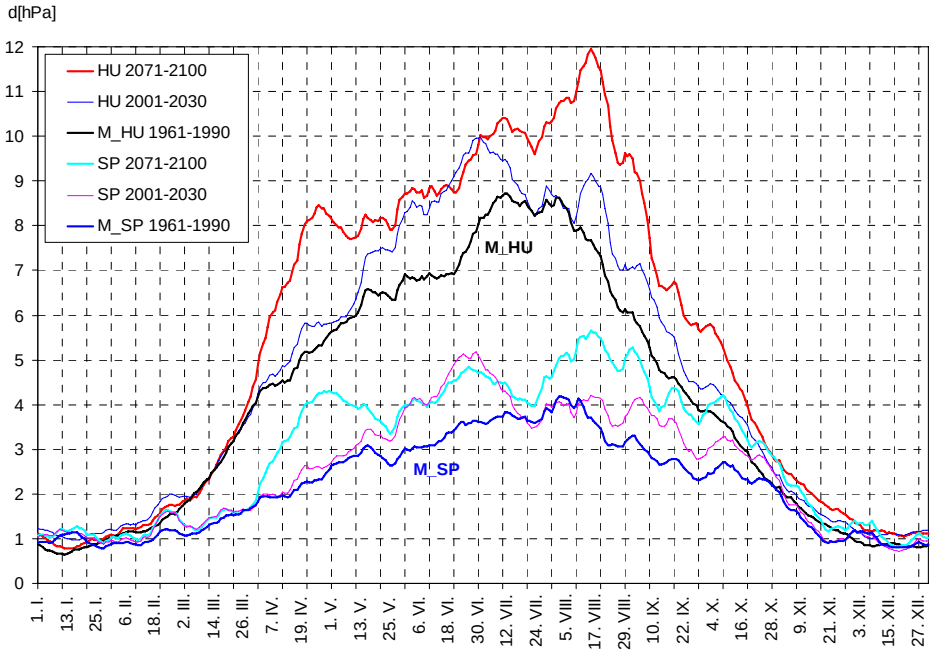

Figure 1: Annual patterns of mean saturation deficit *d* [hPa] at Hurbanovo (HU 115 m a.s.l.) and Strbske Pleso (SP 1360 m a.s.l.), measured (M) in 1961-1990 and modeled in 2001-2030 and 2071-2100 (modified CGCM3.1 SRES A2 model outputs), all 11-day running means, significant d increase is supposed mainly in the April to September season (GS).

REFERENCES

Boer, G. J., Flato, G. & Ramsden D., 2000: A transient climate change simulation with greenhouse gas and aerosol forcing: Projected climate to the twenty-first century. Climate Dynamics, 16: 427–450.

Halmova, D., Melo, M., 2006: Climate change impact on reservoir water supply reliability. IAHS – AISH Publication, Wallingford, 308, 407-412.

Lapin, M., Drinka, R., Kremler, M., Tomlain, J., 2008: Scenarios of Air Humidity and Potential Evapotranspiration Change for Hurbanovo, 16 pp. In: CD Proc. of the XXth Czecho-Slovak Bioclimatological Conference, Mikulov, Czech Republic.

Recommendation on calculation of evaporation from the continent surface 1976. Utverzhdeny GUGMS, Min. melioracii i vodnogo khozyajstva SSSR, Min. seljskogo khoz. SSSR. Gidrometeoizdat, Leningrad. (in Russian)

Étude de l´Impact de la Variabilité du Climat et des Changements Climatiques sur la Guinée-Bissau.

Cherno Luis Mendes

Direction Générale de la Météorologie Nationale de la Guinée-Bissau
E_mail: Cherno_lm@yahoo.fr;

Resumé

Les changements climatiques (augmentation de température, réduction de pluviométrie) qui puissent affecter directement la régénération naturelle des forêts ou les facteurs anthropiques persistants comme le feu de brousse abusifs des aires forestières il aura par conséquent une réduction du revêtement végétal, ce qui obligera les autorités à prendre des mesures de réduction ou de suspension de licences de sciage qui à la fois réduira la production des sciages, menant par conséquent à la réduction de la production des charpenteries et la disparition de certains. Compte tenu de l'évolution de la dégradation du moyen naturel comme conséquence des changements climatiques au niveau national, les entreprises forestières verront certainement leur aires d'exploitation (abattages) réduites à un pourcentage drastique ou à 50 %, ou encore dans une situation de crise majeure de dégradation de forêts voir leur licences supprimés.

1. Introduction

Les services météorologiques nationaux doivent orienter ses actions dans une perspective d´appui au développement socio-économique et coopération international, pour permettre sauver la vie humaine et des biens matériels, la défense civil et l´appui à une large spectre des activités économiques, tels que la agriculture et la production alimentaire, la navigation aérienne, la pêche, et la navigation maritime, la gestion des ressources hydriques, l'industrie, l´énergie, le tourisme et la gestion et protection de l´environnement etc. Les observations climatiques qui permet de caractériser les éléments du climat sont : la température, l'humidité relative, la précipitation l'insolation, le vent etc.

2. La vulnérabilité des secteurs et les impacts des changements climatiques sur ces secteurs, surtout dans les systèmes de production.

Pour ce que concerne la température, et selon le même rapport, les projections pour l'horizon 2100 se traduit dans une augmentation de 2 °C, avec des intervalles de variations de 0,1 à 8,2 °C.

En se basant sur la connaissance del' écologie et les limites de tolérance de certains cultures plus pratiquées dans le pays, on a constaté qu'une augmentation de la température et de pluviométrie qui dépassent les limites de tolérance de ces cultures entraînant des altérations significatives dans la floraison, rendement, odeur, goût, etc. selon les cas. Pour ce qui est de la température, et si on considère que les maximum atteint les entre 32 à 39 °C (mars/mai) et les minimum 20 à 24 °C (décembre à février), une augmentations de 2 °C à l'horizon 2100 déchaînerait possiblement des augmentations de l'ordre de 34 à 41 °C, dans les mois chauds, et 22 à 26 °C pour les mois moins chauds.

Dans ces circonstances, les cultures d'acajou et les horticoles seraient dans des conditions adverses de développement, puisqu'ils dépasseraient les limites de tolérances hydrique et environnementale, parce que la floraison et récolte de acajou devraient coïncider avec les mois de mars, avril et mai. La production horticole serait aussi menacée pourvu qu'elle commence dans les mois novembre jusqu'à mai et juin. De ce fait, la culture serait la plus affectée avec des altérations des températures prévues pour l'horizon 2100, suivie de celle de l'horticole.

3. Température

Les conséquences de l'augmentation des concentrations des gaz à effet de serre les températures moyennes globales ont été obtenues à l'aide du GCM MAGIC/SCENCE. Pour la projection des réchauffements globaux pour les latitudes de la Guinée-Bissau pour l'horizon 2050 et 2100, toutes les sensibilités ont présenté des graduations de valeurs positives dans des conditions du scénario de l'émission IS92a par rapport à la valeur normale 1961-1990. En utilisant les sensibilités 1, 5, 2,5 et 3,5 °C pour l'horizon 2050, le model prévoit une augmentation de température de l'ordre de 1,1 à 1,5 °C et pour l'horizon 2100 une augmentation de 2 °C avec intervalles de variations 0,1 à 2,8 °C.

4. Precipitation

En Guinée-Bissau il a été remarqué une baisse de la pluviométrie, passant de 6 à 5 mois dans l'année (juin à octobre), au contraire des années précédentes. Actuellement, les pluies presque accompagnées de vents forts engendrent des dégâts dans les plantations et cultures. Selon les informations obtenues à partir du service météorologie nationale, les niveaux attendus de diminution de pluviométrie pour l'horizon 2100 seraient d'environ 11,7 %.

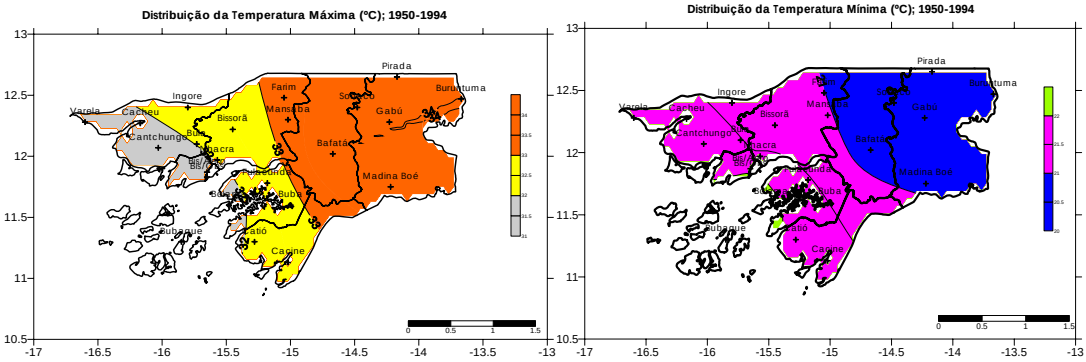

Fig. 1 (a) : Distribution de la température maximale et minimale pour la Guinée-Bissau (période 1950-1994)

Par rapport à ce paramètre climatique, il serait possible d'observer deux situations : notamment des situations des valeurs minimales et maximales. Les spéculations sont faites à partir des valeurs moyennes considérées plus basses. Dans cette situation, une diminution de 11,7 % de pluviométrie produirait une diminution des valeurs minimales de 117 mm dans la zone nord et centre et 176 mm pour la zone sud et les îles. Cela implique que les pluies passeraient de 1000 mm pour 883 mm dans la zone nord et centre, et de 1500 mm pour 1325 mm pour la zone sud et les îles. Si on suit le raisonnement, même, pour les valeurs maximales de 1500 et 2000 mm, il y aurait de même, une diminution de pluviométrie de 1500 pour 1583 mm dans la zone nord et centre, et de 2000 par 1825 mm pour la zone sud et les îles. Donc, la pluviométrie projetée pour l'horizon 2100, malgré sa tendance de diminution, ne posera pas de danger en termes quantitatifs dans le secteur de l'agriculture. De même pour un scénario plus pessimiste, les valeurs estimées se situeront entre 883 et 1383 mm, quantités valables pour une production agricole, dans les conditions d'une bonne distribution du point de vue spatio-temporelle.

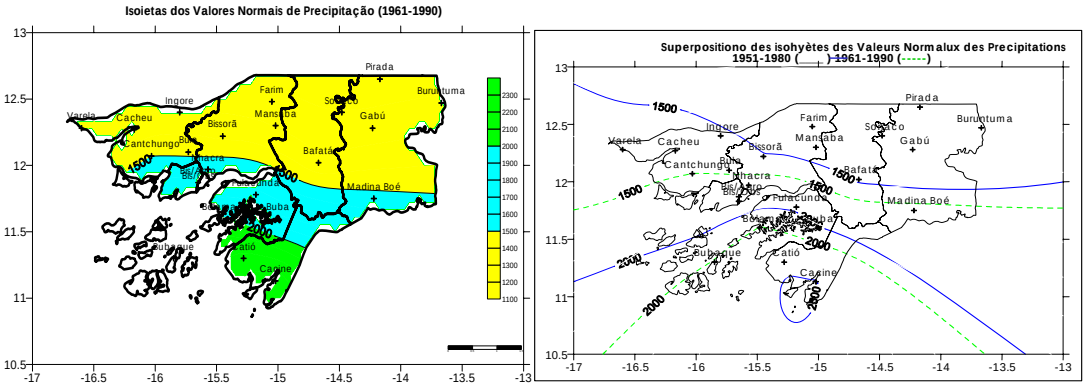

Fig. 2 (b) : Graphiques de la distribution de la pluviométrie et de sa décalage vers le sud de la Guinée-Bissau (période : 1961-1990)

5. Conclusion

Malgré la grande pression dont les forêts guinéennes sont cibles, elles représentant une importante source de séquestration du CO2 atmosphérique, dont la valeur est calculée à 11.288.401 kilotonnes. L'étude de cas, dans le cadre de l'option de mitigation dans le secteur forestier, pour une petite superficie d'une peu plus de mille kilomètres carrés, illustre bien cette capacité de séquestration, la quantité de carbone séquestrée, suite à l'atténuation est estimé à 883.207.649 tonnes (huit cents quatre vingt trois millions, deux cents sept mille et six cents quarante neuf tonnes), en 40 ans d'application des mesures d'atténuation (2005-2044).

D'une manière générale, les données de l'inventaire des GES prouvent que la Guinée-Bissau est loin d'être un pays polluant et émetteur de ces gaz, ce qui laisse conclure que sa part dans l'échauffement global est dérisoire, cela, dans les conditions où les facteurs socio-économiques responsables par les émissions ne s'aggravent pas, ce qui suppose l'adoption des mesures qui tendent à limiter ces émissions.

6. Bibliographie

2006 : Communication Nationale Initiale de la Guinée-Bissau sur les Changements climatiques pp-220.

MODELLING OF NOCTURNAL DRAINAGE WINDS AT METEOR CRATER, ARIZONA USING KLAM_21

Meinolf Kossmann[1], Sebastian W. Hoch[2], C. David Whiteman[2], Uwe Sievers[1]

[1] Deutscher Wetterdienst, Offenbach am Main, Germany. E-mail: *meinolf.kossmann@dwd.de*
[2] Department of Meteorology, University of Utah, Salt Lake City, UT, USA

Abstract: Nocturnal airflow conditions at Meteor Crater, AZ are simulated with the single-layer drainage wind model KLAM_21 to support interpretation of field observations taken during the METCRAX 2006 campaign. A heat budget analysis is conducted to estimate the contribution of intrusions on the bulk nocturnal heat loss inside the crater.

Keywords: *meteor crater, drainage winds, flow splitting, cold air pooling, heat budget*

1 INTRODUCTION

The single-layer cold air drainage model KLAM_21 of the Deutscher Wetterdienst (Sievers, 2005; Kossmann and Sievers, 2007) is used to simulate nocturnal drainage winds at Arizona's Meteor Crater. Results are compared with observational data gathered during the METCRAX 2006 field campaign (Whiteman et al., 2008), which included frequent vertical soundings inside and outside of the crater. The crater is located on the Colorado Plateau about 40 km east-southeast of Flagstaff, AZ. In the vicinity of the crater, the Colorado Plateau is inclined from southwest (Mogollon Rim) to northeast (Little Colorado River) and mostly covered by rocks and bare soil. The depth and the diameter of the crater at the rim are approximately 170 m and 1.2 km, respectively. The crater rim is about 30 to 60 m above the level of the surrounding Colorado Plateau.

Model simulations for idealised nights with no ambient wind have been carried out in a 75 km x 75 km domain with a grid resolution of 50 m in the 10 km by 10 km inner grid and a 250 m resolution outside the inner grid (Fig. 1). Prescribed, spatially and temporally constant local heat loss rates of 30, 20, and 15 W/m^2 were used to account for variations in nocturnal cloud cover.

2 RESULTS

In agreement with observations (Savage et al., 2008), the model simulates the development of regional scale southwesterly drainage winds down the Colorado Plateau, although modelled wind speeds are somewhat lower than those observed. Due to the terrain elevations of the crater rim, these southwesterly drainage winds are deviated around the crater, which is associated with flow deceleration due to blocking and flow splitting on the windward side and flow convergence on the leeward side, while flow acceleration is found on the northwestern and southeastern sides of the crater (Fig. 2). Under cloud-free conditions (30 W/m^2 run) the depth of the southwesterly drainage winds exceeds rim height about 2.5 hours after sunset. The resulting flow of cold air over the rim into the crater generates jet winds above the rim and disturbs the previously decoupled conditions inside the crater (Fig. 2). The 20 and 15 W/m^2 runs simulate the onset of inflow about 3.5 and 5 hours after sunset, due to a slower growth of the depth of the regional southwesterly drainage winds.

Inside the crater the results for all model runs show downslope winds converging towards the crater bottom and a continuously growing cold air lake with extremely weak winds. After the onset of inflow the single-layer physics of KLAM_21 causes all cold air crossing the crater rim to subside into the crater, leading to an accelerated growth of the cold air lake inside the crater. In contrast, observations inside the crater show the development of a two-layer thermal structure early in the night, which is characterised by a strong, approximately 30 m deep temperature inversion at the crater bottom and an almost isothermal layer aloft which extends to rim level (Fig. 3). During the course of the night this two-layer structure is maintained while the crater atmosphere is cooling continuously and a temperature jump develops at rim level. The maintenance of the near-isothermal layer in the crater is indicative to the presence of turbulent mixing processes in the upper part of the crater atmosphere throughout the night. This mixing possibly results from wind shear near rim level and from drainage wind detrainment at the crater sidewalls (Whiteman at al., 2009).

The total nocturnal heat deficit and associated heat loss rates in the crater were estimated from both, model outputs and observations. While the prescribed local loss rates are of similar magnitude as those estimated by Hahnenberger (2008) from vertical temperature soundings outside the crater, it appears that the advective contribution of inflow to the total heat loss inside the crater is clearly overestimated by the model KLAM_21. This finding supports the indirect conclusion that a significant amount of cold air crossing the crater rim is flowing over the crater, while only a fraction of this air actually subsides into the crater, thereby contributing to heat loss in the crater (Fig. 3).

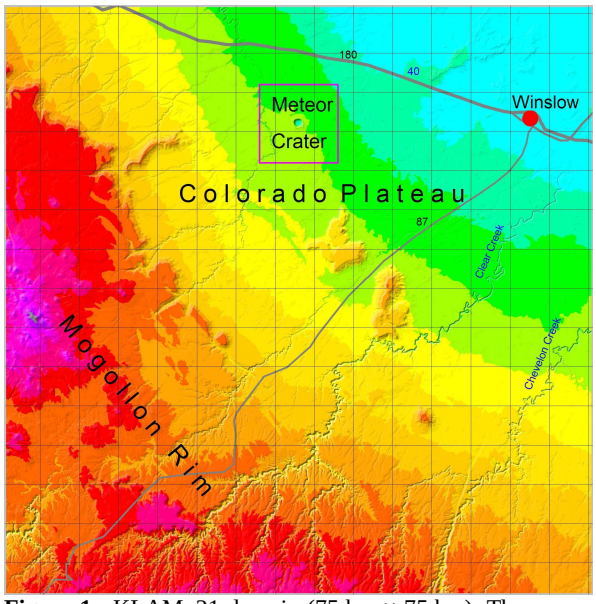

Figure 1. KLAM_21 domain (75 km × 75 km). The square shows the 10 km × 10 km nested high resolution area centred at the crater. Colour shading indicates terrain height with 75 m height intervals.

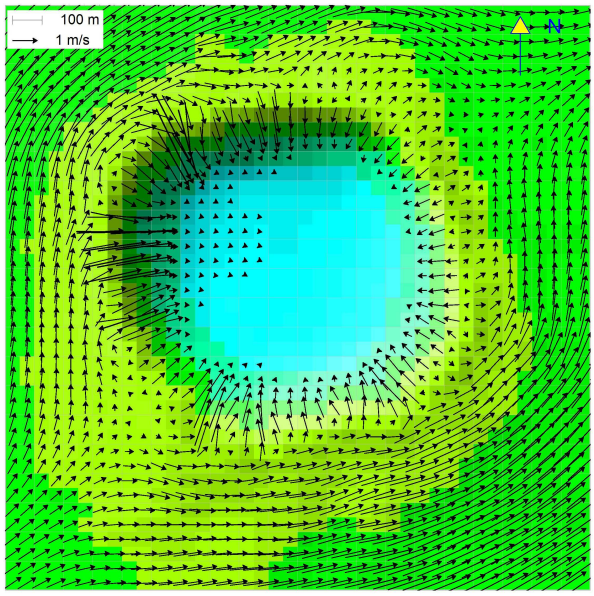

Figure 2. Mean wind vectors in the cold air layer at 3h after onset of surface cooling (30 W/m^2 run). 'Sun shading' is superimposed on the colour shading of the terrain elevation (50 m height intervals) to enhance relief visualisation.

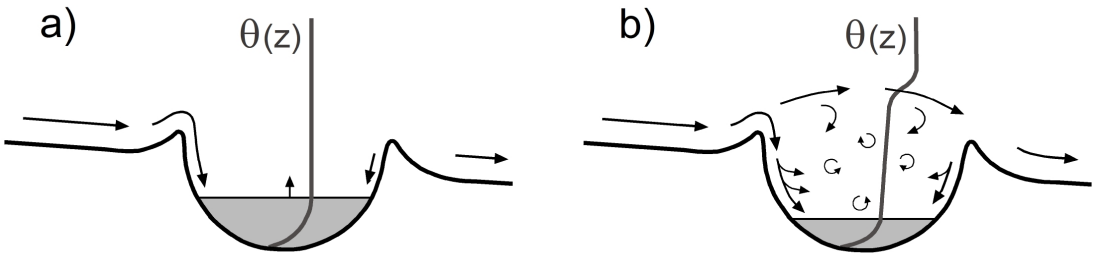

Figure 3. Influence of regional drainage wind intrusions on boundary layer structure and heat loss in the Meteor Crater. The schematic representations illustrate results from KLAM_21 (a) and a hypothesised real world behaviour (b).

3 CONCLUSIONS

Regional southwesterly drainage winds approaching the Meteor Crater and favourite locations of intrusions into the crater are well captured by the KLAM_21 simulations. However, the simulation of the multi-layer structure observed inside the crater is beyond the capabilities of the single-layer drainage wind model KLAM_21. A bulk heat budget analysis of the crater atmosphere suggests that the contribution of inflow to the total heat loss inside the crater is overestimated by KLAM_21. It is therefore hypothesised that a significant fraction of the cold air crossing the crater rim is flowing over the crater and not contributing to heat loss inside the crater. To test this hypothesis, future work will include the evaluation of vertical wind profiles observed within and above the crater and conduction of model simulations with ambient winds of varying speed and direction.

Acknowledgements:
We thank all contributors to METCRAX 2006 for their engagement in the field campaign and data evaluation.

REFERENCES

Hahnenberger, M., 2008: *Topographic effects on nighttime cooling in a basin and plain atmosphere*. MSc thesis, Department of Meteorology, University of Utah, 87 pp.

Kossmann, M. and U. Sievers, 2007: KLAM_21 drainage wind modelling of wintertime air pollution events in Christchurch, New Zealand. *Proc. 29th International Conference on Alpine Meteorology*, Chambery, France, 29–32.

Savage, L.C., S. Zhong, W. Yao, W.O. Brown, T.W. Horst, and C.D. Whiteman, 2008: An observational and numerical study of a regional-scale downslope flow in northern Arizona. *J. Geophys. Res.* 113, D14114, doi:10.1029/2007JD009623.

Sievers, U., 2005: Das Kaltluft-Abfluss-Modell KLAM_21. Theoretische Grundlagen, Anwendungen und Handhabung des PC-Modells. *Berichte des Deutschen Wetterdienstes* 227.

Whiteman, C.D., et al., 2008: METCRAX 2006 – Meteorological experiments in Arizona's Meteor Crater. *Bull. Amer. Meteor. Soc*. 89, 1665-1680.

Whiteman, C.D., S.W. Hoch, and M. Lehner, 2009: Nocturnal cold air intrusions at Arizona's Meteor Crater. *Proc. 30th International Conference on Alpine Meteorology*, Rastatt, Germany.

MINIMUM TEMPERATURES CLASSIFICATION AT THE PYRENEES AREA USING EMPIRICAL ORTHOGONAL FUNCTIONS (EOF)

Josep Ramon Miró, Meritxell Pagès

Meteorological Service of Catalonia, Barcelona, Spain
E-mail: *jrmiro@meteo.cat*

Abstract: In order to forecast temperature in complex terrain areas is important to determine the most likely areas to have Cold Air Pool (CAP) formation. In this work Empirical Orthogonal Functions (EOF) were used to determine the spots where the temperature trends to cool more than the surroundings.
The EOF decomposition is applied to the minimum temperature time series obtained from Automatic Weather Stations (AWS) located in different altitudes along the Segre Valley in the Pyrenees. The EOF decomposition separates the original time series among its variation patterns, which is useful to separate the different sources of variation.

Keywords: *Complex terrain temperature, Empirical Orthogonal Functions, Cold Air Pool, Valley*

1 INTRODUCTION

The idea is to classify the different valleys in order to understand the mechanisms of Cold Air Pool (CAP) formation that are related with the shape and the drainage of these valleys (Eisenbach et al, 2003). The EOF is used to determine where in a valley CAP formation is likely to have (Lundquist et al, 2008). Decomposing the temperature time series among the EOF, it explains the principal variability patterns of the minimum temperatures across the time and the space. As a first work the Segre Valley is analyzed here; this valley has several zones with different shapes and it's very interesting to explore the different temperature behaviour. Moreover, in this valley there are an enough number of temperature sensors that provide us a good knowledge of the temperature behaviour in it.

2 DATA AND METHODOLOGY

2.1 Location

Pyrenees range extents longitudinally 435 km, from Biscay Gulf in the Atlantic Ocean to the Mediterranean Sea, of which 220 km belong to Catalonia in the eastern area where the study takes place. Pyrenees separate the Iberian Peninsula from the rest of Europe, supposing a barrier to advections, especially those from the north. The Segre Valley was chosen due to this valley has different basins and is surrounded by high peaks.

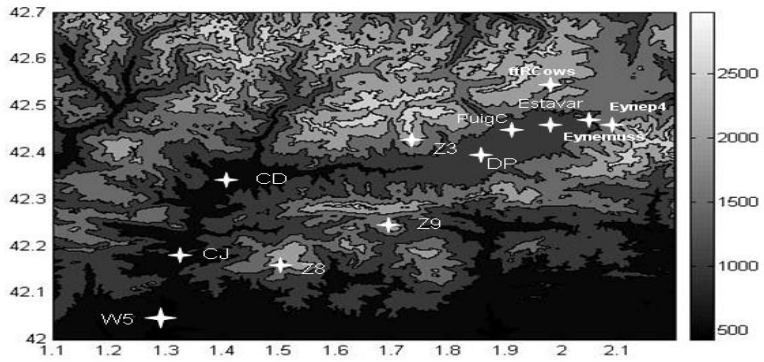

Figure 1. The Segre Valley. The crosses represents the AWS

2.2 Data

The data used was the daily minimum temperatures of different automatic weather stations located both in the top of the mountain and in the floor of the valley (Table 1).

Puigc.	DP	CJ	W5	CD	Z3	Z9	Z8	Estavar	Eyne4p	EyneMus	FtrCows
1210	1097	566	506	849	2310	2149	2300	1268	2305	1559	2111

Table 1. Most Name of the AWS and its height above sea level.

The data was provided by AWS: DP (Das), CJ (Organyà), W5 (Oliana), CD (La Seu d'Urgell), Z3 (Malniu), Z9 (Cadí Nord) and Z8 (Port del Compte), by a Manual Weather Station: Puigc (Puigcerdà) and data recorded by Hobos in an experimental campaign in the Pyrenees: Estavar (Estavar), Eyne4p (Eyne), EyneMus (Eyne) and FtrCows (Font Romeu) (Pepin and Kid, 2006). The data used was from November 2003 until May 2005.

2.3 Methodology

According to (Lundquist et al, 2008), the minimum temperature was decomposed in:

$$T(\vec{x},t) = \overline{T}(\vec{x}) + \overline{T'}(t) + \tilde{T}(\vec{x},t) + \varepsilon \qquad (1)$$

Where $\overline{T(\vec{x})}$ is the mean annual temperature, $\overline{T'}(t)$ is the temporal deviations through measurements and $\tilde{T}(\vec{x},t)$ the local variations through time. $\tilde{T}(\vec{x},t)+\varepsilon$ was decomposed in EOF applying Singular Value Decomposition (SVD). The first EOF is related with days likely that have likely have cold air pools and inversions. Then to discriminate between CAP zone, no-CAP zone or no signal, we choose an adequate threshold for the different spatial weights obtained from the first EOF.

3 RESULTS

A map indicating likely CAP regions, no-CAP regions and no-signal regions are obtained across de Segre Valley (Fig 2)

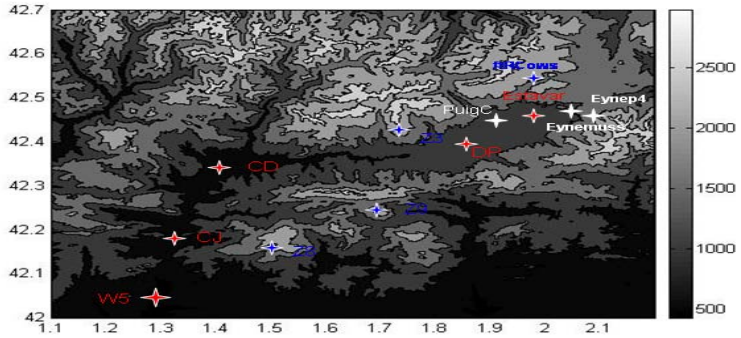

Figure 2. Classification of CAP (red crosses), no-CAP (blue crosses) and no-signal (white crosses)

4 CONCLUSIONS

The results obtained are good and self consistent, but more future works is needed to determine the relationship between the valley shape and the CAP formation. The future work will focus the characterize the CAP with GIS techniques and to relate it to the results obtained with EOF.

Acknowledgements: *We thank Nicholas Pepin and Jessica Lundquist for help us in developing our study and to provide us all we needed. Also we thank Jordi Cunillera, for his support in carrying out our study. Also we want to thank Mònica Herrero, Marc Prohom, Jessica Amaro, Laura Barberia for help us in obtain the data stored in the Meteorological Service of Catalonia.*

REFERENCES

Eisenbach, S., B. Pospichal, C. D. Whiteman, R. Steinacker, and M. Dorninger. 2003. "Classification of Cold Air Pool Events in the Gstettneralm, a Sinkhole in the Eastern Alps." Presented at the International Conference on Alpine Meteorology and MAP, May 18-23, 2003, Brig, Switzerland

Whiteman, C. D., 2000: Mountain Meteorology. Fundamentals and Applications. Oxford University Press.

Lundquist, J.D., N. Pepin, and C. Rochford, 2008. Automated algorithm for mapping regions of cold-air pooling in complex terrain, J. Geophys. Res., 113, D22107

Pepin, N., and D. Kidd (2006), Spatial temperature variation in the eastern Pyrenees, Weather, 61, 300– 310

Lundquist, J.D., N. Pepin, and C. Rochford, 2008. Automated algorithm for mapping regions of cold-air pooling in complex terrain, J. Geophys. Res., 113

FOG WATER COLLECTION WITH SFC DURING THE PERIOD 2000-2008

Marina Mileta

Meteorological and Hydrological Service of Croatia
E-mail: *mileta@cirus.dhz.hr*

Abstract: The highest meteorological station in Croatia, Zavizan (1594 m a.s.l.), is equipped with SFC (standard fog collector). Zavizan is situated on the Velebit Mountain which is the natural boundary between maritime and continental climate. The methodology used was described in Schemenauer and Cereceda (1994). Fog water collection started in the summer 2000. The paper discusses the daily fog water amounts collected during the warm part of the period 2000-2008. Fog water collected in days without precipitation are analysed separately. .Maximum one day – value was 27.8 l / m² while the highest daily rate in days without rain was 19.0 l/m². The maximum highest rates are collected in October, month with maximum days with fog.

Keywords: ICAM, *fog water, mountainous area ,Croatia*

1 INTRODUCTION

The highest mountain meteorological station in Croatia, Zavizan was located on Northern Velebit with a very severe climate. The results of meteorological data from Zavizan included fog water and detailed discussion on the problem of measurements was published in a meteorological monograph (2003), celebrating the 50th anniversary of the weather station. The measurements of fog water in Croatia using Grunow type of fog collector (for the 30-year period) and using the standard fog collector SFC were presented by Mileta (1998, 2003). This paper presents the results of fog water collection by SFC for the period 2000-2008 during the warm part of the year.

2 EXPERIMENT PROCEDURE

2.1 Measurement site and setup

The weather station Zavizan equipped with the SFC was located at the foot of Vucjak Hill on Northern Velebit, 1594 m above sea level (45°49' N, 14°59' E). According to the distribution of wind directions, east is the most frequent wind direction at Zavizan. This wind is a strong bora wind as a consequence of postfrontal cold air advection. The methodology used was described in Schemenauer and Cereceda (1994), and is based on the use of a standard fog collector (SFC) of 1 m² of polypropylene mesh. The results presented here are the daily fog water amounts collected during different long periods in the warm part of 9-year period (2000-2008). The measurements lasted until the air temperature became negative.

3 RESULTS

The daily fog water amounts in the period 2000-2008 during the warm part of the mentioned years have been measured. The data were obtained between July 27 and November 10 in 2000, May 16 and September 27 in 2001, June 26 and October 25 in 2002, July 3 and October 10 in 2003, during June and September (13-24) in 2004, between May 1 and August 31 in 2005, and June 2 and October 17 in 2006, between May 29 and October 12 in 2007 and between May 14 and September 16 in 2008. Maximum daily collected fog water was at the end of October and November, months with maximum days with fog. The maximum one-day value was 27.8 l/m² on October 8, 2003. The highest daily collection rate in days without rain was 19.0 l/m² on October 16, 2002. Synoptic situation on October 7, 2003 was characterised by west upper air current with advection of moist air from Atlantic and on October 16, 2002 was southwest upper current with advection of moist air from Mediterranean.

Tab. A	MAJ			JUN			JUL			AUG			SEP			OKT			NOV		
	SFC	H	%	SFC	H	%	SFC	H	%	SFC	H	%	SFC	H	%	SFC	H	%	SFC	H	%
2000							0,3	1,9	15,8	1,4	7,0	20,0	80,0	247,4	32,3	177,7	278,3	63,9	102,5	211,5	48,5
2001	24,5	36,2	67,7	37,4	153,6	24,3	34,5	67,3	51,3	8,2	10,4	78,8	87,8	241,9	36,3						
2002				14,3	43,5	32,9	21,0	56,0	37,5	99,8	370,4	26,9	128,5	409,4	31,4	165,9	102,1	162,5			
2003							9,0	16,4	54,9	16,6	17,3	96,0	78,2	114,5	68,3	88,2	95,7	92,2			
2004				61,5	104,3	59,0	-			-			44,9	168,8	26,6						
2005	77,1	168,1	45,9	17,4	44,0	39,5	46,9	86,1	54,5	92,1	267,9	34,4									
2006				36,9	97,5	37,8	22,3	80,9	27,6	75,3	247,5	30,4	-			27,1	10,8	250,9			
2007	27,6	47,1	58,6	46,3	130,8	35,4	16,6	26,8	61,9	50,8	193,9	26,2	94,9	258,2	36,7	38,4	12,9	297,3			
2008	46,9	108,1	43,4	41,6	139,5	29,8	10,6	47,6	22,3	18,1	33,1	54,5	32,5	22,8	142,5						

Tab. B	MAJ	JUN	JUL	AUG	SEP	OKT	NOV
	SFC	SFC	SFC	SFC	SFC	SFC	SFC
2000			0,1	.	5,7	32,0	-
2001	7,5	1,2	4,4	2,2	1,2		
2002		4,0	4,4	2,3	5,4	35,5	
2003			0,8	0,3	7,3	7,2	
2004		0,9	-	-	1,0		
2005	0,9	1,6	3,4	10,8			
2006		1,6	0,4	0,5	-	24,9	
2007	.	3,1	2,7	2,6	2,2	2,6	
2008	2,3	1,4	2,5	2,1	0,6		

Table 1. **A** The amounts of fog water collected with standard fog collector (SFC), amounts of precipitation collected with the Raingauge (H) and fog water contribution with respect to rain (%). **B** The amounts of fog water in days without rain.

3 CONCLUSION

The fog water collection on the Velebit Mountain shows that there is a great potential of fog water resource. These results represent opportunities for the restoration of the degraded vegetation after a forest fire. The highest amounts of fog water were collected in autumn when maximum of precipitation occurs. It is caused by the cyclonic activity in this part of the year. The maximum one-day value was 27.8 l / m² on October 8, 2003. The highest daily collection rate in days without rain was 19.0 l/m² on October 16, 2002. Synoptic situation on October 7, 2003 was characterised by the west upper air current with advection of moist air from Atlantic and on October 16, 2002 was the southwest upper current with advection of moist air from Mediterranean.

At the meteorological stations on the Adriatic cost are installed the dew condensers. It is interesting to note that, even in dry conditions such as during the summer 2003, dew continues to provide a consistent (and sometimes only available) amount of water. The installation of dew condenser at the mountain station Zavizan has been planning which could reveal more information about potential of atmospheric water resource.

REFERENCES

Mileta, M., 1998: Fog precipitation on the mountain in Croatia, First International Conference on fog and fog collection, Vancuver, 20-24 July 1998, 413-416.

Mileta, M., 2003: Special Measurements of precipitation and fog water, Zavižan among snow, wind and sun. Meteorological Monography (in Croatian with English summary), Zagreb, 181-190.

Mileta, M., 2004: Results from fog water collection on Mt. Velebit in Croatia, 3rd International conference on fog, fog collection and dew. Cape Town 11-15 October 2004, H4.

Schemenauer, R.S., Cereceda, P., 1994: A proposed standard fog collector for use in high elevation region. Journal of Appl. Meteo., 33, 1313-1322.

THE APPLICATION OF THE COUPLED MODEL IN THE NUMERICAL SIMULATION OF THE LOCAL RADIATION FOG

Lin-lin QI, Xiao-dan WANG and Jian-hua SUN

Institute of Atmospheric Physics, Chinese Academy of Sciences, Beijing, China
E-mail: *niceqll@mail.iap.ac.cn*

Abstract: Fog occurrence is one of the most important events that can lead to low visibility and thus cause casualties and the loss of properties. An effective forecasting method rests upon a perfect initial field and a comprehensive model of the phenomena. The 3D fog model coupling with the MM5 is used to simulate the local winter radiation fog in Chongqing and Changsha respectively. The results show that the unilaterally coupled model can reproduce the circulation and the heavy radiation fog. Especially, the occurrence, location, dissipation and concentration of fog are in accordance with observation. So it is feasible to apply the 3D fog model, coupling with the MM5, in the forecast of fog.

Keywords: *fog, mesoscale model, 3D fog model, unilaterally coupling*

1 INTRODUCTION

Reinforcing the research on the genesis mechanism and structural feature of fog and improving the detection and forecast of fog have become a very urgent task of meteorologic department. Previous studies show that the three-dimension fog numerical model considers the impacts of more factors, adapts to simulate small-scale fog in complicated terrain, approximately describes fog law, needs a relatively short runtime, and thus becomes a good tool to forecast microphysical characteristics of small-scale or single-point fog. However, the model is designed for local fog, and needs the information of atmospheric stratification to run in fixed-point region. Currently, spatial and temporal scales of sounding data used to reflect the information of atmospheric stratification are too sparse, which can not satisfy real-time forecast of local fog. At the same time, a large number of studies (Dong Jianxi et al., 2006; Zhou Mei et al., 2006) show that with the development of mesoscale model, it has also been widely applied to regional fog forecasting. But due to the generality of model, most forecasts provided by mesoscale model are regard to the characteristics and evolution of regional fog. It does not apply to local and rapid, fixed-point forecast of fog. It can be seen that the method coupling fog model with mesoscale model can not only provide the initial field of higher spatial and temporal scales for mesoscale model, but also take the advantages of fog model in the physical mechanism and feedback mechanism of fog. It will be an important direction of development to promto the ability of fog forecasting. Therefore, in the paper we attempt to conduct the research on fog forecasting coupling the MM5 with the three-dimension fog model in order to discuss the feasibility of the application in fog forecasting. It can further provide a basis for operational forecast.

2 BRIEF INTRODUCTION OF MODEL AND SCHEME DESIGN

We simulate the radiation fogs in Chongqing and Changsha, carry out the study of fog forecasting using the MM5 coupling with the three-dimension fog model. Specific simulation program design is as follows: (1) Mesoscale model MM5 uses two-way interactive nested grid. In the experiments, two domains with a grid spacing of 18 and 6 km are nested. The center of model in Chongqing is (29.52°N，106.49°E), the one in Changsha is (28.1°N，113°E). The initial-boundary value uses 1 ° × 1 ° NCEP reanalysis data corrected objectively by the ground and upper-air data. The simulated times respectively are 0000UTC 22 January 2003 ~ 0000UTC 23 January 2003 (Chongqing) and 0000UTC 12 December 2003 ~ 0000UTC 13 December 2003 (Changsha), output frequency is 6 hours.(2) The fog model uses 30 by 30 point staggered grid, grid spacing is 5 km. To reduce effects of lateral boundary, 3 horizontal grids close to the boundary are as extensional grids of model. There are 19 layers in the vertical direction, they are respectively 0, 2, 6, 15, 30, 50, 75, 100, 125, 150, 200, 250, 350, 450, 550, 700, 900, 1200, 1500 m.(3) The initial fields, terrain and standing vegetation of the fog model are from the output of the MM5 domain 2 in order to couple the MM5 with the fog model in one-way mode. The simulated times of Chongqing and Changsha respectively are 1200UTC 22 January 2003 ~ 1200UTC 23 January 2003 (Chongqing) and 1200UTC 12 December 2003 ~ 1200UTC 13 December 2003 (Changsha), output frequency is 30 minutes.

3 RESULTS AND ANALYSIS

Previous studies have indicated that it is regarded as foggy generation when liquid water content reaches 0.01 gkg-1(Shi Chune et al., 1997), therefor, in the paper liquid water content is applied to analyse the simulated fog formation and evolution. According to figure 1, at 1330UTC 22 January 2003, fog first formed in eastern region, the scope was small. At 1500UTC, fog scope expanded and covered most of the simulated region, the contour of eastern region was more intensive, fog concentration was slightly strong. At 2100UTC, mist developed to dense fog, the maximum value of liquid water content in the highlands of eastern region reached 0.63 gkg-1. High value areas of liquid water content were almost consistent with that of topographic contour. Liquid water content of the central region was relatively small, which may be related to urban heat island effect. At 0000UTC 23, liquid water content of the whole region continued to rise, but marginally, when fog developed to the strongest phase. After 0000UTC, solar radiation caused the ground to start warming, with the rise in the

ground temperature, the ground relative humidity decreased, droplet evaporated and the ground fog began to disperse. At 0230UTC 23, radiation fog cleared off entirely, the residual existed in the form of low cloud. From the vertical cross-section for the simulated temperature, relative humidity and liquid water content, we can see that during the development stage, near-surface temperature inversion layer had taken shape, the ground and near-surface layer atmospheric temperatures decreased. In the middle of the region the drop range of temperature was smaller, in the north and south were significant. High value areas of relative humidity were located in southeastern region, corresponding to the one of topographic contour. Relative humidity below 10m reached over 85%, according with observation and helpful to form radiation fog. However, fog thickness was quit thin, only several meters. At the advanced stage, the ground and near-surface layer atmospheric temperatures continued to decrease, relative humidity increased clearly, the air below 30m had been close to saturation, in the central part of the middle and upper layers relative humidity was smaller. Fog developed rapidly in the south. Fog thickness in the highlands was great, about 100m, in the middle was small, less than 40m. With the previous observations that fog thickness in Chongqing is normally 200 ~ 400m, we find that the simulated fog thickness is far less than reality and significantly small.

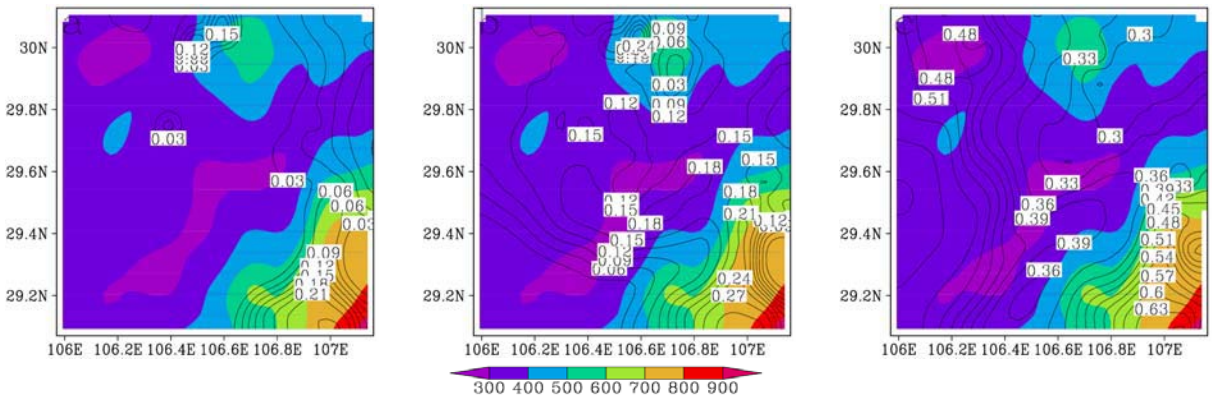

Figure 1. The simulated liquid water content at surface and topography at (a) 1330 UTC 22, (b) 1500 UTC 22,(c) 2100 UTC 22 Jan 2003(contour: liquid water content, units：g kg^{-1}; shaded: topography)

Thus, it does follow that the fog in Chongqing is divided into four stages: (1) formation stage (1330UTC 22 January 2003 ~ 1500UTC 22 January 2003). Because of radiation cooling, the air reached saturation point. Radiation fog came out in the highlands of eastern region at first, then expanded into the central and western region, and basically covered all the simulated zone at 1500UTC. (2) development stage (1500UTC 22 January 2003 ~ 2100UTC 22 January 2003). The air kept cooling, fog concentration and thickness increased, and mist developed into dense fog. (3) maturity stage (2100UTC 22 January 2003 ~ 0000UTC 23 January 2003), the ground temperature stopped decreasing, liquid water content rised, but little, fog top lifted. (4) dissipation stage (0000UTC 23 January 2003 ~ 0200UTC 23 January 2003). The ground temperature went up after the sun came out. To sum up, except for the simulated fog dissipating ahead of reality and fog thickness smaller, the method coupling the MM5 with the three-dimensional fog model can siumulate the macroevolution of fog formation, development, mature and dissipation as well as microstructural characteristics of fog.

Analysis of Changsha case is left out.

4 CONCLUSIONS

At present, there is important significance to enhance fog forecasting. In the paper, the 3D fog model coupling with the MM5 is used to simulate the local winter radiation fog in Chongqing and Changsha respectively. The results show that the unilaterally coupled model can reproduce the evolution, location, dissipation and concentration of heavy radiation fog, especially in complex geographical environments simulation capacity is stronger. Although there is still a certain lack for the simulation of fog thickness and dissipation that need further improve physical mechanisms of model, generally speaking, it is feasible to apply the 3D fog model coupling with the MM5 in fog forecasting. In addition, what deserves special mention here is that fog simulation with the two-way coupled model considering the feedback mechanism of fog will be the focus of our next study.

REFERENCES

Dong Jianxi, Lei Hengchi, Hu Zhaoxia, et al. 2006: Numerical simulation and diagnosis of a dense fog in Beijing and its penumbra.*Climatic and Environmental Research* (in Chinese), **11** (2) : 175 ~ 184.

Zhou Mei, Yin Yan, Wang Weiwei. 2006: A numerical study on the long-lasting wide spread dense fog event during December 24—27, 2006. *Journal of Applied Meterological Sciense* (in Chinese), **19** (5) : 602 ~ 610.

Shi Chune, Cao Bimin, Li Zihua, et al. 1996: umeical simulation of 3D local cirrculation over complicated terrain[J]. *Journal of Nanjing Institute of Meteorology* (in Chinese), **19** (3) : 320 ~ 328.

AERODYNAMIC ROUGHNESS LENGTHS OF SNOW

Christof Gromke[1], B. Walter[1], C. Manes[2] , M. Lehning[1]

[1] WSL Institute for Snow and Avalanche Research SLF, Davos, Switzerland
E-mail: *gromke@slf.ch*
[2] Politecnico di Torino, Department of Hydraulics, Transport and Civil Infrastructures, Torino, Italy

Abstract: Aerodynamic roughness lengths z_0 of snow surfaces have been determined from wind velocity measurements in a boundary layer wind tunnel. Complementary, surface characteristic length scales have been deduced from photographs of these snow surfaces by means of digital image processing and statistical analyses. Both sets of data are confronted in order to reveal possible correlations between the geometric properties of snow surfaces and the associated aerodynamic roughness lengths z_0. The current dataset generally shows increasing roughness lengths z_0 with increasing characteristic length scales.

Keywords: *aerodynamic roughness length, boundary layer velocity profile, structure function, characteristic length scales*

1 INTRODUCTION

The aerodynamic roughness length z_0 is a crucial parameter in the log-law formulation of the boundary layer wind profile and therefore in most model formulations of land-atmosphere interaction. It accounts for the effects of surface roughness on the flow. However, choosing the correct value of the roughness length for diverse surfaces remains a difficult task. Regarding snow surfaces and their corresponding values of z_0, a great lack of knowledge exists. A wide range of values for z_0 spanning two orders of magnitude can be found in literature, making it difficult to choose the appropriate value in model applications.

This work suggests an idea to link the aerodynamic roughness lengths of fresh-snow to characteristic lengths scales of its surface obtained by digital image processing and statistical analyses.

2 METHODS

In the SLF atmospheric boundary layer wind tunnel (situated on 1650 m a.s.l. in Davos, Switzerland) flows over snow covered surfaces and atmosphere-cryosphere interaction processes are studied. The experiments are performed with naturally fallen snow which is collected in custom-made trays positioned outside the wind tunnel facility in a wind sheltered area. The snow laden trays are placed in the wind tunnel providing an 8 m long natural fetch of snow on which a boundary layer develops. Air from outside the wind tunnel facility with ambient temperature is sucked in and the wind tunnel ceiling is adjusted to achieve a vanishing pressure gradient in order to guarantee natural flow conditions.

By measuring vertical profiles of mean horizontal wind velocity using 2D Hot-Wire-Anemometry (HWA) and subsequent curve fitting analysis to the logarithmic velocity profile

$$u^+(z) = \kappa^{-1} \ln\left(\frac{z-d}{z_0}\right), \tag{1}$$

aerodynamic lengths z_0 of snow covered surfaces were determined (approach (i)). For the experiments, the wind tunnel flow velocities were kept small to prevent snow drift and to maintain unaltered snow surface structures during the course of an experiment.

In a complementary procedure (approach (ii)), photographs of the naturally fallen snow surfaces were taken before and after the wind tunnel experiments. The photographs were processed by digital image analysis resulting in contour lines of the snow-air interface to which length co-ordinates of vertical height z and horizontal distance x were assigned (Fig. 1). Based on the contour line co-ordinates, second order spatial structure functions $D_2(r)$, with r horizontal lag, were calculated according to

$$D_2(r) = \left\langle [z(x+r) - z(x)]^2 \right\rangle . \tag{2}$$

The obtained structure functions $D_2(r)$ shown in a double logarithmic chart exhibit 3 distinct regions (Fig. 1). Applying multivariate statistical analysis to fit the second order structure functions by three regression curves yields a total of four characteristic length scales; two horizontal length scales, the crossover length l and the saturation length L, and their corresponding vertical length scales $[D_2(l)]^{1/2}$ and $[D_2(L)]^{1/2}$ (Manes et al. 2008).

The aim of this investigation is to reveal correlations between the aerodynamic roughness lengths z_0 obtained from approach (i) and the surface characteristic length scales obtained from approach (ii).

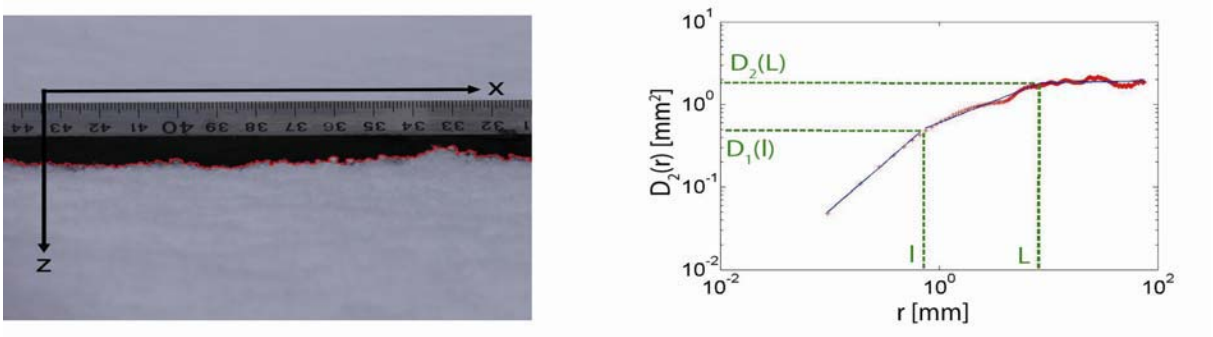

Figure 1. Photograph of snow surface with snow-air interface contour line (left) and diagram of second order structure function $D_2(r)$ with characteristic length scales (right).

3 RESULTS

In January and February 2008/09 five experiments with freshly fallen snow have been performed. Tab. 1 lists the aerodynamic roughness lengths z_0 obtained by approach (i) and the corresponding surface characteristic length scales obtained by approach (ii).

z_0	l	$[D_2(l)]^{1/2}$	L	$[D_2(L)]^{1/2}$
0.01	0.34	0.21	2.82	0.43
0.05	0.55	0.34	9.24	0.91
0.06	0.53	0.43	13.63	1.63
0.07	0.49	0.40	12.62	1.29
0.19	0.71	0.43	4.12	0.80

Table 1. Aerodynamic roughness lengths z_0 and surface characteristic length scales l, $[D_2(l)]^{1/2}$, L, $[D_2(L)]^{1/2}$ sorted by increasing z_0 (units: mm).

4 DISCUSSION AND CONCLUSION

The aerodynamic roughness lengths found are in overall agreement with the results of Clifton et al. (2006) and Andreas et al. (2004) who deduced z_0-values from wind tunnel experiments and field studies in the Arctic and Antarctic, respectively, and provide values $0.01\text{mm} < z_0 < 0.1\text{mm}$.

Analysing Tab. 1 generally shows increasing characteristic length scales with increasing roughness length, except for the roughest case where the length scales associated with the saturation region, L and $[D_2(L)]^{1/2}$, do not fit with this pattern. The data suggest a degressive increase of the characteristic length scales with increasing z_0. Values of z_0 and the crossover length scales l and $[D_2(l)]^{1/2}$ are mostly within one order of magnitude, whereas the saturation length scales usually exceed the roughness lengths by two orders of magnitude. However, the existing data set is still not sufficient to allow for more detailed and universal conclusions.

Moreover, it has to be noted that the roughness Reynolds number criterion $z_0^+ = z_0 u_* / \nu > 2.5$ is not strictly fulfilled for all the measurements. Calculations of the roughness Reynolds number resulted in $z_0^+ = 0.1$, 0.8, 0.9, 0.9 and 3.3 according to the sequence of cases listed in Tab. 1. This indicates that only in the last case an aerodynamically rough regime with a flow independent z_0 is present, whereas otherwise aerodynamically smooth or transitional regimes with z_0 slightly depending on the flow prevail.

The final goal of this work is to bring both approaches, (i) and (ii), together and to constitute a relationship between the aerodynamic roughness length and the characteristic length scales according to

$$z_0 = f\left(l, [D_2(l)]^{1/2}, L, [D_2(L)]^{1/2}\right). \quad (3)$$

However, in order to constitute a functional relationship, a larger dataset of z_0-values and characteristic length scales obtained from wind tunnel measurements and digital image processing/statistical analysis is required.

REFERENCES

Andreas, E. L., R. E. Jordan, P. S. Guest, P. O. G. Persson, A. A. Grachev and C. W. Fairall, 2004: Roughness Lengths over Snow, Proc. 18th Conf. on Hydrology of the American Meteorological Society, Seattle, WA, 11-15 Jan. 2004, pp. 8.

Clifton, A., J. D. Ruedi M. and Lehning, 2006: Snow saltation threshold measurements in a drifting-snow wind tunnel, Journal of Glaciology **52**, pp. 585-596.

Manes, C., M. Guala, H. Löwe, S. Bartlett, L. Egli and M. Lehning, 2008: Statistical properties of fresh snow roughness, Water Resources Research **44**, W11407, doi:10.1029/2007WR006689.

MONITORING THE ATMOSPHERIC BOUNDARY LAYER IN THE ARCTIC (MABLA) - THE GUFUSKÁLAR PROJECT

Haraldur Ólafsson[1,3,4] , Ólafur Rögnvaldsson[2,4], Joachim Reuder[4], Hálfdán Ágústsson[1,2]
Guðrún Nína Petersen[3], Halldór Björnsson[3], Trausti Jónsson[3] and Jón Egill Kristjánsson[5]

[1] Háskóli Íslands (University of Iceland)
[2] Reiknistofa í veðurfræði (Institute for Meteorological Research), Iceland
[3]Veðurstofa Íslands (Icelandic Meteorological Office)
[4]Geophysical Institute, University of Bergen
[5]Institute of Geosciences, University of Oslo
E-mail: *haraldur68@gmail.com*

Abstract: A new project of meteorological observations in a 412 m high mast in the vicinity of Snæfellsjökull Glacier in W-Iceland is described. The project is expected to provide data on various types of orographic disturbances, including corner winds, wakes, blockings and downslope windstorms.

Keywords: *MABLA, Gufuskálar, W-Iceland, mast, boundary-layer monitoring, Arctic, turbulent fluxes*

1 INTRODUCTION

Climate change, new challenges in fine-scale weather forecasting and unanswered questions on the nature of the atmospheric boundary-layer and mountain meteorology have motivated a new project, Monitoring of the Atmospheric Boundary-Layer in the Arctic (MABLA). The first goal of this project is to establish a monitoring of the atmospheric boundary-layer in a more than 400 m high mast at Gufuskálar at the west coast of Iceland (Fig. 1).

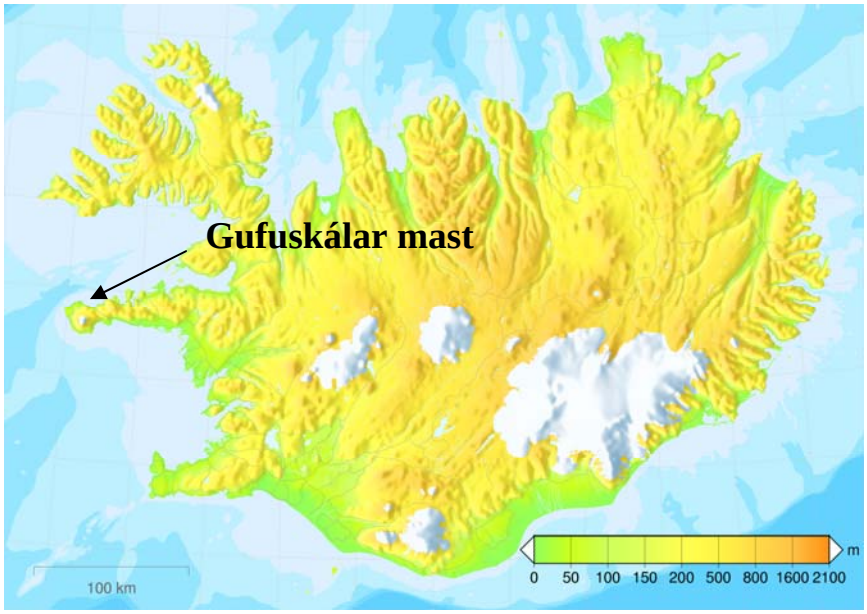

Figure 1. Location of the Gufuskálar mast at the west coast of Iceland.

2 OBSERVATIONS IN THE GUFUSKÁLAR MAST

The Gufuskálar mast is situated at the tip of the Snæfellsnes peninsula, a short distance northwest of the almost 1.5 km high, but rapidly melting Snæfellsjökull Glacier. A manned weather station was operated at Gufuskálar 1970-1994 and an automatic weather station has been operated there since 1994. The Stykkishólmur weather station that has a temperature series dating back to the middle of the 19th century is only a little more than 50 km to the east of Gufuskálar. The main mast of Gufuskálar is 412 m high, while a smaller 40 m high

mast is nearby. The taller mast was erected in 1963 and is currently used for transmitting long wave radio signals. The observations in the masts will consist of automated weather stations recording winds, temperature and humidity at roughly 10, 40, 100, 200 and 400 meters every 10 minutes. In addition, there will be high-frequency observations to assess turbulent fluxes of heat and momentum at 10 and 100 meters and observations of short- and long-wave radiation. Measurements at 10 and 40 metres started in the fall of 2008 and installation of instruments at the remaining levels will be completed during the summer of 2009.

3 SCIENTIFIC OBJECTIVES

The Gufuskálar observations serve a multiple purpose. They are expected to provide a description of the atmospheric boundary-layer inside a corner wind in northeasterly flow, an upstream blocking in northwesterly flow and in wakes or downslope windstorms in southeasterly flows. From a forecasting perspective, the data on turbulent transport of momentum down to the surface of the earth during windstorms is expected to give guidance for tuning of parameterization schemes with the aim of improving forecasts of surface mean winds and surface wind gusts (e.g. Ágústsson and Ólafsson, 2009; Rögnvaldsson et al., 2009). From a climatic perspective, future observations from Gufuskálar are expected to complement the exceptionally long Stykkishólmur time-series of temperature. The Gufuskálar project is a long-term investment. The measurements are expected to monitor a plausible climate change associated with the predicted global warming and the retreat of the sea ice north of Iceland. Being located at the shoreline, observations from Gufuskálar can be expected to be useful in describing the marine boundary-layer and for validating algorithms of remotely observed winds over the sea.

Figure 2. Installation of equipment in one of the two masts at Gufuskálar, W-Iceland in August 2008.

Acknowledgements:
MABLA is supported financially by the the Icelandic Research Fund (RANNÍS) and the Norwegian Research Fund through the THORPEX-IPY project. The access to the Gufuskálar mast is provided by the National Radio Company (RÚV).

REFERENCES

Ágústsson, H. and H. Ólafsson, 2009: Forecasting wind gusts in complex terrain. Meteorology and Atmospheric Physics, in press.

Rögnvaldsson Ó., J.-W. Bao, H. Ágústsson and H. Ólafsson, 2009: Downslope windstorm in Iceland – WRF/MM5 model comparison. Atmos. Chem. and Phys., in revision.

MIXING IN THE STABLE ATMOSPHERE OF AN IDEALIZED ALPINE VALLEY

Yann Largeron[1], Chantal Staquet[1], Charles Chemel[2], Jean-Pierre Chollet[1]

[1] Laboratoire des Ecoulements Géophysiques et Industriels (LEGI), CNRS, Grenoble, France
[2] University of Hertorfdshire, Hatfield, UK
E-mail: *yann.largeron@hmg.inpg.fr*

Abstract: The nocturnal radiative cooling of a sloping ground surface often induces katabatic flows. These natural self-generated flows may account for the major part of the observed atmospheric dynamics over a complex terrain by stable conditions and weak synoptic forcing. One may wonder about the ability of these flows to increase the transport properties of the atmosphere, a necessary step to characterize the dispersion of pollutants in a valley. The aim of the present study is to analyse these transport properties by the computation of a turbulent mixing coefficient, and to propose a parameterization of this coefficient. For this purpose, we perform LES numerical simulations with the ARPS meteorological code and adapt the analysis of mixing of Winters and d'Asaro (1996) to the present configuration.

***K*eywords:** *stable atmosphere, alpine valley, katabatic wind, turbulent diffusivity, ARPS code*

1 INTRODUCTION

In the absence of a strong synoptic forcing, the atmospheric flow in a valley is mainly created by thermal circulations due to the cooling or warming of the ground. For instance, the nightime radiative cooling of the ground leads to a downslope wind (refered to as a katabatic wind). In the present paper we consider the situation of a nocturnal katabatic wind in an idealized valley in which the ground cools by infra-red emission. We also focus on a stably stratified atmosphere.

Our aim is to analyze the turbulent mixing induced by the katabatic wind and we perform LES numerical simulations for this purpose. Our estimate of mixing relies on a method derived by Winters and d'Asaro (1996) which leads to an exact expression for the vertical turbulent mixing coefficient (more precisely, for the turbulent mixing coefficient normal to the isotherms). When adapted to our LES approach, this expression becomes :

$$\kappa_{t_{LES}} = -< \kappa_x \left(\frac{\partial\theta}{\partial x}\right)^2 + \kappa_y \left(\frac{\partial\theta}{\partial y}\right)^2 + \kappa_z \left(\frac{\partial\theta}{\partial z}\right)^2 >_{z_*} \cdot \left(\frac{d\theta}{dz_*}\right)^{-2} \tag{1}$$

in which $(\kappa_x, \kappa_y, \kappa_z)$ is the subgrid scale turbulent mixing coefficient computed by the code; $\theta(\overrightarrow{x}, t)$ is the (virtual) potential temperature field; and $z_*(\overrightarrow{x}, t)$ is the equilibrium altitude of a particle being at $\overrightarrow{x}$ at time t and is constant over an isothermal surface. The coefficient $\kappa_{t_{LES}}$ characterizes the turbulent heat flux resulting from the scales larger than the grid scale (explicitely resolved by the code) but also includes the subgrid contribution to turbulence.

2 SETUP OF THE SIMULATION

The simulations are performed with the "Advanced Regional Prediction System" (ARPS code) which is a non-hydrostatic atmospheric mesoscale model used here as a LES code. The turbulence closure scheme is the classical turbulent kinetic energy scheme (so-called TKE$^{1/2}$). In the simulations, the topography of the valley follows the analytical profile of Rampanelli et al. (2004). The length is 20 km and the width is 1240 m with summits rising at 1700 m. By this way, the valley resembles the Chamonix valley located in the French Alps.

We model a 3 hour long nocturnal episode starting at 22 h. In order to study the influence of a katabatic wind in a stable atmosphere for weak synoptic conditions, we impose no velocity field at initial time. The vertical profile of the potential temperature at $t = 0$, denoted $\theta_{amb}(z)$, increases linearly with height, being equal to $\theta_0 = 271$ K at the bottom of the valley. The Brunt-Väisälä frequency $N_{amb} = \sqrt{g/\theta_0 \left(d\theta/dz\right)_{amb}}$ is therefore constant. We perform different simulations for various values of N_{amb}. We also impose the ground to be colder by 3 K than the adjacent air and use the two-layer soil model of Noilhan and Planton (1989).

Open lateral boundary conditions are applied in both horizontal directions. The velocity field satisfies a no-slip condition at the ground and a Rayleigh damping layer is imposed at the top of the domain. At the ground, thermal fluxes are prescribed by the soil model every time step. The temperature of the soil surface then decreases with time, consistently with real soil behavior.

The horizontal resolution is 200 m and the vertical resolution starts at 5 m and slowly increases with height until 7000 m. The associated number of grid points is then $121 \times 103 \times 140$ and the time step is 0.25 s. We ran 10 differents simulations.

3 RESULTS

We focus upon the value of the turbulent mixing coefficient averaged over the layer of air associated with the katabatic wind. We denote this average by $<>_s$. The turbulent mixing coefficient $< \kappa_{t_{LES}} >_s$ thus obtained is comprised between 0.01 and $2\ m^2/s$ depending on the stability of the atmosphere and the time considered. Very few measurements are available in the litterature but those made in Antartica (Brost and Wyngaard (1978)) gave values between 0.01 à $0.6\ m^2/s$ in the katabatic layer, consistently with what we obtain. In a convective situation by contrast, $\kappa_{t_{LES}}$ typically varies between 1 and $700\ m^2/s$.

Figure 1a displays the temporal evolution of $< \kappa_{t_{LES}} >_s$ during the 3 hours of simulation for different values of the stability parameter N_{amb}. Each profile is quasi-linear for $t \geq 40$ suggesting to scale $< \kappa_{t_{LES}} >_s$ by $\alpha \cdot t$ (with $\alpha = 8.87 \cdot 10^{-3}$ given by a linear regression). The result is displayed versus N_{amb} for different times in Figure 1b. Surprisingly, a unique behavior is observed for $t > 40$.

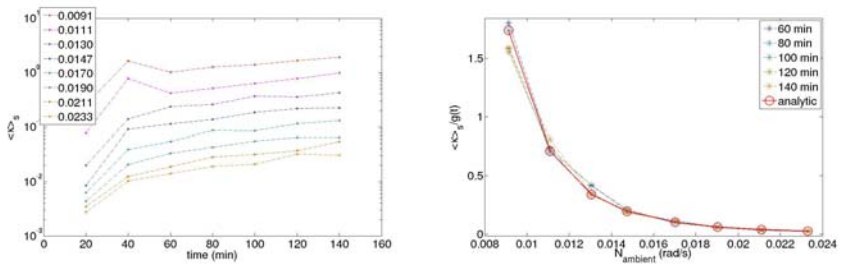

(a) (b)

Figure 1: (a) Evolution of $< \kappa_{t_{LES}} >_s (t)$ for different values of N_{amb}. (b) Colour crosses : Numerical values for $< \kappa_{t_{LES}} >_s (N_{amb})$ scaled by αt (see text). Red circles : Analytical function (2).

As an attempt to understand this behavior, we replaced $\kappa_x = \kappa_y$ and κ_z by their expression from the subgrid scale model. With a few assumptions, the result can be expressed as:

$$< \kappa_{t_{LES}} >_s \approx \frac{A}{N_{amb}^4} + \frac{B}{N_{amb}^5} \tag{2}$$

and is displayed with a red curve on Figure 1b. The curve fits remarkably well the numerical data.

In order to address the dependence of the mixing coefficient upon the subgrid scale model, we ran simulations with another subgrid scale model (the first order Smagorinski-Lilly closure scheme). We observed the same type of dependence of $< \kappa_{t_{LES}} >_s$ upon N_{amb} and found the same order of magnitude for the mixing coefficient (a ratio about 1.5 is found between the two cases). Two different conclusions can be drawn from this result. One may either conclude that the subgrid scale turbulence is correctly parameterized by each subgrid scale model or that the mixing coefficient does not depend upon the subgrid scale model. In both cases, this result ensures that a turbulent mixing coefficient can be estimated from LES.

4 CONCLUSIONS

We computed a mixing coefficient in the katabatic layer from the method of Winters and d'Asaro (1996). This coefficient was found to vary between 0.01 et 2 m^2/s, decreases with the stability of the atmosphere (as $\approx A \cdot N_{amb}^{-4} + B \cdot N_{amb}^{-5}$) and increases almost linearly with time. Most importantly, the mixing coefficient was found not to depend upon the subgrid scale turbulence model, for the two models we considered.

Acknowledgements:
Y.L. is supported by a grant of the région Rhône-Alpes. Computations have been performed on the computers of Joseph Fourier university in Grenoble (Mirage clusters) and on the clusters of the Institut du Développement et des Ressources en Informatique Scientifique (IDRIS).

REFERENCES

Brost, A. and Wyngaard, J., 1978, A model study of the stably stratified planetary boundary layer, *J. Atmos. Sci.*, **35**, 1427-1440

Noilhan, J. and Planton, S., 1989, A simple parameterization of land surface processes for meteorological models, *Mon. Weather Rev.*, **117**, 536-549

Rampanelli, G. and Zardi, D. and Rotunno, R., 2004, Mechanism of up-valley winds, *J. Atmos. Sci.*, **61**, 3097-3111

Winters, K.B. and D'Asaro, E.A., 1996, Diascalar flux and the rate of fluid mixing, *J. Fluid Mech.*, **317**, 179-193

High resolution atmospheric modelling for mountain and valley stations and its applications to complex dispersion conditions

D. Arnold[1], I. Schicker [2], P. Seibert[2], A. Vargas[1]

[1] Institut of Energy Technologies, Technical University of Catalonia, Barcelona, Spain
[2] Institute of Meteorology, University of Natural Resources and Applied Life Sciences, Vienna, Austria
E-mail: *delia.arnold@upc.edu*

Abstract: High resolution modelling with resolutions lower than 1 km is needed when complex topography is involved. Two case studies have been carried out at a valley and a mountain station with MM5V3.7 to evaluate three important topics: the influence of different boundary layer and soil schemes on the results, influences of the orographic shadowing option and the influence of using SRTM 3" satellite topographic data instead of the GTOPO 30" data used by default in MM5.

***K*eywords:** *ICAM, MM5, high resolution modelling, Inn Valley.*

1 INTRODUCTION

Numerical modelling in complex topographical areas is still challenging due to local meteorological phenomena which may lead to very poor air quality conditions. Therefore, high resolution modelling with resolutions lower than 1 km, both in the meteorological and dispersion fields, is needed. In this context, and within a newborn project of the BOKU-Met and the INTE research groups, an analysis of the improvements in the modelling results when using high resolution satellite topography data and land-use data, and better soil initial conditions, has started. First case studies have been carried out for two stations: Penhas Douradas, located on the slope of a mountain ridge in Portugal, and Innsbruck, located in the Inn Valley, Austria. Modelling has been done using the mesoscale meteorological model MM5V3.7 (PSU/NCAR) (Dudhia 1993) with G. Zängl's extensions for Alpine simulations (Zängl 2003) at both stations to evaluate three specific topics. First, the influence of different boundary layer and soil schemes. Second, influences of the orographic shadowing option which is currently not implemented in the distributed memory version of MM5. And third, improvement of the results using SRTM 3" satellite topographic data instead of the, as highest resolution available, GTOPO 30" data used by default in MM5.

2 MODEL SET-UP

MM5 was driven with the 6-hour ECMWF analyses and 3-hour forecasts at 1x1 degrees and standard model levels. The outermost domain was nudged every three hours towards the meteorological input to avoid drifting of the model. Sensitivity tests were performed changing one parameter at a time. A subset of the Innsbruck runs is presented here with MRF and ETA PBL schemes, Noah and 5-layer soil schemes, with and without SRTM 3" data and with and without orographic shadowing (Tab. 1). In all simulations 35 vertical layers and 2-way nesting interaction were used.

MM5run	S1	S2	S3	S4
Domain configuration	50x70, 85x94, 124x142, 115x14, 88x169 64.8 km, 21.6 km, 7.2 km, 2.4 km, 0.8 km			
BL scheme	ETA/MRF	ETA	MRF	ETA
Soil scheme	Noah	Noah/5-layer	Noah	5-layer(IRS)
Oro. shadow.	Yes	Yes	Yes/No	Yes
SRTM3" in D5	No	No	No	Yes/No

Table 1: Specification of configurations of the four sensitivity runs (labelled S1,2,3,4) in Innsbruck.

3 RESULTS

Modelled temperatures for each of the 4 sensitivity runs are compared with the measurements (Fig. 1). In agreement with previous results (Schicker and Seibert 2009) the ETA BL scheme gives in general better results but with too warm nights. The MRF scheme damps the diurnal temperature range. Soil schemes also make a difference in the temperature simulations. Both Noah and 5-layer soil schemes smooth out the diurnal cycles, but maxima temperatures are better simulated with the first one. Orographic shadowing create colder boundary layers. It has also been noticed, that it depends significantly on the BL scheme used in the simulation (not shown here). Additional tests for Penhas Douradas station and other similar locations have shown that those ones located on

mountain slopes are not as much affected as the ones located in the valleys regarding the BL scheme used and the orographic shadowing. However, the shadowing from the valley below may affect the development of thermally driven flows and further studies are being done.

SRTM 3" elevation data has only been tested in Innsbruck. Although during the first period of the run the simulations are in better agreement with the measurements than the ones using GTOPO 30", after some time, the simulations perform clearly worse. Additional work to asses this problem is currently ongoing.

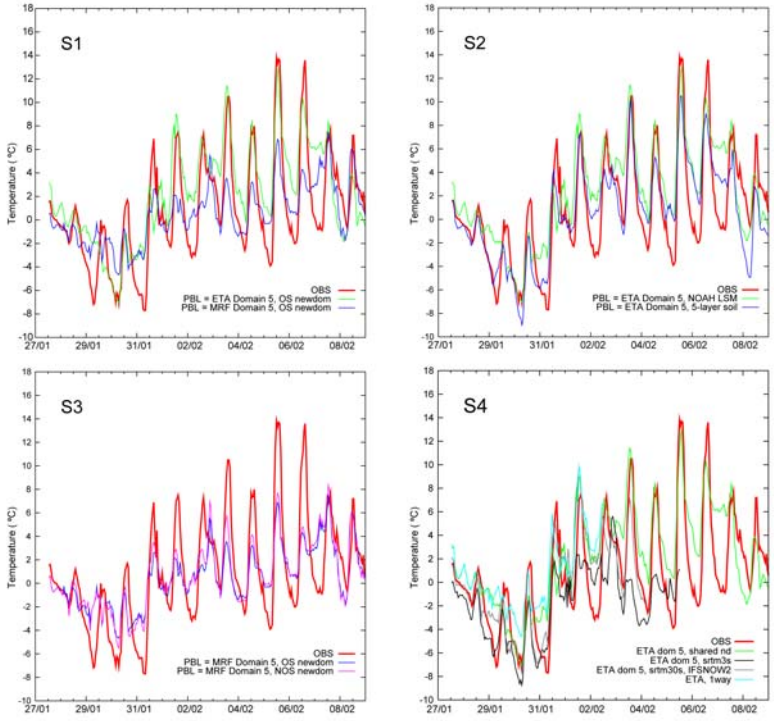

Figure 1: Comparison of the modelled and measured 2 m temperature in Innsbruck for the four runs.

4 CONCLUSIONS

MM5 simulations have been carried out for stations with complex topography and with different configurations and parametrisations. The parametrisations selection strongly influences the modelled results. In Alpine regions, ETA and 5-layer soil model give more realistic results. Orographic influence and the modifications introduced when using satellite elevation data are still under study and need further work. The final implications on the dispersion of radon and CO are currently studied with the Lagrangian particle dispersion model, MM5v3.7-FLEXPARTv6.2, developed specially to work with MM5 output and thus able to simulate complex dispersion conditions specially in the short range.

Computational costs must be considered too, not only regarding storage demands, but also computing time. To downscale from the global fields to such small grid sizes, typically six domains will be needed and thus more storage capacity should be available. Moreover, increasing resolutions in the horizontal and the vertical require small time steps to be numerically stable. This increases significantly the amount of time needed to run the simulation even in HPC.

Acknowledgements:

We thank the EMS for the financial support to assist this conference through a YSTA. We acknowledge the EU-FP6 Network of Excellence ACCENT. ECMWF ERA-40 data used in this study was provided by ECMWF through the Special Project MOTT.

REFERENCES

Dudhia, J., 1993: A non-hydrostatic version of the Penn State-NCAR Mesoscale Model: validation tests and simulation of an Atlantic Cyclone and cold front. *Mon. Wea.Rev.*, **121**, 1493-1513.

Schicker, I., and Seibert, P., 2009: Simulation of the meteorological conditionrs during a winter smog episode in the Inn Valley. *MAP*, **103** (1-4), 211 – 222.

Zängl, G., 2003: A generalized sigma coordinate system for the MM5. *Mon. Wea.Rev.*, **131**, 2875–2884.

MOUNTAIN WAVE RELATED TURBULENCE DERIVED FROM SONIC ANEMOMETERS AND AN ELASTIC BACKSCATTER LIDAR

Željko Večenaj[1], Stephan F.J. De Wekker[2] and Vanda Grubišić[3]

[1]Department of Geophysics, Faculty of Science, Zagreb, Croatia
E-mail: *zvecenaj@gfz.hr*
[2]Department of Environmental Sciences, University of Virginia, USA
[3]Department of Meteorology and Geophysics, University of Vienna, Austria

Abstract: A case study of mountain wave related turbulence during the Terrain-induced Rotor EXperiment in the Owens Valley is presented. Large spatial and temporal variability in aerosol backscatter was observed in the valley atmosphere associated with mountain wave activity. The corresponding turbulence structure along and across the valley was investigated using data collected by three 30 m NCAR towers equipped with 6 levels of ultrasonic anemometers. Time series of turbulent kinetic energy (*TKE*) show much higher levels of *TKE* in the valley center than on the sloping western part of the valley. An analysis of the *TKE* budget shows that mechanical production of turbulence is dominant and balanced by turbulent dissipation in central parts of the valley. The data and analysis from this case study can be used to evaluate and improve turbulence parameterization schemes in atmospheric numerical models.

Keywords: T-REX experiment, turbulent kinetic energy, budget equation, dissipation rate

1 INTRODUCTION

Terrain-induced Rotor Experiment (T-REX) was conducted during spring 2006 in Owens Valley, California. During the Intensive Observation Period 1 (IOP 1) from 0000 UTC on 02 March to 1500 UTC on 03 March 2008 a transition occurred from a quiescent to a disturbed boundary layer accompanied by large spatial inhomogeneities in the aerosol backscatter (De Wekker and Mayor, 2009).The turbulence structure near the surface during these transitions is poorly known and potentially important for the modification of mountain wave activity and the generation of rotors and subrotors on the lee-side of mountains.

Turbulent kinetic energy (*TKE*) is produced and destructed by various processes that are explained by the different terms in the *TKE* budget equation (e.g. Stull, 1988). One of the terms is the eddy dissipation rate (ε) which is parameterized in numerical models (e.g. Mellor and Yamada, 1974) and used in turbulence nowcasting at the airports (e.g. Frech, 2007). By quantifying both the *TKE* and ε, parameterization schemes that are used in these models can be evaluated and potentially improved.

2 FIELD EXPERIMENT, INSTRUMENTATION AND DATA

Data from three towers from the Integrated Surface Flux Facility (ISFF) installed by NCAR and from the Raman-shifted Eye-safe Aerosol Lidar (REAL) are used in this study. Figure 1 shows the map of the site with the towers and REAL indicated.

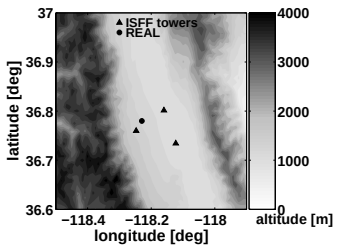

Figure 1. The map of the area of interest together with the locations of the towers and the lidar.

The western tower (WT) was located on the alluvial slope on the western side of Owens Valley. The central tower (CT) and the south tower (ST) were located along the valley's central axis extending from NNW to SSE. Each tower was 35 m tall and instrumented with CSAT3 ultrasonic anemometers collecting data with a sampling rate of 60 Hz at heights of 5, 10, 15, 20, 25 and 30 m. REAL was installed between WT and CT on the alluvial slope providing an undisrupted view in all directions within its range. Vertical and horizontal scans were made using REAL (De Wekker and Mayor, 2009).

3 RESULTS

In Cartesian system, the *TKE* is defined as a sum of variances of all three wind components:

$$TKE = \frac{1}{2}\left(\overline{u'^2} + \overline{v'^2} + \overline{w'^2}\right) \quad (1)$$

The *TKE* budget equation is expressed as (e.g. Stull, 1988):

$$\underbrace{\frac{\partial TKE}{\partial t}}_{I} = \underbrace{\frac{g}{\Theta_v}\left(\overline{w'\theta_v'}\right)}_{II} \underbrace{-\overline{u'w'}\frac{\partial U}{\partial z}}_{III} \underbrace{-\frac{\partial\left(\overline{w'TKE}\right)}{\partial z}}_{IV} \underbrace{-\frac{1}{\rho}\frac{\partial\left(\overline{w'p'}\right)}{\partial z}}_{V} \underbrace{-\varepsilon}_{VI} \qquad (2)$$

Term *I* represents a local storage of *TKE*. Term *II* is the buoyant production/consumption term depending on the sign of the heat flux ($\overline{w'\theta_v'}$). Term *III* denotes mechanical (shear) production term. Term *IV* describes the turbulent transport of *TKE* by the vertical velocity *w* of turbulent eddies. Term *V* is a pressure correlation term that shows how pressure perturbations redistribute *TKE* in the vertical. Finally, term *VI* represents the dissipation of *TKE* by molecular viscosity into heat.

Between 2345 UTC on 02 March and 0115 UTC on 03 March REAL detected interesting features that indicated presence of high levels of turbulence (De Wekker and Mayor, 2009). ISSF towers reveal that *TKE* indeed is strong along the valley (ST, Fig. 2c and CT; Fig. 2b) due to the influence of strong south-easterly flows along the valley. However, *TKE* is considerably weaker at WT (Fig. 2a). REAL data shows that downslope advection of stable stratified air occurs near the western tower leading to the low levels of turbulence there. The *in-situ* measurements do not capture the increased mixing above ~ 1 km revealed by REAL. REAL indicated that this increased mixing is caused by the interaction of the downslope flow and the SE flow along the valley. From Fig. 3 it is obvious that the mechanical term and ε are predominant and almost in balance at all mid-levels at the CT (Fig. 3b) and ST (Fig. 3c). In general, the values at WT are approximately 5 times smaller than at CT and ST, confirming that the turbulence is suppressed at WT. However, ε is noticeable larger than the sum of *TKE* production terms, i.e. mechanical shear and buoyancy, at WT. This indicates that the *TKE* was not produced locally but advected from elsewhere by the downslope flows.

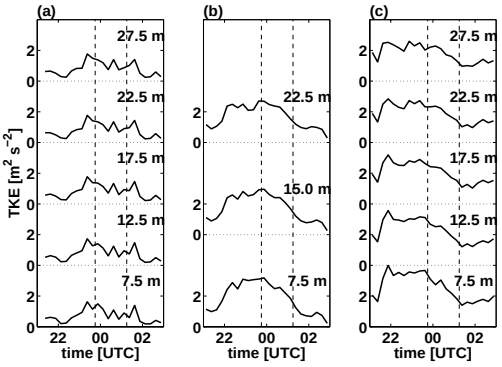

Figure 2. Temporal evolution of the *TKE* evaluated at various mid-levels at WT (a), CT (b) and ST (c). The heights of the various mid-levels are indicated in the figure. Vertical dashed lines depict the period of interest.

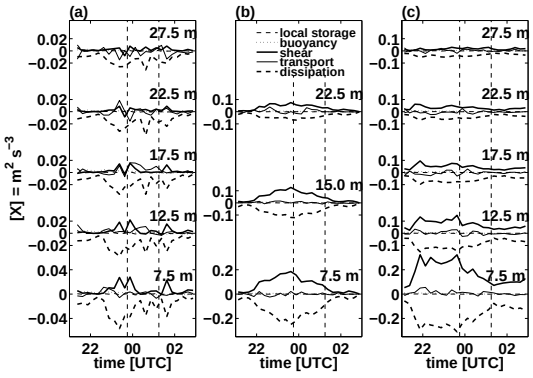

Figure 3. Temporal evolution of the terms from the *TKE* budget equation (equation 2 in text) evaluated at the mid-levels at WT (a), CT (b) and ST (c). The heights of the mid-levels are indicated in the figure.

4 SUMMARY

During T-REX IOP 1, a transition from a quiescent to a disturbed boundary layer is accompanied by large variability in space and time of aerosol backscatter and turbulent kinetic energy. Stably stratified downlope flows suppress the *TKE* on the western side of the valley while the *TKE* is enhanced in the central part of the valley, where a strong interaction between downlope flows, channelled along-valley flows and mountain waves occurs. At the along-valley locations locally produced shear-driven turbulence is balanced by turbulent dissipation while advection effects play an important role at the western slope location. This study exemplifies the benefit of combined in-situ and remote sensing measurements in providing an improved understanding of temporal and spatial turbulence variability in complex terrain.

Acknowledgements:
This study is partially supported by the Croatian Ministry of Science, Education & Sports, projects BORA No. 119-1193086-1311. This work was started while ZV was a visiting student at the University of Virginia.

REFERENCES

De Wekker S.F.J. and S.D. Mayor, 2009: Observations of atmospheric structure and dynamics in the Owens Valley of California with a ground-based, eye-safe, scanning aerosol lidar. J. Appl. Meteor. Climat.In press.

Frech, M., 2007: Estimating the turbulent energy dissipation rate in an airport environment. Boundary-Layer Meteorol. **123**, 385–393.

Mellor, G.L. and T. Yamada, 1974: A hierarchy of turbulence closure models for planetary boundary layers. J. Atmos. Sci. **31**, 1791-1806.

Stull, R.B., 1988: An Introduction to Boundary Layer Meteorology, Kluwer Academic, 666 pp.

ALONG-COAST FEATURES OF THE BORA RELATED TURBULENCE

Željko Večenaj[1], Danijel Belušić[1], Vanda Grubišić[2] and Branko Grisogono[1]

[1]Department of Geophysics, Faculty of Science, Zagreb, Croatia
E-mail: *zvecenaj@gfz.hr*
[2]Department of Meteorology and Geophysics, University of Vienna, Austria

Abstract: The mesoscale bora structure in the along-coast direction (normal to the mean bora flow) is featured by an interchange of jets and wakes related to mountain gaps and peaks. Here we examine the along-coast, off-shore turbulence structure of the bora that occurred on 7 November 1999 during the Mesoscale Alpine Program (MAP) Intensive Observation Period 15. We use the aircraft and dropsonde data measured along the lee side of the Dinaric Alps over the Adriatic by the NCAR Electra aircraft. The results are compared with the output from the WRF ARW numerical model.

Keywords: MAP, bora wind, turbulence, turbulence kinetic energy, dissipation rate, WRF ARW model

1 INTRODUCTION

Along the eastern Adriatic coast, a downslope wind called bora is a common occurence. Bora blows from the northeastern quadrant and is most frequent during the winter season. Bora mean wind speed can surpass 20 m s^{-1} and due to its gustiness can reach speeds in excess of 60 m s^{-1} (e.g. Belušić and Klaić, 2006). During such events, there is strongly developed turbulence in the lee of the coastal mountains.

The mesoscale bora structure in the along-coast direction (normal to the mean bora flow) is featured by an interchange of jets and wakes related to mountain gaps and peaks as documented in Grubišić (2004) for a bora event over northern Adriatic that occurred on 7 November 1999 during the Mesoscale Alpine Programme (MAP) Intensive Observation Period 15. We present here a study of turbulence in the early stage of this bora event. The study is based on the aircraft data measured along the lee side of the Dinaric Alps over the Adriatic by the NCAR Electra aircraft. The data includes two vertically separated flight legs (lower at ~ 370 m, higher at ~ 680 m) and six dropsonde measurements along the legs. The results are compared with the output from the WRF ARW numerical model for this event.

2 OBSERVATIONAL DATA ANALYSIS

During IOP 15, two 216 km long coast-parallel flight legs were flown by the NCAR Electra, one at ~680 m ASL flying SE to NW, and the other at 380 m ASL from NW to SE. High-resolution aircraft data was obtained at the frequency of 25 Hz. The aircraft flew at the mean velocity of 100 m s^{-1}. Two hours ealier, nine dropsondes were released by the aircraft from a 4200 m ASL leg above the low-level flight legs. The area of interest, together with the horizontal wind along the lower flight leg, and the coordinates of the dropsondes, are shown in Fig. 1.

The coordinate system is rotated counter clockwise with the x-axis perpendicular to the flight legs and pointing SW. The y-axis is parallel to the flight legs and points toward SE. The crosspectrum and spectrum analyses of the heat and momentum flux from the aircraft data for both flight legs show the energy gap (e.g. Metzger and Holmes, 2008) at the wave number that corresponds to the wavelength of 120 m. This impelled us to filter the aircraft data using the Moving Average (MA) of 120 m. Consequently, we neglect all of the phenomena on scales greater then this MA. The flight legs are divided into 100 segments of 2160 m. For each segment the turbulent kinetic energy (*TKE*) and *TKE* dissipation rate (ε) are calculated. The latter is calculated using the inertial dissipation method provided by Kolmogorov's 1941 theory (?) (e.g. Večenaj et al., 2007). The *TKE* values are used as the control parameter for the evaluation of ε (Figs. 2a-c). Bulk Richardson number, R_B, (e.g. Stull, 1988) calculated from the aircraft data is compared with the one calculated from the dropsonde data (Fig. 2d).

3 COMPARISON OF MEASUREMENTS AND MODEL RESULTS

This bora event was simulated using the WRF ARW model. While u wind speed component is reproduced successfully along the flight legs, the agreement with the v component, potential temperature (θ) and *TKE* is poorer (Fig. 3). With respect to the aircraft data, the model significantly overestimates v along the entire flight legs while it underestimates θ on the northern part and *TKE* on the southern part of the legs. There is a good agreement between the aircraft and dropsonde data along the flight legs (Fig. 4). Comparison of the modelled with the dropsonde data shows a good agreement with u and θ, while v shows more deviation both in magnitudes and in vertical structure.

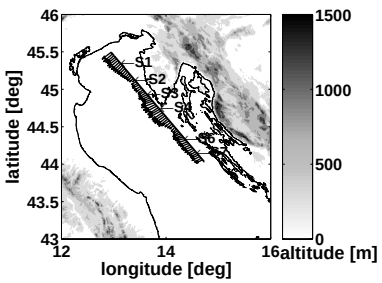

Figure 1. Area of interest together with a lower flight leg (height of 370 m), wind vectors (1600 m means) and positions of dropsondes.

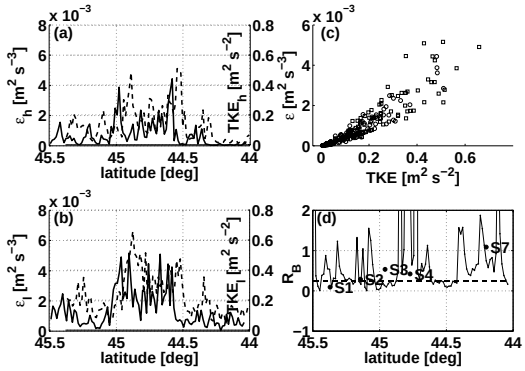

Figure 2. ε (solid line) and *TKE* (dashed line) on (a) higher (b) lower flight leg. (c) ε vs. *TKE* on higher (circles) and lower (squares) flight leg. (d) R_B between flight legs from aircraft data (solid line) and from dropsonde data (diamonds).

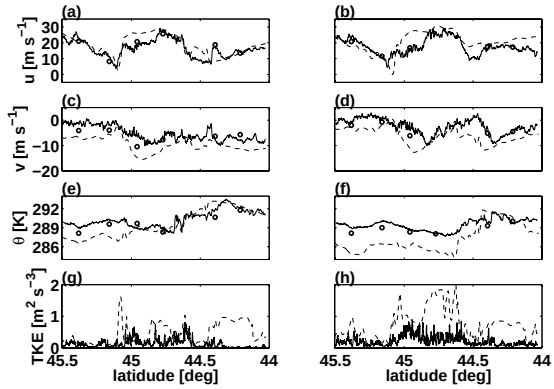

Figure 3. Aircraft (solid line), dropsonde (circles) and modelled data (dashed line) along the higher (a, c, e, and g) and the lower (b, d, f, h) flight leg.

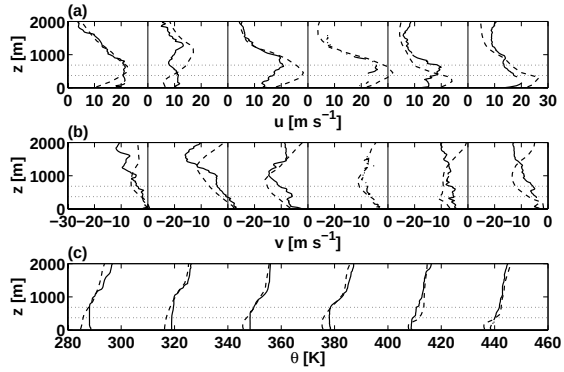

Figure 4. Six dropsonde along flight legs (solid line) and modelled (dashed line) data of (a) u and (b) v. (c) θ is consecutive shifted for 30 K.

4 SUMMARY

A significant spatial variability of *TKE* and ε along the flight legs is revealed in this bora case associated with mesoscale phenomena that are part of bora such as mountain waves, wave breaking, jets and wakes, shear zones, where the jets, wakes and the shear zones are closely related to the terrain complexity of the eastern Adriatic coast.

Variations of *TKE* time series closely follow those of ε which gives the information about robustness and consistency of the ε estimation. As expected, a scatter plot shows that ε increases with *TKE*. The empirical relation between these two variables is yet to be examined.

In general, aircraft in situ data agrees well with the dropsonde data which points out to the degree of measurements reliability. The WRF ARW model reproduces the *u* wind speed component along the flight legs well, while the *v* component and θ are overestimated and underestimated, respectively. Also, *TKE* is well simulated at the northern part of the legs, while it is overestimated at the southern part. As for the vertical range, *u* and θ are reproduced more successful than *v*.

Acknowledgements:
This study is supported by the Croatian Ministry of Science, Education & Sports, projects BORA No. 119-1193086-1311.

REFERENCES

Belušić, D. and , Z.B. Klaić, 2006: Mesoscale dynamics, structure and predictability of a severe Adriatic bora case. Meteorol. Z. **15**, 157-168.

Grubišić, V., 2004: Bora-driven potential vorticity banners over the Adriatic. Q. J. R. Meteorol. Soc. **130**, 2571-2603.

Metzger, M. and H. Holmes, 2008: Time scales in the unstable atmospheric surface layer. Boundary-Layer Meteorol. **126**, 29-50.

Stull, R.B., 1988: An Introduction to Boundary Layer Meteorology, Kluwer Academic, 666 pp.

Večenaj, Ž., D. Belušić, and B. Grisogono, 2007: Estimation of turbulence kinetic energy dissipation rate in a bora event. *Proc. 29th Intern. Conf.on Alpine Meteorology*, Chambery, France, 745-748.

ANALYSIS OF SECOND ORDER MOMENTS OF SURFACE LAYER TURBULENCE IN AN ALPINE VALLEY

Dino Zardi[1], Massimiliano de Franceschi[1,2], Mauro Tagliazucca[3], Francesco Tampieri[3]

[1] Gruppo di Fisica dell'Atmosfera, Università di Trento, Trento, Italy
E-mail: *Dino.Zardi@ing.unitn.it*
[2] Seminario Maggiore, Diocesi di Bolzano-Bressanone, Bressanone, Italy
[3] Istituto di Scienze dell'Atmosfera e del Clima, Consiglio Nazionale delle Ricerche, Bologna, Italy

Abstract: Results from the analysis of field measurements in the atmospheric surface layer in the Adige Valley, south to the city of Bolzano/Bozen in the Alps, are presented. Values of drag coefficient, displacement height and roughness length are similar to those reported in the literature about surface layer turbulence over plain uniform terrain. All the nondimensional standard deviations of wind velocity components are well reproduced with just one Monin-Obukhov similarity relationship. The analysis of temperature fluctuations results in distinct behaviours in the stable and unstable regimes respectively, which require suitable expressions such as those already proposed in the literature. In the present case the coefficients for near neutral conditions are lower than generally reported. The importance of using an appropriately formulated recursive filter to separate low frequency unsteadiness of the mean flow from turbulence signal is also shown.

Keywords: *surface layer turbulence, valley, second order moments*

1 INTRODUCTION

Many recent studies on boundary layer turbulence investigate areas with nonhomogenous terrain, testing appropriate extensions of concepts valid for flat uniform terrain. The present paper focuses on the stability dependence of wind velocity and temperature variances and aims at exploring the applicability of MOST in the central region of a valley floor.

Standard deviations of the three wind components and of air temperature are a basic information concerning the intrinsic statistical properties of surface layer turbulence. Moreover they are required for appropriate parameterization of diffusion processes into the atmosphere. The vertical structure of velocity standard deviations within MOST has been examined by various authors (Doran et al., 2002; Rotach and Zardi, 2007), who explored a rather wide group of situations, including some cases of complex terrain. However so far only few results are available in the literature for the case of mountain valleys and their similarity scaling.

2 DATA AND METHODS

Results are based on turbulence measurements performed in July 1999, under various weather conditions, with a sonic anemometer in the middle of the valley floor (so as to be minimally affected by sidewall effects), in a locally plain and almost horizontal area (down-valley slope everywhere less than 0.2%), rather regularly surrounded by uniformly high apple tree orchards (de Franceschi et al., 2009).

Besides the techniques commonly adopted in the field of micrometeorology (Lee et al., 2004), special care was devoted to the appropriate design parameters of the digital recursive filter used to separate turbulent fluctuations from the mean flow (de Franceschi and Zardi, 2003), as well as to evaluation of the rotation angles required for streamwise alignment (de Franceschi, 2004). Furthermore the analysis of wind velocity standard deviations is based on the well known expression that Panofsky and Dutton (1984) proposed for the vertical component (only) under unstable conditions. In particular, in the present work the following expression

$$\frac{\sigma_i}{u_*} = \alpha_i \left(1 + \beta_i |\zeta|\right)^{1/3} \tag{1}$$

has been assumed as test function for the three wind components (u, v and w) and both stability ranges. Furthermore, for the temperature fluctuations two different expressions have been tested, namely

$$\frac{\sigma_i}{|\theta_*|} = \begin{cases} \alpha_\theta \left(1 - \beta_\theta \zeta\right)^{-1/3} & \zeta \le 0 \\ \alpha_\theta \left(1 + \beta_\theta \zeta\right)^{-1} & \zeta \ge 0 \end{cases} \tag{2}$$

3 RESULTS

The analysis of data from nondimensional standard deviations allows to adopt, for all the wind components, the same Monin-Obukhov similarity relationship in the form of equation (1), thus extending its applicability to the case of winds over a valley floor under slowly varying situations. The best-fit coefficients α_i and β_i are

reported in Table 1. The latter also shows the benefit in terms of reduced scatter around the best fit curve following a correct definition of the design parameters for the digital filter (de Franceschi and Zardi, 2003).

	$\zeta < 0$								
	α_u	β_u	R^2	α_v	β_v	R^2	α_w	β_w	R^2
unf.	2.02±0.07	5.14±0.96	0.29	2.09±0.08	4.81±1.06	0.20	1.06±0.02	6.48±0.56	0.70
McM	1.85±0.05	5.50±0.89	0.40	1.85±0.06	5.80±1.10	0.31	1.13±0.01	4.94±0.32	0.77
dFZ	1.80±0.02	0.78±0.05	0.71	1.63±0.02	1.32±0.10	0.74	1.27±0.01	2.82±0.14	0.97
	$\zeta > 0$								
	α_u	β_u	R^2	α_v	β_v	R^2	α_w	β_w	R^2
unf.	2.02±0.09	22.50±3.92	0.64	2.21±0.10	16.60±3.06	0.50	1.12±0.02	1.42±0.16	0.35
McM	2.01±0.06	12.80±1.63	0.67	1.98±0.09	16.10±2.69	0.57	1.17±0.01	1.48±0.15	0.41
dFZ	1.92±0.02	1.01±0.06	0.69	1.71±0.02	1.68±0.12	0.69	1.32±0.01	0.88±0.06	0.64

Table 1: Best-fit coefficients for eq. (1) for the along-valley wind directions ["unf." = values obtained without any filtering procedure; "McM" = McMillen's (1988) procedure; "dFZ" = de Franceschi and Zardi (2003) correction].

As to temperature variance, two different behaviours are met in the stable and unstable regimes respectively: the expressions (2) seem to reproduce well the data, though with lower coefficient values (Table 2) than commonly reported for near neutral conditions.

	$\zeta < 0$				$\zeta > 0$		
	α_θ	β_θ	R^2		α_θ	β_θ	R^2
unf.	1.47±0.11	21.0±8.82	0.25		1.73±0.05	0.17±0.07	0.07
McM	1.19±0.11	19.0±9.59	0.20		1.55±0.04	0.01±0.02	$6\ 10^{-3}$
dFZ	1.15±0.11	16.9±8.34	0.29		1.21±0.02	$3\ 10^{-3}$±$7\ 10^{-3}$	$1\ 10^{-3}$

Table 2: Best-fit coefficients for eq. (2) for the along-valley wind directions ["unf." = values obtained without any filtering procedure; "McM" = McMillen's (1988) procedure; "dFZ" = de Franceschi and Zardi (2003) correction].

4 CONCLUSIONS

The analysis of turbulence data from a field measurement campaign in an Alpine valley, thanks to suitable data-treatment (de Franceschi and Zardi, 2003) which proved to be effective in filtering out the short-period nonstationarities, allowed a reliable estimation of best-fit parameters for similarity functions.

The results presented here give a new perspective on the behaviour of second order moments in the Surface Layer turbulence in an mountain valley, especially about the validity of MOST over all stability ranges and wind velocity components, for which a single similarity function provides simpler but well reliable description.

Acknowledgements:
This work has been partly supported by: the Bolzano Municipality under the contract "Evaluation of the pollutant dispersion in the Bolzano area"; the Environmental Protection Agency of the Province of Trento under the contract "Study of the Boundary Layer processes in the Adige Valley"; the Italian National Institute for the Scientific and Technological Research on the Mountain (INRM) under the research contract "Study of atmospheric dynamics in Alpine valleys".

REFERENCES

Doran, J.C., J.D., Fast, J. Horel, 2002: The VTMX 2000 Campaign. Bull. Amer. Meteor. Soc., **83**: 537–551.

de Franceschi, M., Investigation of Atmospheric Boundary Layer in Alpine Valleys. Monographs of the School of Doctoral Studies in Environmental Engineering. Università di Trento, 2004. ISBN 88-8443-052-6, 135 pp (http://www.ing.unitn.it/dica/eng/monographs/)

de Franceschi, M., D. Zardi, 2003: Evaluation of cut-off frequency and correction of filter-induced phase lag and attenuation in eddy covariance analysis of turbulence data. Boundary-Layer Meteorol., **108**: 289–303.

de Franceschi, M., D. Zardi, M. Tagliazucca, F. Tampieri, 2009: Analysis of second order moments in the Surface Layer turbulence in an Alpine valley, Q. J. R. Met. Soc., *submitted*

Lee, X., W. Massman, B. Law, 2004: Handbook of Micrometeorology. A Guide for Surface Flux Measurement and Analysis. Kluwer Academic Publishers, Dordrecht.

McMillen, R.T., 1988: An eddy correlation technique with extended applicability to non-simple terrain. Boundary-Layer Meteorol., **43**: 231–245.

Panofsky, H. A. and Dutton, J. A. 1984 Atmospheric Turbulence. Models and methods for engineering applications. Wiley and Sons Inc., New York

Rotach, M., D. Zardi, 2007: On the boundary layer structure over highly complex terrain: key findings from MAP. Q. J. R. Met. Soc., **133**: 937–948.

VALIDATING THE TURBULENCE PARAMETERIZATION SCHEMES OF A NUMERICAL MODEL USING EDDY DISSIPATION RATE MEASUREMENTS IN A TERRAIN-DISRUPTED AIRFLOW

Pak Wai Chan

Hong Kong Observatory, Hong Kong, China
E-mail: *pwchan@hko.gov.hk*

Abstract: A number of turbulence parameterization schemes are available in the latest version (6.0) of the Regional Atmospheric Modelling System (RAMS). Chan (2009) studied the performance of these schemes by simulating the eddy dissipation rate (EDR) distribution in the vicinity of the Hong Kong International Airport (HKIA) and comparing with the EDR measurements of remote-sensing instruments at the airport. For the e-l (turbulent kinetic energy – mixing length) scheme considered in that study, the mixing length is assumed to be a constant. This assumption is removed in the present paper and simulations of EDR fields are repeated for terrain-disrupted airflow in the vicinity of HKIA. It is found that, with a variable mixing length, the performance of the e-l scheme is greatly improved. With suitable choice of the empirical constants in the turbulence closure, the accuracy of the EDR profile (in comparison with LIDAR and wind profiler measurements) is found to be comparable with that predicted by the Deardorff scheme. A study on the sensitivity of the simulation results to these empirical constants has also been performed.

Keywords: *RAMS, turbulence parameterization, e-l scheme*

1 INTRODUCTION

The Hong Kong International Airport (HKIA) is situated in the vicinity of complex terrain. To its south is the mountainous Lantau Island with peaks rising to about 1 km above mean sea level (AMSL) and valleys as low as 400 m in between. The airport is surrounded by sea in the west, north and east. To its northeast, at a distance of 10-12 km, there are a couple of mountains with a height of 500-600 m. Airflow disturbances arising from terrain disruption may bring about significant turbulence to aircraft landing at or departing from HKIA. Following the requirement of the International Civil Aviation Organization (ICAO), the turbulence intensity in aviation is quantified in terms of the cube root of eddy dissipation rate (EDR), ε. Forecasting of $EDR^{1/3}$ by numerical weather prediction (NWP) models would be useful in the provision of turbulence alerting services to aircraft.

Chan (2009) demonstrated that the forecasting of $EDR^{1/3}$ in typical cases of terrain-disrupted airflow around HKIA was possible by running the Regional Atmospheric Modelling System (RAMS) version 6.0 at high spatial resolution. The innermost model domain has a horizontal resolution of 50-200 m. The forecasting results had been shown to depend very much on the choice of the turbulence parameterization scheme. It turns out that the Deardorff scheme appeared to have the best performance in the selected cases. In RAMS 6.0, there are also a couple of new turbulence parameterization schemes available, such as the e-l (turbulent kinetic energy [TKE] – mixing length) scheme of Trini Castelli et al. (2005). However, this scheme is found to give too much turbulence near the ground and $EDR^{1/3}$ drops too rapidly with altitude in comparison with the other turbulence schemes and actual measurements.

The default setting of RAMS 6.0 adopts a constant mixing length for e-l scheme. In the present study, a variable mixing length is applied to two different wind regimes, namely, southwest monsoon in the summer and northeast monsoon in the winter over southern China.

2 E-L SCHEME AND NUMERICAL MODEL SETUP

In e-l scheme, the diffusion coefficient of momentum K_m is determined as:

$$K_m = c_\mu e^{1/2} l \tag{1}$$

where c_μ is a closure empirical constant. Following Xu and Taylor (1997), it has a value of 0.41. This constant is in turn related to the corresponding empirical constant of dissipation term of TKE $\varepsilon_\mu = c_\mu^3$. In the present study, c_μ is made variable and the resulting $EDR^{1/3}$ field is compared with the actual measurements to find out a suitable value for this empirical constant.

The model setup is similar to that in Chan (2009). The initial and boundary conditions for RAMS are obtained from a mesoscale regional spectral model of the Hong Kong Observatory (HKO). Only three nested domains are employed in the present study of RAMS, namely, at spatial resolutions of 4 km, 800 m and 200 m. In the second and third domains, terrain data of Hong Kong at 100 m horizontal resolution is used in order to resolve the major topographical features around HKIA.

3 MODEL SIMULATION RESULTS

A moderate southwest monsoon case is studied. The LIDAR measurements around HKIA at that time are shown in Fig. 1. The model-simulated wind field is found to be generally consistent with the LIDAR data (not shown).

The model-simulated $EDR^{1/3}$ profile at Siu Ho Wan (location in Fig. 2) and the actual measurement by a 1299-MHz wind profiler at that location are compared in Fig. 3. It can be seen that the results from e-l scheme and Deardorff-scheme are rather close to the actual measurements in the first 1 km or so AMSL, whereas Mellor-Yamada (MY) scheme gives rather small $EDR^{1/3}$ values. The root-mean-square difference between model simulated and actual data (at all heights) as a function of c_μ for e-l scheme is given in Fig. 4, which shows that a c_μ value of about 0.45 gives the smallest difference. This is consistent with the results in the literature (between 0.40 and 0.55). Using the e-l scheme with $c_\mu = 0.45$, the simulated $EDR^{1/3}$ field is given in Fig. 2. The turbulence intensity is larger at areas just downstream of the mountains of Lantau Island and decreases gradually several kilometres downstream. The results for a northeast monsoon case near HKIA are basically the same (not shown).

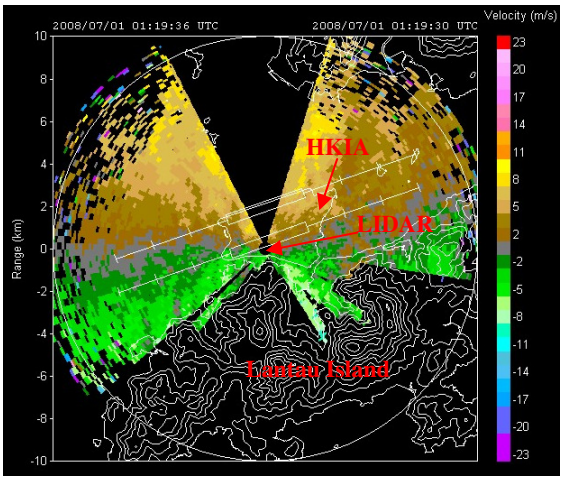

Figure 1. LIDAR velocity image at 3.2-degree conical scan at 01:19 UTC, 1 July 2008.

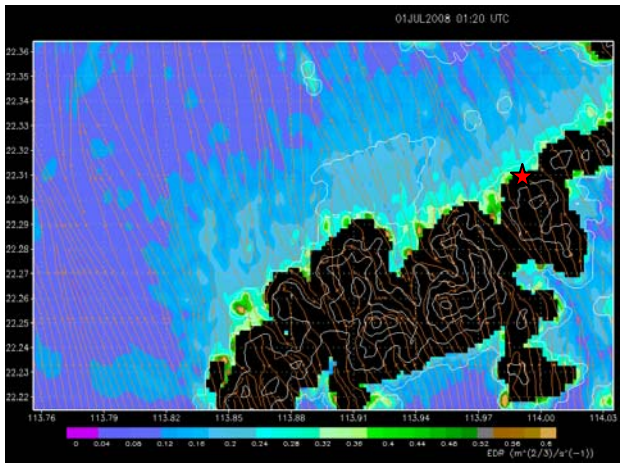

Figure 2. Model simulated $EDR^{1/3}$ field at 50 m AMSL at 01:20 UTC, 1 July 2008. The location of Siu Ho Wan wind profiler is indicated by the star.

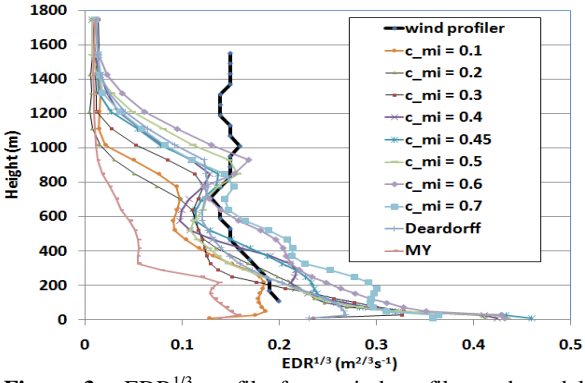

Figure 3. $EDR^{1/3}$ profile from wind profiler and model simulations of different turbulence parameterizations for 1 July 2008 case.

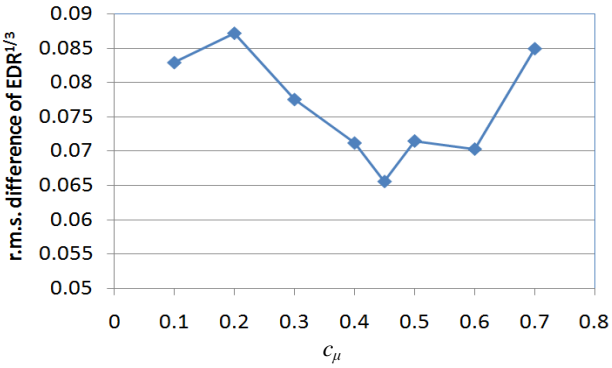

Figure 4. Root-mean-square difference of $EDR^{1/3}$ values as a function of c_μ for 1 July 2008 case.

4 CONCLUSIONS

It has been found that the use of a variable mixing length in e-l scheme in RAMS simulation gives $EDR^{1/3}$ fields comparable with those obtained with Deardorff scheme. The optimal c_μ value (0.45) for model simulation is consistent with those reported in the literature.

REFERENCES

Chan, P.W., 2009: Atmospheric Turbulence in Complex Terrain: Verifying Numerical Model Results with Observations by Remote-sensing Instruments. Meteorol. Atmos. Phys., **103**, 145-157, DOI: 10.1007/s00703-008-0342-3.

Trini Castelli, S., E. Ferrero, D. Anfossi, and R. Ohba, 2005: Turbulence closure models and their application in RAMS. Environmental Fluid Mechanics, **5**, 169–192.

Xu, D., and P.A. Taylor, 1997: On Turbulence Closure Constants for Atmospheric Boundary-Layer Modelling: Neutral Stratification. Boundary-Layer Meteorology, **84**, 267-287.

ESTIMATING AND TESTING THE TOPOGRAPHIC AMPLIFICATION FACTOR USING GIS AND CLIMATE DATA FROM THE WESTERN U.S.

Sharon Zhong, Jessica Van Deusen, Yi Chen, Ashton Shortridge

Department of Geography, Michigan State University
E-mail: *zhongs@msu.edu*

Abstract: High resolution DEM data and GIS tools are employed to identify basins in Western U.S. The value of Topographic Amplification Factor (*TAF*) is estimated for each basin and the usefulness of *TAF* to explain the observed differences in diurnal temperature variations among these basins are explored using climate data.

Keywords: *Topographic Amplification Factor, diurnal temperature range in basins, Western U.S. basins*

1 INTRODUCTION

The Topographic Amplification Factor, or *TAF*, has been used to explain why air in a valley or basin heats or cools more than air over adjacent plains (Steinacker 1984; Whiteman 1990). *TAF* is defined as

$$TAF = \frac{A_{xy}(h)/V_{valley}}{A_{xy}(h)/V_{plain}}$$

where A_{xy} is the horizontal area through which energy enters or leaves the top of the volumes at height *h* above valley floor or plain, and V_{valley} and V_{plain} are the volumes of atmosphere subject to heating or cooling in the two regions, respectively. An elementary integration of first principles of thermodynamics links *TAF* to the differential temperature variations between a valley and a plain. Because the heated or cooled air volume is smaller in a valley than above the plain, the same heating or cooling provides larger increase or decrease of temperature within the valley. Due to its simplicity and intuitiveness, the *TAF* concept has been used to interpret lower minimum temperatures in basins and sinkholes as well as valley wind development.

Using GIS and high resolution DEM data, we have identified basins and sinks in the western United States and estimated their *TAF* values. We have also obtained climate data for a number of basins to examine how well the *TAF* concept may be used to explain the differences in the observed diurnal temperature ranges among the basins.

2 APPROACH

2.1 Finding the basin and estimating *TAF*

To identify basins and estimate *TAF*, we used 1 arc second DEM data and GIS software. Many steps are involved in delineate a basin and determine its *TAF* and the flow chart below outlines the major steps. The basins identified in Western U.S. are shown in Figure 1 and the *TAF* values estimated are listed in Table. 1.

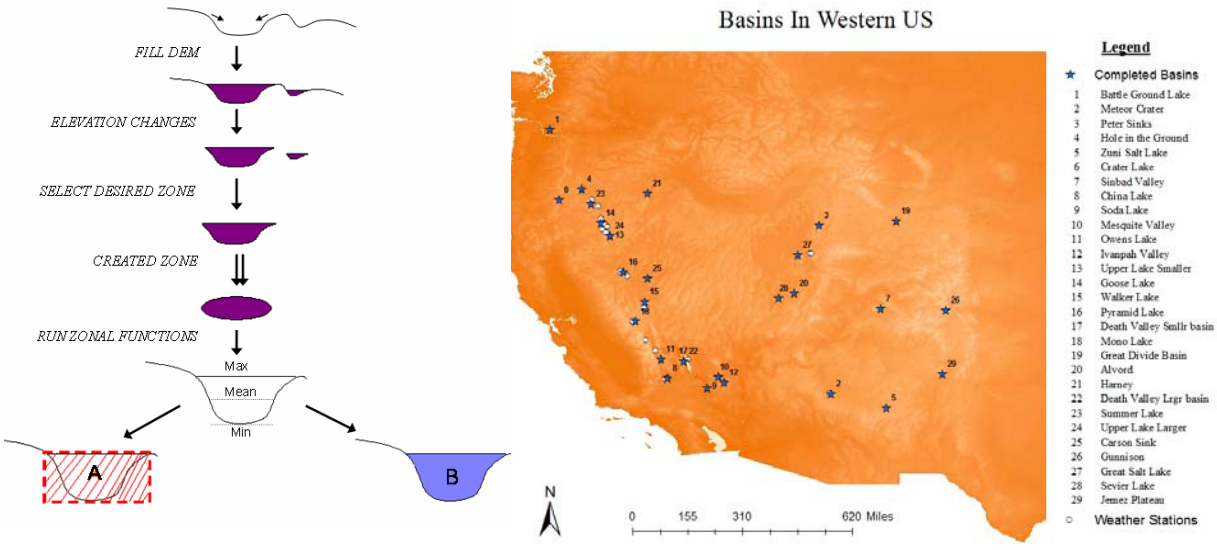

Figure 1. Flow chart (left) showing the major steps in identifying basins in Western U.S. (right). *TAF* is calculated as the ratio B/A. Also shown on the terrain and basin map are locations of weather stations used in the analyses.

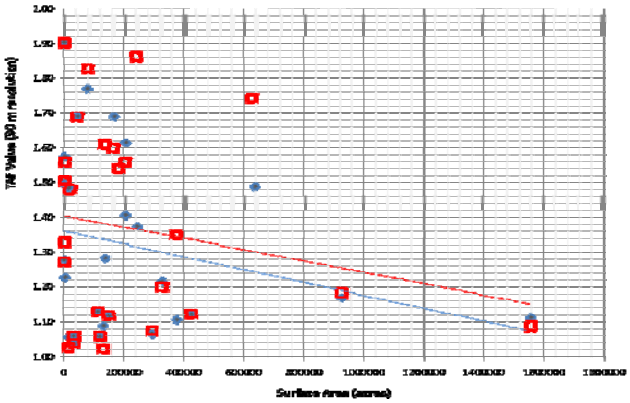

Figure 2 shows *TAF* values as a function of surface area of the basins. As expected, *TAF* value tends to decrease as the surface area of a basin increases. But for small basins, *TAF* values are more sensitive to the slope and shape of the sidewalls.

Figure 2. *TAF* as a function of surface area. The red squares are *TAF* values calculated using 30-m resolution data and the blue diamonds are *TAF* using 90-m data.

Basin Name	TAF	Basin Name	TAF	Basin Name	TAF
Battle Ground Lake	1.270	Mesquite Valley	1.688	Great Divide Basin	1.557
Meteor Crater	1.558	Owens Lake*	1.826	Alvord	1.861
Peter Sinks	1.901	Ivanpah Valley	1.128	Harney	1.073
Hole in the Ground	1.504	Upper Lake (small)	1.057	Death Valley (large)	1.199
Zuni Salt Lake	1.328	Goose Lake	1.022	Summer Lake*	1.349
Crater Lake	1.025	Walker Lake*	1.610	Upper Lake (large)*	1.120
Sinbad Basin	1.478	Pyramid Lake*	1.116	Carson Sink	1.741
China Lake*	1.059	Death Valley (small)*	1.599	Gunnison	1.181
Soda Lake	1.037	Mono Lake*	1.539	Great Salt Lake*	1.086

Table 1. Estimated *TAF* values for basins in Western United States. The * indicates basins having climate data.

2.2 Diurnal temperature range of *TAF*

Climate data are used to determine whether *TAF* or the "volume effect" can be used to explain some of the differences in the maximum and especially the minimum temperature observed in these basins. Because majority of these basins are located in remote areas, only a third of them have climate data available (stared in Table 1). Data from these basins range from 20-30 years and most stations only have temperature and precipitation records which prevented a selection of ideal days with clear sky and weak winds when the volume effect is most prominent. To avoid the errors associate with simple height adjustment in comparing maximum and minimum temperature which may overwhelm the effect of *TAF*, the mean diurnal temperature ranges are compared.

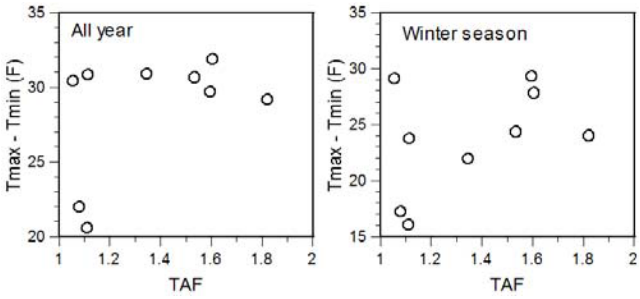

Figure 3. Mean diurnal temperature range and TAF

Figure 3 shows the diurnal temperature variation averaged over days without precipitation as a function of *TAF*. There is no clear relation between the diurnal range and *TAF*. For winter season, there appears to be an indication that larger diurnal range corresponds to larger *TAF* values, but the correlation is weak. Adjustment for density differences did not improve the correlation. The lack of correlation in the current analysis is likely due to other complicating factors affecting energy budget, such as cloudiness, winds, solar radiation, humidity, and vegetation, which could not be controlled in the current analyses. Synoptic maps and output from North American Regional Reanalysis are being used to help better control these factors.

Acknowledgements:
We thank Diane Barach for helping with identifying and downloading climate data. This research is supported by the U.S National Science Foundation through Grants No. ATM 0837860 & ATM 0640206.

REFERENCES

Steinacker, R. 1984: Area-height distribution of a valley and its relation to the valley wind. Contrib. Atmos. Phys. **57**, 64–71.
Whiteman, C.D. 1990: Observations of thermally developed wind systems in mountain valleys, in Atmospheric Processes over Complex Terrain. W. Bluemen ed. Meteorological Monograph, American Meteorological Society, 323 pp.

Winter High Pressure - Mater of mixing air in the Belluno Pre-alpine basin

Robert-Luciani Thierry, Marigo Gianni
E-mail: *tluciani@arpa.veneto.it*
Avalanches Centre of Arabba, ARPA Veneto, Italy

Keywords: synoptic, mixing air, wind, boundary layer, Alps' basin

INTRODUCTION

During winter, High pressures can be present for several days on the Alps with problem of mixing air in the valleys, especially in the Pre-alpine basin like Belluno depression. Normally in this area winds are often very weak, especially during winter, when air viscosity (member of Reynolds) increases appreciably and laminar and stratify flow tends to deposit and almost immovable, without micro-turbulences, so when winds are strong on top of mountains, including in certain situation of Foehn. The absence or long periods of calm of wind without any exchange and strong stagnation of the same air mass in the lower level generate serious problems on the air quality due to high concentration in pollutants (pm10)

DATA AND METHODS

The first step consists to recognize each synoptic configuration observed on meteorological charts at 500, 700, 850 and 950 hPa. In this way to compare the situation in height (free atmosphere) and the same thing at low or ground level (planetary boundary layer) with the aim to create a synoptic database. The complete synoptic classification retains nine different types of weather, but only the first tow type shows principally problems of air mixing. So criteria of the synoptic classification consider wind factor in the low level basin, presence of inversion temperature (Sodar profile), daily temperature range and vertical air motion…

The second step consists to join synoptic situation with wind parameters (speed and direction) in the low layers (six automatic monitoring stations with wind speed and direction at five and ten meters level measurements situated in different and significant point of basin bottom for the needs of present study, added data Sodar in the central part of the basin to evaluate vertical temperature configuration in the first 900/1000 m).

The data of wind have a frequency of 24 mean values/day for the speed and the direction, added value of the strongest gust (max wind speed/24h) registered during all day.

The analysis covers a period of five years 2001-2005, and an other years (2006) with elevated winds analysis and vertical atmospheric data.

Without forgetting a study of cloud cover from HVR and Infrared images of Meteosat8 (2006) to define certain type of day about solar radiation, using 12 images for each day on the Italian oriental Alps.

RESULTS

In Belluno basin 30% of winter period presents problem of mixing air due to very important temperature inversion stratification, absence of wind and no air turbulences in the lowest layers. The weakness of the ventilation associated with the stable situations is a normal fact, but more surprising when anafront arrives with a strong increase of relative humidity and absolute blocking of winds. Paradoxically the situation is more critical within hours which precede the passage of anafront structure. The biggest concentrations of pollutants in the air are observed when temperatures is very cold in the lower levels, with very high humidity and when there is a very important increasing temperatures inversion when warm front reaches Alps.

The worse air mixing conditions correspond in the saturated and cold air or better when there intense and persistent fog in the basin. This last one creates a full-size thermal spatial and vertical homogeneity, preventing any air mixing in the first 50 /100 first meters above ground, thus one almost immobility of air. The moderate movements are of the order of 400 - 600 m/h (speed wind around 0.01, 0.02 m/s) with very high concentration of pm10 at Belluno and Feltre (two biggest city of this Basin)

Another peculiarity of Belluno basin is the absence of winds while on nearest top mountains speed of winds are sometimes strong: 30/50 km/h, but it seems that there are no exchanges between free atmosphere laminar flow

and cold air stratification in the air basin low level. So that it can have a mixing air, is needed vertical dynamics like front crossing or intense Foehn conditions to remove the low layer of cold air. Otherwise the air flow remains very weak, especially during the night, with bad air quality.

The poor quality of air for insufficient ventilation is more often exceeded to Belluno and Feltre than not in Milan. Colder, more humidity and more viscosity determine high stagnation of air with consequent problems, especially in the closed orographic basin, where the erosion of Planetary Boundary layers happens only in case of very dynamical flow conditions.

CONCLUSION

The wind in Valbelluna introduces characteristics of extreme weakness aerologic flow during the stable winter synoptic situation, so during the first phase of disturbance weather. Everywhere in this orographic basin, it possible to observe a very limited dynamic of winds in all the seasons and particularly during the cold semester from October to March, especially in the southern sector where the basin is more closed, with high frequency of fogs or low stratus and high deficit of solar radiation. So during the first phases of wintry disturbance weather, which often appears the worse condition with very high humidity, rather strong temperature inversion and absolute air stagnation. To attended a real remixing of the air, it ‘s necessary to wait the front crossing or Foehn conditions on the Belluno Basin.

REFERENCES

Blackadar A. K. (1957) Boundary layer wind maxima and their significance for growth of nocturnal inversion. Bull. Am. Meteorol. Soc. n° 38, pag . 283-290

Demoor G. (1983); Les théories de la turbulence dans la couche limite atmosphérique. Cours et manuels. Météo-France

Demour G. e Veyre P. (1999). Les bases de la météorologie dynamique. Cours et manuels. Météo-France.

James I. N. (1994); Introduction to circulating atmosphere. Cambridge University Press.

Malardel S. (2005). Fondamentaux de Météorologie, l’école du temps, ed. Cépaduès. Météo-France.

Malardel S. (2005). La couche limite, description e bref aperçu théorique. Cours et Manuel Météo-France

Robert-Luciani Th. (1991). Capitolo sulle situazioni sinottiche sul Nord-Est Italia, pagg. - Tesi di Dottorato

Trom M. (1996) Un’esercitazione di fisica con il foehn, Nimbus 13-14: 99-103

Stull, R. B. (1988). An introduction to Boundary layer Meteorology. Kluwer Academic.

WRF-CHEM STUDY OF THE HIGH OZONE EPISODE DYNAMICS OVER THE COMPLEX TERRAIN OF SLOVENIA

Rahela Žabkar and Jože Rakovec

University of Ljubljana, Faculty of Mathematics and Physics, Chair of Meteorology, Ljubljana, Slovenia
E-mail: *rahela.zabkar@fmf.uni-lj.si*

Abstract: Characteristics of temporal and spatial dynamics of high ozone episodes in Slovenia have been analyzed with the help of a coupled meteorological-photochemistry WRF/Chem model. The ability of model to represent the meteorological conditions and the ozone evolution over the complex terrain of Slovenia has been evaluated.

Keywords: *WRF-Chem model, complex terrain, tropospheric ozone*

1 INTRODUCTION

In Slovenia the highest frequency of exceedances of ozone threshold values during the warm months of the year is usually related to the south-western part of the country, separated from central Slovenia with the Alpine-Dinaric mountain ridge. The rest of Slovenia generally experiences lower ozone daily maxima with occasionally exceeded thresholds.

In the present research we study the temporal and spatial dynamics of high ozone episodes in Slovenia with a coupled meteorological-photochemistry WRF/Chem model. The main purpose is to understand and explain some observed characteristics of the high ozone episodes, e.g. the higher observed ozone maxima in Mediterranean south-western Slovenia (especially during the first part of the episodes) and higher ozone levels in central Slovenia related to the south-western air masses origin (Žabkar et al., 2008), as well as to identify potential direct impact of Po River Basin emissions on ozone levels in Slovenia.

2 METHODOLOGY

Among 50 days in years 2003 to 2005 with ozone daily maxima above 165 μg/m^3 at least at one air quality station, we focus on three episodes (example of measured ozone during one episode shown in Figure 1) for which we explore the characteristics of episode dynamics with a 2.2 version of the WRF/Chem model. Simulations in 27 km, 9 km and 3 km domains (Figure 2) and with 51 vertical levels were performed using a coupled one-way nesting strategy. The initial and boundary meteorological conditions were taken from ECMWF analysis archive data with the 0.25º horizontal resolution and the temporal resolution of 6 hours.

The modelling results were evaluated with ozone measurements from 12 ground level air quality stations and 15 meteorological stations spread over the complex terrain of Slovenia, while vertical structure of atmosphere was compared to radiosounding observations in Ljubljana, Udine and Zagreb.

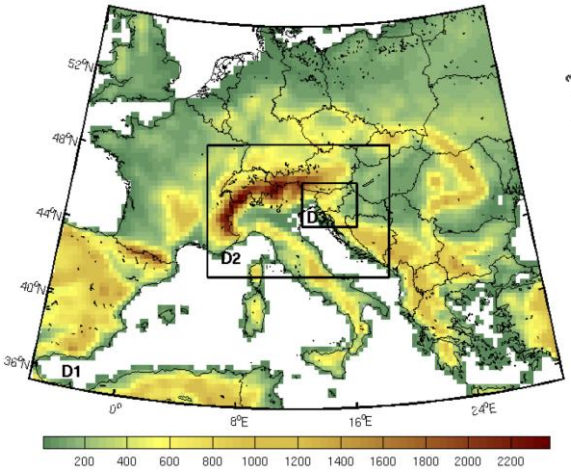

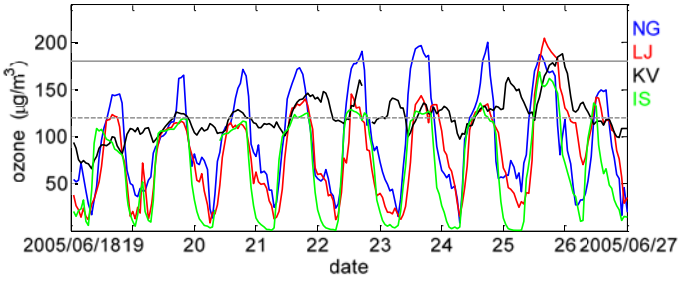

Figure 1. (Above) Measured ozone levels during one of three analyzed episodes at Mediterranean Nova Gorica (NG), elevated Krvavec (KV), rural Iskrba (IS) and urban Ljubljana (LJ) station.

Figure 2. (Left) Configuration of model domains with 27 km (D1), 9 km (D2) and 3 km (D3) resolution. Shown is 27 km orography.

3 RESULTS AND CONCLUSIONS

According to model results all three discussed episodes express a similar temporal evolution, which in general consists of three phases, closely related to the synoptic situation. During the first phase the distinctive air

(re-)circulations, characteristic for the northern Adriatic Sea and its coastal regions (land-sea breezes coupled with thermal mountain winds) enable significant pollutant accumulations in the re-circulating air in the Mediterranean region. Together with favourable meteorological conditions (warm weather, a lot of sunshine and lack of precipitations) this accumulated pollution explains high ozone levels in the south-western Slovenia during the first phase of the episodes, as well as the ozone "jump" at the non-Mediterranean stations during the second phase, when this polluted Mediterranean air is with south-westerly flow advected over Slovenia.

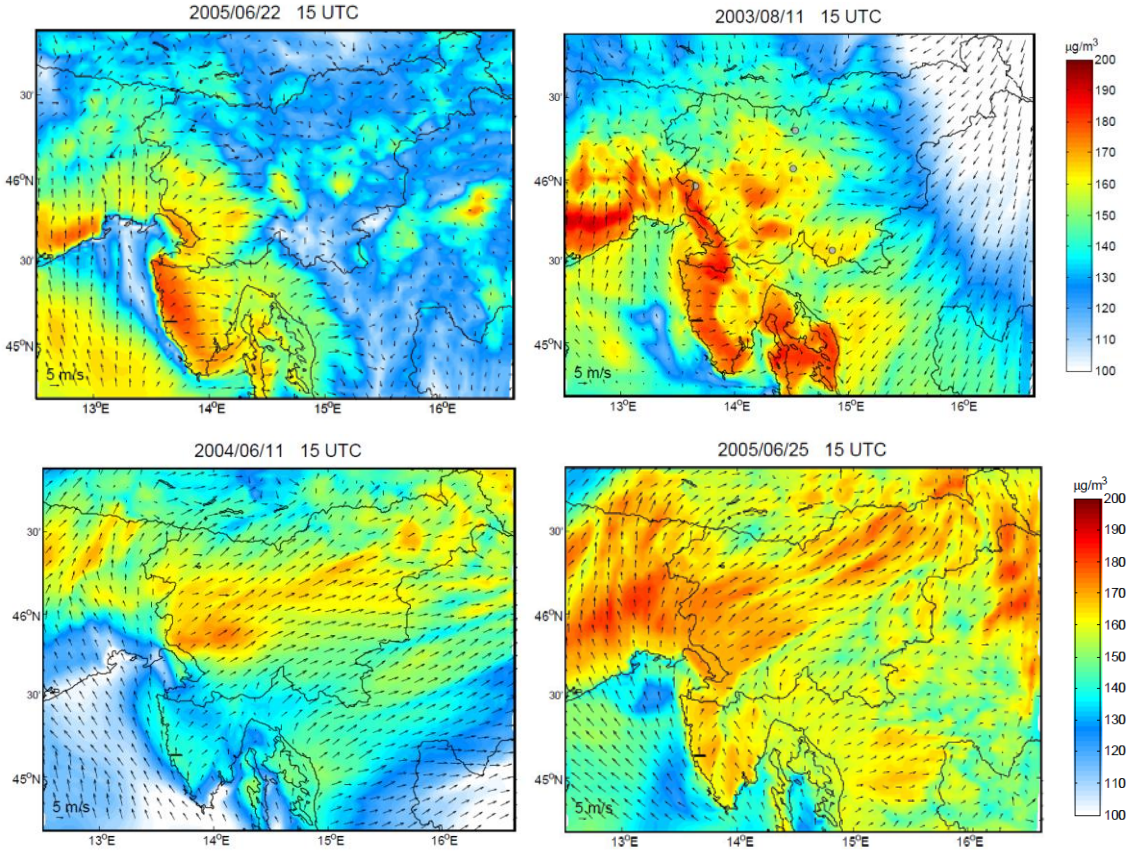

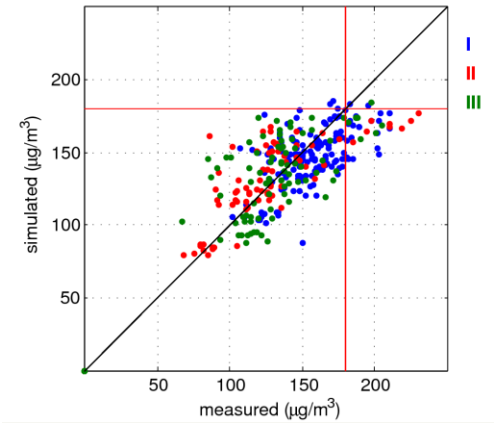

Figure 3. (Above) Examples of simulated near ground ozone and 10 m wind. Upper two panels: during the first phase of the episodes, when near ground ozone levels over coastal areas are significantly higher than over central Slovenia. Lower two panels: during the second phase, when the Mediterranean pollution is with south-westerly flow advected over Slovenia.

Figure 4. (Left) Scatter plot comparing measured and simulated hourly ozone levels for 12 Slovenian stations during three analyzed episodes. Red lines indicate 1-hourl warning threshold value 180 µg/m^3.

With the model we were able to represent the principal characteristics of the episode evolutions, while the accurate representation of location, duration and extension of the highest ozone levels was usually not feasible. The selection of some model parameterization schemes (especially PBL scheme and land surface model) played a significant role in simulated planetary boundary layer meteorological conditions and consequently influenced simulated ozone levels.

REFERENCES

Žabkar R., J. Rakovec, S. Gaberšek, 2008: A trajectory analysis of summertime ozone pollution in Slovenia. *Geofizika*. Volume **25**, 179–202.

HEAT WAVES IN THE ROMANIAN CARPATHIANS DURING THE COLD SEASON

Dana M. Micu [1], Sorin Cheval [2], Mădălina Baciu [2]

[1] Institute of Geography, Romanian Academy, Bucharest, Romania
E-mail: *d_a_n_a_art@yahoo.com*
[2] National Meteorological Administration, Bucharest, Romania

Abstract: Heat waves are a representative index frequently used to analyse the incidence of extreme temperature in a given area. A study was undertaken on the frequency and duration of such phenomena in the Romanian Carpathians during the cold season (September 30-May 31). The STARDEX heat wave definition used reads that: there should be at least five consecutive days with daily maximum temperature deviations higher than 5°C from the multiannual average of the day taken into consideration. Investigations had in view the mountain weather stations located >1,000 m above sea level (27 locations) over the 1961-2007 period. Regional patterns of heat waves were expressed by comparing their severity in terms of persistence for the weather stations located both in the alpine, sub-alpine and forest vegetation belts. The results indicated significant increasing frequency trends of heat wave duration associated to the high temperature anomalies recorded during the cold season, especially in the last quarter of the 20th century and after 2000. Low altitude mountain sites are generally most affected by heat wave occurrence.

Keywords: *heat waves, maximum temperature, Romanian Carpathians*

1 INTRODUCTION

The climate warming process affects the Romanian Carpathians by increased climate variability and extreme events. Even small changes in the means and variations of the key climate variables (temperature and precipitation) might be considered as signals of this process in areas less exposed to a significant temperature increase at high altitude.

Previous studies, focused on the temperature regime and extremes in the Romanian Carpathians at over 1,000 m altitude (Baciu et al., 2004; Cheval et al., 2004; Micu and Micu, 2006 etc.), indicated that highest values were recorded in summer months, while winter and spring warming comes second in terms of statistical significance. In this context, the present study focuses on the temporal and spatial distribution of heat waves during the extended cold season in the Romanian Carpathians. According to the study, the extended cold season is considered to last from September 30 to May 31. Investigations looked at the links between heat wave frequency and duration on the one hand, and the local geographical setting and the atmospheric circulation patterns, on the other.

2 DATA AND METHODS

The study was conducted based on two heat wave indicators defined by the STARDEX project (heat wave duration index and the 90th percentile of heat wave duration). Daily maximum temperature data from 27 weather stations covering the entire Carpathian range and some intra-Carpathian depression areas were analysed in this study over the 1961-2007 period (Fig. 1). The Mann-Kendall and Pettitt statistical tests were applied in order to estimate the trends and detect the shifting years in the cold season time series. The selection of the significance of the corresponding trends and threshold years consider the ≥95% significance level threshold.

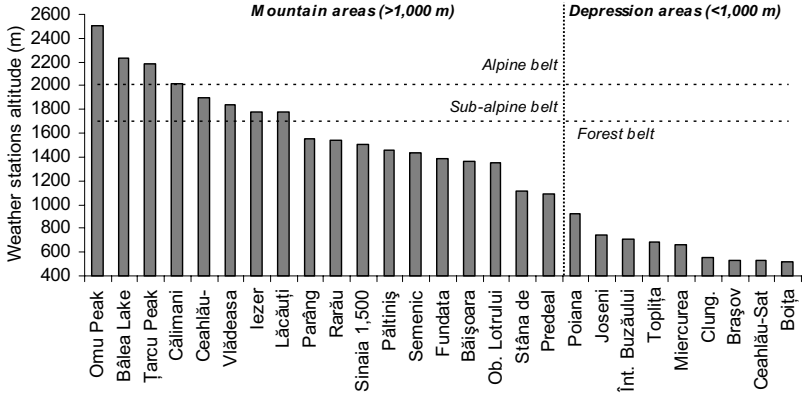

Fig 1. Altitudinal distribution of the 27 weather stations in the Romanian Carpathians, located both in mountain and depression areas.

3 RESULTS

The variability of maximum temperatures in the Romanian Carpathians highlights the heterogeneous character of mountain climate patterns. It is obvious that altitude and the general atmospheric circulation play a very important role in the distribution of temperature values shaping cold season characteristics.

Generally, the Eastern Carpathians show the lowest frequency of heat waves, mainly in the northern part and on their eastern slopes, due to exposure to the circulation of Arctic air masses from the North-Eastern and Northern sectors, causing severe winters and early and prolonged air freeze intervals. It was noticed that heat waves usually cumulated less than 10 days over the entire cold season (47-85% frequency), while durations of 11-20 days count for 9 to 29% over the analysed period. According to statistical tests returns and to these atmospheric circulation patterns, most of the weather stations located in this Carpathian branch showed no significant trends in the variability of heat wave duration over the 1961-2007 period.

The Southern Carpathians and Curvature Carpathians, as well as the Banat Mountains (part of the Western Carpathians) on their western, south-western and southern slopes, are as a rule very much exposed to heat wave duration due to the warm Mediteraneean air mass circulation associated with cyclonic activity. It is worth noting that heat waves in these locations cumulate less than 10 days/season (55-65% frequency) or 11-20 days/season (24-30%).

In terms of the multiannual mean duration of such phenomena the values between the three branches are comparable (Fig. 2).

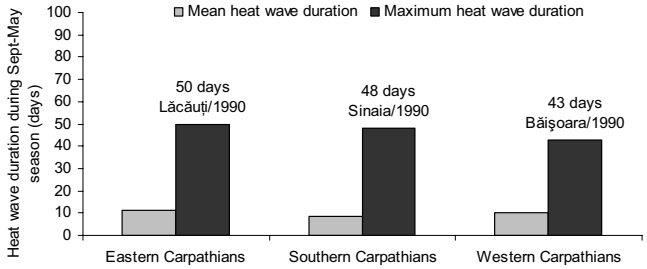

Fig 2. Mean and maximum heat wave durations in the three Romanian Carpathians branches during the cold season.

The data of many forest belt locations in the Western Carpathians (Semenic, Stâna de Vale and Băişoara stations) and in the Southern Carpathians (Parâng, Sinaia 1,500 m and Păltiniş stations) also revealed a higher sensitivity to the climate warming process over the September-May interval. Less visible/or absent even, such influences appeared particularly in the alpine sites, especially those situated above 2,200 m (except for Bâlea Lake where heat waves duration showed increases mostly visible after 2000).

As several climatological studies have already suggested, the Romanian Carpathians recorded higher heat waves frequency during the cold season in most of the studied locations, especially in the last quarter of the 20th century. This finding is also indicated by the Pettitt statistical test to the effect that higher frequency of the shifting years in the heat wave duration occurred during the cold season, after 1990 (66%), than before 1990 (34%).

A low frequency of significant heat waves durations was determined over the late 1960s and the early and mid 1970s, with 11 to 20 days/season at most of the weather stations (especially in the Eastern Carpathians). A better-defined interval of climate warming was delimited starting with 1990 (a record year in terms of maximum heat wave duration in the Romanian Carpathians) particularly since 2000, when most locations (especially the forest belt ones) registered heat waves of 11 to 30 days/season, due to noticeable increase trends of maximum temperature values for most of the mountain areas.

4 CONCLUSIONS

The study has shown that the winter maximum temperature regime of the Romanian Carpathians is clearly influenced by the climate warming process. There is an evident spatial simultaneity in heat waves occurrence especially during the warmest years (e.g. 1990, 2002, 2007). These findings are particularly relevant for forest belt weather stations (located below 1,700-1,600 m), while alpine and sub-alpine sites still maintain their severe winter characteristics. Altitude and the general atmospheric circulation play a very important role in the distribution of temperature values shaping cold season characteristics.

REFERENCES

Baciu, M., Busuioc, A., Breza, T., 2004: Spatial and temporal variability of meteorological phenomena frequency in the cold season, Romanian Journal of Meteorology, **6** (12), 27–39.

Cheval, S., Baciu, M, Breza, T., 2004: The variability of climatic extremes in the Romanian Carpathians, Annals of Western University of Timisoara, Geography series, **XIV**, 59–78.

Micu, D., Micu, M., 2006: Winter temperature trends in the Romanian Carpathians – a climate variability index, Annals of Western University of Timisoara, Geography series, XVI, 141–158.

CASE STUDY OF BURA OF 1ST AND 3RD FEBRUARY 2007

Martina Tudor[1]

[1] Croatian Meteorological and Hydrological Service, Zagreb, Croatia
E-mail: *tudor@cirus.dhz.hr*

Abstract: Two cases when the operational forecast seriously underestimated the wind speed maxima are analysed. The first one in the night between 1st and 2nd February 2007 and the second one in the evening of 3rd February 2007.

Keywords: *bura,*

1 INTRODUCTION

The operational forecast is performed using hydrostatic Aladin model with 8 km horizontal resolution on 37 vertical levels using digital filter initialization (DFI, no data assimilation), semi-Lagrangian horizontal diffusion (SLHD) and prognostic TKE scheme. That forecast is operationally further dynamically downscaled to 2 km horizontal resolution using the procedure described in Ivatek-Šahdan and Tudor (2004).

2 DATA AND METHODS

2.1 General situation

On 1st February 2007, the NW jet-stream moved SW across Croatia. Its edge reached the eastern Adriatic coastline around 12 UTC. Then the direction of the jet stream changes, from NW to NE as the jet strengthens and moves SE along the coast. On 3rd February, at 9 UTC another NW jet-stream reaches Croatia, strengthens and changes the wind direction from NW to NE as it reaches further SE by the evening of the same day. The high level wind is first perpendicular to the Dinaric Alps, but later in the 2nd episode it is parallel to the mountains on eastern Adriatic coast.

2.2 Observed weather

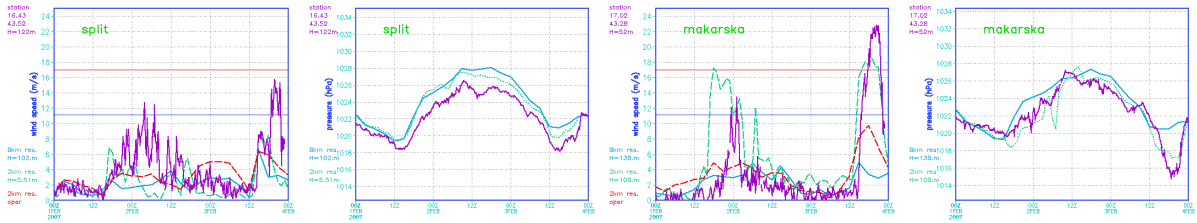

Figure 1. Forecast in 8 km resolution (blue line), 2 km dynamical adaptation (red dashed) and 2 km resolution full run (green dashed) and 10 minute measurements (purple) of 10 m wind and pressure reduced to mean sea level for Split (left) and Makarska (right) locations. The longitude and latitude of the measuring station locations as well as height are also shown.

During the evening and night on 1st and 2nd February 2007, measured 10 m wind speed significantly exceeded the forecast one (Figure 1). Average 10 minute wind speed significantly changed from one interval to the next one. Vertical sounding data (Figure 2) show two temperature inversions, at 850 and at 700 hPa, but the upper one is barely noticeable in the Zadar sounding. The second bura episode, in the evening of 3rd February 2007 was characterized by much stronger and more steady 10 m wind. There were also two temperature inversion layers, one at 900 and 700 hPa.

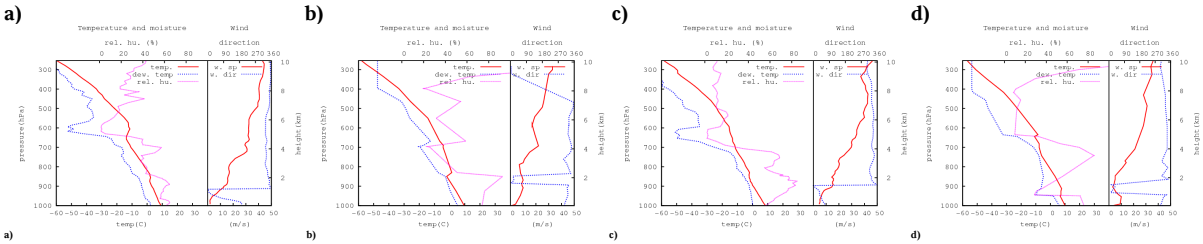

Figure 2. Measured vertical profiles of temperature and wind for Zagreb (a and c) and Zadar (b and d) locations for 12 UTC on 1st (a and b) and 3rd (c and d) February 2007.

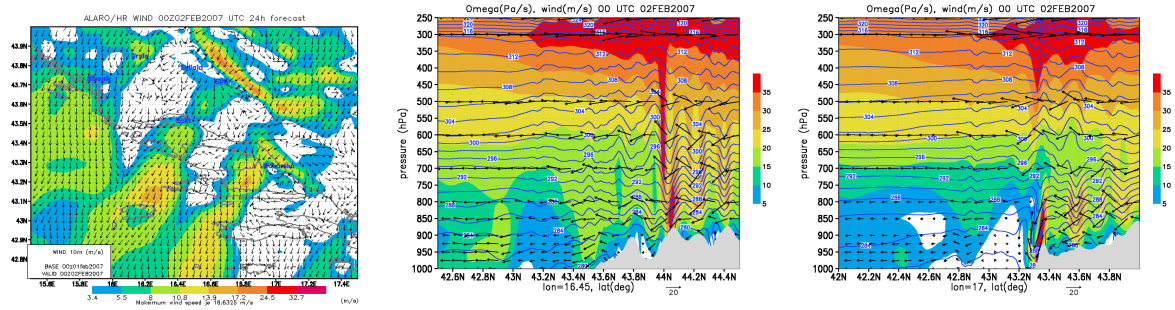

Figure 3. Forecast of wind 10 m above ground (left) and meridional vertical cross-sections through Split (center) and Makarska (right) for 00 UTC 2nd February 2007. Vertical cross-sections show potential temperature in blue lines and arrows show the direction of vertical velocity component.

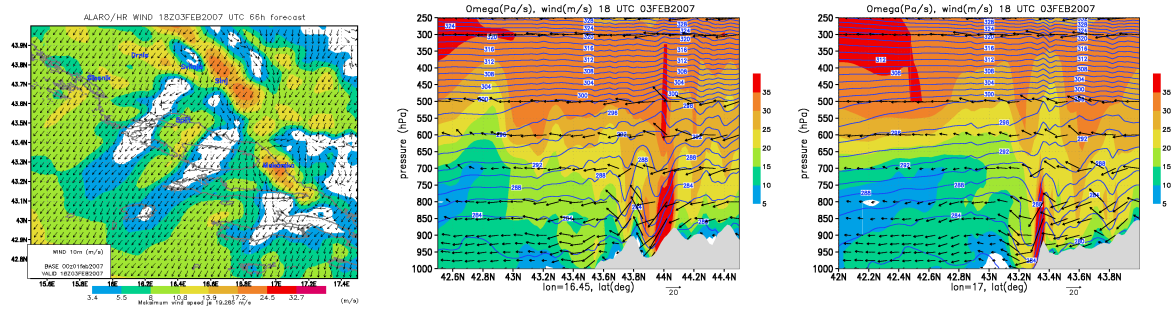

Figure 4. As Figure 3 for 18 UTC 3rd February 2007.

3 MODEL SETUP

The full 2 km resolution forecast alone instead of the operational dynamical adaptation did not improve the forecast, but the full forecast run was used to test the impact of other processes in the model. The possibility that the digital filter initialization (DFI) removed part of the energy of the high-frequency waves from the initial conditions was explored, but the run without DFI did not improve the simulated wind field. There are two horizontal diffusion schemes used simultaneously in the operational model. One is the "standard" 4th order numerical diffusion (ND), and the other is the semi-lagrangian horizontal diffusion (SLHD) scheme. When the intensity of the ND was reduced by a factor of 100, high amplitude waves developed which were responsible for development of the windstorm. Unfortunately not on all locations that were hit by this bura episode.

The first bura episode is characterized by a stable layer above mountains below 700 hPa and less stable layer above (Figure 3) while in the second one the layer up to 500 hPa was far less stable than the one above (Figure 4). In both cases, the high amplitude wave developed on the lee side of Biokovo mountain (right panel of Figures 3 and 4) as well as Dinara mountain upstream of Split (center panel of Figures 3 and 4) but the windstorm is too weak in the Split area (for lat=43.5 in the center panel of Figures 3 and 4).

4 CONCLUSIONS

Usage of non-hydrostatic (NH) dynamics did not improve the 10m wind forecast but it had a positive impact higher in the atmosphere, where usage of SLHD and NH dynamics reduces the TKE as well as values of extreme PV suggesting that removal of those two mechanisms forces other, like vertical turbulent diffusion, to compensate.

Acknowledgements: *The author wishes to thank Ivana Stiperski for advice, literature and for being the patient listener.*

REFERENCES

Ivatek-Šahdan, S. and M. Tudor, 2004: Use of High-Resolution Dynamical Adaptation in Operational Suite and Research Impact Studies. Meteorologische Zeitschrift, 13, No. 2, 1-10

THE COMPLEX BORA FLOW IN THE LEE OF SOUTHERN VELEBIT

Ivana Stiperski[1], Branka Ivančan-Picek[1], Vanda Grubišić[2]

[1] Meteorological and Hydrological Service, Zagreb, Croatia
E-mail: *stiperski@cirus.dhz.hr*
[2] University of Vienna, Vienna, Austria

Abstract: The complex flow structure in the lee of the Southern Velebit is investigated by means of very high-resolution numerical simulations carried out with the NRL COAMPS model. The focus is placed on a wintertime severe bora episode. The spatially complex and temporally highly variable 3D flow structure is characterized by a hydraulic jump over the lee slope and a pronounced wake over the Zadar area. The wake structure appears very sensitive to the upstream flow evolution and is highly non-stationary. The reversed flow along the wake centerline as well as flow separation and rotor formation are observed during different stages of the bora evolution. Sensitivity experiments show the height of Velebit exerting a strong influence on the flow structure, including the onset and strength of the bora flow and the structure of the wake. The terrain of the Zadar peninsula, although significantly lower than that of Velebit, is shown to influence the characteristics of the fully developed bora flow.

Keywords: *bora, critical level, orography, rotors, upstream conditions, wake*

1 INTRODUCTION

The strong bora winds are a common occurrence along the eastern mountainous Adriatic coast, especially in wintertime. The most severe Bora is found in the foothills of Southern Velebit, characterized by significant horizontal and vertical wind speed variability over a relatively small area (e.g. Grubišić, 2004; Belušić and Klaić, 2006). The highest bora windspeed ever recorded in Croatia (69 m/s) was measured in the lee of the southern tip of Velebit. Located only a short distance away, in the lee of one of the highest Velebit peaks (1757m), the area of the city of Zadar (ZD) (Fig. 1) is characterized climatologically by winds considerably weaker compared to its surroundings. In this study we investigate small-scale characteristics and spatial variability of the severe Bora flow in the wider Zadar area with the aim of identifying reason for the "Zadar calm". A severe bora event of 20 December 2004 is examined during which a sodar system was operated at the Zadar Zemunik (ZZ) airport.

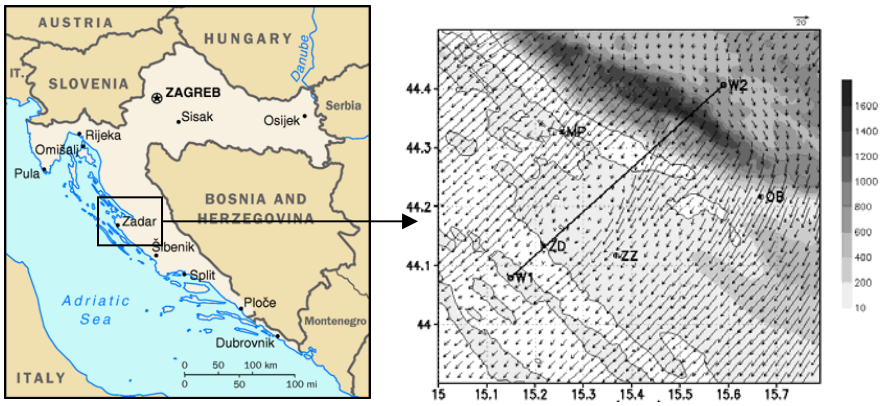

Figure1. Location of Southern Velebit with broader Zadar area (left) and the innermost model domain (right). Letter codes in the right panel indicate stations Zadar (ZD), Zadar airport (ZZ), Obrovac (OB), and Pag Bridge (MB). W1-W2 marks the baseline of the vertical cross section through the wake.

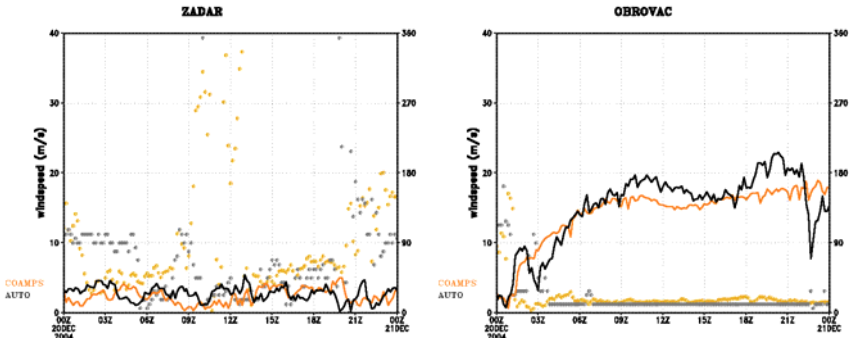

Figure 2. Time series of the measured (grey) and modeled (orange) 10-minute wind speed (solid) and wind direction (dotted line) at Zadar (ZD) and Obrovac (OB).

2 BORA OBSERVATIONS AND MODEL SETUP

The examined bora event developed under the influence of a lee cyclone in the Gulf of Genoa and a high-pressure system over central Europe. The upstream flow impinging on the Velebit was characterized by a synoptically induced critical level at 3.2 km and several inversions with the bases at 0.6, 1.3 and 2.3 km. The bora flow showed significant spatio-temporal variability as seen by comparing the winds measured at the automatic weather stations Pag Bridge and Obrovac with those at Zadar, where the wind was distinctly weaker (Fig. 2). The simultaneous sodar measurements at ZZ reveal a weak low-level flow and the maximum bora speeds above 300 m MSL (Ivančan-Picek et al. 2007). The analysis of the

spatial and temporal bora flow variability was facilitated by real-data three-dimensional numerical simulations, carried out with the nonhydrostatic NRL's COAMPS model with 6 nested domains. The horizontal resolution in the innermost domain was 333 m. In addition to the baseline run, two sensitivity experiments were conducted, one with the reduced Velebit height (rhV), and the other in which the topography of the Zadar peninsula was removed (nZ).

3 RESULTS

The numerical results shown in Fig. 3 show a hydraulic jump over the steep lee slopes of the Velebit, followed further downstream by a pronounced wake over the city of Zadar and beyond. The wake is spatially and temporally highly variable (Gohm et al. 2008). It is especially well developed in the initial stages of the bora development (Fig. 3 left and center), when a reversed flow is present along the wake centerline (Schär and Smith 1993). The reversed flow at the ground is also present towards the end of the examined period (from 21-23 UTC; Fig. 4), with trapped lee waves and weak and shallow lee-wave rotors over the Zadar peninsula (Hertenstein and Kuettner 2003), suggesting a possibility of the lee wave resonance (Grubišić and Stiperski 2009). The reduction of the Velebit height leads to the disappearance of the wake; instead the high-speed flow at low levels extends far downstream (Fig. 3 right). The removal of the Zadar peninsula affects most strongly the flow separation and the rotor zone (Fig. 4 right), with the reversed flow that is both stronger (> -5ms^{-1}) and higher reaching.

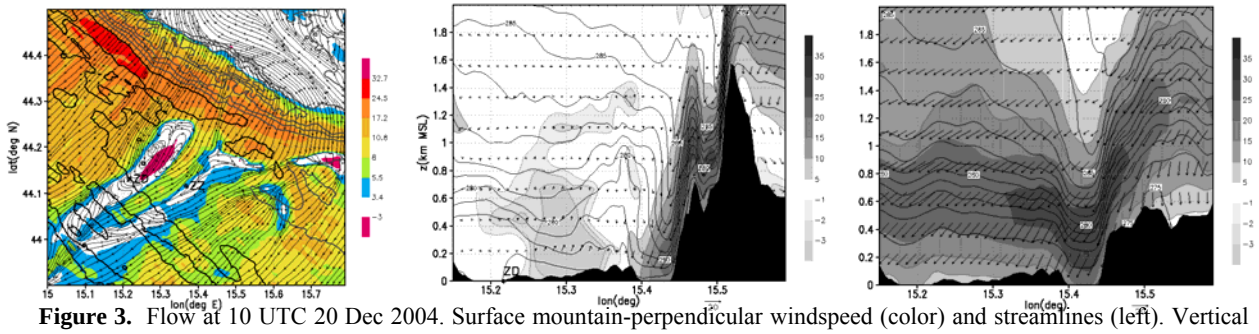

Figure 3. Flow at 10 UTC 20 Dec 2004. Surface mountain-perpendicular windspeed (color) and streamlines (left). Vertical cross-sections of mountain-perpendicular windspeed (gray shade), potential temperature (lines) and horizontal wind direction (arrows) along W1-W2 for the baseline run (center) and the rhV run (right).

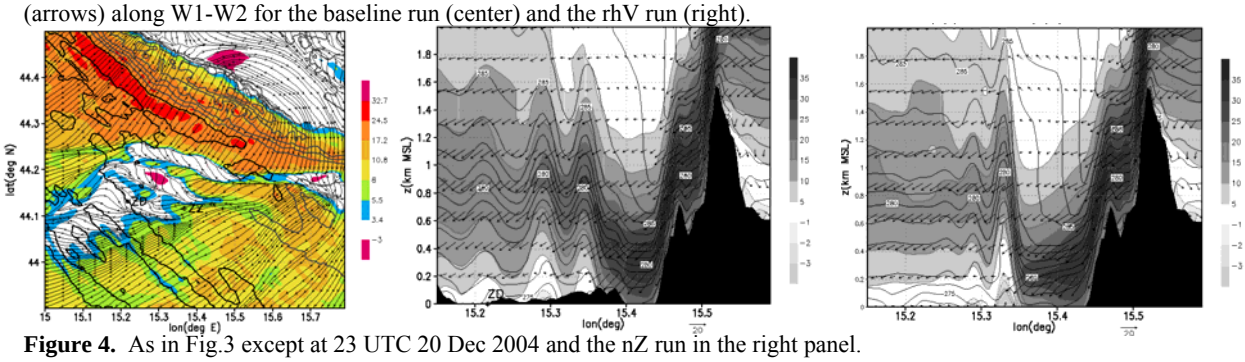

Figure 4. As in Fig.3 except at 23 UTC 20 Dec 2004 and the nZ run in the right panel.

4 CONCLUSIONS

The new observations and numerical simulations of the flow in the lee of Southern Velebit provide an insight into the nature of the "Zadar calm", which lies within the wake of the highest terrain. The wake is strongly influenced by the upstream flow evolution and shows high spatio-temporal variability. Both the terrain of the Southern Velebit and the low-elevation Zadar peninsula were found to exert a strong control of the wake flow.

REFERENCES

Belušić, D., Z. B. Klaić 2006: Mesoscale dynamics, structure and predictability of a severe Adriatic bora case. *Meteorol. Z.*, **15**, 157–168.

Gohm, A., G. J. Mayr, A. Fix, and A. Giez, 2008: On the onset of bora and formation of rotors and jumps near a mountain gap. *Quart. J. Roy. Meteor. Soc.*,**134**, 21-46.

Grubišić, V., 2004: Bora-driven potential vorticity banners over the Adriatic. *Quart. J. Roy. Meteor.Soc.,* **130**, 2571-2603.

Grubišić, V., and I. Stiperski, 2009: Lee wave resonances over double bell-shaped obstacles. *J. Atmos. Sci.,* In press.

Hertenstein, R.F., and J.P. Kuettner, 2003: Rotor types associated with steep lee topography: influence of the wind profile. *Tellus*, **57**, 117-135.

Schär, C., and R.B. Smith, 1993: Shallow-water flow past isolated topography. Part I: vorticity production and wake formation. J. Atmos. Sci. **50**, 1373-1400.

Ivančan-Picek , B., V. Grubišić, I. Stiperski, M. Xiao, and A. Bajić, 2007: "Zadar calm" during severe bora. *Proc. 29th Intern. Conf. on Alpine Meteorology*, Chambery, France, 261–264.

OROGRAPHIC ENHANCEMENT OF SEVERE WINDSTORMS IN THE AUSTRIAN ALPS: TWO CASE STUDIES

Florian Pfurtscheller[1], Alexander Gohm[1]

[1] Institute of Meteorology and Geophysics, University of Innsbruck, Innsbruck, Austria
E-mail: *Florian.Pfurtscheller@student.uibk.ac.at*

Abstract: This study investigates two different types of windstorms that occurred in winter 2008. The analysis is based on observations from an operational network of automatic weather stations and high-resolution numerical simulations with the mesoscale model RAMS. The study shows the similarities and differences between the two windstorms regarding the wind speeds on the northern and southern side of the Alps and demonstrates the ability of RAMS to simulate the storms in a regional scale.

***K*eywords:** *winterstorms, RAMS, north foehn*

1 INTRODUCTION

Mid-latitude windstorms in wintertime, associated with intense cyclones and jet streams, are among the natural hazards that cause the greatest damage to vegetation, infrastructure, and human life. For example, the windstorm Kyrill that occurred in January 2007 was responsible for 49 fatalities and insured losses over 2.4 billion of US dollars in central and northern Europe (Munich Re Group, 2008). Over flat terrain such storms often cover large areas influencing many countries. In complex terrain such as the Alps the wind field is modified by the orography and the severity of the associated winds decreases or even enhances depending on the location. Our goal is to analyze two windstorms, which occured in the winter 2008, to investigate the performance of a mesoscale numerical model to simulate the intensity and pattern of the wind field in regional and local scale.

2 DATA AND MODEL

The data consists of measurements from automatic weather stations (AWS) of the Austrian national weather service ZAMG and several avalanche warning services, as well as from SYNOP-stations. The numerical model used for the analysis is the Regional Atmospheric Modeling System RAMS (Cotton et al., 2003). The model domain consists of three nested grids with horizontal grid spacing of 32, 8 and 2 km. The outermost grid covers whole Europe while the innermost grid covers the area of the Eastern Alps including Austria (Fig. 1). Sensitivity simulations were conducted with an additional fourth grid with horizontal grid spacing of 0.7 km (see black boxes in Fig. 1a–b)

3 RESULTS

Our first case, the windstorm Paula, occurred between 18 UTC 26 January and 06 UTC 28 January 2008 and was associated with a jet stream that caused northerly winds over eastern Europe. The eastern parts of the

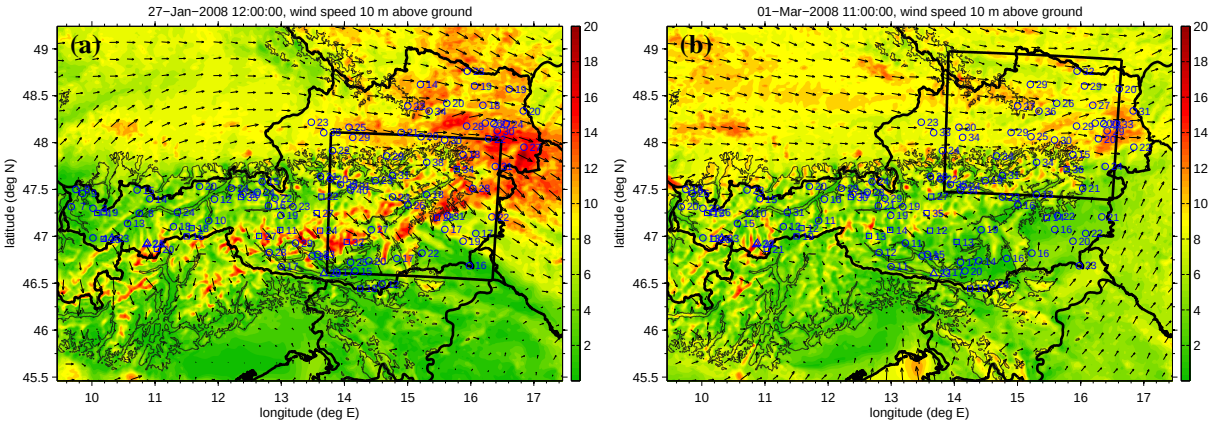

Figure 1: RAMS simulated wind speeds (m s^{-1}) and wind vectors of model domain three at 10 m above ground at (a) 12 UTC 27 January 2008 with observed maximum wind gusts on 27 January 2008 and at (b) 11 UTC 01 March 2008 with observed maximum wind gusts on 01 March 2008

Austrian Alps were most affected by the windstorm. Sustained wind speeds at mountain stations typically exceeded 30 m s^{-1}, with gusts up to 64 m s^{-1}. In valleys and over flat areas sustained winds typically exceeded 20 m s^{-1}. The simulation and observations (Fig. 1a) of the first case show that the highest wind speeds were caused by flow channelling in the Danube River Valley (northwestern Austria), by a corner jet at the eastern edge of the Alps and by north foehn in the valleys on the southern side of the Alps. Stations affected by the north foehn measured exceptionally high wind gusts of up to 40 m s^{-1} in the valleys between eastern Tirol and Burgenland (12-17°E). The time series of Graz (Fig. 2) shows that the RAMS simulation with four grids is able to capture the breakthrough of the north foehn. However, both simulations have problems to reproduce the low-level cooling during the calm conditions in the night before, which is associated with a very strong, only 400 m thick, surface inversion. The radiosonde of Graz at 03 UTC (not shown) reveals a strength of this inversion of more than 12°C . With the turbulence parameterization of Deardorff (Deardorff, 1980) the wind speeds in the four-grid simulation better agree with the observed gusts, while the surface winds in the simulation with three grids and with the turbulence parameterization of Mellor-Yamada (Mellor and Yamada, 1982) are closer to the observed sustained wind speeds. The second case occurred between 00 UTC 01 March and 06 UTC 03 March 2008. It can be separated into two windstorm events: Emma and Fee. Our focus is on Emma, and in contrast to Paula, this storm affected greater parts of central and northwestern Europe. The synoptic scale flow was from northwesterly directions. Fig. 1b shows that in contrast to Paula the strongest winds exceeding 30 m s^{-1} occurred north of the Alps. The highest wind speeds were also caused by flow channelling in the Danube River Valley and a corner jet at the eastern edge of the Alps, while the southern side was partly sheltered by the Alpine barrier. With the approach of an intense cold front and thunderstorms, winds on the northern side of the Alps increased. With the passage of front north foehn was reported in some valleys on the southern side of the Alps.

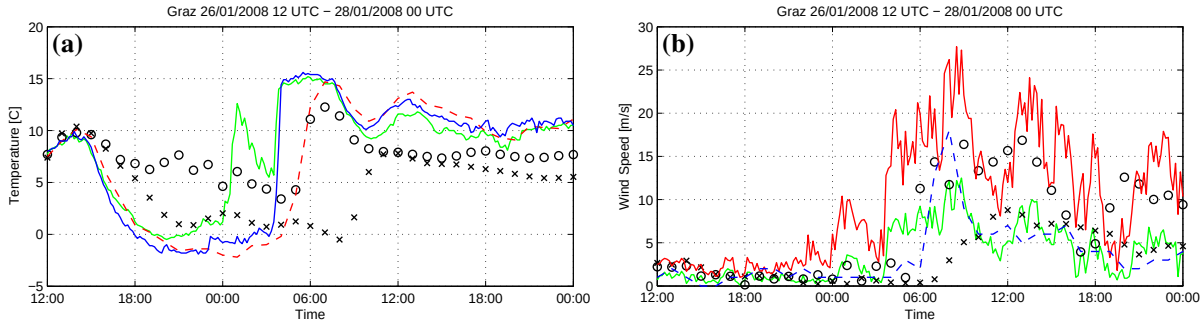

Figure 2: (a) Time series of temperature of two AWS at the town of Graz (solid green and blue line) and of the SYNOP-station at the airport of Graz (dashed) compared with the three-grid simulation (crosses) and four-grid simulation (circles). (b) Time series of wind speed (green) and gusts (red) at the 'green' AWS shown in (a) and the wind speed at the airport of Graz (dashed) compared with the wind speeds of the three-grid simulation (crosses) and four-grid simulation (circles), respectively.

4 CONCLUSIONS

The RAMS simulations are able to capture the wind speeds at a regional scale, but have problems in a local scale. Both events are characterized by wind modification and enhancement by flow channeling in the Danube River Valley and by a corner jet at the eastern edge of the Alps. In contrast to the first case Paula, Emma did not cause severe winds and gusts at the mountains and in the valleys on the southside of the Alps.

Acknowledgements: *We thank Manuela Lehner for her support in conducting the simulations and the ZAMG and several Austrian avalanche warning services for providing the observations.*

REFERENCES

Cotton, W.R., R.A. Pielke, R.L. Walko, G.E. Liston, C.J. Tremback, H. Jiang, R.L. McAnelly, J.Y. Harrington, M.E. Nicholls, G.G. Carrio, and J.P. McFadden, 2003: RAMS 2001: Current status and future directions. *Meteor. Atmos. Phys.*, **82**, 5–29.

Mellor G.L., T. Yamada, 1982: Development of a turbulence closure model for geophysical fluid problems. *Rev. Geophys. Space Phys.*, **20**, 851–875

Deardorff J.W., 1980: Stratocumulus-capped mixed layers derived from a three-dimensional model. *Bound. Layer Meteor.*, **18**, 495–527

Munich Re Group, 2008: *Highs and lows–Weather risks in central Europe.* Munich Reinsurance Company, Munich, 58 pp. http://www.munichre.com/pulications/302-05482_en.pdf, accessed 08 April 2009

FOEHN DIAGNOSIS AND MODEL VERIFICATION

Klaus Burri[1], Bruno Dürr[2], Thomas Gutermann[3], Christian Häberli[4], Patrick Hächler[4], Alfred Neururer[5], Hans Richner[6], and Richard Werner[7]

[1] Working Group Foehn-Research Rhine Valley/Lake Constance
E-mail: *knburri@swissonline.ch*
[2] Sunergy GmbH, Buchs, Switzerland
[3] formerly MeteoSwiss, Zurich, Switzerland
[4] MeteoSwiss, Zurich, Switzerland
[5] Central Institute for Meteorology and Geodynamics (ZAMG), Regional Office for Tyrol and Vorarlberg, Innsbruck, Austria
[6] Institute for Atmospheric and Climate Science, ETH Zurich, Zurich, Switzerland
[7] Salzachwind GmbH, Dornbirn, Austria

Abstract: The strong foehn case of December 8, 2006 is analysed and used as testbed for the mesoscale model COSMO-2. The investigations are a joint effort of Austrian, German and Swiss researchers and focus on the Rhine Valley and Lake of Constance.

Keywords: *ICAM, foehn, case study, model verification, forecasting, climatology*

1 INTRODUCTION

The "Working Group Foehn-Research Rhine Valley/Lake Constance" (AGF, Arbeitsgemeinschaft Föhnforschung Rheintal/Bodensee) collects and archives meteorological parameters and investigates foehn phenomena in the Rhine Valley since the early 1970's. The main task of the Working Group is to find plausible criteria and methods for a more reliable foehn forecast.

At present, a report is being prepared which studies in detail the foehn case of December 8, 2006. This foehn case produced high wind velocities and was reaching quite far; it was one of the rare cases when foehn was observed north of Lake of Constance.

2 WHAT IS FOEHN?

Despite the fact that even professional meteorologists believe that foehn can be identified unambiguously, there are uncertainties when defining a particular weather pattern as "synoptic foehn situation". Similarly, there are no generally accepted criteria for foehn-typical parameters such as cross-ridge pressure gradient, wind direction and speed, temperature, and humidity that would give a clear YES or NO decision for foehn at a specific location. Because different meteorologists use different definitions, a comparison of foehn statistics is difficult, sometimes impossible.

An objective, computer-based method for determining foehn at a given station has recently been developed. The criteria are based on data supplied by the automatic network Swissmetnet (formerly ANETZ). Threshold values for the various parameters are station-specific; they were determined by using elaborate statistical methods. As a test, the automatic method was compared to the most careful, subjective classifications of the weather situation for the two primary foehn stations Altdorf and Vaduz, this for the period January to November 2008. For Altdorf, the objective method yielded 70, the subjective one 69 foehn incidents, however, they agreed only on 67; hence, objectively there were 3, subjectively 2 additional – but different! – incidents. For Vaduz, the methods agreed on 58 incidents, the objective one produced 3, the subjective one 6 additional unrelated foehn incidents. Details of the objective classification procedure are to be published soon.

3 THE FOEHN CASE OF DECEMBER 8, 2006

Fig. 1 shows the synoptic situation at the surface for December 8, 2006. In the previous week, cold air intrusions between Newfoundland and Greenland caused the formation of troughs over the Atlantic. On their leading edge, large regions of Europe were in a mild southwesterly flow. Repeatedly, there were strong cyclogeneses between Iceland and Great Britain. On December 7, steered by a low over Scotland, cold polar air moved southward. On December 8, the low had moved over the North Sea, and over the Benelux a secondary low formed which must be regarded as the trigger for the strong foehn situation over the Alps. As can be seen in the surface analysis (Fig. 1), the eastward moving, associated cold front was retarded by the formation of a wave. The surface pressure difference between Locarno-Monti and Vaduz increased to 13.3 hPa at 09 UTC, between Bozen and Innsbruck to 8.5 hPa at 12 UTC.

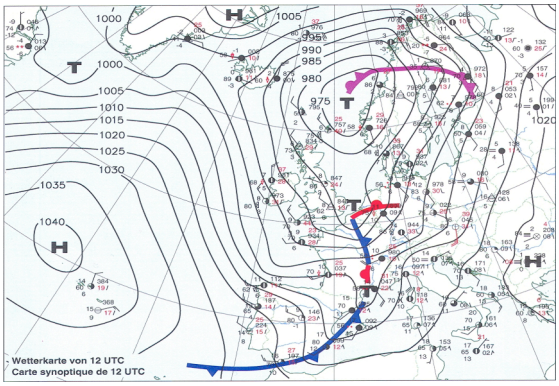

Figure 1. Synoptic surface chart for December 8, 2006. (Provided by MeteoSwiss)

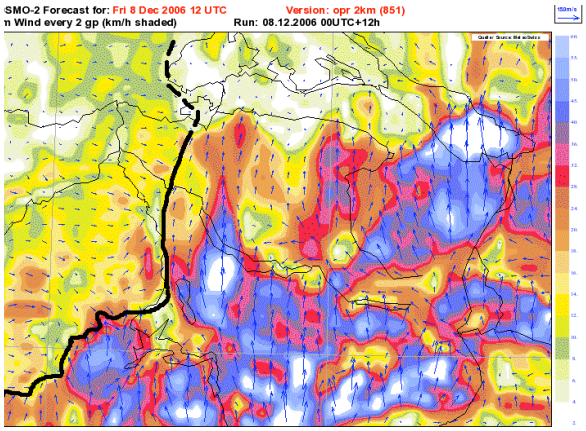

Figure 2. COSMO-2 forecast for the Rhine Valley region.

4 MESOSCALE ANALYSES

A significant event as this foehn case offers a perfect possibility to test forecasting procedures. For 12 UTC of December 8, VERA analyses were produced for the parameters pressure, potential temperature, surface wind direction and speed, and equivalent-potential temperature (VERA: Vienna Enhanced Resolution Analysis). Subsequently, the 12-hour forecast of the COSMO-2 model of MeteoSwiss (Fig. 2) was compared to actual observations at specific stations and to the detailed analysis.

In general, the model produces the main features on the larger scale quite well; fields for pressure, temperature, humidity, and wind do show the major characteristics. Wind speed over the Alpine ridge is reasonable. The (too) high wind speeds east of Lake of Constance are most likely caused by underestimating friction over the smooth water surface, and possibly by the fact that the model assumes a slightly higher temperature of the water. This increases the instability, making it easier for the air mass to penetrate the surface boundary layer.

When it comes to details, several shortcomings of the forecast must be noted: Despite the 2-km resolution, features that are induced by the topography are not represented satisfactorily. In particular, the specific representation of winds in valleys (lack of channelling and too low wind speed, important issues for forecasting a foehn storm) and of the diffluence of the flow at the valley exits (wind speeds over the Lake of Constance are unrealistically high) is inadequate.

Cloudiness and relative humidity fields exhibit the classical pattern for a prefrontal foehn: clouds over the Alpine ridge, frontal cloudiness from the Jura Mountains to the Black Forest. Relative humidity over the Swiss Plateau is – as consequence of the penetrating foehn air – below 50 percent (Fig. 3).

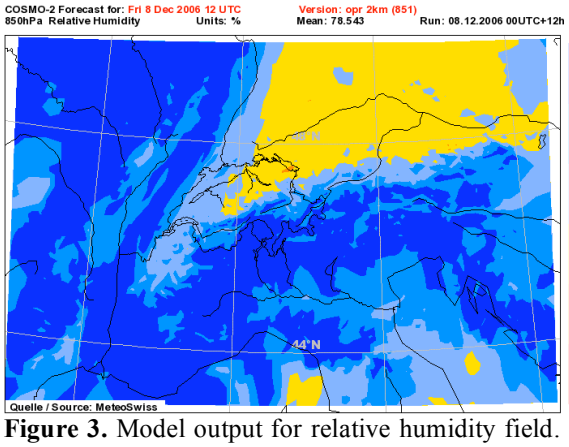

Figure 3. Model output for relative humidity field. Yellow indicates humidity below 50 percent.

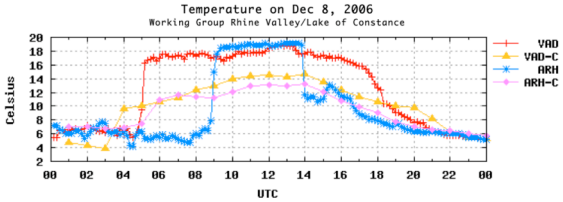

Figure 4. Observed and forecast temperature for Vaduz (VAD) and Altenrhein (ARH). The forecast values are labelled with VAD-C and ARH-C, respectively.

A time series analysis (Fig. 4) shows that the model is not (yet) capable to forecast the onset and breakdown of foehn at a specific location. The change of the air mass, expressed by significant changes in wind, temperature, and humidity is represented unsatisfactorily; the changes occur too early and are much too small.

Acknowledgements:
We thank MeteoSwiss for supplying the data used in our study. In particular, we are indebted to Emanuele Zala (MeteoSwiss) who provided the model data for the comparisons.

LABORATORY EXPERIMENTS ON MOUNTAIN INDUCED ROTORS

Christoph Knigge[1], Dieter Etling[1], Alexandre Paci[2], Olivier Eiff[3]

[1] Institut für Meteorologie und Klimatologie, Leibniz Universität Hannover, Hanover, Germany
[2] Centre National de Recherches Météorologiques Toulouse, Météo-France, Toulouse Cedex, France
[3] Institut de Méchanique des Fluides de Toulouse, Université de Toulouse, Toulouse, France
E-mail: *knigge@muk.uni-hannover.de*

Abstract: We present laboratory experiments on stratified flows over isolated obstacles which were aimed at the simulation of atmospheric rotors. An elevated density inversion above the obstacle height, which seems to favour the development of mountain induces rotors, was introduced compared to the classical tank experiments. In fact our experimental setup was guided by the simulations of Vosper (2004), which provided systematically the upstream conditions under which mountain rotors are expected. We were able to confirm the results from these numerical simulations over a wide range of parameters.

***K*eywords:** *Rotor, inversion, lee wave*

1 INTRODUCTION

The problem of mountain-induced rotors has received considerable interest in recent years, which cumulated in the large international field experiment T-REX (Grubisic et al, 2008). Also several numerical simulations on the formation of rotors have been published recently (e.g. Vosper 2004, Doyle and Durran 2007). Although much insight into the rotor problem has been gathered through these activities, some additional information might be provided by laboratory experiments in stratified towing tanks. This kind of research has been used frequently with respect to the lee wave problem (e.g. Eiff and Bonneton 2000), but not many systematic laboratory experiments on the rotor problem have been performed.

The mayor finding of recent numerical simulations that an elevated inversion above the mountain greatly supports the rotor formation has motivated our experimental work because this kind of stratification profile has not been used very often before.

2 EXPERIMENTAL SET UP

The experiments have been performed in the fluid dynamical facilities of Météo-France/CNRM at Toulouse consisting of two towing tanks. The dimensions of the tanks are: length: 22 m, width: 3 m; height: 1 m (large tank) and 7 m x 0.8 m x 0.7 m (medium tank). In both tanks we used a bell-shaped obstacle of 13 cm respectively 3.5 cm height. The stratification was set up as guided by the simulations of Vosper (2004): A neutral bottom layer below a density jump $\Delta\rho$ at the height z_i (inversionheigth) followed by a linear density profile above ($N > 0$). In practice, inversion height and density jump were not as sharp as in the principle schematic. The simulations by Vosper have shown, that rotor formation depends on the non dimensional mountain height H/z_i and the inversion Froude number F_i defined as:

$$F_i = \frac{U}{\sqrt{g\frac{\Delta\rho}{\rho_0}z_i}} \,. \tag{1}$$

The experiments were run for different combinations of F_i and H/z_i by varying the towing speed U, the inversion height z_i and the density jump $\Delta\rho$.

The documentation of the experiments was performed by different cameras making photos and videos of the flow field. The velocity fields within lee waves and rotors were obtained by a PIV method. To get a quantitative impression of the flow, streak line photos were made. Due to the differences in the used laser systems (continuous laser in the large tank and pulsed laser in the medium tank), streakline photos could only be made in the large tank.

3 RESULTS

53 experiments in the medium tank and 26 experiments in the large tank have been performed for various combinations of the inversion Froude number F_i and the non-dimensional obstacle height H/z_i. The former were mainly used for checking the parameters under which rotors can be observed in the laboratory experiments and also helped us in preparing the experiments in the large tank, which were more complex to set up.

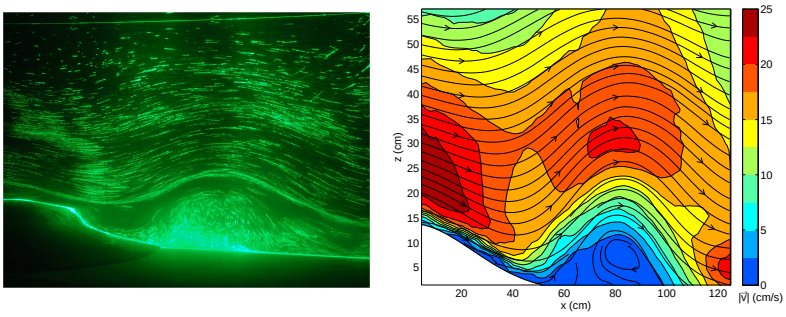

Figure 1: Observations of a Rotor case for $H/z_i = 1.1$ and $F_i = 0.90$ showing part of the lee wave and rotor below the crest. Flow is from left to right. Left: Streak lines; right: Streamlines and velocity field.

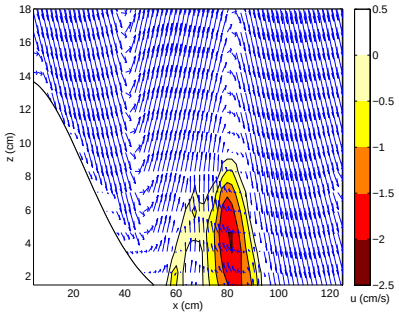

Figure 2: Close-up of the velocity field of the rotor case shown in Fig. 1. The area of backward flow towards the obstacle is shaded.

Here we present detailed analyses of the rotors flows only for the large towing tank, where streakline photos could be made. All flow phenomena described in the simulations by Vosper (2004) have been found in the laboratory, which are lee waves, hydraulic jumps and rotors.

We define a rotor as a flow situation where there is a counter-rotating vortex behind the obstacle beneath the first wave crest. In the strict sense there should be also a near surface flow toward the obstacle (full rotor) but a stagnant fluid in this region might be also termed as rotor. Figure 1 shows a rotor case for $F_i = 0.9$ and $H/z_i = 1.1$. A vortex structure under the wave crest can clearly be seen as indicated by somewhat chaotic behaviour of the streak lines (Fig. 1, left). This is also evident in the velocity field as obtained by a PIV (Fig. 1, right). A clear flow towards the obstacle can be observed in the layer close to the surface, which is even more evident in the zoom in Figure 2, where the velocity vectors are shown and only the flow component backwards toward the obstacle is coloured.

All observed flow phenomena are summarised in Fig. 3. Compared to the results obtained by Vosper (solid and dashed lines in Fig. 3) the boundaries of the observed rotor cases do not coincide exactly.

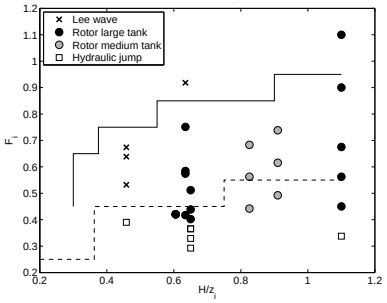

Figure 3: Flow regimes as observed in the experiments as depending on F_i and H/z_i. The flow regimes as obtained in the numerical simulations of Vosper (2004) are also indicated as follows: Solid line separates lee waves from rotors, dashed line separates rotors from hydraulic jumps.

Nevertheless the experiments have captured the main physics of the rotor simulation that an elevated inversion above the mountain top is favourable for rotor formation.

4 CONCLUSIONS

Our experiments guided by recent numerical simulation of Vosper (2004) confirm, that an elevated inversion is supporting the formation of rotors in the lee side of mountains, as was already indicated in numerical simulations mentioned above. A flow regime diagram as in Vosper (2004) is showing the dependence of the observed phenomena (lee wave, rotor and hydraulic jump) of the relevant flow parameters F_i and H/z_i.

Acknowledgements:

The experiments have been performed within the EU framework HYDRALAB III under grant 022441(RII3). We thank B. Beaudoin, J-C. Boulay, J.-C. Canonici, M. Morera, S.-L. Pigat and H. Schaffner of the Météo-France/CNRM fluid mechanics laboratory for their kind support during the experiments.

REFERENCES

Doyle, J.D. and D.D. Durran, 2007: Rotor and sub-rotor dynamics in the lee of three-dimensional terrain. *J.Atmos.Sci.*, **64**, 4202–4221.

Eiff, O. S., F. Huteau, J. Tolu, 2005: High Reynolds-number orographic wave-breaking experiments. *Dyn. Atmos. Oceans*, **40**, 71–89.

Grubisic, V. and coauthors, 2008: The terrain-induced rotor experiment: A field campaign overview including observational highlights. *Bull. Amer. Metor. Soc.*, **89**, 1513–1533.

Vosper, S. B., 2004: Inversion effects on mountain lee waves. *Quart. J. Roy. Meteor. Soc.*, **130**, 1723–1748.

THE CAPE TOBIN JET

Haraldur Ólafsson[1,3,4] , Hálfdán Ágústsson[1,2]
Melvyn A. Shapiro[4,8], Jón Egill Kristjánsson[5], Idar Barstad[6] and Andreas Dörnbrack[7]

[1] Háskóli Íslands (University of Iceland), [2] Reiknistofa í veðurfræði (Institute for Meteorological Research), Iceland, [3]Veðurstofa Íslands (Icelandic Meteorological Office), [4]Geophysical Institute, University of Bergen [5]Institute of Geosciences, University of Oslo, [6]Bjerknes Centre for Climate Research, Bergen, [7]Deutsche Luftfahrts und Raumforschung (DLR), Oberplaffenhofen, Germany, [8]NOAA/CIRES, Boulder, USA
E-mail: *haraldur68@gmail.com*

Abstract: A case of strong northerly winds close to Cape Tobin in E-Greenland is discussed with the help of dropsondes and a numerical simulation. Winds of about 45 m/s are observed at only 900 hPa, in a very stably stratified air mass. The jet extends about 200 km away from the coast of Greenland. When the jet impinges the high topography of E-Greenland, parts of the low-level cold air is lifted and mixed with the warm air above, leading to a "cold föhn" at levels close to 850 hPa on the downstream side.

Keywords: *IPY, THORPEX, GREENEX, Cape Tobin, East-Greenland, low-level jet,*

1 INTRODUCTION

When easterly flow impinges the mountains of Greenland, north of approximately 69°N, strong winds along the E-Greenland coast are generated. These winds blow into the Denmark Strait, north of NW-Iceland and form a jet that we choose to call the Cape Tobin Jet. As a part of the IPY-THORPEX and GREENEX programmes, a case of a Cape Tobin Jet was explored with dropsondes on 9 March 2008. This short paper describes the observations and a few details of the flow as simulated numerically.

2 THE CAPE TOBIN JET

Figure 1 shows the simulated surface winds and two-metre temperatures on 9 March 2008 at 12 UTC. There is strong acceleration at the coast of Greenland and strong flow into the Denmark Strait. The low-level air mass in the jet is very cold, which corresponds with the fact that the area is mostly covered with sea ice. Figure 2 shows the temperature profiles of the northernmost (upstream) and the westernmost (downstream) dropsondes shown in Fig. 1. Upstream, there is a very strong inversion close to 900 hPa, while downstream of the approximately 3000 m high topography, the air mass is close to neutral up to about 800 hPa. The upstream winds below the inversion are about 22 m/s, and the winds are stronger inside the inversion. The 800-850 hPa layer is much colder downstream than upstream. Figure 3 shows that the jet has a maximum of about 45 m/s inside the stable layer at about 900 hPa. The flow has been simulated with the numerical model WRF with boundary conditions from the ECMWF and horizontal resolution of 9 km. Figure 4 shows two cross sections of the simulated flow, one along the flow, across the E-Greenland mountains and one across the jet off the coast of Greenland. The cross section along the flow shows that some of the low-level dense air is lifted across the mountains and ends up in a downslope windstorm. The cross section across the flow shows that the jet is indeed confined to the inversion layer and that it extends about 200 km away from the mountains of E-Greenland. Apart from weak observed winds in the wake of the E-Greenland topography (a wake), the simulation is in quite good agreement with the observations.

3 DISCUSSION AND CONCLUSIONS

Both the observations and the simulations show extreme winds at only about 600 metres above the sea in the Cape Tobin Jet. As these winds appear not to reach down to the surface, they can not be detected with the QuikSCAT technology, and even if they did, such data would probably not be reliable because of extensive sea-ice cover in the region. Indications of very strong winds in this region have however been presented by Moore and Renfrew (2005) and Kolstad (2008). Winds of this kind present a challenge for calculations of turbulent transport of horizontal momentum in numerical models, and they may presumably be brought down to the surface by turbulent mixing, as the air mass flows over open sea and becomes less stable.

The trajectory of the air mass impinging the E-Greenland topography is a little unusual: in most cases, air at low levels does not climb 3000 m high mountains. The kinetic energy of the flow is so great that some of the

low level cold air is able to climb the mountains and mix with warmer air above. Consequently, the downslope flow at levels above the upstream inversion is relatively cold. This could be called a "cold föhn".

Further work with the Cape Tobin Jet will consist of dynamic analysis of the forces at stake, the role of the sea ice and the variability of the jet in past climate and future climate projections. From a forecasting perspective and development of numerical tools, the jet will provide a testbed for vertical mixing of momentum.

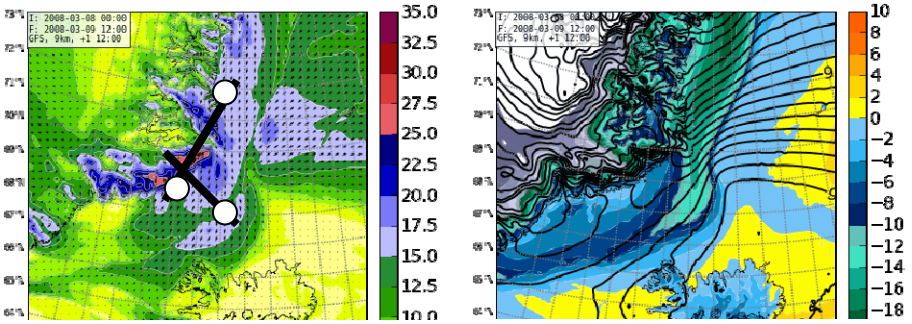

Figure 1. Simulated surface wind speed (left) in m/s and two-metre temperature (right) in °C. The approximate position of the dropsondes in Figs. 2 and 3 and the cross sections in Fig. 4 are shown on the left panel.

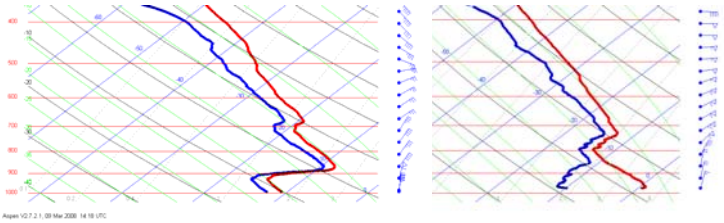

Figure 2. Vertical profiles from dropsondes upstream of the E-Greenland mountains (left) and downstream of the E-Greenland mountains (right)

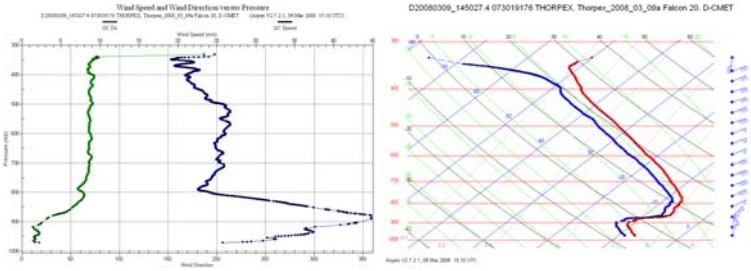

Figure 3. The vertical profile of winds (left), temperature and humidty (right) from the southernmost dropsonde shown in Fig. 1. The peak winds are 45 m/s

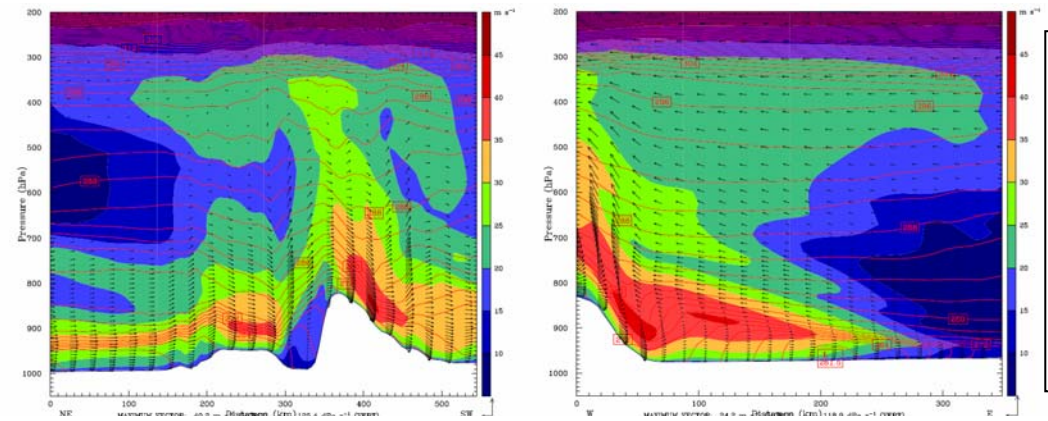

Figure 4. Simulated vertical profiles along the flow from the NE to the SW (left) and across the flow, from the NW to the SE (right), showing wind speed (m/s) and potentital temperature (K). The positions of the sections are shown in Fig. 1.

Acknowledgements:
The observations presented here were provided with support from EUFAR, within the framework of GREENEX and with support from the Norwegian Research Fund (IPY-THORPEX).

REFERENCES

Moore, G. W. K. and I. Renfrew, 2005: Tip jets and barrier winds: A QuikSCAT climatology of high wind speed events around Greenland. *J. Climate*, **18,** 3713–3725

Kolstad, E. W., 2008: A QuikSCAT climatology of ocean surface winds in the Nordic seas: Identification of features and comparison with the NCEP/NCAR reanalysis, *J. Geophys. Res.*, 113, D11106, doi:10.1029/2007JD008918.

SIMULATIONS OF MESOSCALE FLOW OVER AN ARCTIC FJORD

Tiina Kilpeläinen[1,2], Haraldur Ólafsson[2,3]
[1] The University Centre in Svalbard, Norway
E-mail: *tiina.kilpelainen@unis.no*
[2] University of Bergen, Norway
[3] University of Iceland, Iceland

Abstract: **Mesoscale flow over Isfjorden, Svalbard, was simulated applying the Weather Research and Forecasting (WRF) model. The direction of the large scale flow affects local wind-, temperature- and humidity fields as well as the spatial distribution of the turbulent fluxes. Spatial differences are largest when the large scale wind is blowing along the fjord.**

Keywords: *Arctic fjord, mesoscale simulation, topographical effects*

1 INTRODUCTION

Fjords, narrow and deep inlets of the sea, are features of mountainous regions and are distributed at high latitudes in both hemispheres. The local meteorological conditions in fjords are affected by surrounding complex topography, possible sea ice and oceanographic phenomena. The atmospheric boundary layer over fjords is poorly understood and many processes occur on spatial scales that cannot be resolved by climate and weather prediction models. This study addresses the spatial variability of wind, temperature and humidity, and its effect on the turbulent fluxes over an Arctic fjord.

2 SIMULATIONS

The Weather Research and Forecasting (WRF) model, initialized with ECMWF operational analysis data, was used to simulate spatial variability over Isfjorden, Svalbard (Fig. 1). The model system consists of three polar stereographic domains at horizontal resolution of 9 km, 3 km and 1 km. Three real cases, representing different large scale flow directions, were chosen: 19/02/2008 northwesterly wind, 13/02/2008 northeasterly wind and 26/02/2009 southeasterly wind. Isfjorden was ice-free apart from the innermost parts of the fjord, and the sea surface temperature in the ice-free area was set to constant. Simulated temperature and wind speed show fairly good agreement with weather mast measurements performed on the southern coast of Isfjorden.

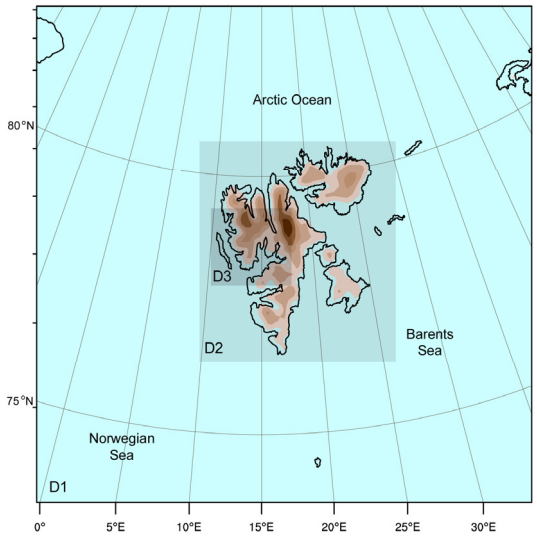

Figure 1. The three domains used in WRF model.

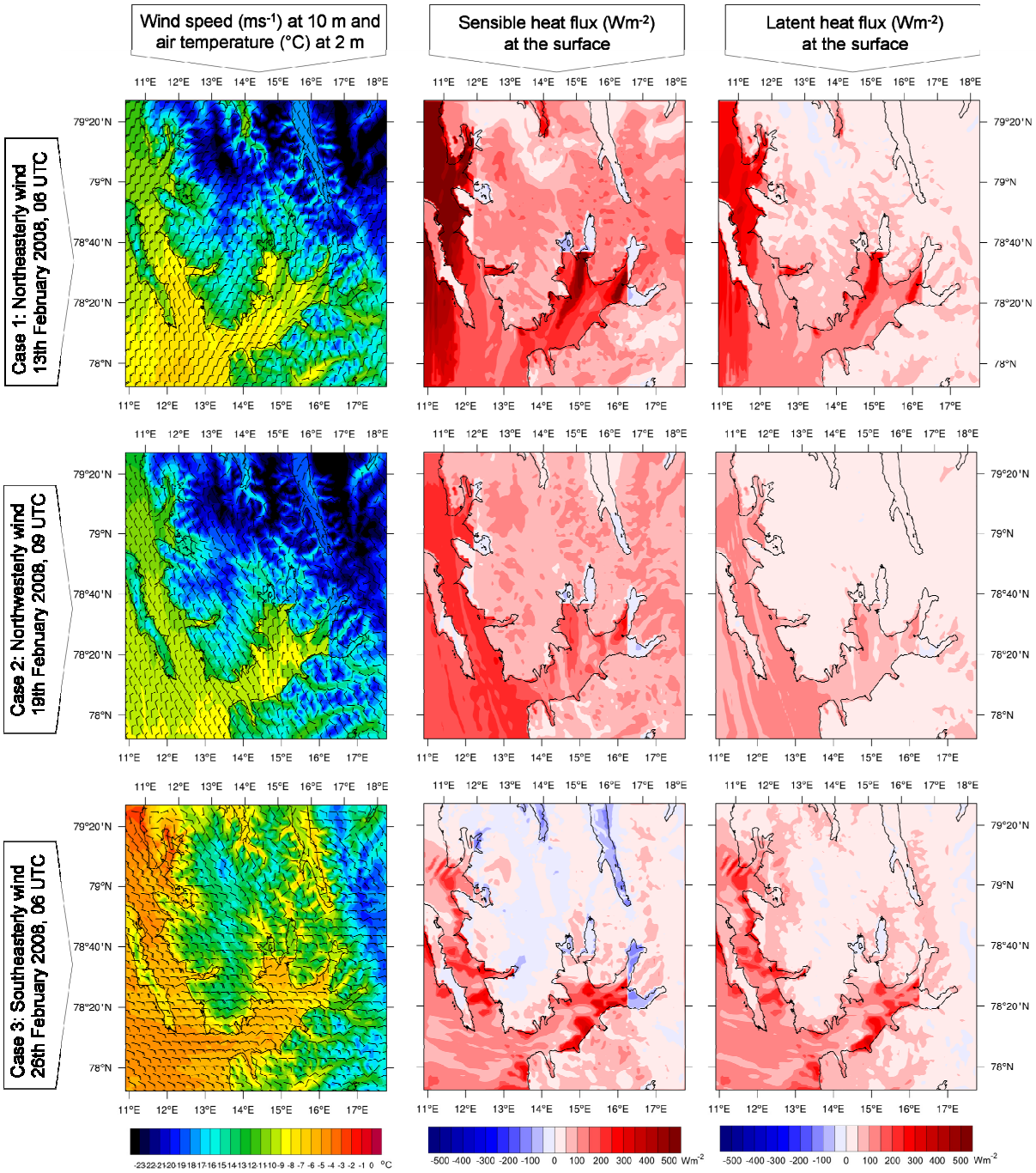

Figure 2. The left panel shows horizontal wind vectors at 10 m level and temperature at 2 m for domain 3. The sensible heat flux and latent heat flux are shown in the middle panel and the right panel, respectively.

3 SPATIAL VARIABILITY

The simulations indicate that the direction of the large scale flow has an influence on the spatial distribution of wind speed, air temperature and humidity over Isfjorden, especially on the location of maxima and minima, and as a consequence of these also the spatial distribution of the turbulent fluxes is largely influenced (Fig. 2). When the wind has a northerly component, cold air is transported over the fjord through the valleys in northeast, creating pronounced local minimum of air temperature and maxima of wind speed and the turbulent fluxes. Local differences within the ice-free area of Isfjorden, caused by the topography, can exceed 400 Wm^{-2} for sensible heat and 350 Wm^{-2} for latent heat flux. The spatial differences are largest when the large scale wind is blowing along the fjord.

SEVERE TURBULENCE IN THE WAKE OF SOUTHEAST-ICELAND

Hálfdán Ágústsson[12], Haraldur Ólafsson[134]

[1] Háskóli Íslands (University of Iceland), Iceland
E-mail: *halfdana@gmail.com*
[2] Reiknistofa í veðurfræði (Institute for Meteorological Research), Iceland
[3] Veðurstofa Íslands (Icelandic Meteorological Office), Iceland
[4] Bergen School of Meterology, Geophysical Institute, Bergen, Norway.

Abstract: On 18 November 2008 a commercial aircraft encountered severe turbulence while flying in westerly flow across the wake of SE-Iceland. The situation is simulated with horizontal resolutions down to 1 km. The simulations show a type 1 rotor (Hertenstein and Kuettner, 2005), which is in agreement with the vertical profile of wind and temperature. Very strong shear-turbulence is reproduced in the lee-wave and inside the rotor. The lee-waves and the turbulence patterns are not stationary and as the upstream vertical windshear increases, the lee-wave becomes less steep, but the turbulence increases. From a forecasting perspective, this event could have been foreseen quite accurately, but not with the NWP tools that are currently in use for aviation forecasts. Their resolution is typically of 9 to 27 km and even more, and that is not adequate. This event underlines the urgency of delivering products from fine-scale simulations over complex terrain to pilots.

Keywords: *Wake, severe turbulence, rotor, complex orography, ICAM, Iceland*

1 INTRODUCTION

There is mounting evidence in the scientific literature that turbulence aloft may be successfully forecasted using fine-scale numerical simulations of weather. Observations of such turbulence are currently limited to large experiments using specialized aircraft, e.g. as in the Greenland Flow Distortion Experiment (Renfrew et al., 2008) or to aviation incidents where commercial airplanes accidentally fly into regions of severe turbulence. One such incident is described in Ólafsson and Ágústsson (2009), where an international flight encounters severe turbulence and breaking waves in easterly flow over Greenland. In this case the incident could presumably have been avoided as fine-scale simulations reproduced the turbulence which reached up to the tropopause.

Here we investigate an incident where a domestic flight along the south coast of Iceland encounters severe turbulence in the wake of Southeast-Iceland in the afternoon of 18 November 2008. The airplane first encounters the turbulence at 8.000 ft east of Mt. Öræfajökull and the severe turbulence continues for 5-7 min. while the airplane descends towards Höfn. There was no warning, i.e. SIGMET, for this region until after the incident. Winds were strong and westerly in the troposhere (Fig. 1), and the Keflavik sounding (SW-Iceland) shows a forward vertical windshear and an inversion at 900 hPa at 12 UTC (not shown). At 12 UTC a downslope windstorm was initiated at Kvísker on the eastern side of Mt. Öræfajökull with winds increasing suddenly from 5 m/s to 40 m/s and a significant warming and drying of the air. Kvísker is close to the track of the airplane through the wake and the previous study of Ágústsson and Ólafsson (2008) shows that the current situation is in fact characteristic for downslope windstorms and a turbulent wake of Southeast-Iceland.

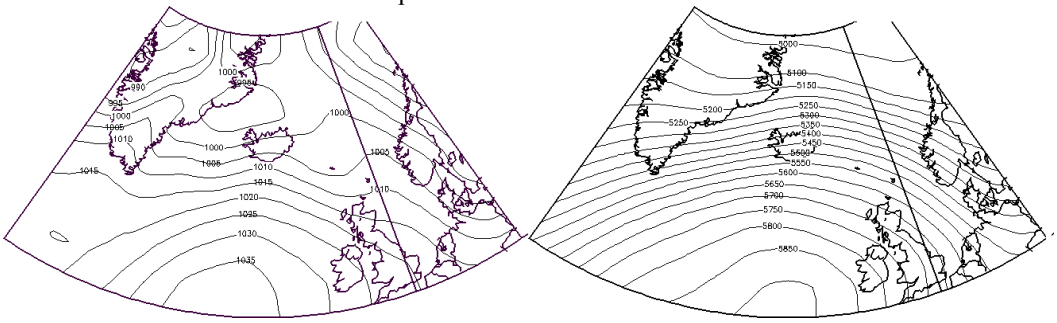

Figure 1. Analysis from NCEP/NCAR provided by NOAA/ESRL physcial science division. The figures are valid at 18 UTC on 18 November 2008 and show the mean sea level pressure [hPa] (left) and the 500 hPa geopotential height [m] (right).

2 RESULTS

The atmospheric situation is reproduced using the WRF-model (Skamarock et al., 2005) with three nested grids using a resolution of 9, 3 and 1 km and 40 sigma-layers. The model was forced using the ECMWF-analysis on model levels. Apart from the 1 km grid, the setup is similar to what is used for operational forecasting at Veðurstofa Íslands and published online at: "http://belgingur.is", by Reiknistofa í veðurfræði.

The simulated wind field in Southeast-Iceland reveals a great dependence on the horizontal resolution of the model (Fig. 2). A resolution of at least 3 km is necessary to reproduce the leeside windstorm and the wave pattern in the wake. The model successfully reproduces the observed winds and temperature at a resolution of 1 km at Kvísker while the agreement is worse at coarser resolutions (not shown). The winds at 950 hPa reveal the same wave pattern and patches of strong turbulence in the wake while section A across Mt. Öræfajökull and into the wake reveals a series of large amplitude waves with large values of turbulence kinetic energy (TKE) in the region of strong wind shear below the waves (Fig. 3). This wave pattern is not stationary and the waves become less steep and the turbulence increases as the upstream vertical windshear increases (not shown).

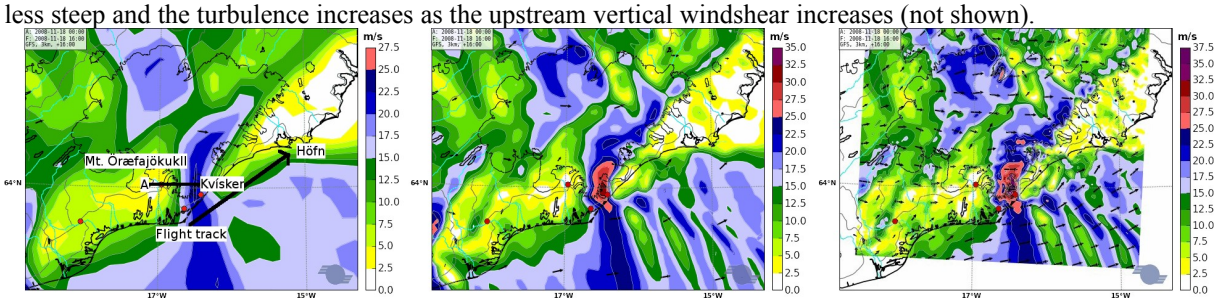

Figure 2. Simulated surface winds [m/s] at a horizontal resolution of 9 km (left), 3 km (middle) and 1 km (right) in Southeast-Iceland at 16 UTC on 18 November 2008. Also shown are locations mentioned in the text, the track of the airplane and section A.

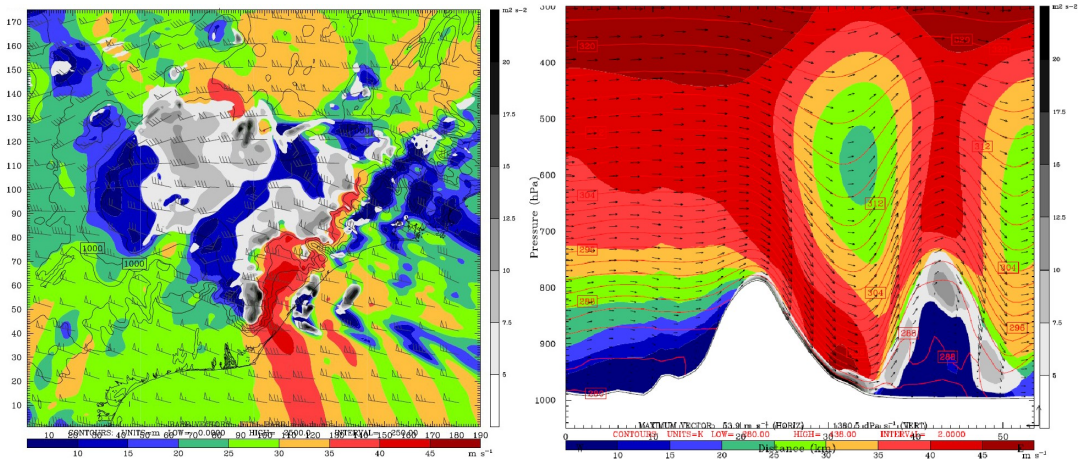

Figure 3. Simulated winds [m/s], turbulence kinetic energy [J/kg] and potential temperature [K] at 950 hPa (left) and in section A (right) at 16 UTC on 18 November 2008. The section only shows the first wave in a series of lee waves.

3 CONCLUSIONS

In this paper, a case of a type 1 rotor as classified by Hertenstein and Kuettner (2005) is presented. The structure of the rotor is in agreement with the upstream vertical profile of wind and temperature. There is strong shear-turbulence in the lee-wave and inside the rotor. It is evident that this event could have been forecast quite accurately, but not with the NWP tools currently used in aviation forecasts. Their horizontal resolution is typically 9 to 27 km or even coarser, which is simply not adequate. This study underlines the urgency of delivering products from fine-scale simulations over complex terrain to pilots.

Acknowledgement:
We thank the pilot, Aðalsteinn Marteinsson for providing detailed information on the turbulence incident.

REFERENCES

Ágústsson H. and H. Ólafsson, 2008. Variability in the Kvísker downslope windstorms. *Proc. Amer. Meteorol. Soc. Conf. Mountain Meteorology*, Whistler, Canada.

Hertenstein, R. F. and J. P. Kuettner, 2005. Rotor types associated with steep lee topography: influence of the wind profile. Tellus 57A, pp. 117-135.

Ólafsson H. and H. Ágústsson, 2009: Gravity wave breaking in easterly flow over Greenland and associated low level barrier- and reverse tipjets. In press, Meteorology and Atmospheric Physics, March 2009.

Renfrew, I. A., G. W. K. Moore, J. E. Kristjánsson, H. Ólafsson, S. L. Gray, G. N. Petersen, K. Bovis, P. R. A. Brown, I. Føre, T. Haine, C. Hay, E. A. Irvine, A. Lawrence, T. Ohigashi, S. Outten, R. S. Pickart, M. Shapiro, D. Sproson, R. Swinbank, A. Woolley, and S. Zhang, 2008. *Bulletin of the American Meteorological Society,* 89 (9), pp. 1307–1324.

Skamarock, W. C., J. B. Klemp, J. Dudhia, D. O. Gill, D. M. Barker, W. Wang and J. G. Powers 2005. A description of the Advanced Research WRF version 2. Technical Report NCAR/TN-468+STR, National center for atmospheric research.

GREENLAND AND EXTREME NORTHERLY WINDS IN THE NORDIC SEAS

Beathe Tveita[1], Haraldur Ólafsson[3,4], Anne Dagrun Sandvik[5] and Berit Hagen[2]
[1]Storm Weather Centre, Bergen, Norway
[2]Norwegian Meteorological Institute
[3]Háskóli Íslands (University of Iceland)
[4]Bergen School of Meteorology, Geophysical Institute, University of Bergen
[5]Institute for Marine Research, Bergen, Norway
E-mail: *beathe.tveita@storm.no*

Abstract: A study of the impact of Greenland on the atmospheric flow in the Nordic Seas in the case of an extreme northerly windstorm north of Iceland is presented. Removing Greenland leads to much warmer air at low levels east of Greenland, a much weaker frontal jet north of Iceland and no jet at Cape Tobin. The surface pressure is much higher everywhere over the Nordic seas north of ca. 69N when Greenland is present. The wake area at the east coast of Greenland, west of Iceland is much colder when Greenland is not present.

Keywords: *Greenland, Cape Tobin Jet, Wake, damming, extreme winds, Nordic Seas, WRF, QuikSCAT.*

1 INTRODUCTION

Several authors have elaborated on the role of Greenland in the play of weather and climate on different time scales. Kristjánsson and McInnes (1999) studied how Greenland contributed to the Icelandic Trough when a synoptic cyclone moved to the northeast between Iceland and Greenland. Petersen et al. (2004) showed that on a climatological time scale, Greenland contributes to a positive pressure anomaly at its east coast, extending across the N-Atlantic towards Scandinavia.

In this study, a case of an extreme northerly windstorm is simulated with and without Greenland. The flow is initialized at 18 UTC on 4 March 2000 and the fields are compared 24 hours later. The simulations are carried out with the WRF model with boundaries from the ECMWF and horizontal resolution of 9 km. More details on this case are given in Tveita et al., (2009).

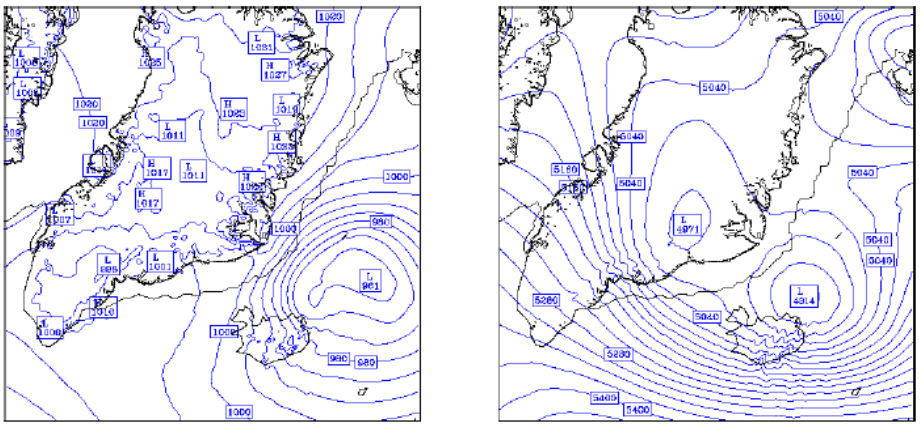

Figure 1. MSLP (left) and geopotential height at 500 hPa (right) valid at 18 UTC on 5 March 2000. The simulation is initialized 24 h earlier.

3 RESULTS

The results are presented in Figures 1-3 and schematically in Fig.2 (right). The main features when Greenland is present are i) cold air damming east of Greenland and a positive surface pressure anomaly extending very far to the east, ii) a warm wake at the coast of Greenland, west of Iceland, extending to the east of Iceland, iii) very strong winds in a frontal zone north of Iceland and also close to Cape Tobin, but weak winds in the wake of Greenland further south.

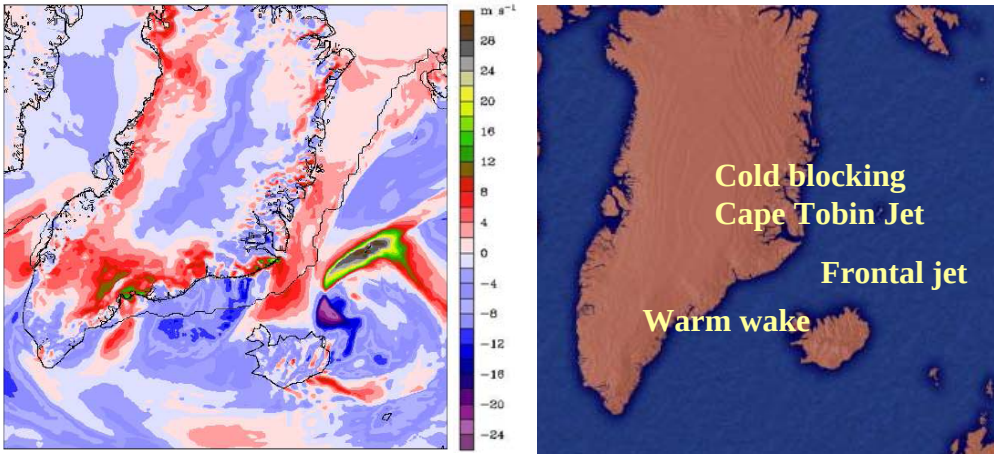

Figure 2. Surface wind speed in the NOGREEN simulation subtracted from the CONTROL simulation (left) and a schematic overview of the main features of the fields of difference between NOGREEN and CONTROL.

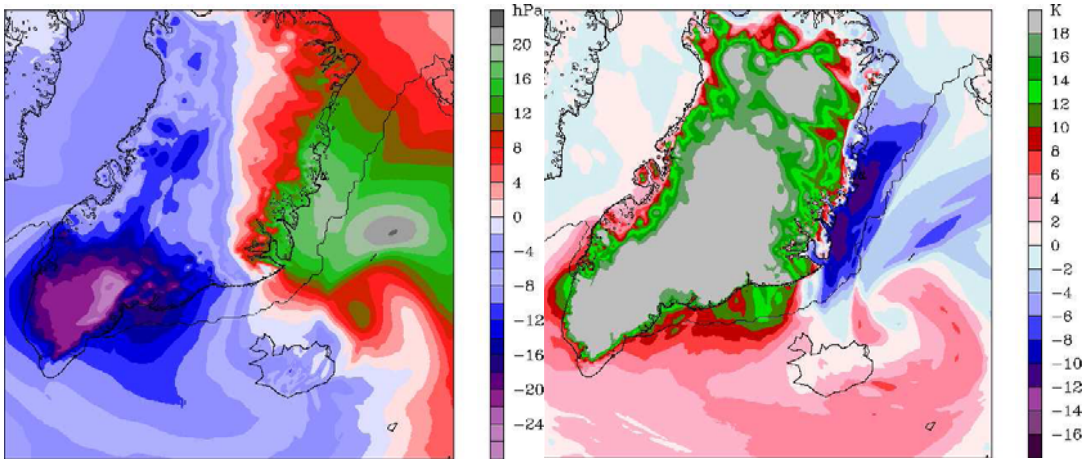

Figure 3. Difference fields (CONTROL-NOGREEN). Left: MSLP (hPa); Right: Temperature at 850 hPa (K) at 18 UTC on 5 March 2000.

3 DISCUSSION

None of the key features described in the previous section are surprising, except perhaps the magnitude and the extent of the sea level pressure difference north of Iceland. It does however correspond to the climatological study by Petersen et al. (2004). As expected, Greenland has in a case like this a very strong positive effect on the surface winds in the vicinity of Cape Tobin, and a negative effect in the wake area further south. The greatest impact is however in the frontal zone, further to the east where the cold dammed air meets warmer air in the southeast. A difference in wind speed of 25-30 m/s between the two simulations (CONTROL-NOGREEN) gives a solid foundation for stating that the extreme windstorm was indeed generated by Greenland.

REFERENCES

Kristjánsson, J. E., McInnes, H., 1999: The impact of Greenland on cyclone evolution in the North Atlantic. Quarterly Journal of the Royal Meteorological Society, 125(560), 2819-2834.

Petersen, G. N., J. E. Kristjánsson and H. Ólafsson, 2004: Numerical simulations of Greenland´s impact on the Northern Hemisphere winter circulation. Tellus 52A, 102-111.

Tveita, B., H. Ólafsson, A. D. Sandvik, B. Hagen, 2009: A numerical study of an extreme windstorm in the Greenland Sea. Submitted to Meteorology and Atmospheric Physics.

FORECASTING EXTREME WINDS IN THE NORDIC SEAS - THE GREENLAND DAMMING

Berit Hagen[1], Haraldur Ólafsson[2,3], Anne Dagrun Sandvik[4] and Beathe Tveita[5]
[1]Norwegian Meteorological Institute
[2] Háskóli Íslands (University of Iceland)
[3]Bergen School of Meteorology, Geophysical Institute, University of Bergen
[4]Institute for Marine Research, Bergen, Norway
[5]Storm Weather Centre, Bergen, Norway
E-mail: *berit.hagen@met.no*

Abstract: A study of QuikSCAT data reveals that a large proportion of extreme wind cases in the Nordic Seas appear to be linked to damming of low-level dense air east of Greenland. Forecasts with different lead times of one Greenland-damming windstorm and three extreme windstorms that were not influenced by Greenland are compared and the Greenland-damming storm forecast has the best skill. Simulations of all the four cases suggest little sensitivity of the extreme winds to parameterization of the PBL and horizontal resolution in the range from 3 to 27 km.

Keywords: *Greenland, damming, extreme winds, Nordic Seas, WRF, QuikSCAT.*

1 INTRODUCTION

Accurate forecasting of extreme winds is of utmost importance, both for security and economic reasons. In recent years, continuous wind observations have been made available by the QuikSCAT remote sensing system. Here, cases of extreme winds in the Nordic Seas, recorded by QuikSCAT are studied. A case where Greenland plays a strong role through damming of low-level air is compared to cases where such effects are not important. Details on the QuikSCAT data processing and the numerical simulations are given in Hagen et al. (2009).

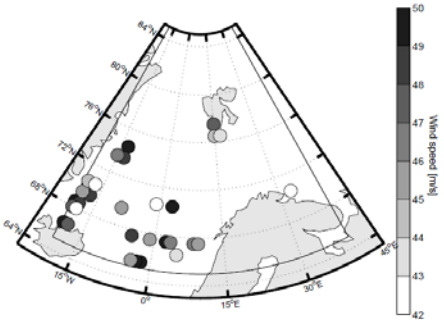

Figure 1. Position of the most severe wind events in the Nordic Seas 2000-2006, detected by QuikSCAT.

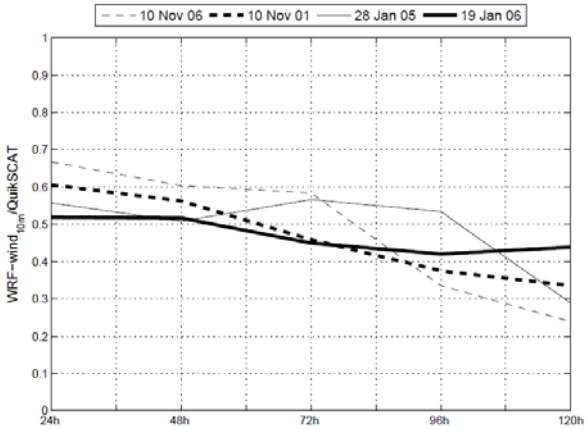

Figure 2. Forecast skill in 4 of the cases in Fig. 1, simulated with different lead time with initial conditions and boundaries from the ECMWF and horizontal resolution of 9 km.

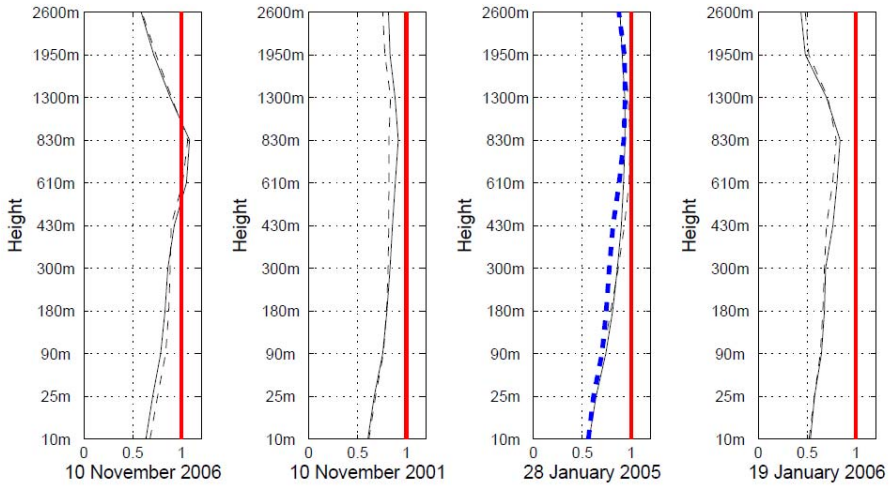

Figure 1. Simulated wind profiles in four cases of extreme surface winds, normalized with the observed QuikSCAT value at the surface. Solid lines show results when using the MYJ PBL scheme, while dotted lines show results from the YSU scheme. A bold dotted line indicates results from a simulation with 65 vertical levels (instead of 33 levels as in all the other simulations).

2 RESULTS

Figure 1 shows the distribution of the 30 strongest wind cases 2000-2006. There is a large concentration of cases just east of Greenland. These cases are linked to damming of low-level dense air, leading to very strong northerly surface winds in reverse vertical wind-shear situations. Four of the extreme wind cases are simulated, with the WRF model and boundaries from the ECMWF. One of the cases is a Greenland-damming case (10 November 2006), while the three other cases are not. Figure 2 shows the skill of the forecasts of the extreme winds at different lead times. All the forecasts underestimate the winds, giving typically about 30 m/s while the QuikSCAT indicated about 45 m/s. Of all the four forecasts, the Greenland-damming case has the best skill at lead times of 24, 48 and 72 hours. There was not much sensitivity of the forecasts to horizontal resolution of the simulations (not shown).

Figure 3 shows the wind profiles from 24 h forecasts of the four cases. While in all of the cases, the surface winds are underestimated, the simulated winds at typically 600-800 meters height do come close to the observed surface winds. In the Greenland-damming case, the simulated winds exceed the observed surface winds at these levels. There is quite limited sensitivity to the two parameterization schemes that were tested, as well as to the vertical resolution.

4 DISCUSSION AND CONCLUSION

The fact that the orographic windstorm has the best forecast skill has of course no statistical significance, but from a dynamic standpoint, this is not entirely surprising, since the damming of cold air by Greenland is quite a straightforward process to simulate, provided that the topography and the surface fluxes are reasonably correct. From this study, one may state that there is an indication that extreme winds associated with cold-air damming by Greenland may be better forecasted than extreme winds associated with “ordinary” extratropical cyclones. Although all the short-range forecasts do predict a strong windstorm, the skill of the forecasts is far from outstanding. There are several possible reasons for this. Firstly, the simulated cyclones may be to shallow or the pressure gradients not as steep as in reality. Secondly, the vertical mixing of horizontal momentum may be underestimated by the models. The parameterization schemes are not tuned for extreme winds and there are quite limited observations of vertical profiles in extreme situations. Such observations are planned (Ólafsson et al., 2009). Finally, the QuikSCAT procedures may overestimate the surface wind speed.

REFERENCES

Hagen, B., H. Ólafsson, A. D. Sandvik, B. Tveita, 2009: Forecasting wind extremes in the Nordic Seas. Submitted to Meteorology and Atmospheric Physics.

Ólafsson, H., Ó. Rögnvaldsson, J. Reuder, H. Ágústsson, G. N. Petersen, H. Björnsson, T. Jónsson and J. E. Kristjánsson, 2009: Monitoring the atmospheric boundary-layer in the arctic (MABLA) – the Gufuskálar project. An extended abstract in this issue.

"UP-HILL EFFECT" ON WINDS AT THE HONG KONG INTERNATIONAL AIRPORT IN STRONG NORTHERLY WINDS ASSOCIATED WITH TROPICAL CYCLONES

Pak Wai Chan[1] and T.C. Cheung[2]

[1] Hong Kong Observatory, Hong Kong, China
E-mail: *pwchan@hko.gov.hk*
[2] Chinese University of Hong Kong, Hong Kong, China

Abstract: The Hong Kong International Airport (HKIA) is built on a reclaimed island surrounded by complex terrain from the E to SW directions. It is however exposed to the Pearl River Estuary to the N and NW. Given this geographical setup, it may be expected that, in northwesterly airflow, the effect of the complex terrain in the vicinity of HKIA would be insignificant and the winds over the airport would be rather uniform. Nevertheless, uneven wind distribution on the airfield has been observed in strong northwesterly winds associated with tropical cyclones. For instance, the winds at the north runway were found to be stronger than those over the south runway by as much as 10 – 15 knots. The uneven wind distributions over HKIA in strong northwesterly winds associated with tropical cyclones are studied in this paper. They appear to arise partly from an "up-hill effect" when winds are forced to climb over the mountainous Lantau Island to the south of the airport. High-resolution numerical simulation is performed using the Weather Research and Forecasting (WRF) model version 2.2. The model successfully reproduces the wind speed difference between the north and the south runways of the airport.

Keywords: *up-hill effect, tropical cyclone, WRF*

1 INTRODUCTION

The Hong Kong International Airport (HKIA) is situated to the north of the mountainous Lantau Island. It is exposed to the Pearl River Estuary to the north and northwest. With this geographical setup, airflow disturbances are expected to appear in the airport area due to terrain disruption when east to southwesterly winds prevail, whereas more uniform winds may occur over the airport for north to northwesterly airflow. However, rather uneven wind distribution is observed over HKIA for strong northwesterly winds associated with tropical cyclones or winter monsoon. The winds at the two runways of the airport (locations in Fig. 1) may become very different in those situations. The wind speeds measured at the anemometers over the north runway were found to be larger than those over the south runway by as much as 10-15 knots. This could have significant implications for aircraft operation. For instance, the crosswind at the north runway may be too strong for aircraft to land. As such, the aircraft may need to land at the south runway, which is closer to the terrain. This may render the wind more turbulent.

The uneven wind distribution over the airport in northwesterly winds associated with tropical cyclones is presented in this paper. Its cause is studied by high-resolution numerical simulation.

2 UNEVEN WIND DISTRIBUTION IN TYPHOON NURI

In the morning of 22 August 2008, Typhoon Nuri was situated to the southeast of Hong Kong bringing gale force north to northwesterly winds to the territory. The wind distribution around HKIA at about 10 a.m. on that day is shown in Fig. 1. It can be seen that there is quite significant wind difference between the two runways of the airport. The north runway recorded north-northwesterly gales of about 35-40 knots. On the other hand, the south runway had strong winds of only about 25 knots. Normally, aircraft would land at the north runway of HKIA. However, because of the gale-force crosswind at that runway, they could only opt to land at the south runway from the west. The airflow turned out to be quite turbulent near the threshold of the south runway (cube root of eddy dissipation rate of about 0.4 $m^{2/3}s^{-1}$, as determined by onboard flight data, indicating moderate turbulence) for the aircraft to operate. After a couple of hard landing events, it was decided to stop the aircraft operation until the wind subsided or changed direction.

The time series of the anemometer data at the two runways of HKIA in Typhoon Nuri case (22 and 23 August 2008) are shown in Fig. 2. The measurements from the pair of anemometers at the eastern end, near the middle and at the western end of HKIA are compared. It could be seen that, for wind directions of about 300 to 360 degrees, the wind speed difference between each pair of anemometer becomes larger. In general, this difference is more pronounced for the anemometer pair at the western part of the airport. These anemometers are closer to the terrain of Lantau Island (Fig. 1) and it seems that the wind difference may be related to terrain effect on the airflow in *northwesterly* winds.

3 OTHER TROPICAL CYCLONE CASES WITH STRONG NORTHWESTERLY WINDS

The wind data of other tropical cyclone cases since HKIA opened in 1998 have also been reviewed to see whether or not the wind difference as noted in Section 2 above occurred only in the case of Typhoon Nuri. Two

other strong northwesterly wind cases due to tropical cyclones were identified, namely, Typhoon Sam and York in August and September 1999 respectively. The wind records for Typhoon Sam are shown in Fig. 3. It could be seen that, similar to Typhoon Nuri, wind speed differences between the anemometer pairs were the largest in north to northwesterly winds. Moreover, this difference was slightly larger for anemometers near western end of HKIA.

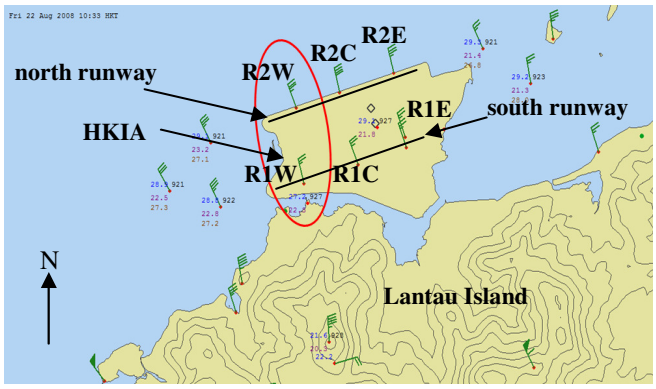

Figure 1. Surface wind distribution around HKIA at 10:33 a.m., 22 August 2008. Runway length: about 4 km.

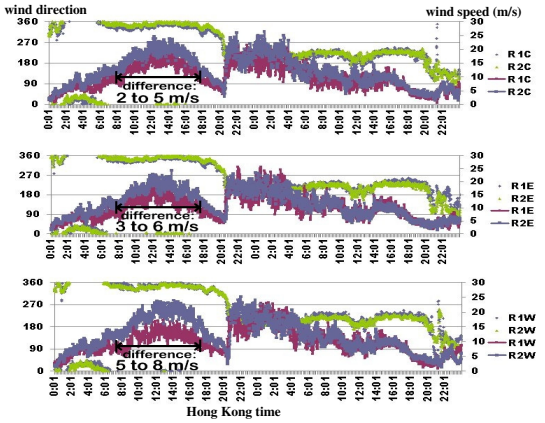

Figure 2. Time series of HKIA anemometer readings on 22-23 August 2008 during the passage of Typhoon Nuri. Anemometer locations: see Fig. 1.

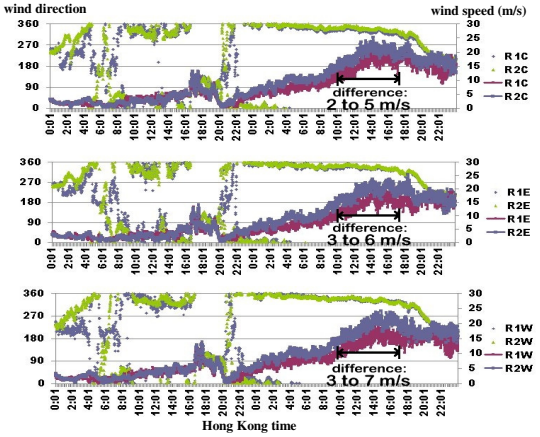

Figure 3. Time series of HKIA anemometer readings on 21-22 August 1999 during the passage of Typhoon Sam.

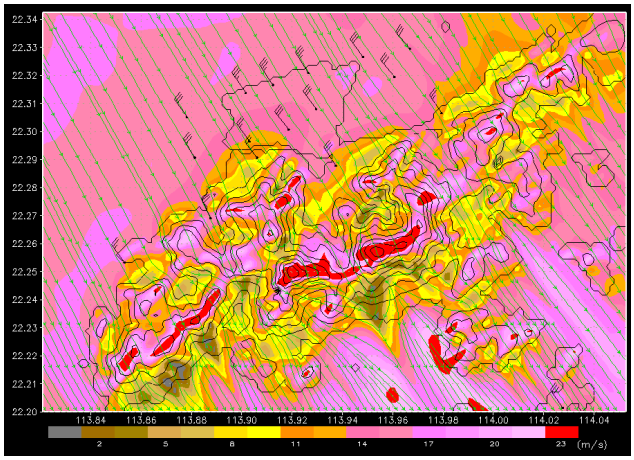

Figure 4. WRF-simulated wind speed distribution at the surface at about 02 UTC, 22 August 2008.

4 NUMERICAL SIMULATION

The uneven wind distribution over HKIA is studied numerically using the Weather Research and Forecasting (WRF) model version 2.2. Three nested domains are used, from southern China to areas around Lantau Island. The innermost domain has a spatial resolution of 200 m. The Typhoon Nuri case is considered and the winds near the airport in gale-force north to northwesterly wind condition are shown in Fig. 4. It could be seen that the wind speed differences between the two runways, viz. about 10 knots at the western end and about 5 knots for middle and eastern end, are reasonably reproduced. A sharp gradient of surface wind speed is successfully simulated near the foothill of Lantau Island, which covers the southern part of the airport. The model simulation results suggest that the wind speed difference could be due to "up-hill effect" on the airflow when the winds start to climb up the mountains of Lantau Island. Similar "up-hill effect" has been discussed in the literature (e.g. Stull (2004)).

5 CONCLUSIONS

Uneven wind distribution between the two runways of HKIA is observed in the strong northwesterly wind cases associated with tropical cyclones in Hong Kong. The difference is in the order of 10-15 knots and could have significant implication to aircraft operation. Based on WRF simulation results, it could be related to "up-hill effect" as the winds start to climb over the mountains of Lantau Island.

REFERENCES

Stull, R. B., 2004: An Introduction to Boundary Layer Meteorology, Kluwer, 670 pp.

ARE TORNADOES POSSIBLE ALSO IN SLOVENIA? CASE STUDY OF AN EXTREME EVENT OF 13 AND 14 JULY 2008

Uroš Strajnar

Environmental Agency of the Republic of Slovenia, Ljubljana, Slovenia
E-mail: *uros.strajnar@gov.si*

Abstract: Extreme convective events also appear frequently in Slovenia, but tornadoes are very unlikely. In the paper the most catastrophic convective event in year 2008 is discussed, when the damage to the houses and forests was similar to tornado's.

Keywords: *extreme event, tornado, downburst*

1 INTRODUCTION

It is well known that tornadoes can occur in most European countries. Rough estimation based on survey of average tornadic activity in Europe conducted among the participants of the European Conference on Severe Storms 2002 (Dotzek, 2003) is more than 300 tornadoes per year in Europe.

Even in the Alps tornadoes sometimes form, especially at the eastern flanks. In Slovenia's neighbouring countries Austria, Italy, Hungary and Croatia, there is significant occurrence of tornadoes very close to the Slovenia border. According to Holzer (2000) the tornado density in the period from 1946 to 1971 in South-Eastern Austria is 0.9 tornadoes per 10000 km² per year, while Giaiotti's (2005) statistics for the period from 1991 to 2000 for Eastern Italy (Friuli) is roughly 10 tornadoes per 10 years. In Hungary average number of tornadoes is 3 to 5 per year (Sárközi, 2005).

On the other hand there is no official statistics for Slovenia and there are only a few tornado occurrences, despite that this region has one of the highest number of thunderstorms in the Alps. The most reliable estimation based on number of volunteer observed tornadoes between 2000 to 2007 (European Severe Storms Laboratory, http://www.essl.org/research/tornado/) is 0 to 0.3 tornadoes per 10000 km² per year. Because a tornado is unusual phenomenon in Slovenia and the major threats are hail, heavy precipitation and downburst winds, there are only volunteer organised observation and no official tornado warning system is in operation.

The case of 23 August 1986 is known as a strongest tornado, when estimated wind speed reached 60 m/s. At that time there was no synoptic observation of tornado and the wind speed estimation and the synoptic diagnose of that event was made from the damage caused by tornado. The last evidences of tornadoes near Slovenia are pictures of waterspouts over the Trieste bay on 8/8/2008 and Piran bay on 28/5/2007.

2 DISCUSSION

In the paper an extreme event of 13 and 14 July 2008 is discussed when several heavy thunderstorms developed and produced large hail, heavy precipitation and heavy winds, which caused damage similar to the tornado's. On 13/7/2008 a deep and quite intense, quasi-stationary upper long-wave trough was covering the western parts of Europe, slowly beginning to evolve into an upper cut-off cyclone over the Alpine regions late in the period. In the lower levels there were warm and moist south to south-westerly winds, which blew ahead of the cold front which has reached the region during the night. A deep layer shear (0 to 6 km) was present with values higher than 25 m/s and lifting condensation level 690 m which is favourable for supercell development. After the cold front passage there was a slight stabilisation of atmosphere, but during the 14/7/2008 upper trough again destabilised the air mass.

The most intense event during this period was a pre-frontal storm from 10:00 to 14:00 UTC 13/7/2008 which travelled from west to north-east Slovenia. Figure 1 shows radar images for the period when the most damage was done are presented. At 12:10 UTC the most developed convective system was in centre of Ljubljana plane in Medvode with reflection more than 57 dBZ and the shape close to the hook. There was rather weakly argumented observation of tornado sent to European Severe Weather Database (http://www.essl.org/ESWD/), some damage to the buildings, but no images of tornado. Nevertheless, this case is now verified as tornado. On a zoomed picture of radar measured radial velocities field (Fig. 2 right) in the centre of white circle there are some pixels changing from 15 m/s to -15 m/s which could indicate some rotation.

Afterwards system travelled to the mountain region of Gozd where several large forest areas were destroyed. According the nearest automatic reporting station the wind gusts exceeded 23 m/s. Unfortunately the most affected regions have not been covered by the reporting network. On the basis of aerial photos and the pattern of destroyed trees there was a strong scientific and public debate about possibility of tornado, but officially it was

deduced that the most probable reason for the destruction was a downburst. There was no photo or any other direct evidence of tornado cloud. At 13:10 UTC the system travelled to the east and the maximum precipitation rate 33 mm per 15 minutes was measured in Celje with return period of 100 years.

Considering radar maximum echoes and radial velocities the possibility of tornado on Ljubljana flatland at 12:10 UTC could not be denied, on the other hand the radar vertical cross-section through the storm (Fig 2. left) shows that instead of hook echo two separate cells are more likely.

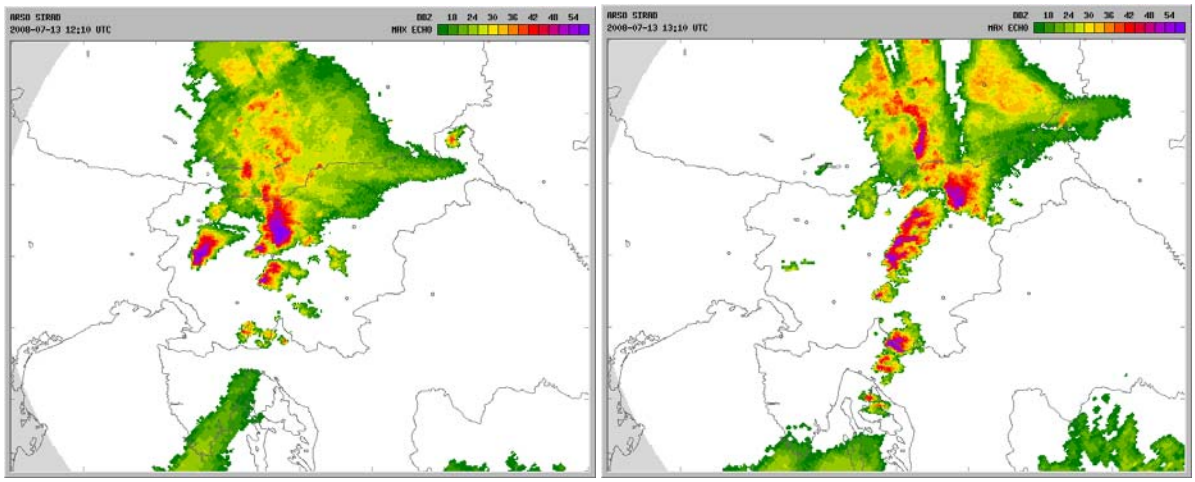

Figure 1. Maximum echoes from Lisca radar (Slovenia) for 13/7/2008 12:10 and 13:10 UTC.

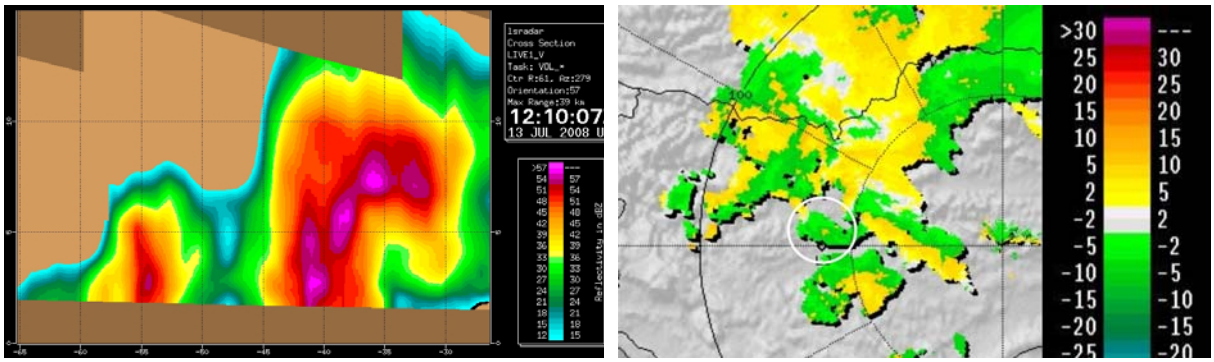

Figure 2. Left: Radar (Lisca) echoes vertical cross-section in SW–NE direction trough the centre of the white circle on the right figure for 13/7/2008 12:00 UTC; right: radar radial velocities at 4 degrees elevation on 13/7/2008 12:10 UTC. The scale is in m/s.

3 CONCLUSIONS

Although the climatology of neighbour countries shows that tornadoes are possible in the area, there was no case in Slovenia with a photo or record found till now. The possible reason for such small number of tornadoes comparing with neighbouring countries is that terrain in Slovenia is unfavourably shaped and complex with few and not extensive flatlands.

The presented case showed that the possibility of tornado at 13/7/2008 12:10 could not be denied. For the further work detailed analysis of storm relative mean radial velocities will be done, which is at moment as operational product not available. It would, besides the limitation in complex terrain and resolution, give better description of the dynamics of the extreme event.

REFERENCES

Giaiotti, D. B., M. Giovannoni, A. Pucillo, F. Stel, 2005: The climatology of tornadoes and waterspouts in Italy. Atmos. Res. **83**, 534–541.

Holzer, A. M., 2000: The Tornado climatology of Austria. Atmos. Res. **56**, 203–211.

Sárközi, Sz., 2005: A systematic approach to synoptic tornado climatology of Hungary for the recent years (1996–2001) based on official damage reports. Atmos. Res, Chambery, France, 263–271.

Dotzek, N., 2003: An updated estimate of tornado occurrence in Europe. Atmos. Res. **67-68**, 153–161.

Sioutas, M. V., A. G. Keul. 2007: Waterspouts of the Adriatic, Ionian and Aegean Sea and their meteorological environment. Atmos. Res. **83**, 542–557.

TRANSPORT AND CHEMICAL CONVERSION IN CONVECTIVE SYSTEMS ABOVE COMPLEX TERRAIN

W. Wilms-Grabe[1], U. Corsmeier[1], W. Junkermann[1], Ch. Kottmeier[1], F. Holland[2], H. Geiss[2] and B. Neininger[3]

[1]Institute for Meteorology and Climate Research, Karlsruhe Institute of Technology (KIT)
E-mail: *Walburga.Wilms-Grabe@imk.fzk.de*
[2]Institute of Chemistry and Dynamics of Geosphere, Research Center Jülich [3]MetAir Switzerland

Abstract: The COPS-TRACKS campaign of summer 2007 was focussed on the transport and chemical conversion of air pollutants under convective conditions. In this context the Karlsruher city plume was investigated, applying several airborne platforms. The results show a positive correlation between O_3 and CO in remote parts of the plume, which is an indicator for longer-distance transport and underlines the importance of the terrain structure for local trace gas distributions.

Keywords: *TRACKS, complex terrain, air pollution, O_3/CO correlation, transport processes, convective boundary layer*

1 INTRODUCTION

In July 2007, the COPS-TRACKS campaign (Transport and Chemical Conversion in Convective Systems) was carried out in southwestern Germany in order to study the transport of atmospheric trace gases and aerosols under convective conditions. One focus of this experiment was to investigate the dilution of air pollutants due to dynamical and chemical processes above complex terrain. Therefore, the dispersion of the plume of Karlsruhe, a city with moderate anthropogenic emissions, has been detected by coordinated measurements of ground based stations and different airborne platforms, namely three aircraft and a zeppelin.

2 MEASUREMENT PERFORMANCE

Karlsruhe is located in the upper Rhine valley between the Palatine mountains and the Black Forest. The transport of air masses is deeply influenced by this orographical situation (fig. 1). The day of measurement is the 25/07/2007. The weather conditions in the upper Rhine valley are characterized by a high pressure situation with occasionally 1/8 cloudiness and a maximum ground temperature of about 24 °C. The wind arises from westerly directions and ranges between 3 and 8 m/s during the measurement time period. The 25/07/2007 represents a frequently occurring summer situation with medium-sized convective conditions. The anthropogenic emissions of air pollutants mainly result from traffic and industry and also represent typical conditions of a usual summer day in the region of Karlsruhe.

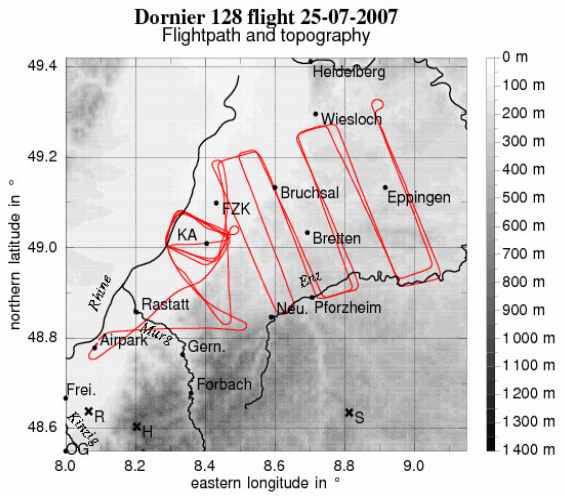

In the lee of Karlsruhe, three aircraft – *Dornier* (IMK Karlsruhe), *Dimona* (MetAir) and *Ultralight* (IMK Karlsruhe/Garmisch-Pat.) – and the *Zeppelin NT* (Jülich) flew between 13:20 UTC and 17:40 UTC inside the convective boundary layer in order to detect the city plume in different distances to Karlsruhe. Each aircraft chose a special flight pattern (example fig. 1). The measured components comprised meteorological variables as well as standard trace gases and aerosols. Ground based monitoring stations of LUBW completed the measurements.

Figure 1. Two-dimensional view on the flight patterns of Dornier in the lee of Karlsruhe. The abbreviation '*KA*' symbolizes *Karlsruhe*, '*FZK*' denotes the *Research Center of Technique and Environment Karlsruhe*.

3 RESULTS

Some selected results are presented in the following analyses, concerning the relationship between O_3 and CO. Usually, near to industry emissions one would expect enhanced CO-concentrations (because of uncomplete combustion) and low ozone concentrations at the same time. However, special situations can lead to positive correlations of both species, for example biomass burning plumes in the boundary layer (*Takegawa et al., 2003*) or the impact of remote pollution sources (*Ancellet et al., 2009*).

Fig. 2 shows the ozone concentration, measured by the Dornier aircraft in the lee of Karlsruhe, in a three-dimensional view of the mattress pattern, one leg around 750 m height and a second leg in 1000 m height above sea level. Both legs reveal moderate ozone concentrations about 53 ppb above the city area of Karlsruhe and in the direct easterly neighbourhood of the city, i.e. downstream of the wind direction. This occurs due to the reduction of background ozone mainly by NO_x-emissions. With increasing distance to Karlsruhe, ozone is enhancing up to 60 ppb as result of the common photochemical production of O_3 by NO_x-, VOC- and CO-chemistry. Also in the north-south direction the measurement shows a gradient in the O_3-distribution with higher concentrations up to 63 ppb at the borders and lower concentrations inside the mattress pattern, likely reflecting the shape of the Karlsruhe city plume, directly crossed by the aircraft.

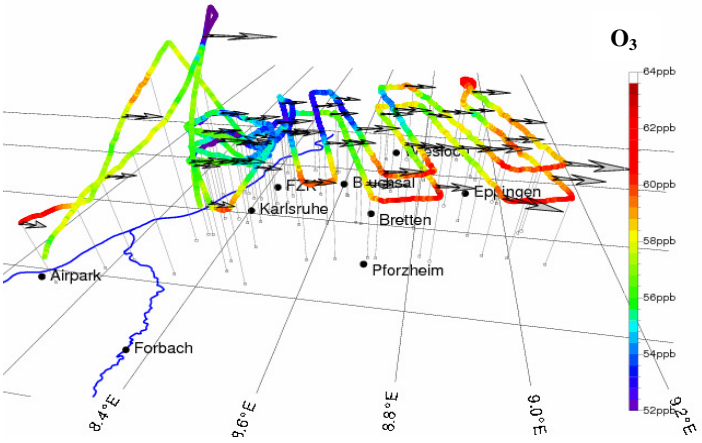

Figure 2. Ozone distribution, measured by the Dornier at 25/07/07 between 13.22 UTC and 16.55 UTC. The arrows specify the wind.

The Dornier measurements of CO (not shown here) offer moderate concentrations between 100 ppb (background concentration) and 124 ppb, but indicate the same principle distribution pattern as O_3: lower values inside the mattresses, higher values at the leg borders. Fig. 3 demonstrates the correlation of O_3 and CO for the data obtained in the remote lee area of Karlsruhe, at least 20 km away from the city emission sources. The $\Delta O_3/\Delta CO$ ratio is found to be 0.46 which is higher than the biomass burning $\Delta O_3/\Delta CO$ ratio (= 0.12) calculated by *Takegawa et al. (2003)*. The coefficient of determination amounts to 0.71, therefore the positive correlation is noteworthy and possibly gives a hint on transport mechanisms from remote emission sources.

In contrary, for the region directly bordering to the city of Karlsruhe the O_3/CO-correlation (not shown here) is unassigned, the coefficient of determination comes to only 0,26. This discrepance in the O_3/CO-correlation as function of the distance between city plume and emission source area provides an indicator for possible long-distance transport of air pollutants from remote emissions.

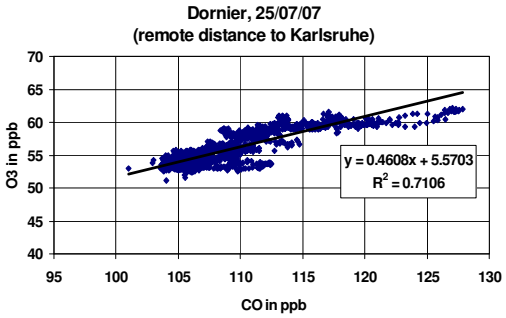

Figure 3. Correlation of O_3 and CO in the remote lee area of Karlsruhe.

4 CONCLUSIONS

On 25/07/07, the city plume of Karlsruhe was transported easterly in the Kraichgau region. The positive correlation between O_3 and CO in the lee area remote of Karlsruhe gives a hint, that the measured concentrations derive not only from the city plume itsself, but are considerably determined by mesoscale transport processes in the existing complex terrain formation and by the accompanying chemical conversion conditions. To gain more detailed information about the significance of the different dynamical and chemical interactions, a study with a regional transport model can provide essential understanding. Especially OH-radicals, which are important in the O_3- and CO-chemistry but which have not been measured during TRACKS, have to be taken into account.

This study addresses not to extreme atmospheric conditions, but to an ordinary summer situation with moderate anthropogenic emissions, a frequently occurring situation. The results help to determine the general significance also of vertical transport of trace gases during a whole summer season and to estimate human exposure to air pollutants under common summer conditions in the upper Rhine Valley.

REFERENCES

Ancellet, G., J. Leclair de Bellevue, C. Mari, P. Nedelec, A. Kukui, A. Borbon, and P. Perros, 2009: Effects of regional-scale and convective transports on tropospheric ozone chemistry revealed by aircraft observations during the wet season of the AMMA campaign. Atmos. Chem. Phys., 9, 383-411.

Kottmeier, Ch., N. Kalthoff, U. Corsmeier, et al., 2008: Mechanism initiating deep convection over complex terrain during COPS. Meteorol. Z., 17 (6), 931-948.

Takegawa, N., Y. Kondo, M. Ko, M. Koike, K. Kita, D. R. Blake, W. Hu, C. Scott, S. Kawakami, Y. Miyazaki, J. Russell-Smith, and T. Ogawa, 2003: Photochemical production of O_3 in biomass burning plumes in the boundary layer over northern Australia. Geophys. Res. Let., vol. 30, n°10, pp. 7.1-7.

DYNAMICAL AND PHYSICAL PROCESSES CHARACTERIZING UPPER-LEVEL CUT-OFF LOWS IN WINTER

Andrea Buzzi[1], Lorenzo Catania[2]

[1] Institute of Atmospheric Sciences and Climate (ISAC-CNR), Bologna, Italy
E-mail: *A.Buzzi@isac.cnr.it*
[2] ARPA-Piemonte (ext. collab.), Torino, Italy

Abstract: Upper level cut-off lows are cold-core cyclonic vortices, associated with positive potential vorticity anomalies in the upper troposphere – lower stratosphere, that are conducive to severe convection in summer and cold spells and snowfalls in winter. In the latter season, especially when travelling over continents, they can survive for many days and sometimes exhibit intensification even while migrating at relatively low latitudes, away from the main polar vortex from which they originate. Their maintenance and possibly intensification are explored using real and idealized numerical simulations. The presence of significant IR radiative cooling in a moist and cloudy troposphere, lying just under the lowest tropopause and surmounted by very dry stratospheric air, is found to significantly contribute in reinforcing the vortex strength, due to intensification of the lower portion of the positive PV anomaly.

Keywords: *Cut off low, upper level vortex, potential vorticity anomaly, atmospheric radiation*

1 INTRODUCTION

Upper level cut-off lows (ULCL's), detached from the arctic polar vortex and wandering for several days over mid-latitude belts, have been recognized as distinct from usual cyclones. They can convey important weather phenomena, like sudden snowstorms and convection, in the case they migrate over warmer surfaces. ULCL's are characterized by a tropospheric cold temperature anomaly, often without a clear signature in the m.s.l.p. field. ULCL's are associated with a sharp positive anomaly of potential vorticity (PV) in the upper troposphere, due to a downward protrusion of stratospheric air, superimposed on the tropospheric cold pool. The dynamical structure of ULCLs, including the implications of the PV distribution and of the related patterns of wind and potential temperature, has been the subject of numerous studies (for example, Eliassen and Kleinschmidt, 1957; Thorpe, 1985).

The problem of maintenance and intensification of ULCL's by radiative transfer processes is considered here, after the ULCL has acquired a quasi-circular symmetry, away from the region of formation. The working hypothesis is that atmospheric radiation contributes significantly to increase the PV maximum in the upper troposphere by means of vertical differential heating. A few case studies of ULCL's events that affected Europe in winter, moving with an east-to-west component from north-eastern Europe to southern Europe and the Mediterranean (Catania, 2008), indicate that the ULCL's can get reinforced, in terms of PV maximum, temperature minimum and circulation strength, in the mid-upper troposphere, well after their formation stage, while travelling over land in a latitude belt comprised between about 45°-60° N. Satellite imagery and meteorological analyses indicate that such ULCL's are characterized by the presence of rather compact cloud layers lying just below the dynamical tropopause, the latter being typically situated around 400-500 hPa. The combined presence of almost saturated air and clouds below the tropopause and very dry air above it (typically less than 10% of relative humidity) favours a strong radiative cooling of a layer embracing the cloud top and the base of the PV anomaly, favouring a growth of the PV maximum where the vertical derivative of diabatic heating is higher, according to the equation:

$$\frac{d\,P}{d\,t} = \frac{\vec{\zeta}}{\rho} \cdot \nabla\,\dot{\theta} \qquad (1)$$

where P is the Ertel PV, $\vec{\zeta}$ is the absolute vorticity vector, $\dot{\theta}$ is the diabatic heating/cooling and ρ is air density. In the case considered here, in the vortex core, the horizontal and vertical velocity is small, therefore $dP/dt \approx \partial P/\partial t$ and both $\vec{\zeta}$ and $\nabla\,\dot{\theta}$ are approximately vertical.

Previous studies of the impact of radiative transfer in atmospheric phenomena that bear some similarity with ULCL's, namely PV filaments (Esler et al, 1999; Forster and Wirth, 2000) and formation of arctic air masses (Emanuel, 2006), have documented its relevance on the evolution of such systems, including destabilization and convective mixing of the saturated air.

2 DATA, METHODS AND MODEL

The real ULCL events of 10-14 Dec. 2001 and 13-16 Dec. 2007 (Fig. 1) have been studied using ECMWF analysis fields, both for direct diagnostics and for running numerical experiments with the limited area BOLAM

model at a resolution of 0.25°x0.25° (Catania, 2008). Various sensitivity experiments were performed with full physics, with or without radiation (the BOLAM model uses a combination of Morcrette, 1991, Ritter and Geleyn, 1992, and Mlawer et al, 1997, radiation schemes), with or without precipitation processes, surface fluxes etc. In addition, a model based experimental approach has been undertaken by simulating idealized ULCL's structures, using the same BOLAM model with fixed or periodic lateral boundary conditions and with a horizontal grid distance of 20°x20°. The ULCL structures have been prescribed by defining a dipolar (in the vertical) Gaussian temperature anomaly (cold in the troposphere and warm in the stratosphere), superimposed on a horizontally uniform atmosphere with a tropopause, as suggested by the observed thermal structure of ULCL's (Fig. 1). A gradient wind balance, taking into account the thermal wind relationship, has been prescribed, imposing a lower condition of vanishing wind and geopotential perturbation. Most experiments have been run with constant Coriolis parameter, in which case a quasi steady state can be easily obtained in quasi inviscid conditions. The model humidity field has been defined in order to have a saturated cloudy layer in the tropospheric part of the ULCL and very dry air above, where PV attains stratospheric values. Experiments have been performed in which radiation, moisture, microphysics, horizontal and vertical diffusion have been prescribed in various manners in order to evaluate mainly the contribution of the IR radiative transfer.

3 RESULTS

The analysis of numerical experiments on real cases has revealed an important role of radiation, if combined with the presence of moist air and clouds in the cold dome. Since removal of radiation has important effects also far away from the ULCL, it is preferable to consider idealized simulations in which only the IR radiation fluxes *anomalies* are considered, after subtracting the far field radiation. In this way the effects of radiation due only to the particular temperature and moisture anomalies associated with the baroclinic vortex are isolated, as shown in Fig. 2. Relative cooling prevails near and just below the cloud top, situated at 440 hPa, and warming above, while PV increases by about 5 PV units in a layer between 400 and 450 hPa and decreases around 300-350 hPa, in agreement with eq. 1.

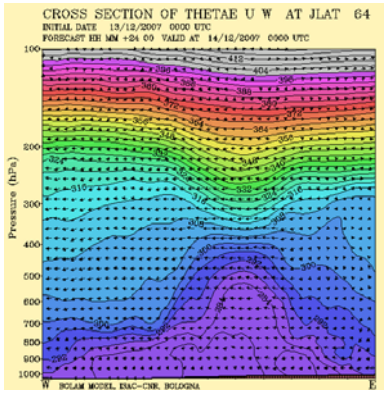

Figure 1. Vertical cross-section of equivalent potential temperature and wind vector (u, w) on the same plane across the ULCL of Dec. 2007, over eastern Europe.

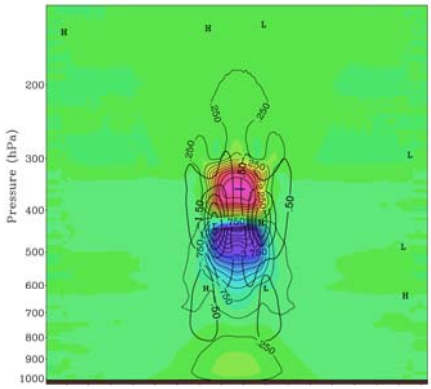

Figure 2. Vertical cross-section of radiative heating/cooling (thin lines and red/blue colours) in the ideal ULCL, and related changes of the normal velocity field (thick lines), after 4 days.

4 CONCLUSIONS

Simulations of real and idealized ULCL's indicate that the radiative transfer in the anomalous profiles of temperature and moisture can sustain and even reinforce the ULCL strength, by augmenting the amplitude of the PV anomaly and of the cyclonic flow in a thick layer situated in the upper portion of the cold pool.

REFERENCES

Catania, L., 2008: Processi radiativi e dinamici di mantenimento di vortici freddi in quota alle medie latitudini. Dissertations (*Tesi di Laurea*) in Physics. University of Bologna.

Esler, J. G., L. M. Polvani and R. A. Plumb, 1999: On the mix-down times of dynamically active potential vorticity filaments. *Geophys. Res. Lett.*, **26**, 2953-2956.

Emanuel, K., 2008: Back to Norway: an essay. *Synoptic-Dynamic Meteorology and Weather Analysis and Forecasting - A Tribute to Fred Sanders.* L. F. Bosart and H. B. Bluestein Ed., American Meteorological Soc., Boston, 87-96.

Eliassen, A., and E. Kleinschmidt, 1957: Dynamic Meteorology. *Handbuch der Physik*, **48**, 1-154.

Forster, C., and V. Wirth, 2000: Radiative decay of idealized stratospheric filaments in the troposphere. *J. Geophys. Res*., **105**, 10,169-184.

Mlawer, E. J., S. J. Taubman, P. D. Brown, M. J. Iacono, and S. A. Clough, 1997: Radiative transfer for inhomogeneous atmospheres: RRTM, a validated correlated-k model for the longwave. *J. Geophys. Res.*, **102D**, 663-16, 682-16.

Morcrette, J.-J., 1991: Radiation and cloud radiative properties in the ECMWF operational weather forecast model. *J. Geophys. Res.,* **96D**, 9121-9132.

Ritter, B. and J.F. Geleyn, 1992: A comprehensive radiation scheme for numerical weather prediction models with potential applications in climate simulations. *Mon. Wea. Rev.*, **120**, 303-325.

Thorpe, A. J., 1985: Diagnosis of balanced vortex structure using potential vorticity. *J. Atmos. Sci*., **42**, 397-406.

VERY HIGH RESOLUTION MODELLING OF FLOW OVER STEEP OROGRAPHY USING A TERRAIN-INTERSECTING MESH

A. Gadian[1], S. Lock[2], A. Coals[1], S. Mobbs[1]

[1] NCAS, University of Leeds, LS2 9JT, UK
[2] ICAS, University of Leeds, LS2 9JT, UK
E-mail: *alan@env.leeds.ac.uk*

Abstract: This poster presents results for idealised orographic stratified flows generated in a Microscale Model with a cut-cell representation of orography, resulting from a terrain-intersecting mesh. Comparisons with analytical solutions and other orographic models show promising results for the accuracy of the method. Further results demonstrate the potential of the cut-cell approach for steeper and more complex terrain.

Keywords: *Cut-cells, terrain-intersecting grids, modelled orographic flows*

1 INTRODUCTION

A generation of numerical atmospheric models has developed based on terrain-foll owing vertical coordinate systems due to their computational simplicity — of o perating on a rectangular grid regardless of the shape of the underlying orograp hy; of the lowest vertical level always coinciding with the orographic surface; and of the lowest few vertical levels being naturally positioned for application of a boundary layer scheme.

However, many studies (e.g. Sundqvist (1976) and Janjic (1989)) have demonstrated problems associated with the terrain-following approach — the generation of spurious winds in the vicinity of hills, and instabilities associated with distorted grid-cells near steep orographic gradients.

Massive growth in computing capacity and the resultant move to finer grid-resolu tions means the errors and instabilities associated with terrain-following grids above steep gradients are becoming an unavoidable hindrance. As grid resolutio ns increase, steeper and more complex gradients in the underlying orography are being resolved by the model grid. The numerical schemes in high-resolution mode ls must be capable of reliably and accurately solving flows over those steep gra dients.

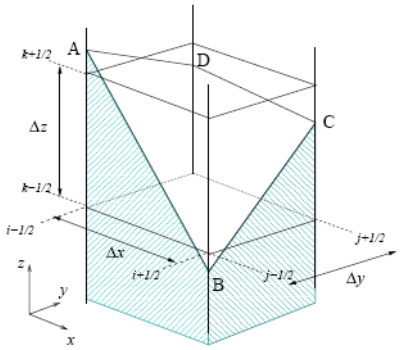

Figure 1: An example cut-cell in a terrain-intersecting model: $ABCD$ repr esents the orographic surface that intersects the model levels

2 METHODS

There has recently been some investigation of the potential for terrain-*in tersecting* grids, where the vertical levels remain horizontal throughout the do mian. In the presence of uneven orography, the vertical levels intersect the lo wer boundary resulting in some grid-cells that are *cut* by the orography. Figure 1 illustrates an example cut-cell within a terrain-inter secting model domain.

To solve the flows through irregularly-shaped cut-cells, Adcroft et al. (1997) explor ed the use of a finite-volume approach in an incompressible ocean model, where t he ocean-bottom topography was represented with cut-cells. The cut-cell method was seen to produce smooth solutions, where more rigid step-representations of o rography had failed. The method was extended and further explored in Bonaventura (2000), Steppeler et al. (2002), and Steppeler et al. (2006), resulting in a cut-cell method being implemented in the high-resolution numerical weather prediction model at the Deutscher Wetterdienst — the COSMO-DE model.

This work explores the potential for the cut-cell method in a very high resolution model. The Microscale Model is designed for exploring dynamics and moist processes at grid resolutions of $\Delta x < 100$m, with a particular focus on flows over steep gradients.

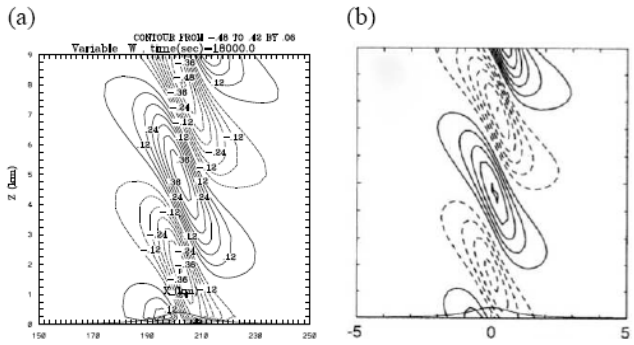

Figure 2: Results for stratified flow over a 2D bell-shaped hill, with half-width 10km, as described in Gallus et al. (2000): plots show the vertical velocity field, with a contour interval of 0.1 from (a) the Microscale Model; and (b) the analytical solution reproduced from Gallus et al. (2000)

3 RESULTS AND CONCLUSIONS

Results from the model compare well with linear solutions for well-studied idealised test cases (see Figure 2). At higher resolutions, resolving steeper gradients, the results for dry inviscid flows over orography look promising and will be presented here. In addition, routines for computing latent heat exchange between water vapour and liquid water have been implemented and tested. Current work is focusing on exploring the potential of the cut-cell Microscale Model for moist orographic flows.

REFERENCES

Adcroft, A., Hill, C., and Marshall, J., 1997: Representation of topography by shaved cells in a height coordinate ocean model. *Mon. Wea. Rev.*, **125**.

Bonaventura, L., 2000: A Semi-implicit Semi-Lagrangian Scheme Using the Height Coordinate for a Nonhydrostatic and Fully Elastic Model of Atmospheric Flows. *J. Comp. Phys.*, **158**.

Gallus, W. and Klemp, J., 2000: Behavior of flow over step orography. *Mon. Wea. Rev.*, **128**.

Janjic, Z. I.,1989: On the pressure gradient force error in σ-coordinate spectral models. *Mon. Wea. Rev.*, **117**.

Steppeler, J., Bitzer, H., Minotte, M., and Bonaventura, L., 2002: Nonhydrostatic Atmospheric Modeling using a z-Coordinate Representation. *Mon. Wea. Rev.*, **130**.

Steppeler, J., Bitzer, H.-W., Janjic, Z., Schättler, U., Prohl, P., Gjertsen, U., Torrisi, L., Parfinievicz, J., Avgoustoglou, E., and U. Damrath, 2006: Prediction of Clouds and Rain Using a z-Coordinate Nonhydrostatic Model. *Mon. Wea. Rev.*, **134**.

Sundqvist, H., 1976: On vertical interpolation and truncation in connection with use of sigma system models. *Atmosphere*, **14**.

THE SUMMER OF COPS-2007: MULTI-SCALE DYNAMICS VISUALIZED BY VARIABLE-SPEED TIME-LAPSE SATELLITE IMAGERY

Hans Volkert

Deutsches Zentrum für Luft-und Raumfahrt, Institut für Physik der Atmosphäre, Oberpfaffenhofen, Germany
E-mail: *Hans.Volkert@dlr.de*

Abstract: Some 9000 Meteosat images at 15' intervals span the full 3 months of the COPS field phase. Their display in variable-speed time-lapse loops provides an intuitive and persuasive synopsis of generation, motion and decay of cloud systems of differing horizontal scale and at distinct atmospheric levels.

Keywords: *ICAM, Meteosat, cloud motions, synoptic meteorology*

1 INTRODUCTION

Atmospheric dynamics focus on the interplay of the acting forces, mainly in the horizontal direction, e.g. the pressure gradient force in approximate balance to the Coriolis force on the rotating globe, modulated by friction and resulting individual acceleration of air parcels. Physical processes like cloud generation induced by the significantly smaller vertical motions (due to buoyancy forces) can eventually lead to the fall-out of precipitation. Synoptic, i.e. combined-view, horizontal charts at various levels are still the standard medium when insights about the evolving state of the atmosphere are sought, be it directly from observations or from computer generated analysis or forecast fields. Vertical sections provide an upright perspective, but tend to overemphasize height over distance and along-section motions to perpendicular ones.

Since more than 40 years satellite imagery has been providing an additional perspective. In an early study, Warnecke et al. (1968) combined multi-wavelength composite imagery by polar orbiting satellites with conventional observations to investigate the life cycle of a tropical cyclone. Since the late 1960s, weather satellites in geosynchronous orbit allow through their fixed relative position the direct production of time-lapse loops (short films). At the poster we present for the COPS field phase (June-August 2007) a 3-month-long sequence from multi-channel SEVIRI images obtained from Meteosat-8 at 15' (or 900") intervals on a stereographic weather map projection with overlaid geographical grid.

2 THE COPS-2007 CLOUD MOTION LOOP

Multi-spectral data of the SEVIRI instrument on the Meteosat Second Generation satellites are regularly received and processed by DLR-IPA, e.g. for the detection and tracking of convective cells over central Europe (Zinner et al., 2008). For all regular scan scenes from Meteoat-8 (15' intervals) a 3-channel (high resolution visible and two infrared channels) colour composite was created on a weather map projection (10ºE as vertical meridian) resulting in 8832 images for the COPS field phase from 1 June to 31 August 2007. They are online available for scientific users under password protection from www.pa.op.dlr.de/cops/msg_vis_archive.html which is linked to the general site www.cops-2007.de branch "operational products / satellite products / MSG imagery".

But only when combined to a video-clip with standard image frequency of 25 frames/s and displayed at relative speeds of 0.5, 1.0, 2.0 the full "drama of weather" (Shaw, 1933; admirable juxtaposition of atmosphere and antique theatre) becomes evident for the high-speed viewing system of human eyes and brain. The considerable time-lapse factors ('speed-ups') of 11250-, 22500- (=25x900"), and 45000-fold provide a breath-taking impression of ceaseless motions, much more rotational than translatory, under the quick successions of longer day-light and shorter dark night periods. Opposing motion directions at low and high elevations are frequent. The full three-month clip has 402 MB and can be run at variable speeds with, e.g., MS-MediaPlayer.

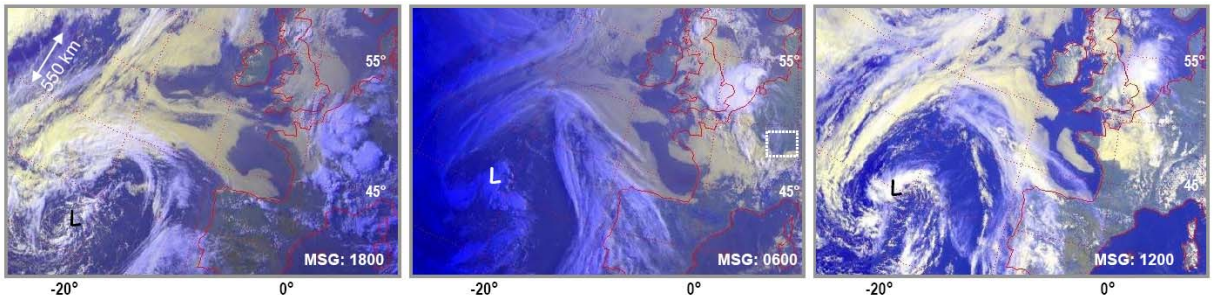

Figure 1. Three snapshots of spiralling cloud bands around a cyclone (L: low pressure centre) west of Portugal on 7 (18 UT) and 8 June 2007 (06, 12 UT). Three channel composite of SEVIRI sensor aboard Meteosat-8, transformed on a stereographic weather map projection (5º x 10º lat./lon. dotted grid; 10ºE vertical). The small dotted frame indicates the inner COPS area.

3 GLIMPSES TO A FEW "STILL LIFES"

While the moving dynamics of the atmosphere over Europe and the east Atlantic during summer 2007 can only be inferred from the video-clip, we present here two examples in a sequence of single frames.

During four days (6-9 June) a cyclone 'danced' west of Portugal sending its frontal cloud bands onto the continent (cf. Fig. 1 for three glimpses during the central period) before a following larger low pressure system covered the ocean area around 20º–10ºW for full five days (10-14 June). Sequences of fast moving high-level cirrus bands indicate frequent streamers, most likely connected with stratospheric intrusions (Appenzeller and Davies, 1992).

The end of June saw an impressive '*pas de deux*' of two cyclones over the eastern Atlantic and the North Sea, respectively, linked by an elongated, curved cloud band as if they were holding hands (Fig. 2). The detailed cloud structures and their vertical extent become best visible during the hours when the sun is rising or setting over Europe. Inspection of close-ups from rapid scans (at 5' minute intervals) allow during daylight periods the detailed identification of embedded convection. After a parallax correction their position can be precisely located.

4 CONCLUSION

Short sequences of cloud motions are regularly presented in TV weather forecasts, both observed during the previous hours and pre-determined from short-range NWP model output. Web-based access to Meteosat loops is also available for schools (cf. Dudek, 2009).

However, it is felt that the research community does not sufficiently use video technology combined with satellite data and classical synoptic experience. A regular archive of temporal complete, spatially well resolved and navigated multi-channel satellites scenes, put together in overlapping month-long loops for both normal (15') and rapid (5') scans over carefully selected areas has a huge potential *(i)* of inspiring researches; *(ii)* of educating students, teachers and pupils; and *(iii)* of impressing the public at large regarding the true nature of the weather producing atmosphere and the astonishing daily successes of providing skilful forecasts for the seemingly chaotic medium, at the ground of which we spend our days.

Discussions are sought with participants of ICAM-2009 during and after the conference. The video-clip COPS-Jun JulAug2007.avi is available from the author for non-commercial usage.

Acknowledgements:
I want to thank my colleagues Luca Bugliaro and Hermann Mannstein for their efforts to process and archive the multi-channel SEVIRI data obtained from EUMETSAT. Bernhard Mayer kindly assembled the videoclip in avi-format. The inspiration to look at extended loops of satellite imagery stems from my student days in the late 1970s with Prof. Günter Warnecke (FU Berlin), who extensively used the then novel loops from geostationary satellites for his undergraduate courses.

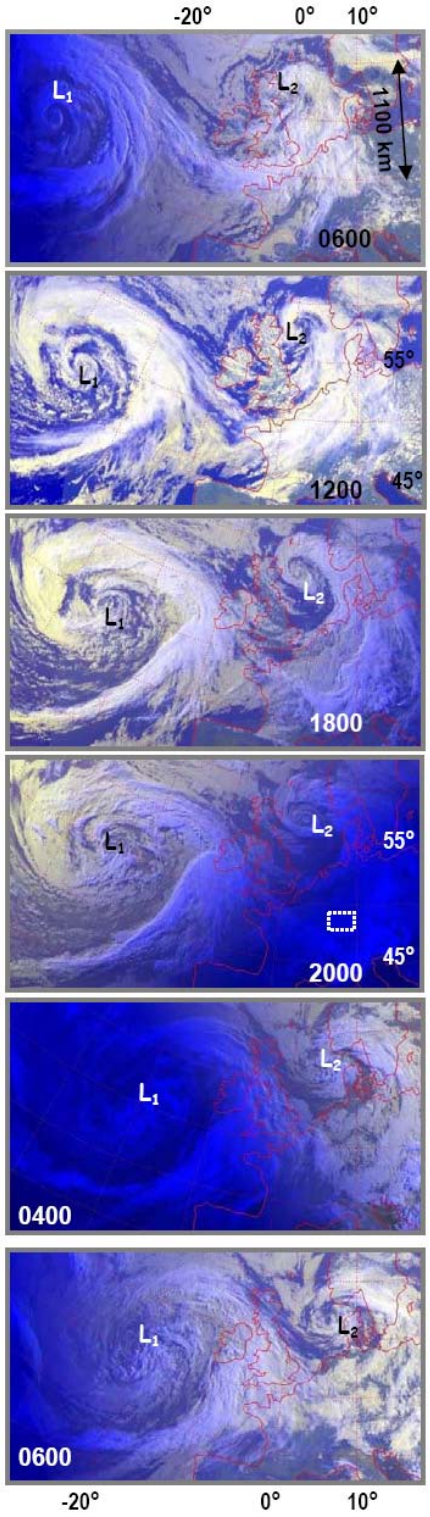

Figure 2. Top to bottom: Cloud band developments around two cyclones over eastern Atlantic (L_1) and North Sea (L_2) on 29/30 June 2007. Details analogous to Figure 1.

REFERENCES

Appenzeller, C. and H.C. Davies, 1992: Structure of stratospheric intrusions into the troposphere, *Nature* **358**, 570–572.

Dudek, P., 2009: Website "http://sat-sh.lernnetz.de/wetterfilme/msg/ " ,Weather films for schools (in German; accessed April 2009)

Shaw, N., 1933: *The drama of weather*. Cambridge University Press, Cambridge, UK, xiv + 269 pp.

Warnecke, G., L.J. Allison, E.R. Kreins and L.M. McMillin, 1968: A satellite view of the typhoon Marie 1966 development. NASA Technical Note TN D-4757, 94 pp.; online available from http://ntrs.nasa.gov/ (search for "typhoon Marie").

Zinner, T., H. Mannstein, A. Tafferner, 2008: Cb-TRAM: Tracking and monitoring severe convection from onset over rapid development to mature phase using multi-channel Meteosat-8 SEVIRI data. *Meteorol. Atmos. Phys.* **101**, 191–210.

Relationship between morphology PARAMETERS and duration of snow cover at microscale: preliminary study in several major ski areas of the territory of Trentino (Italian Eastern Alps)

Massimiliano Fazzini[1], Mauro Gaddo[2],
[1] Università di Ferrara – Dipartimento di Scienze della Terra
E-mail: *massimiliano.fazzini@unife.it*
[2] Provincia Autonoma di Trento - Ufficio Previsione ed Organizzazione

Abstract: The duration of stay of snow on the ground in areas of medium and high Alpine mountains, is very uneven and depends on many morphological variables, starting from the altitude and the exposure to hillside. A special case concerns the valley, the highlands and karst areas where the thermal effect together with that of the "sky wiew factor" difficult to determine hardly modelling situations. In this study, it was decided to consider the longest continuous period during which snow remains on the ground at the different exposure finding a relationship with the exposure itself and to hillside, in three sample areas identified in extended ski areas, located in different areas of the Alps Tridentine: thus district of Pampeago-Latemar, San Martino di Castrozza-Passo Rolle and Passo Tonale. Statistical reports, researched by a simple and a multiple linear regression analysis of the forward kind, show results in some respects surprising and very useful for climatological-tourism applications in ski areas.

Keywords: *Snow duration, exposition, microscale, ski district*

1 INTRODUCTION

Beginning from the ’80, we witness a strong decrement of seasonal fresh snow quantities, that can vary, depending on geographical area and altitude, from 3 to 5 cm per season (Fazzini *el al*., 2004). This signal, together with an evident increment of winter average temperatures, that can be quantified, in the same period, between 0.3 and 0.5 °C, comes from a proportional decrement of days with snowfalls. Consequently, a decrement of days with snow on the ground can be observed. All that gives rise to strong repercussion on the skiability of middle and low altitude ski areas, and the alpine ski tracks facing South are feasible for a limited number of days (Fazzini, 2008; Fazzini e Bisci, 2008). Trento Province relies, since winter 1981-1982, on a well organized nivometeorological network; moreover, a recent Provincial Law on avalanche sites control in ski areas, promoted a higher density of such measuring sites. Thanks to the relative abundance of data, their remarkable quality and their geographical positioning, including all main aspects, in important ski areas, it is possible to attempt a microscale climate study that can better clear the existing relationships between morphology and snow parameters in a territory.

Figure 1. Study areas position

2. DATA AND METHODS

A climatological analysis has been carried out on a series of nivometric data belonging to 2005-2006, 2006-2007, and 2007-2008 seasons for those measuring sites located in Pampeago – Ski Center Latemar and San Martino di Castrozza – Passo Rolle (Pale di San Martino Group) ski areas. In the Passo Tonale area, nivometric data are available for the season 2007-2008 only, so results have not been considered since they were not comparable with those of the two other study areas. In the Pampeago area - situated in Val di Fiemme and representative of the Dolomites - data have been sampled at altitudes ranging from 1,750 to 2,100 m a.s.l in the four major aspects. In San Martino di Castrozza, representative of the south Dolomites, data are relative to altitudes between 1450 and 2050 m a.s.l for all major aspects. For all the stations listed in this work, data from the current, extremely snowy season, are being collected. As soon as snow will melt on all sites, new data will be integrated and analyzed with the existing ones. Up till now, nivological daily data, man measured at 8.00 am, have been analyzed. For each measuring site, monthly and seasonal fresh snow contributions have been calculated, as well as the summation of days characterized by snow coverage of the ground, continuous (*Len cont*) and total (*Len tot*). Only *Len cont* values have been used. At the same time, to try describing quantitatively the environment surrounding each site, 16 measures, both morphometrical and topographic, have been calculated, to be correlated with the nivological

variable. A stepwise type multiregressive statistical analysis has been performed, considering the nivological variable as a dependent, and the morphological measures as independent ones. Angular parameters have been linearized using *sinus* and *cosinus*.

AREA SAN MARTINO	Elev	Expos	Slope	Htot	Len tot	Len cont
S.MARTINO DI C.ZZA	1461	47	2	342	130	123
PASSO ROLLE	2004	214	6	448	179	174
CALAITA	1602	14	5	344	137	129
VAL CIGOLERA	1878	106	13	425	148	144
COL VERDE	1879	221	18	375	129	116
AREA PAMPEAGO	Elev	Expos	Slope	Htot	Len tot	Len cont
PAMPEAGO VILLAGE	1780	147	20	275	137	134
GARDONE'	1675	94	9	229	129	124
MONSORNO	2000	195	14	342	153	152
AGNELLO	2065	345	13	387	171	170

Table.1 – Topographical and nivological parameters for the sites used in the analysis: Elev: elevation above sea level – m; Expos: Aspect of slope °; Htot: average of seasonal fresh snow, cm; Len tot: duration of total snow cover, days; Len cont: duration of continuous snow cover, days.

3 RESULTS

From the analysis of nivological data, comes into sight that, at the same altitude, San Martino di Castrozza area is more snowy than Pampeago one, because of its location, more external in regard to Alpine range, and for the arrangement of the valleys. The Pale di San Martino group is actually more exposed than the Latemar group to Mediterranean currents that, statistically, bring the heaviest snowfalls (Fazzini et al 2005); the mouth of San Martino valley (Val Cismon) faces south, favouring the entrance of mild advections, which afterwards undergo a heavy convergence - uplift process at the head of the valley. Nevertheless, due to a higher thermal continentality of Pampeago area, no substantial differences can be observed with regards to the duration of snow on the ground. On Passo Tonale area, measures made at the same altitude of 1880 m a.s.l. on N and S aspects showed a difference of 23 days in the persistence of the snow on the ground. The analytical relationship between altitude and snow persistence results to be found only in Pampeago area (R^2 = 0.93), with an increase of snow coverage of 10,8 days/100 meters of altitude increase. The corresponding values for San Martino area are R^2 = 0.43 and 6,7 days/100 meters. The multiple linear regression analysis raised the level of explained variability to 0.98 in Pampeago area, thanks to the statistical contribution of site aspect and the gradient ratio of the slope overhanging the site. Similarly, the explained variability of San Martino area reached values of 0.93 thanks to statistical contribution of site aspect, the *sinus* of the azimuth of the valley axis, and the *cosinus* of slope steepness.

4. CONCLUSIONS

With the analysis of the statistical relationship of multivariate type between morphological parameters and continuous presence of snow cover, flattering results have been obtained. Using the data of current season, and therefore using the data from Passo Tonale area too, the model could be further improved; using the information coming from morphological measures used in the study areas, a regionalization of the model could be tried.

Acknowledgements: *We thank Enrico Filaferro for an critical rewiew of analisys and PAT and ITAP - Pampeago nivologist.*

REFERENCES

Massimiliano Fazzini., Simona Fratianni, Augusto Biancotti, & Paolo Billi, 2004: "Skiability condition in several skiing complexes on Piedmontese and Dolomitics Alps. Meteorologische Zeitschrift, Gerard Borntraeger ed, Berlin, Stuttgard Volume .**13.3**, 253-258

Fazzini M., Giuffrida A., Frustaci G., 2005: Snowfall analisys over peninsular Italy in relationship to the different types of synoptic circulation: first results – *Proc. 28th conference on Alpine Meteorology, Zadar*, Croatian Meteorological Journal, Volume **40**, 650-653.

Massimiliano Fazzini and Carlo Bisci, 2008: Alpine climatology and touristic application of a skiability index in Paneveggio-Pale di San Martino park area (easter trentino region, italian Alps - Studia Crescent, Volume **2-2008**; 41-49.

Massimiliano Fazzini, 2008: Impact du changement climatique sur l'enneigement dans les Pré-Alpes du Trentino: le cas de Folgaria – *Proc XXI colloque Internationale AIC Montpellier*, 234-239

SNOW PRECIPITATION VARIABILITY IN THE WEST ALPS IN ITALY: EVALUATION OF AN ALGORITHM FOR THE SURVEY OF SNOW COVER THROUGH SATELLITE IMAGES

Terzago S.[1], Cassardo C.[2], Cremonini R.[3], Fratianni S.[1]

[1] University of Torino, Department of Earth Science, Torino, Italy
E-mail: 315697@*studenti.unito.it*
[2] University of Torino, Department of Physics, Torino, Italy
[3] Regional Agency for Environmental Protection, Torino, Italy

Abstract: Snow cover greatly influences the climate in the Alpine region and it is one of the most important factors in the analysis of the climate change because of its interconnections with other phenomena: the different distribution and amount of snow precipitation during the winter season influence energy, radiation and hydrologic budgets, as well as atmospheric circulation.
In this paper the results of the analysis of snow precipitations in North-West Italy in the period 2000-2009 are presented: nivometric measurements performed in 10 automatic meteorological stations of ARPA Piemonte Network were used. In the studying of Alpine climatology satellite data can be exploited to achieve information on temporal and spatial variability of snow cover extent: for this purpose MSG's SEVIRI snow cover algorithm was evaluated for 19 cases of study in the period 2007-2009 using at-ground stations.

Keywords: *snow, climate, MSG snowcover algorithm, Alps*

1 INTRODUCTION

Snow cover over Alps influences climate both at large and local scale as snow reflects most of the solar radiation, varying surface radiation, energy and hydrologic budgets. Ground-based meteorological stations and satellite data can provide complementary information on snow cover: the first ones about the nivometric statistical parameters and the climate trends for local scale, the second ones about the extension of snow cover, the snow line and the reflectance of snow covered areas on large scale. The analysis of snow precipitation variability through these two different point of view will allow to achieve a global understanding of snow processes and dynamics in the Alpine Region.

In this paper the first results of the analysis of 10 ground-based stations measurements in the South-West Piedmont Alps in the period 2000-2009 are presented: time series are continuous and homogeneous in this period so the results can be compared.

For a future exploitation of satellite data in climatological studies, the quality of satellite snow cover products need to be assessed and improved: daily SEVIRI snow cover was generated for 19 clear-sky days in the period 2007-2009 and validated with 111 at-ground measurements in Piedmont and Aosta Valley. It was quantified the snow product accuracy in presence of fresh snow, for different snow depths and different seasons.

2 DATA

Snow depth measurements performed in the automatic meteorological stations have been considered to evaluate the monthly mean snow depth over the period 2000-2008 and the results are reported in Table 1. The standard deviation is generally high for the strong annual variability of snow precipitation. Fresh snow depth records have been used to determinate the number of snowy days per month which shows little fluctuations. In Figure 1 the monthly-averaged snow depth and the number of snowy days for the Acceglio station are represented: as in all the other stations, the highest peak for snow depth corresponds to the last snow season (2008-2009), when heavy snowfalls occurred over Piedmont. In January 2009 the monthly mean snow depth is 112 cm, in February it is 124 cm: in both cases the values exceed two standard deviations the month average, however, in order to classify them as anomalous events, they should be compared to the mean value of a 30-years time series.

At-ground snow depth and fresh snow depth measurements have been used for the validation of SEVIRI snow cover product which discriminates snow covered and snow free areas. The quality of the SEVIRI snow cover has been determinated using contingency tables and statistical indices, as reported in Table 2: the probability of a correct classification of snow covered areas is CSI=0.74 and the probability of overestimation of snow cover (FAR=0.17) is comparable to the probability of underestimation (BIAS=1.04). Further analysis show that the quality of snow cover is higher in Winter than in Spring, when snow is overestimated. It was observed

that the accuracy of the snowcover product is very high in presence of fresh snow or if snow depth higher than 30 cm (CSI=0.95). When snow depth is lower than 10 cm the probability of misclassification increase.

Station	Elevation a.s.l. [m]	UTM_x	UTM_y	Mean Snow Depth [cm]					
				Nov	Dec	Jan	Feb	Mar	Apr
Acceglio	1610	339567	4927939	13±13	39±29	41±27	45±30	31±23	3±2
Argentera	1680	335978	4918048	16±15	57±36	60±37	63±39	50±35	8±5
Boves	575	385442	4910296	1±2	9±11	10±8	8±6	2±3	0±0
Castelmagno	1755	354208	4918133	17±15	52±29	49±32	55±36	42±28	10±8
Paesana	1265	362370	4947015	8±12	19±26	21±14	27±19	22±19	2±1
Piaggia	1645	398488	4880823	4±4	29±33	36±36	46±47	34±37	8±7
Pian delle Baracche	2135	351816	4934725	30±21	73±43	73±38	84±38	85±41	72±30
Pontechianale	1575	345555	4941889	11±12	29±25	19±16	21±15	13±9	3±3
Rifugio Mondovì	1760	398757	4894142	15±11	56±38	59±41	73±47	73±47	49±36
Valdieri	1390	361709	4896272	18±18	67±37	79±48	97±48	89±55	31±27

Table 1. Monthly mean snow depth and standard deviation calculated over the period 2000-2008 for 10 ARPA Piemonte ground stations.

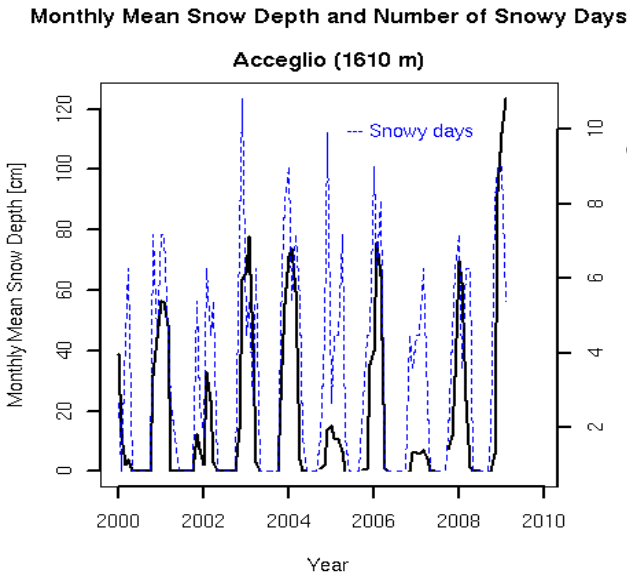

Figure 1. Monthly-averaged snow depth and number of snowy days in the period from January 2000 to February 2009.

GROUND STATIONS	SEVIRI no snow	SEVIRI snow
no snow	413 (correct negatives)	110 (false alarms)
snow	85 (misses)	550 (hits)

$$POD = \frac{hits}{hits+misses}$$

$$CSI = \frac{hits}{hits+false\ alarm+misses}$$

$$FAR = \frac{false\ alarm}{hits+false\ alarm}$$

$$BIAS = \frac{hits+false\ alarm}{hits+misses}$$

POD = 0.87
CSI = 0.74
FAR = 0.17
BIAS = 1.04

Table 2. Validation of SEVIRI snow cover with in-situ measurements: contingency table and statistical indices.

3 CONCLUSIONS

A first analysis on snow precipitation features over Alps in North-West Italy has identified the monthly mean snow depth during the period 2000-2008 in 10 at-ground stations: a strong variability in the abundance of snow has been pointed out. Longer time series are necessary to determinate climate trends and to investigate on the heavy snowfall of the 2008-2009 winter.

The quality of SEVIRI snow cover product is better in Winter than in Spring when snow cover is overestimated, probably due to the stronger solar illumination: snowcover algorithm test threshold should be optimised to have a constant accuracy during the snow season. Deep snow and fresh snow are correctly identified while shallow snow should be detected with a more liberal test threshold.

REFERENCES

Kidder S. Q., Vonder Haar T. H., 1995: Satellite Meteorology: an introduction. Academic Press.

Parajka J., Bloschl G., 2006: Validation of MODIS snow cover images over Austria. Hydrology and Earth System Sciences, 10.

Schmetz J., Pili P., Tjemkes S., Just D., Kerkmann J., Rota S., Ratier A., 2002: An introduction to Meteosat Second Generation (MSG). Bulletin of American Meteorological Society.

Using polar-orbiting weather satellite data to estimate the snowline of central-European mountains

Ralf Becker[1], Peter Bissolli[2], Thomas Reich[3]

[1] Deutscher Wetterdienst, Remote Sensing Division, Offenbach
E-mail: ralf.becker@dwd.de
[2] DWD, Dept. Climate and Environment, Offenbach,[3] DWD, Dept. Hydrometeorology, Berlin

Abstract: The utilization of atmosphere and surface parameters derived from satellite remote sensing is of increasing importance to describe status and changes of weather, climate and the regarded processes in the biosphere. Even in regions with good coverage concerning ground based measurements satellites contribute to fill temporal and spatial gaps. Imaging radiometers provide information on surface snow and ice based on multispectral algorithms with a spatial resolution from 500 m to 3000 m. Verification with respect to ground based measurements shows very good results.

Keywords*: snowline, mountains, satellite remote sensing, AVHRR, MODIS*

INTRODUCTION

Snow and glacier ice play an important role in the description of the hydrological cycle by acting as a reservoir for water. The real-time monitoring of snow cover contributes to improve the water management. In the mid-latitudes of central Europe this is of special interest in and near the Alps and highlands like the Black forest and the Bavarian forest. Standard methods to detect and monitor snow cover are based on synoptical data as input and kriging techniques to handle the heterogeneous spatial distribution of stations and orographic effects. In orograpical structured area there is a lack of accuracy of such methods.

DATA AND METHODS

Observations of operational satellite systems namely Meteosat second generation, Noaa/MetOp AVHRR and Terra/Aqua MODIS have the potential to provide snow products on a daily basis with spatial resolution comparable or better than grid increment of the hydrological models. The work presented here shows the applicability of an automatic scheme evaluating AVHRR and MODIS data to determine the snowline in mountainous areas. A well-established algorithm, developed within the framework of the Satellite Application Facility for Nowcasting (NWCSAF, Dybbroe et.al. 2005), is used to detect snowy pixels in the AVHRR imagery. For MODIS a dedicated algorithm was set up: a multi-spectral thresholding of calibrated radiances is applied to separate clear land and sea from cloudy and snow-covered scenes. It is independent of other non-static data like numerical model forecasts and outputs a combined snow/cloudmask that is finally convoluted with background topography information (GIS), allowing for the calculation of snowlines. The core snow and ice detection is mainly based on a NDSI module (*normalised difference snow index*, Hall et.al. 2001). The first processing step separates pixels that can be classified for sure by its spectral features as snow meanwhile the others remain uncertain. The second, box-based step analyses the neighborhood of these pixels to catch pixels with mixed spectral features. A set of regions has been defined to cover low mountain ranges, like Thuringian forest in the middle and Black forest in the southwest of Germany, as well as parts of the Alps. In a postprocessing step an automatic quality assessment is conducted. It checks whether cloud coverage of the scene is tolerable in terms of absolute coverage as well as vertical distribution of snowy pixels.

COMPARISON AND VERIFICATION

A comparison study of MODIS to Nowcasting SAF software results - the validated PPS algorithm - is enabled by setting up a processing with preprojected data on a spatial scale of 500 m. The data ranges from May 2007 to August 2008. According to that the results for MODIS are in a good agreement facing a correlation of .94 but systematic overestimation of MODIS vs. AVHRR snowline of about 200 m is considered. A verification was carried out for the same time range by taking into account all European synoptical and climatological snow measurements with snow heights of at least 1 cm. The scores show a clear seasonal cycle with PODs of .2 in summer (both) and .86 (AVHRR) and .82 (MODIS) in winter months. Bad figures during summertime can be explained by more mixed pixels with less snow contribution over central Europe at this time.

APPLICATIONS

The hydrological model SNOW is simulating the snow cover evolution up to 72 hours lead time. Additional initial data on snow cover extent based on AVHRR and MODIS are feeded into the model to improve some critical aspects of conventional snow assimilation like melting phase heterogeneity (neighborhood of snowy and snowfree picture elements) and insufficient correlation with terrain height as exploited by kriging techniques. First results of adjustment examples using AVHRR snowmask show that the speed of melting is accelerated considerably. The goal of the project SnowClim is to build a European snow climatology to serve as input for touristical applications, regional climate monitoring, water management and traffic a.o. In a first step the satellite based values shall help to identify wrongly coded data of snow cover in the synop database and to compare the duration times of snow cover especially in regions with less dense ground based measurements.

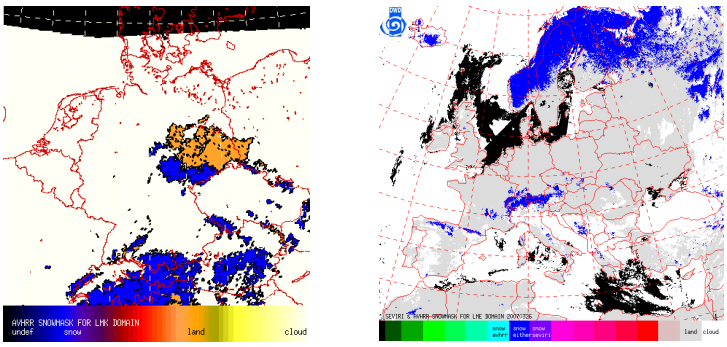

Figure 1: Sample AVHRR snowmask mapped for the domain of COSMO-DE model at 2.8 km scale (left, valid for 20071225, snow=blue, cloud=white). Input are two NOAA-17 midmorning overpasses (8:00 to 10:30 UTC), processed on 1 km scale using NWCSAF/PPS software. Merged AVHRR and SEVIRI snowmask for the COSMO-EU domain (right). Higher importance of polar orbiter data given at higher latitudes due to decreased applicability of SEVIRI data north of 60 degrees.

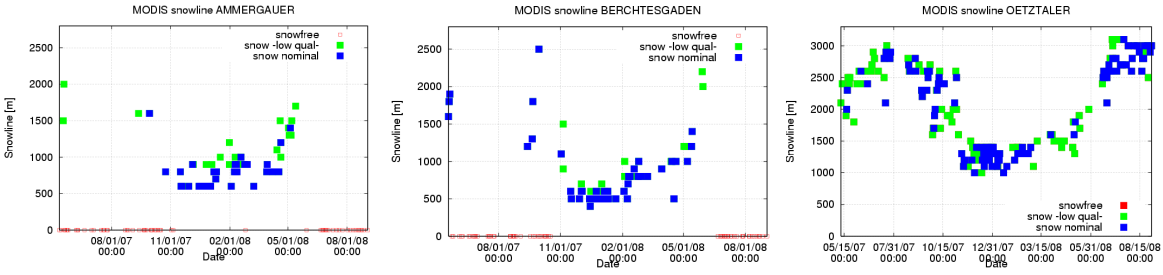

Figure 2: Snowline evaluations covering the winter season 2007/08 based on MODIS for some selected regions – the Ammergau and Berchtesgaden mountains as examples for the northern Alps and Oetztal as part of the central Alps. Blue squares are associated with nominal quality referring to almost cloudfree conditions and near-nadir viewing geometry. Green squares mark evaluations that lack one of these boundary conditions, still usable but larger error bars. If there was no snow detected an open red square is drawn. Note that results of a central alpine area characterized by permanent snow and glaciers (right panel valid for Oetztal, time range here from May 15, 2007 to Aug 15, 2008) do reflect the seasonal variation of snowline.

OUTLOOK

The very promising results enable the utilization of a merged (MODIS/AVHRR/SEVIRI) snowmask in the assimilation scheme of the SNOW model on a 1 km scale, maintained by the department of hydrometeorology of DWD. In the context of the DWD-project SnowClim (European snow climatology) the satellite-based evaluation shall be used as comparison and potential correction regarding a climatological derivate like duration of snow cover with respect to its height dependency.

REFERENCES

Droz, M. and S. Wunderle, 2002. Snow line analysis in the Alps based on NOAA/AVHRR data spatial and temporal patterns for winter and springtime in 1990, 1996 and 1999, Proceedings of the EARSeL-LISSIGWorkshop: Observing our cryosphere from space, Bern (CH) March 11-13

Dybbroe, A., K.G. Karlsson and A. Thoss, 2005. AVHRR cloud detection and analysis using dynamic thresholds and radiative transfer modelling – part one: Algorithm description. J. Appl. Met., 41(1):3954.

Hall, D.K., G.A. Riggs and V.V. Salomonson, 2001. Algorithm Theoretical Basis Document (ATBD) for the MODIS Snow and SeaIce Mapping Algorithms. http://modis-snow-ice.gsfc.nasa.gov/atbd.html

A NEW DEVICE FOR ACCURATE MEASUREMENTS OF METEOROLOGICAL PARAMETERS IN A SNOW RICH ENVIRONMENT

Manfred Dorninger

Department of Meteorology and Geophysics, University of Vienna, Vienna, Austria
E-mail: *manfred.dorninger@univie.ac.at*

Abstract: A deep snow pack, remote locations, no external power supply and very low temperatures are often the main ingredients when it comes to the deployment of meteorological stations in mountainous terrain. WMO recommendations concerning distance of the sensors to the surface are hardly fulfilled especially due to the varying snow depths. The accurate position of the sensor related to the snow surface is normally not known since a daily inspection is not possible. Even worse, the sensor might be completely snow-covered. The paper introduces the so called "METLIFT" which has been developed at the department recently. A snow height sensor measures the distance to the snow surface. If certain limits are exceeded the whole station is adapted accordingly. The lift can deal with a snow depth of up to 4 m. Accumulators recharged by solar panels guarantee the internal power supply. Data transfer is possible via radio transmission and/or GSM.

Keywords: *WMO, snow depth, mountainous terrain, meteorological instruments*

1 INTRODUCTION

WMO recommends a height between 1.2 m and 2 m above ground level for the measurement of air temperature and humidity (WMO, 2008). The height above ground level is specified to take care of the possible strong vertical temperature and humidity gradients at the lowest layers in the atmosphere. Especially in snow rich and remote locations it may be hardly possible to follow this advice. Therefore most of the meteorological stations in mountainous terrain are situated at mountain tops where strong winds will blow off the snow or in valleys where a daily inspection of the sensors is possible. In other unpopulated mountainous areas, e.g. basins, plateaus, the distance of the sensor to the snow surface is not known or the sensor will be snow-covered. Figure 1 shows two examples of our Gruenloch basin experience from recent winter campaigns.

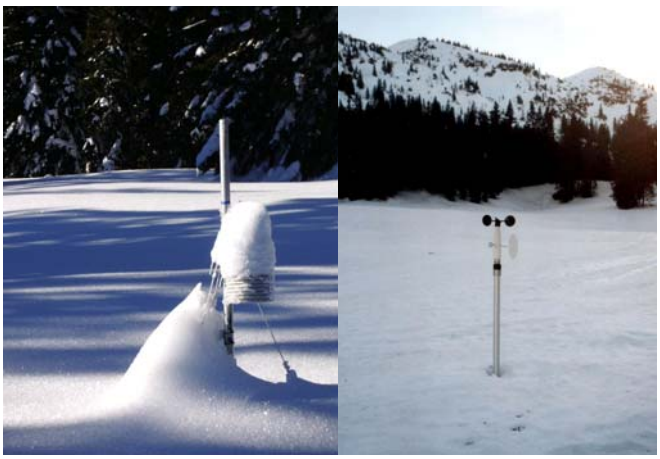

Figure 1. Snow cover in Gruenloch area; left: Temperature/Humidity sensor about 50 cm above snow surface; right: weather station almost completely snow-covered. In both cases: snow depth about 3 m.

2 METLIFT

In close cooperation with the technical high school in Waidhofen/Ybbs, Lower Austria, a new device was developed to guarantee the sensor height above surface within the WMO limits in harsh and remote environments. An ultrasonic snow height sensor measures the distance to the snow surface. If it exceeds certain limits due to snow accumulation or snow melt the lift adapts its height accordingly.

2.1 Overall set-up

Figure 2 shows the prototype of METLIFT. The lift is 6 m high and can pull out for another 4 m. Sensor arms are mounted every meter to allow the connection of additional sensors or to measure a profile of a certain

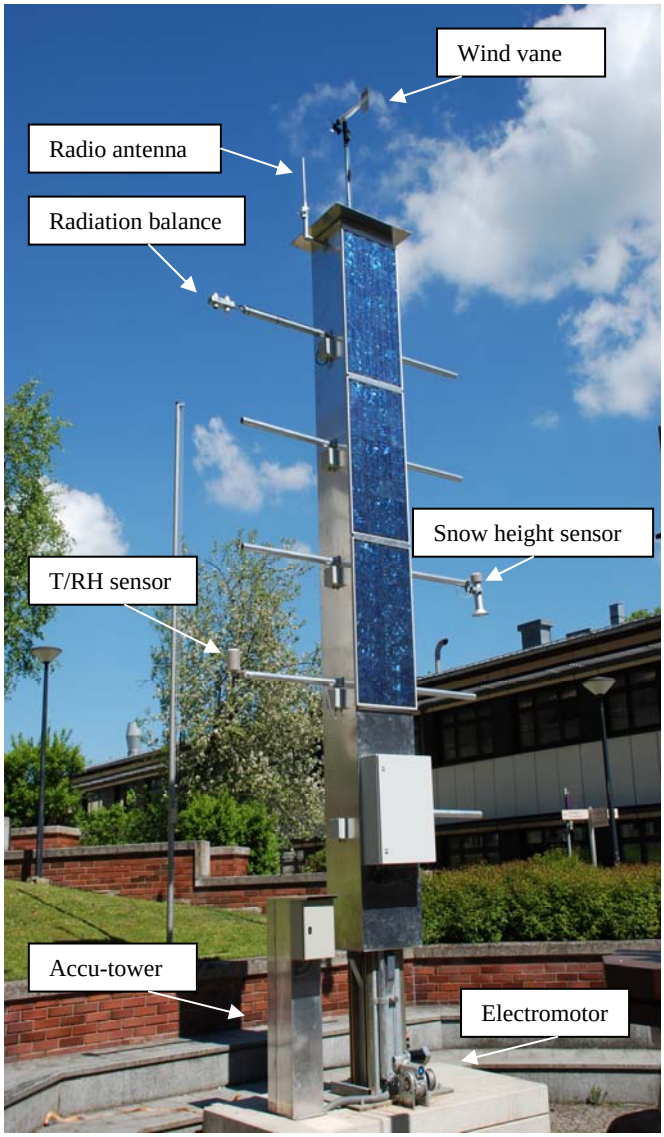

Figure 2. Prototype of METLIFT. Protective housing for the electromotor and for the accu-tower will be added in the final set-up.

parameter of the lowest 5 m above surface. Sensors can be added easily since cable wiring is provided to each sensor arm. Horizontal winds are measured at 7 m height above surface.

2.2 Some technical details

METLIFT is independent of external power supply. Three lead gel accumulators (12V, 85Ah) recharged by three solar panels provide the energy necessary for the sensors, the data loggers, the data transmission components and for the electromotor to lift the system. It has to be ensured that the temperature in the accu-tower stays within the operation temperature limits of the accumulators to avoid a loss of power or even worse a destruction of the accumulators. The accu-tower is insulated and a heat pipe provides additional energy to the interior of the accu-tower to keep the temperature high enough. METLIFT is energy optimised to keep the energy consumption at low levels.

The components of the lift device consist of a 12V electromotor with a worm gear with a transmission rate of 2856:1. This means that the lift moves extremely slow. The lifting is realized via a winch, a steal rope and a return shaft.

Basins represent very often dead zones for GSM signals. Therefore, METLIFT is equipped with a radio transmission system. The radio signal is sent to a nearby mountain station and then converted into a GSM signal.

All electronic units are checked for temperatures down to -70 degree Celsius.

3 SYSTEM CHECKS

Several tests have been performed during the winter season 2008/2009. The data transmission check verified the data flow from the logger via the radio signal and GSM signal to a server and the real-time availability on a webpage. The power consumption of each sensor, of the logger, of the data transmission system and of the control unit for the lift has been measured and optimized in the energy consumption check. Icing conditions have been simulated by sprinkling the tower during very cold days.

4 FURTHER OUTLOOK

METLIFT will be brought into the field in the upcoming summer season in the Dachstein region in Austria. Due to the very remote location all components have to be transported via helicopter. First field data are expected in autumn 2009.

REFERENCES

WMO, 2008: Guide to Meteorological Instruments and Methods of Observation. WMO-Nr. **8**, 681pp.

EXTENDED ABSTRACT TEMPLATE FOR ICAM-2009: A CASE-STUDY OF VOLUNTARY COOPERATION (12 PT BOLD CENTRED)

Hans Volkert [1] and Günther Zängl [2] (10 pt centred)

[1] Deutsches Zentrum für Luft-und Raumfahrt, Institut für Physik der Atmosphäre, Oberpfaffenhofen, Germany
E-mail: *Hans.Volkert@dlr.de*

[2] Deutscher Wetterdienst, Forschung und Entwicklung, Offenbach, Germany (10 pt centred)
Email: *Guenther.Zaengl@dwd.de*

Abstract: This example presents all layout details for an easy production of a two-page Extended Abstract for each oral and poster presentation which was accepted for the 30th International Conference on Alpine Meteorology (ICAM) to be held in Rastatt, Germany, from 11-15 May 2009. The abstract should briefly summarize the main contents of your contribution. Recommended maximum size 10 lines using Times new roman 9pt. The sample is reproduced here as it may be useful at future occasions.

Keywords: *ICAM, group dynamics (9 pt in italics)*

1 INTRODUCTION (headline in CAPITALS, 10 PT BOLD)

The extended abstracts will be gathered in the preprint volume for the 30th International Conference on Alpine Meteorology. In order to have similar format for all abstracts of the conference volume, this document gives some recommendations to the authors when elaborating their extended abstract. The extended abstract should be formatted **in A4 format** (210 mm x 297 mm) with page margins of 25 mm on the left and right sides and 25 mm on the top and bottom. The **maximum allowed size is 2 pages**. Pages **must not** be numbered as the pagination will be done during the final editing process.

The first page must begin with the paper title in capital letters centred. All authors' names and affiliations appear just below the title. The email address is only necessary for the first author. An abstract and keywords directly follow directly.

The text should be divided in several sections, e.g. INTRODUCTION, DATA AND METHODS (or MODEL SETUP for numerical modelling papers), RESULTS and CONCLUSION. The title of each section should be in capital letters. Sections can be divided in sub-sections with subtitles. The text must be in a **single column format**. For the body, the text must be single-spaced and justified, using preferably Times new Roman font. Sizes are specified at various locations. It should be structured in paragraphs, new paragraphs begin indented without an empty line. The paper should be written in English. SI units should be used.

References will appear at the end of the extended abstract. List citations alphabetically in the reference section. Three examples of citations are given in this document (Bougeault et al. 2001, Houze 1993, Schwitalla et al. 2007). Acknowledgements is an optional item placed just before the references section.

2 TABLES, FIGURES AND EQUATIONS

2.1 Tables and figures (10 pt bold)

A caption must be provided for each table and figure. Captions should be below the figures/tables and must be numbered (Tab. 1; Fig. 1). Figures may be provided in colour, but should also be readable when printed in greyscale, because the printed Extended Abstract Volume will not contain colour figures. However, colour figures will be available in the online version of the extended abstracts.

2.2 Equations

Equations should be marked with numbers at the right side, equation (1) is an example:

$$ax + b = c \tag{1}$$

Presentation type / Session topics	BoundLayer	Climate	Dynamics	Num.Wea.Pred.	Precipitation	Snow
Oral (#talks, #sessions)	18 in 3	6 in 1	14 in 3	12 in 2	34 in 7	6 in 1
Poster	31	17	27	–	24	7

Table 1. Distribution of presentations in topical groups (cf. programme on pp. ii-xvii; as of 15 April 2009) – Example of a table with columns and lines filled with some quantitative information (entries in 10 pt; caption in 9 pt).

Figure 1. Two versions of the ICAM-2009 logo. Left: towering cumulus above the Black Forest as viewed from Baden Airpark during COPS-2007; right: view from the northern Black Forest heights into the Rhine valley under the cover of high cirrus (9 pt).

Figure 2. View of the venue of ICAM-2009. Right: Spacious foyer, where some of the poster boards will be placed; middle: lecture hall with large elevated screen; the outside garden next to the river Murg invites for informal discussions and relaxing moments during breaks.

3 SUBMISSION OF EXTENDED ABSTRACT

The extended abstract should be produced with MS-Word or LaTeX. For both formats, templates are provided *(ICAM-ExtAbsTemplate.doc* and *ICAM-ExtAbsTemplate.tex)* on the ICAM-2009 web page (www.pa.op.dlr.de/icam2009/downloads/). Of course, other word processing systems can be used as well, in that case, the authors are encouraged to follow the recommendations given in this example. The file should be converted in **pdf-format before submitting your abstract** to **icam2009@dlr.de**. When pdf conversion is not possible, a MS-Word (.doc) or a postscript file (.ps) is also acceptable.

Please submit your extended abstract not later than 3 April 2009. **Note that if you do not submit an extended abstract, your contribution will not appear in the Volume of Extended Abstracts.** Please use the following naming convention to help us producing the Volume of Extended Abstracts:

`ICAM-Name_of_first_author-{Oral|PosterCode}.pdf`

Your PosterCode is given in the programme (cf. www.pa.op.dlr.de/icam2009/programme/ICAM-agenda.pdf), starting with a capital letter (B, C, D, P, or S) followed by two digits.

4 CONCLUSIONS

This Volume shows to what extent the 125 co-authoring teams found the provided guidelines useful. The example got updated with overview figures of presentations in categories oral and poster and in topical groupings (Tab. 1). It is included in the Extended Abstract Volume to make a bit more explicit how an international scientific community – though diverse in many respects – is willing to cooperate on a voluntary basis. A short deadline before the meeting with some flexibility for late-comers and the avoidance of an extra charge appear to have contributed to the considerable number of contributions. It is hoped that the Volume of Extended Abstracts eases personal selections during the conference and preserves some of its contents.

Acknowledgements: *(9pt italics)*
We thank all contributors for their cooperation on a voluntary basis. The five sponsoring agencies DWD, DLR, KIT, NEC and WMO are acknowledged for their support and their trust in the organizers of ICAM-2009.

REFERENCES (e.g. article, book, proceedings; in 9 pt; second line indented for better distinction)

Bougeault, P., P. Binder, A. Buzzi, R. Dirks, R. Houze, J. Kuettner, R. B. Smith, R. Steinacker, and H. Volkert, 2001: The MAP Special Observing Period. *Bull. Amer. Meteorol. Soc.* **82** , 433–462.

Houze, R. A., Jr. 1993: *Cloud dynamics*. International Geophysics series, Volume **53,** Academic Press, 573 pp.

Schwitalla, T., G. Zängl, H.-S. Bauer, and V. Wulfmeyer, 2007: Convective initiation in the Black Forest region in high-resolution MM5 simulations. *Proc. 29th Intern. Conf. on Alpine Meteorology*, Chambery, France, 261–264.